Experimental and computational investigations of heterofluorene oligomers

by

Leah Shawn Coumont

A thesis submitted in partial fulfillment of the requirements for the degree of

Doctor of Philosophy

Department of Chemistry
University of Alberta

Abstract

In response to an increasing global need for inexpensive, energy efficient electronics, the field of organic semiconductors has experienced tremendous growth over the last 3 decades. In addition to their low cost, and interesting electronic and optical properties, organic semiconductors offer the additional benfits of being composed largely of earth-abundant elements, having electronic properties that are easily tailored through structural modifications, and can be solution processed to form flexible films. In particular, the heterofluorene structure has become a popular structural motif in organic semiconductors as a result of their straightforward preparation, and excellent electronic properties which have made them popular materials for devices ranging from transistors to solar cells. In this thesis, I present the results of original research on the subject of heterofluorene oligomers based on two structural motifs: i) macrocyclic carbazole tetramers, and ii) linear trimers of group 14-bridged spirobifluorenes.

The early chapters of this thesis outline the preparation of a family of shape persistent macrocycles based on a carbazole monomer unit through the coupling of 3,6-dibromocarbazole and a series of N-alkylated derivatives with bis-(1,5-cyclooctadiene)Nickel(0) (*i.e.,* $Ni(COD)_2$). The macrocycles produced using this methodology were then used as building-blocks for the preparation of soft carbon nano and micromaterials through polarity induced self-assembly in acetone/water and THF/water co-solvent mixtures. The impact of the assembly process on the optical properties of the tetramers was also studied, and revealed that the alkyl-free derivative underwent aggregation-induced emission

enhancement. The substitution of the tetramers with larger N-alkyl substituents disrupted the aggregation process leading to this favourable behaviour, but allowed the preparation of a range of morphologies from twisted nanofibers through microrods, ribbons and paddlewheels, the nature of which depended on the length and steric bulk of the N-alkyl substituent.

The latter work in this thesis presents the results of a theoretical investigation into a series of linear trimers based on a spirobifluorene monomer unit in which the identity of the spiro-bridging atom is varied from C, Si, Ge and Sn. The potential for spiro-conjugation based charge transfer was calculated at three levels of theory, and suggested that the carbon and silicon analogues are most appropriate for spiroconjugation-based off-chain charge transfer in these trimers. The use of long-range corrected functionals dramatically decreased the charge transfer contributions to the singlet excited states of the trimers, and increased the estimated band gaps to values that were more comparable to experimental results obtained using the carbon-bridged trimer.

Dedicated to my family.

"An expert is a man who has made all the mistakes which can be made in a narrow field."

- *Niels Bohr*

Acknowledgements

Firstly, I would like to thank my supervisor, Prof. Jon Veinot. You took a chance on me some 8 years ago when you agreed to take me on as a summer undergrad. I have learned a lot from you over the years; you are a talented scientist and dedicated supervisor and I hope to continue to learn from you as I progress in my career. I would also like to thank the members of my supervisory committee- Prof. Mariusz Klobukowski and Prof. Eric Rivard for your endless help, guidance and patience over the years. You have gone above and beyond your required roles as members of my supervisory committee, and have helped teach me to ask questions, and admit when I am wrong.

Secondly, I would like to thank the army of support staff that have helped me with administrative issues and characterizing my materials. In particular I would like to thank the members of the Mass Spectrometry lab, Analytical and Instrumentation lab, Scanning Electron Microscopy lab, NMR Spectroscopy lab, X-Ray Crystallography lab, the Alberta Centre for Surface Engineering and Science and Information Services and Technology, and Anita Weiler for their endless hours of help during my PhD. Furthermore, I would like to personally thank George Braybrook, Dimite Karpusov, Wayne Moffatt and Randy Whittall who have helped immensely with acquisition and analyses of mountains of results.

Thanks are also due to the members of the Veinot Research Group, all 4 of the generations that I have had the pleasure of working with. I have gotten to learn from some great scientists in my short career. Special acknowledgement is

required for Polymer Team alumni Shaune McFarlane, Matthew Sirtonski, Lydia Glover, and Larissa Smith for their unending enthusiasm and willingness to learn along with me. I would also like to thank Brenna Brown who has always been my cheerleader, and a good friend. Her passion for the "problems" in chemistry have taught me to remain engaged when my research was failing. Additional special thanks go to Mita Dasog, whose strong example has encouraged me to ask better questions, and whose kindness helped pull me through some very stressful times. I am fortunate to have gotten the opportunity to work with these two very skilled researchers, and wonderful human beings.

Finally, I would like to thank my family for their limitless support, encouragement, and patience. I have not been a joy to deal with over the course of my PhD studies, but I promise your kindness will not be forgotten as I embark on this next, and hopefully more successful, chapter of my life.

Table of Contents

List of Figures

List of Tables

List of Abbreviations and Symbols

Å: Angstrom

Δ: Stokes' shift

°C: Degrees Celcius

δ: Chemical shift

λ: Wavelength

Φ: Fluorescence quantum yield

η: refractive index

A: absorbance

AIE: aggregation-induced emission

AIEE: aggregation-induced emission enhancement

AIQ: aggregation-induced quenching

Bpy: 2,2′- bipyridyl

Cbz: carbazole

CEP: compact effective potential

COD: 1,5-cyclooctadiene

CT: charge transfer

DCTB: trans-2-[3-(4-tert-Butylphenyl)-2-methyl-2-propenylidene]malononitrile

DFT: density functional theory

DLS: dynamic light scattering

DMF: N,N-dimethylformamide

DMG: dimethyl glyoximate

DSC: differential scanning calorimetry

ECL: effective conjugation length

E_g: HOMO-LUMO gap

E_s: Energy of singlet electronic transition

eV: electron volt

f: oscillator strength

HOMO: highest occupied molecular orbital

HPLC: high performance liquid chromatography

HRMS: high resolution mass spectrometry

LUMO: lowest unoccupied molecular orbital

MALDI FTICR: matrix assisted laser desorption-ionization Fourier transform ion cyclotron resonance mass spectrometry

MALDI-TOF: matrix assisted laser desorption-ionization time of flight mass spectrometry

MEH-PPV: Poly[2-methoxy-5-(2-ethylhexyloxy)-1,4-phenylenevinylene]

π-MO: pi molecular orbital

MS: mass spectrometry

NA: naphthenic acid

NMR: nuclear magnetic resonance

t-PA: transpolyaceylene

PANI: polyaniline

PCbz: polycarbazole

PF: polyfluorene

PL: photoluminescence

PLE: photoluminescence excitation

PPE: polyparaphenylene ethylene

PPP: polyparaphenylene

PPV: polyparaphenylene vinylene

PPY: polypyrole

PSC: polymer solar cell

PT: polythiophene

QY: quantum yield

SBF: spirobifluorene

SEM: scanning electron microscopy

SPM: shape persistent macrocycle

TD-DFT: time dependent density functional theory

TEM: transmission electron microscopy

TGA: thermogravimetric analysis

THF: tetrahydrofuran

X_{aq}: mole fraction of water

XPS: X-ray photoelectron spectroscopy

XRD: X-ray diffraction

Chapter 1:

Introduction

1.1. Conjugated polymers and carbon nanomaterials

Recent advances in the development of conductive polymers and carbon-based nanomaterials have inspired countless researchers worldwide. For example, a search in Web of Science shows that in 2014 alone, 538* papers had been published in the field of carbon nanomaterials. In part, this excitement has been fueled by the awarding of Nobel Prizes in Chemistry (1996 and 2000) and Physics (2010) for the discovery of Fullerenes,[1] conductive polymers,[2] and graphene.[3] These discoveries and the associated ongoing research form a foundation for a "new" generation of carbon-based materials with far reaching applications including catalysis,[4] separations,[5] drug delivery,[6] sensors,[7] gas storage,[8] energy applications,[9] and electronics.[10, 11]

Carbon has long been central to materials chemistry/science.[12] From the obvious and seemingly mundane applications of coal and diamond, to the use of chars in paints and pigments,[13] carbon is ubiquitous. The appeal of carbon as a functional material arises from its chemical versatility,[14] ready availability,[15] and biocompatibility.[16] Much of its chemical versatility arises because it has a propensity to catenate and it can participate in σ- and π-bonding, which allows synthetic chemists to define the localization of electron density by modifying the carbon-carbon bonding environment.[17] This ability to tailor bonding affords researchers the opportunity to rationally design materials such as polymers and solid pyrolytic carbons by selectively modifying the carbon-carbon bonding environment.[18] The following chapter offers a brief summary of functional

* Search performed using keywords "carbon nanomaterial"

carbon-based materials with the intent of providing context for the present thesis that describes investigations into the synthesis and properties of two novel families of materials based upon the carbazole and fluorene structural motifs. In particular, linear and cyclic oligomers of a general heterofluorene type will be investigated as structural units for the preparation of functional organic nano- and micromaterials using a bottom-up approach, and will include theoretical investigations into novel oligomers as potential materials for electronic applications such as light-emitting diodes and solar cells.

1.1.1. Carbon-based π-conjugated systems

As mentioned above, the varied bonding modes of carbon make it attractive for designing functional materials.[19] Of particular note, carbon-carbon π-bonds contribute to the ability to tailor carbon-based materials; they increase bond dissociation energy,[20] shorten internuclear separations,[21] and can provide a pathway for electron delocalization/conduction.[21, 22]

Trans-polyacetylene (t-PA) is the most structurally simple conductive polymer and provides a useful conceptual starting point for describing the electronic structure of this intriguing class of materials (Figure 1-1).[21] An elementary understanding of the band structure of t-PA can be realized from a thought experiment in which sp^2 hybridized C atoms are sequentially added to a growing polymer chain. When two sp^2 carbon atoms are linked by one σ-bond and one π-bond 2 bonding and 2 antibonding orbitals result with 1 bonding orbital, and 1 antibonding orbital of π-symmetry (*i.e.*, n = 1 in Figure 1-1). The sequential addition of more carbon atoms with sp^2 hybridization and alternating

double and single bonds leads to an increase in the number of π-molecular orbitals (π-MOs).[22] As new states are added they appear above the HOMO (highest occupied molecular orbital), and below the LUMO (lowest unoccupied molecular orbital) and the HOMO-LUMO band gap narrows (*i.e.*, E_g, Figure 1-1). As a result, an infinite chain of conjugated carbon atoms of this type should conceptually exhibit $E_g = 0$, leading to fully conductive, metallic properties along the backbone of the molecule.[23]

Contrary to what might be expected from this straightforward model, dopant free t-PA shows an experimental E_g = 1.8 eV.[22, 24] The explanation for this observation is found in a phenomenon referred to as Peierls' distortions, which describes the observation of a non-zero E_g in polyacetylene-type molecules. In a conjugated molecule (*i.e.,* where π-bonds are formed from the overlap of neigbouring p_z-orbitals) Peierls' distortions arise from the relative positions of nodes in the π-system in the frontier molecular orbitals. In the HOMO the p_z-orbitals are in phase across the shorter double bonds, stabilizing this electronic state (Figure 1-1, lower right).[25] In the LUMO, nodes occur across the shorter double bonds, which increases the energy of this state, manifesting in a larger E_g.[25] These distortions are also the source for bond length alternation (*i.e.,* the observation of alternating long and short bonds corresponding to single and double bonded carbons, respectively) and limit the extent of electron delocalization within a given π-system.[25] Electron delocalization in π-conjugated materials is commonly quantified in terms of the effective conjugation length (ECL), which can be determined from the UV-visible spectra of oligomers of

growing chain length and confirmed by computational modelling of the HOMO for a given polymer or oligomer.[26, 27] The size of the ECL influences the electronic structure and optical properties of conjugated polymers, which manifests in periodic loss of mutual planarity between π-segments within the backbone of t-PA, and greater bond length alternation.[28] In this respect the degree of bond length alternation within a polymer can provide chemists with insight into its relative conductivity, and help in estimating the magnitude of its E_g.[29]

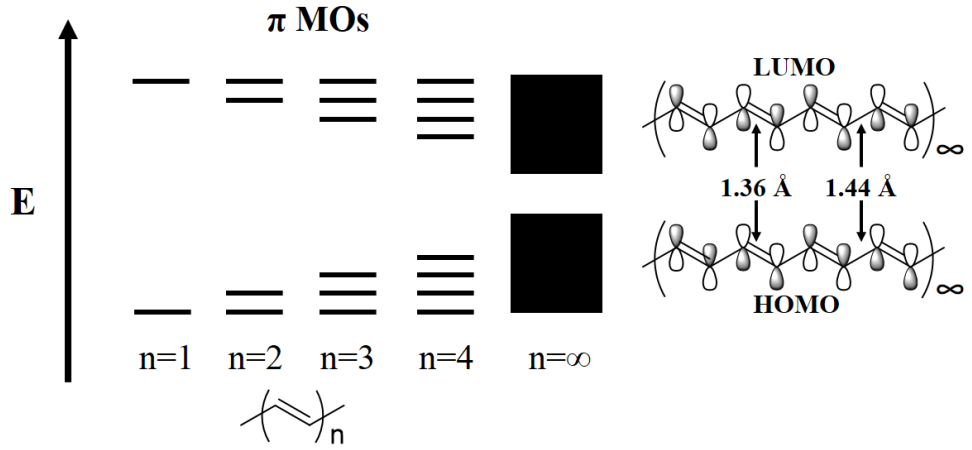

Figure 1-1. The evolution of π-MOs with increasing chain length in a growing t-PA molecule.

Even complex polymer structures like some of those shown in Figure 1-2, contain a polyacetylene-type structural motif.[24] In these materials, bond length alternation between bridging C-C bonds and phenyl- or pyrrole-based C=C bonds can be determined from crystal structures of model short chain oligomers.[30-32] This parameter can serve as a measurable manifestation of effective conjugation length which arises from the formation of quinoid

structures in the excited state (Figure 1-2).[33, 34] Electron delocalization over a larger area - whether it is the result of conjugation, or intramolecular interactions - generally leads to a narrower HOMO/LUMO gap (*i.e.,* smaller E_g), and can facilitate intermolecular charge migration, and thus 1D conduction.[23, 35] In this context, knowing and controlling the degree of bond length alternation is an essential tool to the synthetic materials chemist who aims to tailor a material for a specific application.[36, 37]

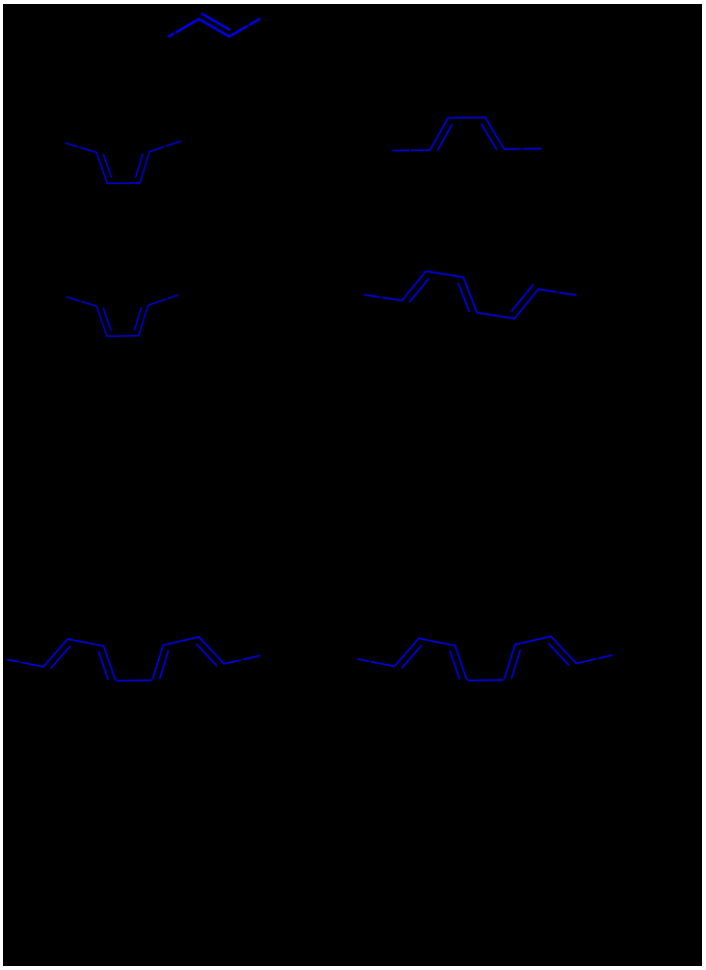

Figure 1-2. Structures and nomenclature for some common conductive organic polymers. For clarity the polyacetylene structural motifs are highlighted in blue.

1.1.2. Electronic considerations for π-conjugated molecules

The discussion thus far regarding the electronic structure of π-conjugated polymers/oligomers neglects some important aspects of their electronic structure that are essential to understanding the materials investigated as part of the research described in this thesis. The elementary energy band diagram pictured in Figure 1-1 is adequate for describing some aspects of the electronic structure of simple solid-state materials. However, the tightly-bound electrons in carbon-based polymers result in weak intermolecular electronic coupling, and limitation of electronic conduction to 2D.[22, 38] As such, the properties of solid π-conjugated molecules and polymers are best described using a combination of band theory, and MO based electronic structure determinations.[18, 25, 39] Complicating matters, the electronic structure of these "soft" materials is very sensitive to geometric factors such as the degree of rotation and folding experienced by the conjugated backbone in the solid state.[40] Consequently, while molecules in solution can still possess many of the spectral features of isolated molecules, this is seldom the case for their tightly packed, more planar solid state couterparts, in which the π-orbitals are better aligned.[41]

Isolated conjugated molecules and polymers undergo strong electron-vibrational coupling associated with the C=C stretching vibration, leading to electronic absorption and emission spectra that display vibronic structure (Figure 1-3).[42] This structure arises because molecules must rearrange to achieve a geometry that coincides with an energetic minimum for the density distribution in the excited state (Δ, Figure 1-3).[24] For π-conjugated molecules these

rearrangements typically involve C=C breathing motions and rotational distortions about the conjugated backbone.[42-44] The energy difference between the initial excited state and the vibrationally relaxed excited state can be measured spectroscopically from the Stokes shift (*i.e.*, the difference in energy between the absorption and photoluminescence, PL, maxima).[45] Often the appearance of a large Stokes' shift suggests photoexcitation of a molecule induces significant geometric reorganization.[43, 46]

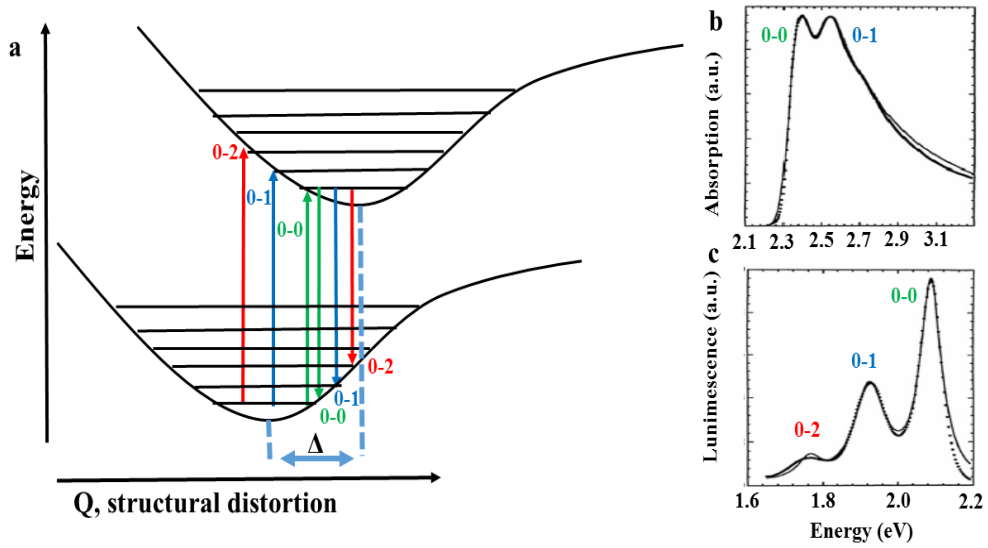

Figure 1-3. a) A Jablonski diagram summarizing the electronic transitions responsible for the PL response of organic molecules. Δ represents the relaxation of the excited state molecule that leads to the Stokes shift. b) Absorption and c) emission spectra for poly[2-methoxy-5-(2-ethylhexyloxy)-1,4-phenylenevinylene] (MEH-PPV) highlighting the impact of vibronic coupling on the spectra. (Spectra reprinted with permission from Hagler *et al.*)[47]

The accessibility of different vibrational modes through excitations of slightly different energy is integral to processes such as charge transfer,[48] and

can provide a spectroscopic "handle" for evaluating the behavior of the molecule in a solution,[49] assembly,[50] or aggregate.[51] For example, spectra arising from isolated molecules often show better defined vibronic structure than the same molecule in the solid state because of restricted molecular motion in the solid (Figure 1-4).[52, 53]

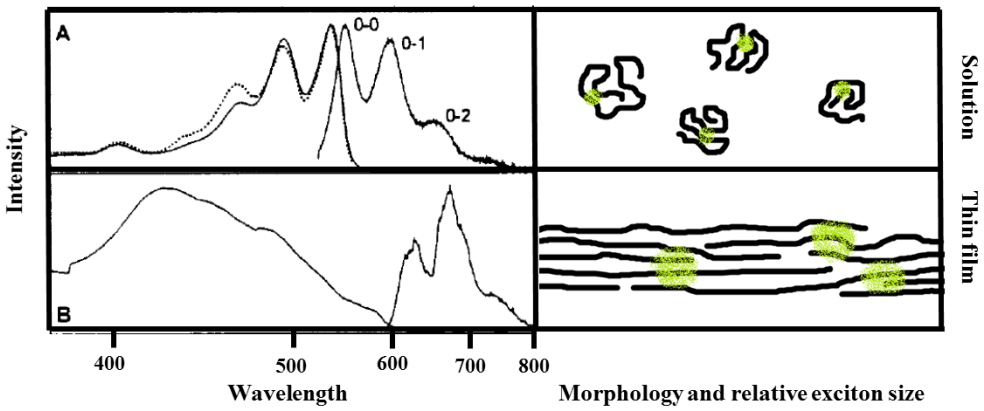

Figure 1-4. The PL (left) and absorption (right) spectra of MEH-PPV in solution (A) and as an H-aggregated film (B) (Spectra reprinted with permission from Meskers et al.).[54]

1.2. Structural motifs in organic semiconducting materials

Much like t-PA all organic semiconductors possess conjugated double bonds, but the specific properties of a given molecule depend upon numerous other factors. In addition to the length of the π-system, molecular electronic properties can also depend upon π-system planarity,[55] the presence of dominant structural motifs contain 5 or 6 membered rings or linear acetylene groups,[56] and the identity and positions of heteroatoms.[57] In the sections that follow specific

examples illustrating the impact of these factors on materials relevant to the content of this thesis will be discussed.

1.2.1. Fluorene-based polymers and oligomers

Polyparaphenylene (PPP) based materials, in which chains of arene rings are joined though single C-C bonds in their para-positions, are an important family of conjugated organic semiconductors (Fig. 1-2). Despite their advantageous properties, two drawbacks to this arrangement of carbon atoms exist: i) conductivity is limited, and ii) the E_g is large.[58] These limitations arise from a lack of structural rigidity within polymer backbones which allows rotation about the long axis of the polymer chain that disrupts orbital overlap between phenylene units. This limitation is compounded by the repulsions between neighboring solubilizing groups,[59] and the presence of successive 6-electron π-systems which ties up the π-electrons in individual phenyl units, and reduces electronic communication between backbone units.[22, 59]

To partially address these issues, one solution developed by the community involves introducing a bridging methylene group like that seen in the structure of fluorene (Figure 1-5).[59] This structural change simultaneously forces neighboring aryl units into a mutually planar geometry,[60] and destabilizes adjacent π-systems.[58] Polyfluorene (PFs) are widely known for their efficient blue PL, and straightforward functionalization.[60] This structural motif also provides a good balance between the electronic benefits of a structurally rigid π-system, and solubility provided by the rotational freedom in between fluorene

units.[60] Still, PFs suffer from oxidative instability and the lack of heteroatoms can limit their range of utility.[58]

Figure 1-5. Structural representations and nomenclature of some important molecules based upon the fluorene-type scaffold. For clarity the bridging methylene group in PF is highlighted in blue, while the heteroatoms are highlighted in green in the other derivatives.

1.2.2. Heteroatom containing fluorene-like materials

The introduction of a bridging methylene group in fluorene introduces a cyclopentadiene-like structural unit into the polymer backbone. By analogy, the bridging carbon atom could be substituted by any atom of appropriate size and electron configuration to produce the corresponding dibenzometallole.[61] Metalloles themselves have been studied theoretically and experimentally for a variety of electronic applications.[62,63] The potential benefits arising from introducing a heavier element in dibenzometalloles include: i) enhancements to optical properties such as two-photon absorption and intersystem crossing,[64,65] ii) increased control over the location of electron density in the ground and excited states, which allows optimization of charge transfer character.[66-69]

The most widely studied heterofluorene is carbazole, in which the bridgehead carbon is replaced by a nitrogen atom. As a result of this structural

change, carbazole (Cbz) has a low lying HOMO which renders this structural unit air stable and, when copolymerized with a more electron withdrawing comonomer to lower E_g, an ideal donor material organic solar cells.[70,71] In addition, the neutral carbazole structural unit has an intact lone pair of electrons that can participate in hydrogen bonding.[72] This lone pair renders oligo- and poly-carbazoles where R = H (see Figure 1-5) susceptible to oxidation under appropriate conditions through the formation of kinetically trapped quinoid structures, similar to those exploited in electrochromic applications (Figure 1-6).[73]

Figure 1-6. Electrochemical dimerization of carbazole (a) and subsequent oxidation to the quinoid based b) pre-emeraldine type monocation, and c) emeraldine-like dication.

1.3. The importance of morphology in organic materials research

While the structure of an individual molecule can be relatively straight-forward to predict and molecular properties are routinely measured in solution or the gas phase, information from these types of studies provide limited insight into the behavior of molecules and polymers in the solid state.[74] Conceptually the simplest model one can construct for a solid-state material involves individual molecules randomly surrounded by, and interacting with many of the same type of molecule. Clearly considering an isolated molecule is not enough as it does little to predict how it will behave in a condensed state – it is important to identify the chemical environment of molecules if material properties are to be understood and exploited.[75] Unfortunately, many molecular and polymeric materials exhibit poorly-defined extended structures or morphologies when cast rapidly from solution, without additional processing steps to induce long-range order.[76-79] In the best cases, with careful study and preparation, the multi-molecule environment or short-range morphology can be accurately modelled on a nanometer scale,[80] but even the thinnest films used in devices are tens of nanometers thick, with areas that fall well into the macroscopic scale.[81]

This difference in scales between what the molecules "see", and what the device requires leaves a substantial window for uncertainty resulting from the introduction of defects, impurities, and/or problems encountered during fabrication that can effectively "undo" whatever *chemical* improvements may have been attempted through rational molecular design.[82, 83] In this context, investigations into the solid state morphology of an organic semiconductor serve

as the first steps in determining whether or not a given material is suited to its target application on a practical scale (Figure 1-7).[40]

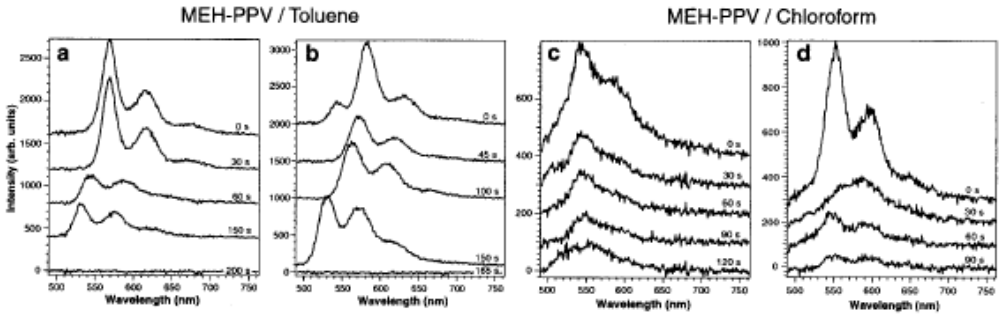

Figure 1-7. The impact of solvent and resulting morphological differences on the optical properties of MEH-PPV. Note: There is a red-shift in emission maxima in the well solvated polymer (left, in toluene) and the poorly solvated polymer (right, chloroform), accompanied by an increase in emission intensity. (Reprinted with permission from T. Huser *et al.* Copyright (2000) National Academy of Sciences, U.S.A.) [84]

The first two sections of this introductory chapter have addressed the chemical structure of organic semiconductors and how it influences material electronic properties. A significant portion of the research outlined in this thesis (*i.e.*, Chapters 2 and 4) involves the assembly of π-conjugated organic molecules based upon the carbazole scaffold into solid micro- and nano-structures, as such, an understanding of the solid-state properties of these materials is useful. In the sections that follow, we will turn our attention to how π-conjugated organic molecules behave as solids. This discussion will encompass which morphologies are accessible by organic semiconducting materials and what is known about how a given morphology impacts the properties of a material.

1. 3. 1. A brief overview of π-conjugated polymer morphology

To more fully appreciate the importance of the work presented herein, the reader will benefit from a thorough understanding of what solid state morphologies are observed in π-conjugated materials, as well as their associated benefits and drawbacks. In general, π-conjugated materials are classified as ordered or amorphous; the internal structure of an ordered material can range from semi-crystalline, to polycrystalline, and even single crystals. Amorphous materials are made up of constituent molecules that exhibit no evidence of folding, stacking, or long-range order.[85] Historically, an amorphous morphology has been preferred over ordered morphologies for π-conjugated polymers used in optoelectronic applications.[58] The amorphous films benefit from an inherent lack of molecular ordering which provides favorable isotropic material properties (*i.e.*, flexibility, conductivities, transparency and luminescence).[86]

The optical and electronic properties of conjugated polymers are influenced by their solid state morphology - a disordered structure has historically been viewed as beneficial to device applications.[87] A large amount of disorder helps inhibit close approach of the polymer backbones that may otherwise lead to deleterious effects such as exciton annihilation,[88] exciplex formation (*i.e.,* a bonded excited state complex), or defect-based quenching (Figure 1-8, b-d).[43] Additionally, by maintaining an amorphous morphology the conductivity and carrier mobilities remain consistent throughout the film which can help in designing more efficient device morphologies, and prevent electrical shorting.[88]

Unfortunately, the benefits associated with employing an amorphous polymer often come at the cost of those properties that make the constituent molecules ideal for electronic applications.[28] For example, the flexibility and ease of solution processing offered by an amorphous polymer film often accompanies a randomized backbone structure which limits conduction in 3D,[28] and results in poor device efficiencies.[89] Additionally, this disorder in the molecular ordering can lead to conformational changes that limit the ECL and lead to variable optical properties.[90] More importantly, excitons (*i.e.*, an electrostatically bound electron/hole pair) can be confined to a single polymer chain - this limits carrier mobilities and can lead to an increase in electron trapping in defect sites that manifests as blinking or a change in luminescence wavelength (Figure 1-8 b).[54, 84, 91, 92]

To ameliorate the poor electronic characteristics associated with amorphous polymers, a common strategy has been to increase crystallinity within the polymer, which improves carrier mobility.[30, 93] Unfortunately, by inducing crystallinity to the previously amorphous solid polymer network, the increased carrier mobilities result in larger exciton diffusion radii, and as such the probability of a carrier encountering a trapping site increases exponentially.[94] Clearly, polymer chemists are often faced with a difficult challenge when designing materials for optical and electronic devices - the optical and electronic properties of solid state materials are often at odds and must be balanced against one another.

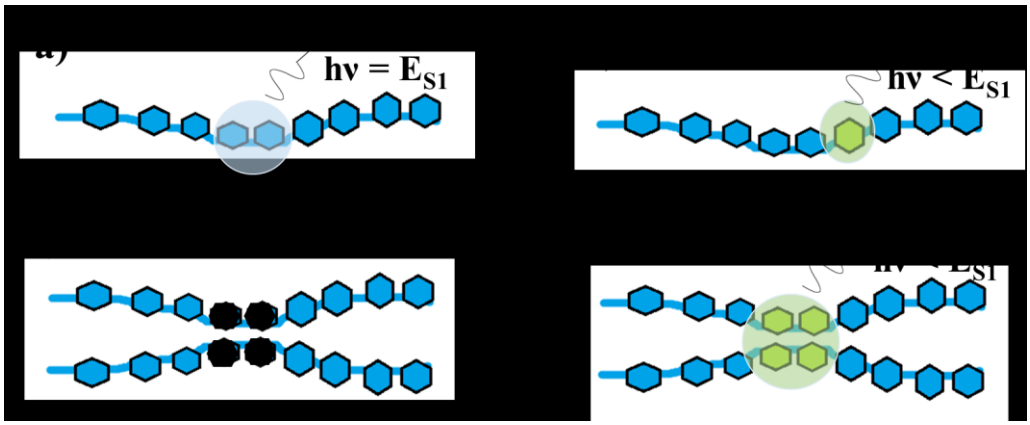

Figure 1-8. a) A pictorial representation of an exciton on single polymer chain, and proposed mechanisms for electron-trapping on a representative polymer. b) The green monomer represents a chemical defect that decreases E_g, c) two nearby chains, both in the excited state undergo exciton annihilation which quenches the luminescence, and d) the two neighboring chains in the excited state interact and undergo radiative recombination in the form of a low energy exciplex.

1.3.2. Small molecules vs. polymers

Unlike polymers, small molecules experience no additional physical benefit from assuming an amorphous morphology other than the isotropy in their optical properties. As their size is limited, the amorphous state for small molecules is generally a disordered molecular arrangement, which yields thin films that are as brittle and inflexible as the corresponding crystalline films. The advantage of using π-conjugated small-molecules in organic electronics is their crystallization behavior is straightforward to identify, modify and implement on a large scale.[95] This property imparts films of small molecules with much greater

carrier transport abilities than their amorphous or even semi-crystalline polymer counterparts,[96] and can make available properties that are unique to the crystals themselves.[55]

The majority of the materials discussed in Chapters 2-5 of this thesis are oligomers; small molecular mass versions of the conventional poly(heterofluorene) and polycarbazole discussed earlier in this Chapter. While both oligomers and polymers are molecules that consist of a repeating monomer unit, the standard criteria used to differentiate these two molecular classes are: a polymer is a molecule in which the addition or subtraction of a single monomer unit *does not* significantly alter the properties of that molecule, whereas the addition or subtraction of a single repeat unit *does* change the properties of an oligomer.[97] Considering the intimate dependence of the properties of oligomers on relatively small structural changes, these materials generally fall into the category of small molecules. For convenience the term small molecule as it is used in this thesis will also include oligomers.

1.3.3. Self-assembly of organic molecules and polymers

Formally, a self-assembled material is defined as one that is composed of chemically discrete molecules which are reversibly ordered in a manner in which small changes in their molecular structure, or the surrounding environment will alter their 3D structure.[98] In their perspective article that described the importance of self-assembly to science and engineering, Whitesides and Grzybowski identified self-assembly as the thread that binds the universal goal of simplicity with the human goal to make things more complicated.[98] This

sentiment exemplifies the field of self-assembled organic materials as a whole - very small structural changes to a molecule can convert it from molecule that favors an amorphous state, to one that will preferentially self-assembles to form a more sophisticated nano or microscale morphology under the appropriate conditions by exploiting very simple intramolecular forces.[99] While this appears straightforward, self-assembled materials can become very complex; the fundamentals of life- structural proteins, enzymes, cells, *etc.* are all complex supramolecular structures formed via self-assembly.[98] Even the simplest self-assembled structures, like the 1D and 0D structures discussed in Chapters 2 and 4 of this thesis, require the concerted and coordinated involvement of intramolecular and intermolecular interactions,[100] as well as kinetic and thermodynamic considerations for assembly to occur.[101-103] The need to manage these factors makes designing molecules for self-assembly very difficult.

In general, certain structural motifs in a small molecule are known to induce self-assembly into certain preferred geometries. For example, high molecular weight conjugated polymers prefer a rigid-rod type quasi-helical geometry,[104] whereas the presence of long aliphatic chains pendant on the conjugated center of small molecules and polymers drives lateral self-assembly into 2D geometries.[105] More generally, solvophobic interactions,[106] hydrogen-bonding,[107] formation of coordination complexes,[108, 109] and ion-pair interactions,[110] are modes of action that have proved useful in promoting supramolecular self-assembly of organic molecules.

Regardless of the challenges associated with designing molecules that will self-assemble into targeted morphologies, the number of applications that require well-defined nano- and micro-structured organic materials is increasing.[96, 100] In particular, these types of assemblies are being investigated for application in sensing,[111] catalysis,[112] photonic devices,[113] and electronic applications.[114] This rapid growth in applications-based research demands novel assemblies of semiconducting organic materials to meet the growing need for well-ordered device components and architectures (Figure 1-9).[115-117]

Figure 1-9. Examples of small molecules used in field effect transistors (left), solar cells (center), and light-emitting diode (right).

1.3.4. Molecular dynamics in solution

Understanding the behaviour of molecules in solution is crucial to controllably forming self-assembled nanomaterials;[118] environmental variations (*e.g.,* stirring rate,[119] temperature,[120] concentration,[121] *etc*.) can have a dramatic impact on the environment that the molecules experience and by extension how they self-assemble.[84] While the general principles of self-assembly are transferable between molecular systems, a thorough understanding of the

solution dynamics of each system is critical if materials with the desired/predictable properties are to be realized.

Solvophobic interactions provide a strong driving force for molecular self-assembly. Molecules with extended π-conjugated systems are inherently solvophobic; even when dissolved in "good" solvents these molecules tend to aggregate and participate in π-stacking (a tendency that is pivotal to self-assembly of these materials into nanostructures).[122] Hydrophobic effects are also commonly exploited in guiding the formation of molecule-derived nanostructures.[114] As a result, nanostructures formed from π-conjugated molecules are often formed using binary solvent mixtures consisting of a "good" solvent-e.g., tetrahydrofuran (THF) , acetone, or acetonitrile- and water, which acts as an antisolvent, to induce nucleation (Figure 1-10).

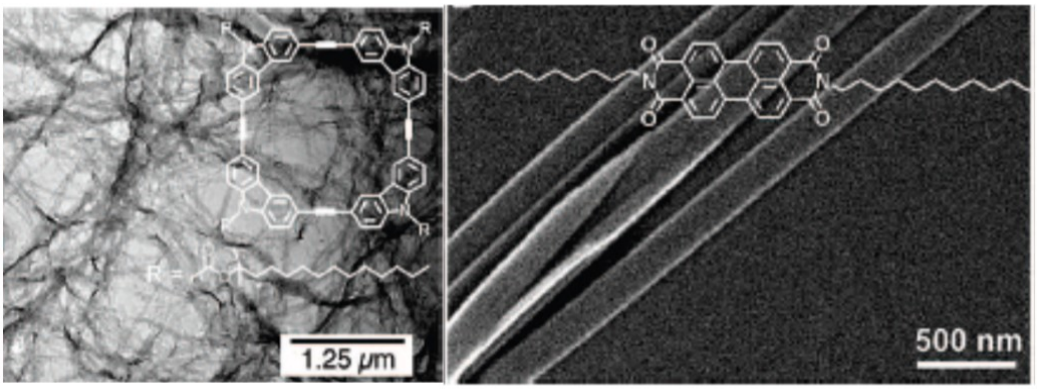

Figure 1-10. Self-assembled 1D nanowires induced upon the addition of water to THF solutions of molecules based on a macrocyclic carbazole structure (left) and perylenediimide structure (right). (Reprinted with permission from Zang *et al.*)[94]

1.3.5. A special case of solution dynamics: shape persistent macrocycles

Macrocycles are attractive materials because their structures combine the benefits of a monodisperse small molecule with the properties of a moderate/high molecular weight linear oligomer or polymer. A significant challenge associated with employing small molecules in device structures is, unlike amorphous polymers, these molecules generally do not form thin-films with uniform properties. As opposed to trying to force these small molecules into an amorphous geometry, an alternative strategy is employed which involves tailoring the molecular structure to induce ordering. This strategy assists in producing a bulk material with predictable properties that approach those of a single crystal, instead of an amorphous material.[123]

One class of materials specifically designed to meet this need are the shape-persistent macrocycles (SPMs). These molecules consist of a "shape-persistent" conjugated core that, unlike a crown ether-type macrocycle, adopt a rigid conformation enveloped by an extaannular corona of oligo(alkane) moieties that are pendant to the central core.[124] SPMs are prone to self-assemble, but the interactions driving this assembly are non-specific. The formation of superstructures occurs because the side chains tend to order,[125, 126] and the π-system is solvophobic.[127] Consequently, SPMs often self-assemble into 1D[126, 128] or 2D nanostructures,[129] can accept molecular guests into their central cavity,[130-132] and can exhibit liquid crystalline properties (Figure 1-11).[133] SPMs have successfully been designed to afford materials that exhibit predictable two-photon absorption, and charge transfer properties, in addition to self-assembly.[134]

While both linear oligomers[135] and SPMs[124] composed of π-conjugated structural units are known to self-assemble, oligomers are subject to rotational degrees of freedom about their backbones which can disrupt the self-assembly process. The fixed molecular geometries encountered in SPMs allow exquisite control over the position of pendant functional groups (*i.e.,* intraannular or extraannular) as well as their relative position in 3D space.[124] While these features assist in preparing molecules which will form specific assemblies, their synthesis and purification is often difficult and low yielding, making investigation of their properties impractical.[136]

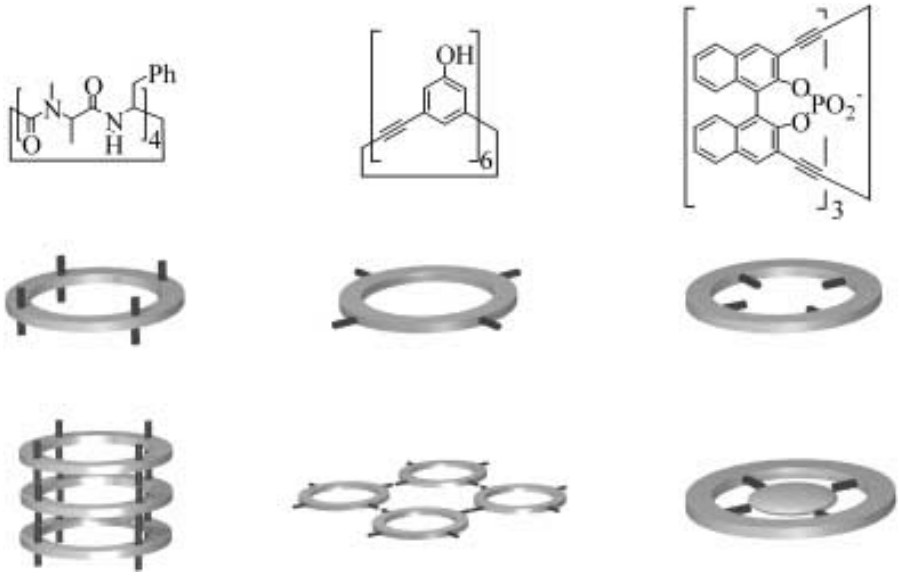

Figure 1-11. Representative examples of SPMs and pictorial representation sof how the orientation pendant groups can guide supramolecular self-assembly.(Reprinted with permission from S. Hoger)[124]

1.3.6. Aggregation and optical response: quenching versus enhancement of luminescence

The first step in the self-assembly of aryl-based π-conjugated materials is molecular aggregation. Even very dilute (*c.a.* 10^{-5} M)[118] solutions of π-conjugated small molecules show evidence of dimerization.[137] As discussed previously, this propensity to assemble is driven by molecular π-stacking and solvophobic interactions. The π-stacking interactions involve constructive overlap of π-orbitals through face-to-face molecular alignment, driven by electrostatic quadrupolar interactions, which are generally weak (e.g., 0.8 to 2.8 kcal/mol)[138] and active over short distances (< 5 Å).[139] These interactions lead to partially-bonded electronic states that can induce polaron trapping and facilitate intramolecular electronic communication.[140] Though the exact nature of these interactions depends upon the molecular structure of the participants, and relative orientation of the molecules involved (Figure 1-12). [141]

There are two general classes of aggregates common in π-conjugated molecules that are investigated for optoelectronic applications: H-aggregates and J-aggregates (Figure 1-12). The optical response of these molecules is dependent upon the changes in electron localization of the electrons in the excited state (*i.e.*, transition dipole).[22] Intramolecular charge transfer can bring about changes in optical absorption arising from the orientation of molecular dipoles within the aggregates.[113] Generally J-aggregates exhibit a slip-stacked molecular arrangement, with transition dipoles oriented in a head-to-tail manor.[111] This dipole arrangement assists in holding the aggregates together, while stabilizing

charge-transfer excited states across the aggregate as a whole. This orientation of transition dipoles is generally accompanied by decreases in the energy of both excitation and emission of the aggregate relative to the fully solvated molecule (Figure 1-12, 2). [142, 143]

In H-aggregates the π-systems are better aligned resulting in more effective π-overlap and a higher probability of excitonic coupling (Figure 1-12, 1).[144] This coupling interaction is believed to induce non-radiative relaxation of electrons from the singlet excited state that would otherwise contribute to the overall luminescence intensity. As such the H-aggregates in solid state organic emitters, particularly carbazole, have historically been implicated as the most likely cause of the low oscillator strengths associated with the emitting states in the π-conjugated solid.[145, 146]

1.3.7. Aggregate properties and aggregation-induced emission enhancement

The most common way to distinguish between J- and H- aggregates through evaluation of their electronic absorption and emission spectra (Figure 1-12).[145] Due to the presence of strong electron vibrational coupling in H-aggregates, excitons are shared between several polymer chains;[54] hence the emission spectra of molecules interacting in this way are usually broad and featureless, and are observed to exhibit longer fluorescence lifetimes consistent with larger exciton diffusion radii (recall Figure 1-4).[143]

Transition dipoles of molecules within aggregates can assume two possible orientations that impact their optical properties; in H-aggregates an

arrangement in which the transition dipoles oppose one another is the only allowed electronic transition. This transition is higher energy than that of the non-aggregated constituent molecules, hence, a blue-shift in the optical absorption is observed relative to the free molecule (Figure 1-12, 1).[147] Occasionally the formation of H-aggregates will also manifest as a red-shift in the emission spectra of a given assembly, but this is considered to arise only because of the larger π-system of the aggregate.[145]

The orientations of the dipoles in J-aggregates can introduce a new emitting species analogous to the exciplex defects mentioned previously. These chromophores have allowed optical transitions in which transition dipoles in the constituent molecules are aligned head to tail (Figure 1-12, 2). As a result of this orientation, J-aggregates often display charge transfer character that can induce red-shifted absorption and emission spectra, and smaller fluorescence lifetimes than those observed for the solvated molecules.[52] Photoemission from J-aggregates exhibit unique spectral profiles (*e.g.*, emission maxima) that differ from the solvated, non-aggregated molecule.[148] Because photo-excitation in J-aggregates is an intramolecular process, there is poor electron-vibrational coupling hence the corresponding spectra often lack vibronic structure.[142]

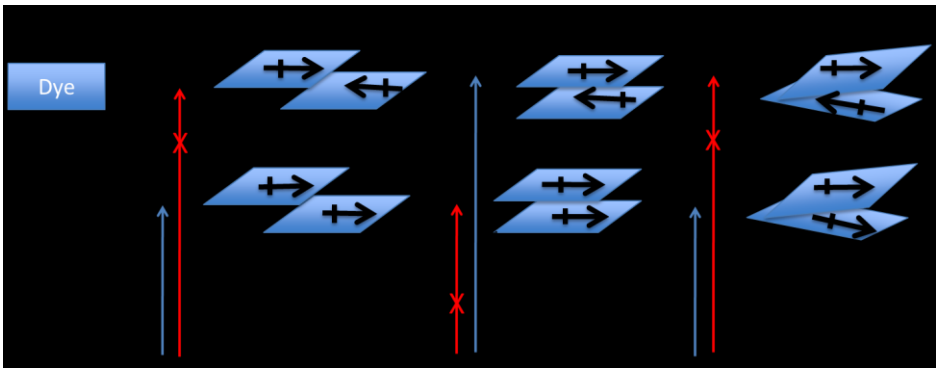

Figure 1-12. A pictorial representation of the electronic transitions accessible upon photoexcitation of 1) an isolated dye molecule, 2) J-aggregates of dye molecules, 3) H-aggregates of dye molecules, and 4) randomly oriented aggregates. Arrows represent the direction of the transition dipoles of the dye molecules within the aggregates.

There is a longstanding debate regarding whether H-aggregates are the true source for non-radiative losses in organic π-conjugated luminophores.[145] Early reports proposed side-to-side stacking typical of H-aggregates reduced PL quantum yields through exciton annihilation.[149] More recently, an increasing number of compounds have been investigated that display all of the optical trademarks of H-aggregates, but are still capable of efficient luminescence.[145] These observations prompted researchers to suggest a defect-based electron trapping model would be more appropriate in describing the non-radiative losses in H-aggregated systems.[145] One of the mechanisms proposed for the emission enhancement observed from H-aggregates, involves the restriction of rotational distortions about C-C bonds.[150] Within this mechanism, the aggregation process fixes the molecular geometry such that it approximates the geometry of the

vibrationally relaxed excited state.[151] The result is a material that has spectral signatures of H-aggregates (*i.e.,* long lifetimes and blue-shifted absorption) with the added benefit of high quantum yields. Because the emission processes in the aggregates are the same as the solvated molecules these properties are commonly referred to as aggregation-induced emission enhancement (AIEE). The phenomenon of AIEE arising from H-aggregates will be discussed in great detail when covering the optical properties of the carbazole-based assemblies presented in Chapters 2 through 4 of this thesis.

1.3.8. Nanomaterials formed from self-assembly of π-conjugated materials.

Given the predictability with which π-conjugated materials tend to self-assemble, much success has been realized in developing new small-molecules and polymers with the specific goal of producing novel "soft" organic nanomaterials. The field of self-assembled organic nanomaterials has grown to encompass structural motifs ranging from spheres,[152] to hollow tadpoles,[153] through fibres,[46] plates,[50] and even advanced structures thought to only be accessible to inorganic solids[154] (*e.g.*, onion[155] and rosebud[156] motifs; Figure 1-14).

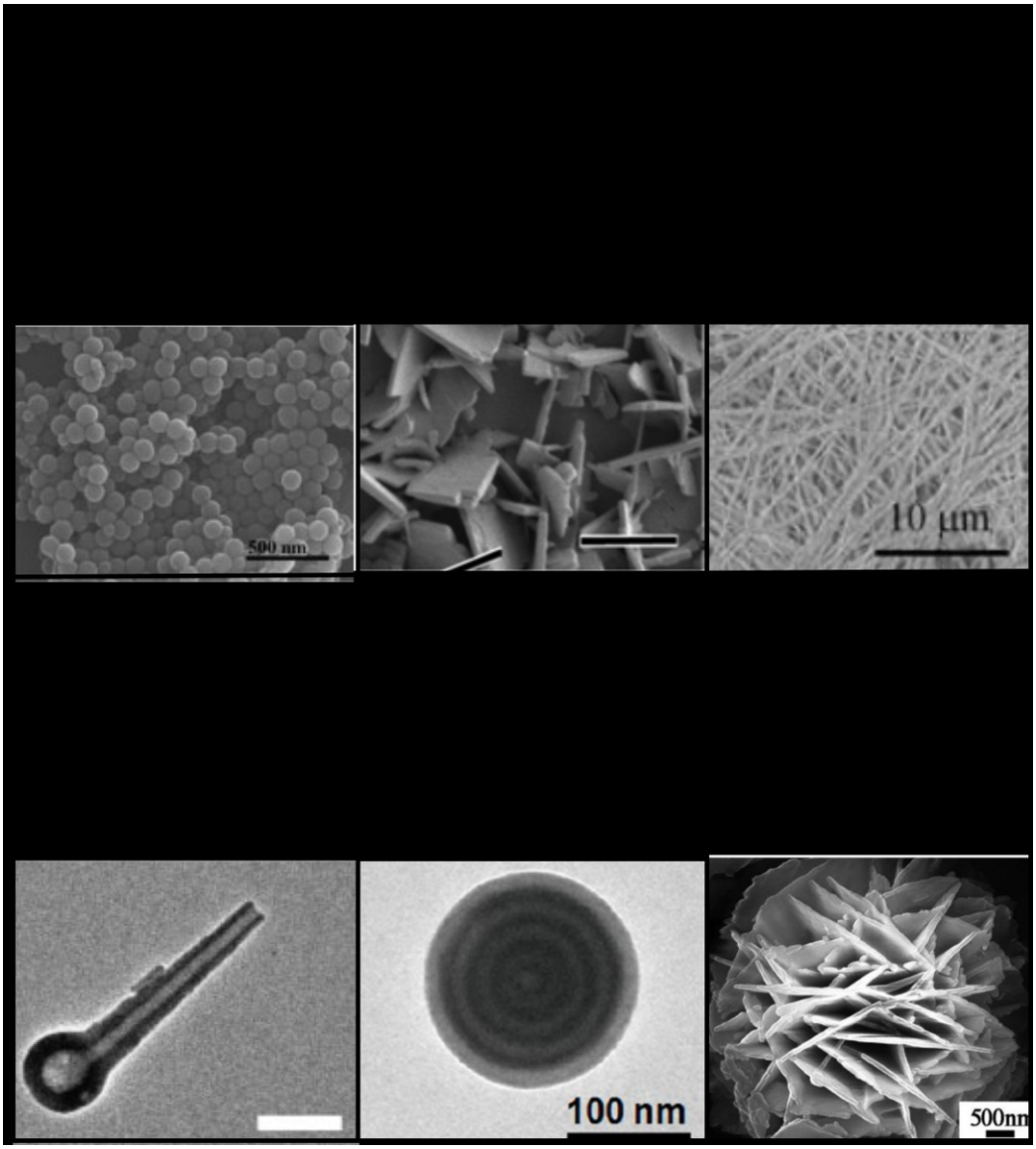

Figure 1-13. Some micro- and nano-structure assemblies of molecular systems. Images adapted from figures in references a) 149, b) 50, c) 46, d) 153, e) 155, f) 156 (Images reprinted with permission).

Much like their inorganic counterparts, the benefits of organic nanomaterials are found in their high surface-area to volume ratio, and sizes that are on the same regime as many thin-film type devices. These features render these materials ideal for gas adsorption, catalysis, and solar applications.

Additionally, there are many reasons why self-assembled nano-materials would be preferred over traditional (often inorganic) "hard" solid-state nanomaterials.

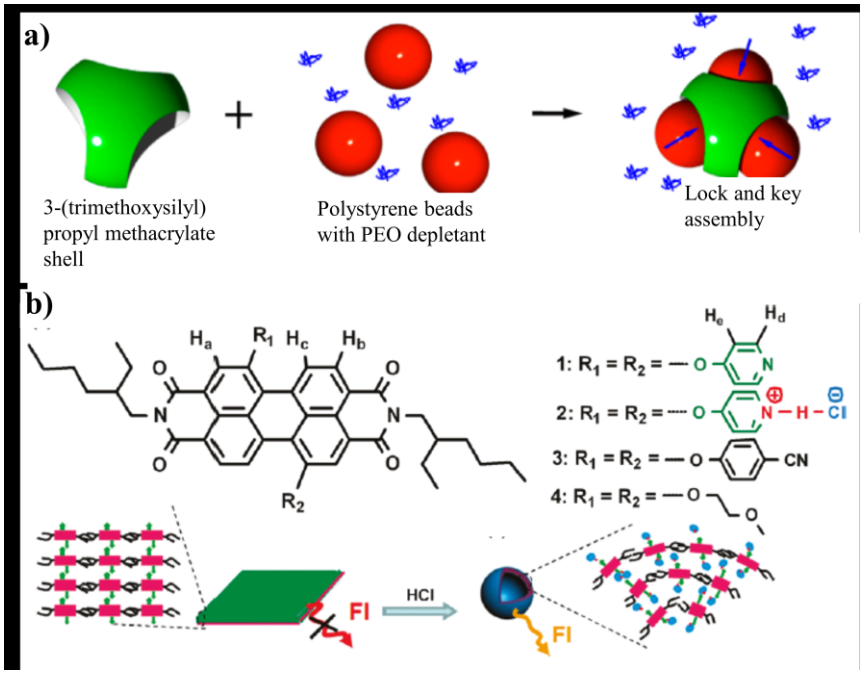

Figure 1-14. Representative stimulus responsive nanomaterials formed from π-conjugated molecules. a) The formation of a lock and key assembly from a 3-(trimethoxysilane)propyl methacrylate lock and polystyrene beads in response to the addition of polyethylene oxide.[160] b) Morphological switching and fluorescence response of perylenediimides in response to changes in HCl concentration.[159] (Images adapted and reprinted with permission)

For example, "soft" nanomaterials can be specifically designed to undergo morphological changes in response to external stimuli. Soft nanomaterials have also been designed to participate in entropy driven lock-and-key assembly,[157, 112] dynamic photo-switching,[158] concentration dependent hydrochloride salt formation,[159] and polarity sensitivity[50] (Figure 1-14).

Furthermore, these materials can be tailored to simultaneously adopt an optimum morphology for a target application.

1.4. Thesis Outline

This thesis describes investigations involving the synthesis and properties of oligomers based on carbazole and heterofluorene scaffolds. The work can be divided into two broad categories. Chapters 2, 3 and 4 describe the synthesis, solution dynamics, and exploration of various applications of a family of all-carbazole SPMs (Figure 1-15). These experimental chapters explore the question; can varying the length of the alkyl substituent appended to carbazole SPMs be used to tailor the morphology of the assemblies formed through precipitation of the molecules from solution?

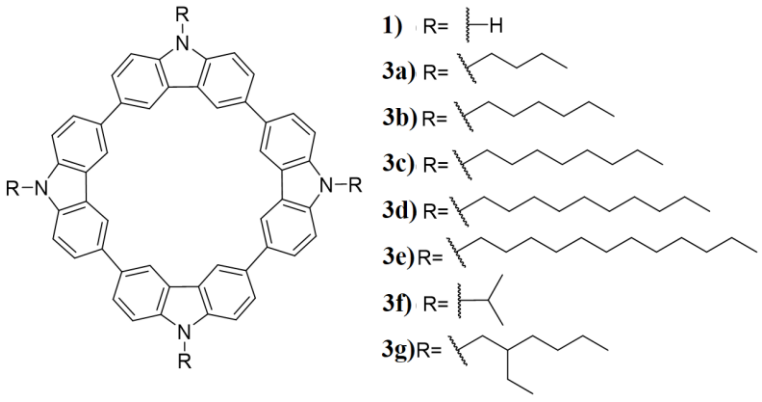

Figure 1-15. Structural representation of the carbazole-based macrocycles prepared and studied in Chapters 2, 3 and 4.

Chapter 5 describes a computational investigation of oligomers based upon the spirobifluorene scaffold in which the identity of the spiro-bridgehead atom is substituted by successively heavier Group 14 elements (Figure 1-16).

The research in this Chapter aimed to determine the impact changing the spiro-atom on spiroconjugation, and how such changes would influence the molecular charge transfer characteristics. The specific question that Chapter 5 attempts to answer is if substituting the spirobifluorene trimer **5a** with heavier Group 14 elements can be predicted to promote charge transfer states in this system using computational methods?

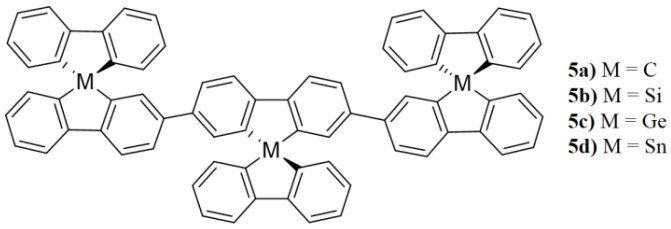

Figure 1-16. Structures of the compounds studied computationally as part of the studies described in Chapter 5.

This thesis will conclude with Chapter 6 by summarizing how the research discussed in Chapters 2-5 helps to provide answers to the questions posed above. Additionally this chapter will contain a discussion of future work which could be completed to further the understanding of the materials discussed as a part of this thesis and outline new projects which could investigate their properties.

1.5. References

(1) Kroto, H. W.; Heath, J. R.; O'Brien, S. S.; Curl, R. F.; Smalley, R. E. *Nature* **1985**, *318*, 162.

(2) Shirakawa, H.; Jouis, E. J.; MacDiarmid, A. G.; Chiang, C. K.; Heeger, A. J. *J. Chem. Soc. Chem. Commun.* **1977**, 578.

(3) Nobel Media, A. The Nobel Prize in Physics 2010 <http://www.nobelprize.org/nobel_prizes/physics/laureates/2010/>.

(4) Yang, L.; Zhao, Y.; Chen, S.; Wu, Q.; Wang, X.; Hu, Z. *Chinese J. Catal.* **2013**, *34*, 1986.

(5) Ye, N.; Shi, P. *Sep. Purif. Rev*. **2014**, *44*, 183.

(6) Wang, Q.; Huang, X.; Long, Y.; Wang, X.; Zhang, H.; Zhu, R.; Liang, L.; Teng, P.; Zheng, H. *Carbon* **2013**, *59*, 192.

(7) Zhang, R.; Chen, W. *Biosens. Bioelectron.* **2014**, *55*, 83.

(8) Arenillas, A.; Drage, T. C.; Smith, K.; Snape, C. E. *J. Anal. Appl. Pyrolysis* **2005**, *74*, 298.

(9) Paraknowitsch, J. P.; Thomas, A. *Energy Environ. Sci.* **2013**, *6*, 2839.

(10) Chung, D. D. L. *J. Mater. Sci.* **2004**, *39*, 2645.

(11) Shenderova, O. A.; Zhirnov, V. V.; Brenner, D. W. *Crit. Rev. Solid State Mater. Sci.* **2002**, *27*, 227.

(12) Dresselhaus, M. S. *Annu. Rev. Mater. Sci.* **1997**, *27*, 1.

(13) Cullers, R. L. Carbon (C). *Salem Press Encyclopedia of Science*, **2013**.

(14) Stwertka, A. *A Guide to the Elements*; **2012**; p. 191.

(15) Dubey, N.; Leclerc, M. *J. Polym. Sci. Part B Polym. Phys.* **2011**, *49*, 467.

(16) Li, W.; Zhang, Z.; Kong, B.; Feng, S.; Wang, J.; Wang, L.; Yang, J.; Zhang, F.; Wu, P.; Zhao, D. *Angew. Chem. Int. Ed. Engl.* **2013**, *52*, 8151.

(17) Coville, N. J.; Mhlanga, S. D.; Nxumalo, E. N.; Shaikjee, A. *S. Afr. J. Sci.* **2011**, *107*, 1.

(18) Barford, W. *Electronic and Optical Properties of Conjugated Polymers*; Birman, J.; Edwards, S. F.; Friend, R.; Rees, M.; Sherrington, D.; Veneziano, G., Eds.; Oxford University Press, **2005**; pp. 1–25.

(19) Clayden, J.; Greeves, N.; Warren, S.; Wothers, P. *Organic Chemistry*; **2001**; Vol. 40, pp. 1990–1992.

(20) Housecroft, C. E.; Sharpe, A. C. *Inorganic Chemistry*; **2005**; pp. 338–384.

(21) Erlandsson, R.; Salaneck, W. R.; Lundström, I. *Mater. Des.* **1986**, *7*, 246.

(22) Moliton, A.; Hiorns, R. C. *Polym. Int.* **2004**, *53*, 1397.

(23) Hoffmann, R.; Janiak, C.; Kollmar, C. *Macromolecules* **1991**, *24*, 3725.

(24) Heeger, A. J. *Chem. Soc. Rev.* **2010**, *39*, 2354.

(25) Soos, Z. G.; Hayden, G. W.; Ramaseshan, S. *Solid State Ionics* **1989**, *32/33*, 567.

(26) Meier, H.; Stalmach, U.; Kolshorn, H. *Acta Polym*. **1997**, *48*, 379.

(27) Chen, R.-F.; Liu, L.-Y.; Fu, H.; Zheng, C.; Xu, H.; Fan, Q.-L.; Huang, W. *J. Phys. Chem. B* **2011**, *115*, 242.

(28) Garnier, F. *Acc. Chem. Res.* **1999**, *32*, 209.

(29) Rossi, G.; Chance, R. R.; Silbey, R. J. *Chem. Phys.* **1989**, *90*, 7594.

(30) Hutten, P. F. V. A. N.; Krasnikov, V. V; Hadziioannou, G. *Acc. Chem. Res.* **1999**, *32*, 257.

(31) Van Bolhuis, F.; Wynberg, H.; Havinga, E. E.; Meijer, E. W.; Staring, E. G. J. *Synth. Met.* **1989**, *30*, 381.

(32) Hotta, S.; Waragai, K. *J. Mater. Chem.* **1991**, *1*, 835.

(33) Gieseking, R. L.; Mukhopadhyay, S.; Risko, C.; Marder, S. R.; Brédas, J.-L. *Adv. Mater.* **2014**, *26*, 68.

(34) Brédas, J. L. *J. Chem. Phys.* **1985**, *82*, 3808.

(35) Karl, N. *Synth. Met.* **2003**, *133-134*, 649.

(36) Beaujuge, P. M.; Reynolds, J. R. *Chem. Rev.* **2010**, *110*, 268.

(37) Kushmerick, J. G.; Holt, D. B.; Pollack, S. K.; Ratner, M. A.; Yang, J. C.; Schull, T. L.; Naciri, J.; Moore, M. H.; Shashidhar, R. *J. Am. Chem. Soc.* **2002**, *124*, 10654.

(38) Bässler, H.; Köhler, A. *Chem. Rev*. **2012**, *312*, 1.

(39) Tiago, M.; Rohlfing, M.; Louie, S. *Phys. Rev. B* **2004**, *70*, 193204.

(40) Bolinger, J. C.; Traub, M. C.; Brazard, J.; Adachi, T.; Barbara, P. F.; vanden Bout, D. A. *Acc. Chem. Res.* **2012**, *45*, 1992.

(41) Fischer, F. S. U.; Tremel, K.; Link, S.; Kayunkid, N.; Brinkmann, M.; Delgado, M. C. R.; Ludwigs, S. *Macromolecules* **2013**, *46*, 4924.

(42) Karabunarliev, S.; Baumgarten, M.; Bittner, E. R.; Müllen, K. *J. Chem. Phys*. **2000**, *113*, 11372.

(43) Saragi, T. P. I.; Spehr, T.; Siebert, A.; Fuhrmann-Lieker, T.; Salbeck, J. *Chem. Rev.* **2007**, *107*, 1011.

(44) Oliveira, F. A. C.; Cury, L. A.; Righi, A.; Moreira, R. L.; Guimarães, P. S. S.; Matinaga, F. M.; Pimenta, M. A.; Nogueira, R. A. *J. Chem. Phys.* **2003**, *119*, 9777.

(45) Brédas, J. L.; Cornil, J.; Heeger, A. J.; Briidas, B. J. *Adv. Mater.* **1996**, *8*, 447.

(46) Liu, X.; Xu, D.; Lu, R.; Li, B.; Qian, C.; Xue, P.; Zhang, X.; Zhou, H. *Chem. Eur. J.* **2011**, *17*, 1660.

(47) Hagler, T. W.; Pakbaz, K.; Voss, K. F.; Heeger, A. J. *Phys. Rev. B* **1991**, *44*, 8652.

(48) Coropceanu, V.; André, J. M.; Malagoli, M.; Brédas, J. L. *Theor. Chem. Accounts Theory, Comput. Model.* **2003**, *110*, 59.

(49) Maus, M.; Rettig, W.; Bonafoux, D.; Lapouyade, R. *J. Phys. Chem. A* **1999**, *103*, 3388.

(50) Zhang, Z.; Zhan, C.; Zhang, X.; Zhang, S.; Huang, J.; Li, A. D. Q.; Yao, J. *Chem. Eur. J.* **2012**, *18*, 12305.

(51) Beckers, E. H. A.; Meskers, S. C. J.; Schenning, A. P. H. J.; Chen, Z.; Würthner, F.; Marsal, P.; Beljonne, D.; Cornil, J.; Janssen, R. A. J. *J. Am. Chem. Soc.* **2006**, *128*, 649.

(52) Spano, F. C. *Acc. Chem. Res*. **2010**, *43*, 429.

(53) Wang, W.; Li, L.-S.; Helms, G.; Zhou, H.-H.; Li, A. D. Q. *J. Am. Chem. Soc.* **2003**, *125*, 1120.

(54) Meskers, S. C. J.; Janssen, R. A. J.; Haverkort, J. E. M.; Wolter, J. H. *Chem. Phys.* **2000**, *260*, 415.

(55) Wang, C.; Dong, H.; Hu, W.; Liu, Y.; Zhu, D. *Chem. Rev.* **2012**, *112*, 2208.

(56) Patil, A. O.; Heeger, A. J.; Wudl, F. *Chem. Rev.* **1988**, *88*, 183.

(57) Henson, Z. B.; Müllen, K.; Bazan, G. C. *Nat. Chem.* **2012**, *4*, 699.

(58) Grimsdale, A. C.; Müllen, K. *Adv. Polym. Sci.* **2006**, *199*, 1.

(59) Jansen, M.; Baldus, H. P.; Patent, U. S.; Jaschek, R.; Russel, C.; Solids, J. N.; Grimme, B. J.; Kreyenschmidt, M.; Uckert, F.; Müllen, K.; Scherf, U. *Adv. Mater.* **1995**, *292*, 292.

(60) Neher, D. *Macromol. Rapid Commun.* **2001**, *22*, 1365.

(61) Xie, L.; Yang, S.; Lin, J.; Yi, M.; Huang, W. *Philos. Trans. R. Soc. London A* **2013**, *371*, 20120337.

(62) Li, Z.; Dong, Y. Q.; Lam, J. W. Y.; Sun, J.; Qin, A.; Häubler, M.; Dong, Y. P.; Sung, H. H. Y.; Williams, I. D.; Kwok, H. S.; Tang, B. Z. *Adv. Funct. Mater*. **2009**, *19*, 905.

(63) Ferman, J.; Kakareka, J. P.; Klooster, W. T.; Mullin, J. L.; Quattrucci, J.; Ricci, J. S.; Tracy, H. J.; Vining, W. J.; Wallace, S. *Inorg. Chem.* **1999**, *38*, 2464.

(64) Geramita, K.; Mcbee, J.; Tilley, T. D. *J. Org. Chem.* **2009**, *74*, 820.

(65) Yin, J.; Zhang, S.-L.; Chen, R.-F.; Ling, Q.-D.; Huang, W. *Phys. Chem. Chem. Phys.* **2010**, *12*, 15448.

(66) Geramita, K.; Tao, Y.; Segalman, R. A.; Tilley, T. D. *J. Org. Chem*. **2010**, *75*, 1871.

(67) Zheng, C.; Tao, Y.; Cao, J.-Z.; Chen, R.-F.; Zhao, P.; Wu, X.-J.; Huang, W. *J. Mol. Model.* **2012**, *18*, 4929.

(68) Pujari, B. S.; Gusarov, S.; Brett, M.; Kovalenko, A. *Electr. Chem. Soc. Trans.* **2011**, *41*, 129.

(69) Duan, C.; Cai, W.; Huang, F.; Zhang, J.; Wang, M.; Yang, T.; Zhong, C.; Gong, X.; Cao, Y. *Macromolecules* **2010**, *43*, 5262.

(70) Gendron, D.; Leclerc, M. *Energy Environ. Sci.* **2011**, *4*, 1225.

(71) Ahmad, A.; Durocher, G. *Photochem. Photobiol.* **1981**, *34*, 573.

(72) Martin, M. M.; Brohoret, E. *J. Phys. Chem.* **1982**, *177*, 107.

(73) Morin, J.-F.; Leclerc, M.; Adès, D.; Siove, A. *Macromol. Rapid Commun.* **2005**, *26*, 761.

(74) Kodali, H. K.; Ganapathysubramanian, B. *Comput. Methods Appl. Mech. Eng.* **2012**, *247-248*, 113.

(75) Shi, Q.; Chen, H. *Sci. China Chem*. **2013**, *56*, 1271.

(76) Xue, F.; Jiang, S. *Polymers* **2014**, *6*, 2116.

(77) Shi, Y.; Liu, J.; Yang, Y. *J. Appl. Phys.* **2000**, *87*, 4254.

(78) Schwartz, B. J. *Annu. Rev. Phys. Chem*. **2003**, *54*, 141.

(79) Liu, J.; Shi, Y.; Yang, Y. *Adv. Funct. Mater.* **2001**, *11*, 420.

(80) Vehoff, T.; Baumeier, B.; Andrienko, D. *J. Chem. Phys.* **2010**, *133*, 134901.

(81) Gupta, D.; Hong, Y. *Org. Electron.* **2010**, *11*, 127.

(82) Malliaras, G.; Friend, R. *Phys. Today* **2005**, *58*, 53.

(83) Balakrishnan, K.; Datar, A.; Naddo, T.; Huang, J.; Oitker, R.; Yen, M.; Zhao, J.; Zang, L. *J. Am. Chem. Soc.* **2006**, *128*, 7390.

(84) Huser, T.; Yan, M.; Rothberg, L. J. *Proc. Natl. Acad. Sci. U. S. A.* **2000**, *97*, 11187.

(85) O'Reilly, J. M. *Crit. Rev. Solid State Mater. Sci.* **1987**, *13*, 259.

(86) Facchetti, A. *Chem. Mater.* **2011**, *23*, 733.

(87) Grimsdale, A. C.; Mullen, K. *Adv. Polym. Sci.* **2008**, *212*, 1.

(88) Nguyen, T.-Q.; Yee, R. Y.; Schwartz, B. J. *J. Photochem. Photobiol. A Chem.* **2001**, *144*, 21.

(89) Kumar, B.; Kaushik, B. K.; Negi, Y. S. *Polym. Rev.* **2014**, *54*, 33.

(90) Huser, T.; Yan, M. *J. Photochem. Photobiol. A Chem.* **2001**, *144*, 43.

(91) Street, R.; Northrup, J.; Salleo, A. *Phys. Rev. B* **2005**, *71*, 165202.

(92) Brédas, J.-L.; Cornil, J.; Beljonne, D.; Dos Santos, D. A.; Shuai, Z.; *Acc. Chem. Res.* **1999**, *32*, 267.

(93) Newman, C. R.; Frisbie, C. D.; Da Silva Filho, D. A.; Brédas, J.-L.;Ewbank, P. C.;Mann, K. R. *Chem. Mater.* **2004**, *16*, 4436.

(94) Zang, L.; Che, Y.; Moore, J. S. *Acc. Chem. Res.* **2008**, *41*, 1596.

(95) Mas-Torrent, M.; Rovira, C. *Chem. Soc. Rev.* **2008**, *37*, 827.

(96) Shirota, Y.; Kageyama, H. *Chem. Rev.* **2007**, *107*, 953.

(97) Jenkins, A. D.; Kratochvil, P.; Stepto, R. F. T.; Suter, U. W. *Pure Appl. Chem.* **1996**, *68*, 2287.

(98) Whitesides, G. M.; Grzybowski, B. *Science* **2002**, *295*, 2418.

(99) Ding, Z.; Xing, R.; Sun, Y.; Zheng, L.; Wang, X.; Ding, J.; Wang, L.; Han, Y. *RSC Adv.* **2013**, *3*, 8037.

(100) Kim, F. S.; Ren, G.; Jenekhe, S. A. *Chem. Mater.* **2011**, *23*, 682.

(101) Korevaar, P. A.; de Greef, T. F. A.; Meijer, E. W. *Chem. Mater.* **2014**, *26*, 576.

(102) Ruiz, L.; Keten, S. *J. Phys. Chem. Lett.* **2014**, *5*, 2021.

(103) Tambara, K.; Olsen, J.-C.; Hansen, D. E.; Pantoş, G. D. *Org. Biomol. Chem.* **2014**, *12*, 607.

(104) Hu, X.-D.; Jenkins, S. E.; Min, B. G.; Polk, M. B.; Kumar, S. *Macromol. Mater. Eng.* **2003**, *288*, 823.

(105) He, C.; Wu, D.; Zhang, F.; Xue, M.; Zhuang, X.; Qiu, F.; Feng, X. *Chem physchem* **2013**, *14*, 2954.

(106) Zhang, K.-D.; Tian, J.; Hanifi, D.; Zhang, Y.; Sue, A. C.-H.; Zhou, T.-Y.; Zhang, L.; Zhao, X.; Liu, Y.; Li, Z.-T. J. *Am. Chem. Soc.* **2013***, 135*, 17913.

(107) Mes, T.; Smulders, M. M. J.; Palmans, A. R. A.; Meijer, E. W. *Macromolecules* **2010**, *43*, 1981.

(108) Chakrabarty, R.; Mukherjee, P. S.; Stang, P. J. *Chem. Rev.* **2011**, *111*, 6810.

(109) Chen, L.-J.; Zhao, G.-Z.; Jiang, B.; Sun, B.; Wang, M.; Xu, L.; He, J.; Abliz, Z.; Tan, H.; Li, X.; Yang, H.-B. *J. Am. Chem. Soc.* **2014**, *136*, 5993.

(110) Wang, Z.; Medforth, C. J.; Shelnutt, J. A. *J. Am. Chem. Soc.* **2004**, *126*, 15954.

(111) Che, Y.; Gross, D. E.; Huang, H.; Yang, D.; Yang, X.; Discekici, E.; Xue, Z.; Zhao, H.; Moore, J. S.; Zang, L. *J. Am. Chem. Soc.* **2012**, *134*, 4978.

(112) Dong, Z.; Luo, Q.; Liu, J. *Chem. Soc. Rev.* **2012**, *41*, 7890.

(113) Li, Y.; Liu, T.; Liu, H.; Tian, M.-Z.; Li, Y. *Acc. Chem. Res.* **2014**, *47*, 1186.

(114) Schenning, A. P. H. J.; Meijer, E. W. *Chem. Commun*. **2005**, *41*, 3245.

(115) Brunner, K.; van Dijken, A.; Börner, H.; Bastiaansen, J. J. A. M.; Kiggen, N. M. M.; Langeveld, B. M. W. *J. Am. Chem. Soc.* **2004**, *126*, 6035.

(116) Beaujuge, P. M.; Fréchet, J. M. J. *J. Am. Chem. Soc.* **2011**, *133*, 20009.

(117) Sun, Y.; Welch, G. C.; Leong, W. L.; Takacs, C. J.; Bazan, G. C.; Heeger, A. J. *Nat. Mater.* **2012**, *11*, 44.

(118) Jonkheijm, P.; van der Schoot, P.; Schenning, A. P. H. J.; Meijer, E. W. *Science* **2006**, *313*, 80.

(119) Stolnik, S.; Illum, L.; Davis, S. S. *Adv. Drug Deliv. Rev.* **2012**, *64*, 290.

(120) Korevaar, P. A.; Schaefer, C.; de Greef, T. F.A.; Meijer, E. W. *J. Am. Chem. Soc.* **2012**, *134*, 13482.

(121) Dong, J.; Yin, C.; Zhang, Y.; Zhang, Q. *J. Polym. Sci. Part B Polym. Phys.* **2014**, *52*, 450.

(122) Zhao, Y. S.; Fu, H.; Peng, A.; Ma, Y.; Xiao, D.; Yao, *J. Adv. Mater.* **2008**, *20*, 2859.

(123) Zhao, T.; Liu, Z.; Song, Y.; Xu, W.; Zhang, D.; Zhu, D. *J. Org. Chem.* **2006**, *71*, 7422.

(124) Höger, S. *Chemistry* **2004**, *10*, 1320.

(125) Finke, A. D.; Gross, D. E.; Han, A.; Moore, J. S. *J. Am. Chem. Soc.* **2011**, *133*, 14063.

(126) Balakrishnan, K.; Datar, A.; Zhang, W.; Yang, X.; Naddo, T.; Huang, J.; Zuo, J.; Yen, M.; Moore, J. S.; Zang, L. *J. Am. Chem. Soc.* **2006**, *128*, 6576.

(127) Aggarwal, a V.; Jester, S.-S.; Taheri, S. M.; Förster, S.; Höger, S. *Chemistry* **2013**, *19*, 4480.

(128) Yang, Y.; Feng, W.; Hu, J.; Zou, S.; Gao, R.; Yamato, K.; Kline, M.; Cai, Z.; Gao, Y.; Wang, Y.; Li, Y.; Yuan, L.; Zeng, X. C.; Gong, B. *J. Am. Chem. Soc.* **2011**, *133*, 18590.

(129) Pan, G.; Cheng, X. J.; Höger, S.; Freyland, W. *J. Am. Chem. Soc.* **2006**, *128*, 4218.

(130) Huang, W.; Zhao, T.-Y.; Wen, M.-W.; Yang, Z.-Y.; Xu, W.; Yi, Y.-P.; Xu, L.-P.; Wang, Z.-X.; Gu, Z.-J. *J. Phys. Chem. C* **2014**, *118*, 6767.

(131) Kong, Q.; Qian, H.; Bo, H.; Zhang, C.; Liu, K.; Zhang, X.; Wang, J.; Li, J.; Gao, G. *Synth. Met.* **2011**, *161*, 2361.

(132) Jung, S.-H.; Pisula, W.; Rouhanipour, A.; Räder, H. J.; Jacob, J.; Müllen, K. *Angew. Chem. Int. Ed.* **2006**, *45*, 4685.

(133) Li, T.; Yue, K.; Yan, Q.; Huang, H.; Wu, H.; Zhu, N.; Zhao, D. *Soft Matter* **2012**, *8*, 2405.

(134) Heimel, G.; Brédas, J.-L. *Nat. Nanotechnol.* **2013**, *8*, 230.

(135) Di Maria, F.; Olivelli, P.; Gazzano, M.; Zanelli, A.; Biasiucci, M.; Gigli, G.; Gentili, D.; D'Angelo, P.; Cavallini, M.; Barbarella, G. *J. Am. Chem. Soc.* **2011**, *133*, 8654.

(136) Zhao, D.; Moore, J. *Chem. Commun.* **2003**, *34*, 807.

(137) Catalan, J. *J. Phys. Chem. A* **2007**, *111*, 8774.

(138) Sinnokrot, M. O.; Valéev, E. F.; Sherrill, C. D. *J. Am. Chem. Soc.* **2002**, *124*, 10887.

(139) Martinez, C. R.; Iverson, B. L. *Chem. Sci.* **2012**, *3*, 2191.

(140) Spano, F. C. *Annu. Rev. Phys. Chem.* **2006**, *57*, 217.

(141) Lim, J. M.; Kim, P.; Yoon, M.-C.; Sung, J.; Dehm, V.; Chen, Z.; Würthner, F.; Kim, D. *Chem. Sci.* **2013**, *4*, 388.

(142) Yamagata, H.; Pochas, C. M.; Spano, F. C. *J. Phys. Chem. B* **2012**, *116*, 14494.

(143) Spano, F. C.; Silva, C. *Annu. Rev. Phys. Chem.* **2014**, *65*, 477.

(144) Yamagata, H.; Spano, F. C. *J. Chem. Phys.* **2012**, *136*, 184901.

(145) Gierschner, J.; Luer, L.; Milian-Medina, B.; Oelkrug, D.; Egelhaaf, H. *J. Phys. Chem. Lett.* **2013**, *4*, 2686.

(146) Hong, Y.; Lam, J. W. Y.; Tang, B. Z. *Chem. Commun.* **2009**, *45*, 4332.

(147) Belletête, M.; Bouchard, J.; Leclerc, M.; Durocher, G. *Macromolecules* **2005**, *38*, 880.

(148) Xu, B.; He, J.; Dong, Y.; Chen, F.; Yu, W.; Tian, W. *Chem. Commun.* **2011**, *47*, 6602.

(149) Eisfeld, A..; Briggs, J. S. *Chem. Phys.* **2006**, *324*, 376.

(150) Li, Z.; Dong, Y. Q.; Lam, J. W. Y.; Sun, J.; Qin, A.; Häubler, M.; Dong, Y. P.; Sung, H. H. Y.; Williams, I. D.; Kwok, H. S.; Tang, B. Z. *Advanced Functional Materials*, **2009**, *19*, 905.

(151) Wu, W.; Ye, S.; Huang, L.; Xiao, L.; Fu, Y.; Huang, Q.; Yu, G.; Liu, Y.; Qin, J.; Li, Q.; Li, Z. *J. Mater. Chem.* **2012**, *22*, 6374.

(152) Busseron, E.; Ruff, Y.; Moulin, E.; Giuseppone, N. *Nanoscale* **2013**, *5*, 7098.

(153) Huang, C.; Wen, L.; Liu, H.; Li, Y.; Liu, X.; Yuan, M.; Zhai, J.; Jiang, L.; Zhu, D. *Adv. Mater.* **2009**, *21*, 1721.

(154) Guo, S.; Wang, E. *Acc. Chem. Res.* **2011**, *44*, 491.

(155) Deng, R.; Liang, F.; Li, W.; Yang, Z.; Zhu, J. *Macromolecules* **2013**, *46*, 7012.

(156) Tao, J.; Yang, M.; Gao, H.; Yu, J.; Wang, G. *Colloids Surf. A* **2014**, *451*, 117.

(157) Sacanna, S.; Pine, D. J.; Yi, G.-R. *Soft Matter* **2013**, *9*, 8096.

(158) Kosa, T.; Sukhomlinova, L.; Su, L.; Taheri, B.; White, T. J.; Bunning, T. J. *Nature* **2012**, *485*, 347.

(159) Ke, D.; Zhan, C.; Xu, S.; Ding, X.; Peng, A.; Sun, J.; He, S.; Li, A. D. Q.; Yao, J. *J. Am. Chem. Soc.* **2011**, *133*, 11022.

(160) Wang, Y.; Wang, Y.; Zheng, X.; Yi, G.-R.; Sacanna, S.; Pine, D. J.; Weck, M. *J. Am. Chem. Soc.* **2014**, *136*, 6866.

Chapter 2:

Formation of carbazole macrocycles in polymerizations over $Ni(COD)_2$- optimization, purification and self-assembly [*]

2.1 Introduction

[*] Fluorescence lifetime measurements were performed by Glenda Del Los Reyes under the supervision of Prof. Frank Hegmann, Department of Physics, at the University of Alberta.
Part of the syntheses in section 2.2 were assisted by Larissa Smith.
TEM was performed by Morteza Javadi and Dr. Tapas Purkait.

Recent research aimed at preparing and tailoring carbon-based nanomaterials has been gaining momentum partly because of their chemical resilience and ease of functionalization.[1-2] As a result, the number of potential applications is growing and now encompasses optoelectronics,[3-5] gas adsorption,[6] biological imaging,[7] drug delivery, [6, 8] and sensing.[9] Generally, carbon-based nanomaterials may be divided into two broad classes, the first being solid-state nanocarbons, or "hard" carbons, such as amorphous,[10] graphitic,[11] and turbostratic carbon;[1] these materials are often prepared using top-down approaches.[12] A second carbon nanomaterial family, the "soft" carbons, are nanostructures produced from the self-assembly of molecular, oligomeric, and polymeric building blocks. This bottom-up approach exploits weak interactions such as H-bonding, van der Waals forces, and π-π interactions to yield 2D sheets, fibers and spheres.[3] Many examples of materials from both families exhibit photoluminescence (PL); generally, "hard" carbon dots exhibit low quantum yield (QY) emission[13] that is characteristic of these particles and is often insensitive to external factors (*e.g.*, solvent environment, aggregation, etc.).[1] In contrast, "soft" carbon nanomaterials produced from the assembly of π-conjugated small molecules frequently show aggregate-dependent PL response that can be influenced by the orientation of the building blocks.[14-18]

Materials derived from carbazole-based small molecules, oligomers, and polymers have been extensively studied because of their useful optical and electronic properties. They have found widespread application in photovoltaics,[20] organic light-emitting diodes,[20] and field-effect transistors.[21, 22]

Recently, a family of carbazole-ethynylene macrocycles was prepared and used as building blocks in self-assembled "soft" 1D and 2D nanomaterials.[23, 24] This family of compounds possesses a near-planar π-conjugated backbone that assists 1D assembly through π-stacking.[26] In addition, pendant aliphatic chains aid in inducing solubility and can interact leading to lateral molecular assembly.[25] The π-interactions between carbazole sub-units in similar carbazole-based molecular systems, allows the assemblies to display unique optical properties including, aggregation-induced emission,[27-29] and have expanded the range of applications accessible to carbazole-based structures to include heavy metal sensing,[30] and explosive vapour detection.[26, 31] As a result of their high porosity and affinity for CO_2, crosslinked, high molecular weight polycarbazoles have found use in gas adsorption;[31, 32] to our knowledge, high surface area nanomaterials derived from shape persistent carbazole macrocycles have yet to be investigated for these applications.

Nitrogen-doped "hard" carbon nanomaterials have been reported to be effective adsorbents in low-pressure post-combustion CO_2 sequestration.[34] In particular, bulk N-doped carbons prepared from the pyrolysis of nitrogen-containing polymers adsorb notably higher quantities of CO_2 relative to N-free materials – this behaviour is enhanced at elevated temperatures.[35, 36] Similarly, N-doped carbon prepared from glucose pyrolysis using carbazole as a N source provides superior CO_2 adsorption capacity when compared equivalent materials prepared using to other N sources.[37] It has been proposed that this important

material property arises because of the high nitrogen content, and the electron rich nature of the nitrogen center.

In this context, the question arises whether self-assembled nanostructures derived from carbazole-based macrocycles will provide effective precursors to porous N-doped carbon nanomaterials suitable for gas adsorption applications. In this report, we describe the preparation of an alkyl-free, all carbazole macrocyclic tetramer that exhibits quasi-planar geometry. This new molecule self-assembles to controllably form nanospheres and gels that exhibit aggregation-induced emission enhancement (AIEE). Subsequent carbonization of these nanostructures preserves particle morphology and yields N-doped carbon structures that were comprehensively characterized and evaluated for CO_2 adsorption.

2.2. Experimental

2.2.1. Materials and Instrumentation

3,6-Dibromocarbazole, 2,2'-bipyridyl, 1,5-cyclooctadiene, sodium hydroxide and dimethylglyoxime were purchased from Sigma Aldrich, bis(1,5-cyclooctadiene)nickel(0) was purchased from Strem Chemicals, and all were used as received.

NMR spectroscopy was performed in toluene-d8 using an Agilent/Varian Dual Cold Probe 500 MHz spectrometer. Low and high resolution mass spectra were acquired using an AB Sciex Voyager Elite MALDI-TOF spectrometer and Bruker 9.4T Apex-Qe MALDI-FTICR instrument, respectively using trans-2-[3-

(4-tert-butylphenyl)-2-methyl-2-propenylidene]malononitrile (DCTB) matrix. All toluene used in the synthesis and sample preparation was distilled over Na/benzophenone immediately prior to use. All binary solvent mixtures were prepared using triple distilled water and HPLC grade acetone.

Samples for scanning electron microscopy (SEM) were prepared by spin-coating cooled solutions onto silicon wafers and sputtered with chromium prior to imaging. SEM imaging was performed using a JEOL 6301F Field Emission Scanning Electron Microscope with a 5 KV beam. Samples for transmission electron microscopy (TEM) were prepared by dropcoating the colloidal suspensions onto carbon TEM grids and dried under vacuum for 1 week prior to imaging. TEM was performed using a JEOL 2010 TEM (LaB_6 electron gun) using an accelerating voltage of 200 kV.

X-ray diffraction (XRD) was accomplished by placing a small volume of powder onto Si wafer mounted onto an XRD sample holder and run using an Inel MPD Multi-Purpose Diffractometer System equipped with a CPS 120 curved position sensitive X-ray detector and copper Kα radiation source.

X-ray photoelectron spectroscopy (XPS) was performed on a Kratos Axis 165 X-ray Photoelectron Spectrometer on the solid powdered products. Spectra were fitted using CASA XPS software with Shirley type background subtraction, and calibrated to the C1s peak to a value of 284.8.[37]

Dynamic light scattering (DLS) experiments were completed using a Malvern Instruments Zetasizer Nano ZS in quartz cuvettes without dilution of the original particle suspensions.

Photoluminescence (PL) and excitation (PLE) spectra were recorded in a quartz cuvette using a Cary Eclipse fluorometer at a scan rate of 2 nm per second.

Differential scanning calorimetry (DSC) and thermogravimetric analyses (TGA) were achieved using a Perkin Elmer Pyris 1 DSC at a heating rate of 10 °C/min and Perkin Elmer Pyris 1 TGA at a heating rate of 25 °C/min respectively all under a nitrogen atmosphere.

2.2.2. Preparation of Cyclotetra(carbazol-3,6-diyl) (1)

3,6-Dibromocarbazole (3.16 g, 9.72 mmol) was loaded into an argon charged Schlenk flask equipped with a reflux condenser and dissolved in 100 ml of anhydrous DMF. A second Schlenk flask was charged with bis(1,5-cyclooctadiene) nickel(0) ($Ni(COD)_2$, 7.70 g, 28.0 mmol), 2,2'- bipyridine (5.10 g, 32.4 mmol), and 1,5-cyclooctadiene (COD, 4.2 ml , 44.0 mmol) and 100 ml toluene under an argon atmosphere in a glove box. The purple solution was heated to 80 °C for 30 minutes, after which it was transferred via cannula to the flask containing the 3,6-dibromocarbazole/DMF solution. The purple mixture was heated at 70 °C for 4 days, and quenched by pouring into 1 L of methanol. The resulting brown/black precipitate was collected in the thimble of a soxhlet extractor and washed with methanol for 24 hours followed by extraction with acetone for 2 days. The green solid residue was dried, and suspended in 400 ml

of ethanol containing 0.86 g of sodium dimethyl glyoximate (NaDMG) and stirred at room temperature for 4 hours. 500 ml of dH_2O was then added and the brown suspension was isolated by vacuum filtration and washed with 500 mL of toluene. The product was isolated from the red $Ni(DMG)_2$ complex by extraction into THF and gravity filtration, and evaporation to yield 1.07 g of brown solid (67 %). HRMS (m/z); $[M]^+$ calculated for $C_{48}H_{28}N_4$, 660.23139; found, 660.23084, Mean error (ppm); 0.61. ^{1}H NMR (Toluene-d8, 27 °C, 500 MHz); δ (ppm): 8.63 (d, 8H, 7.5 Hz, Ar-H 2,7), 8.51 (s, 8 H, Ar-H 4,5), 7.27 (m, 8 H, Ar-H 1,8), 6.75 (s, 4 H, N-H). ^{13}C NMR (Toluene-d8, 27 °C, 125 MHz); δ (ppm): 149 (C1', C8'), 137 (C1, C8), 136 (C3, C6), 123 (C4', C5'), 123 (C4, C5), 121 (C2, C7).

Particle suspensions were prepared by stirring solid **1** in refluxing acetone and water solvent mixtures (X_{aq} = mole fraction of water) for 5 minutes with stirring to yield a 3 mM solution. All hot solutions were clear and yellow, with the exception of X_{aq} =0.8 which appeared cloudy, and all cooled to form slightly opalescent yellow liquids. The organogel was prepared dissolving 1.0 g of **1** in 10 ml of THF, and sonicated until it was transparent at which time the volume was reduced to 3 ml by evaporation of the solvent and a brief period of agitation yielded a brown gel that remained suspended from the bottom of the flask following its inversion.[38]

2.2.3. Carbonization and CO_2 Adsorption

3 mM colloidal suspensions of **1** were dropcast onto silicon wafer and removed with a spatula following drying. The gel sample prepared in THF was dried in a

vacuum oven at 100 ºC for 1 hour and placed in an alumina boat. 50 mg of each sample was heated in a quartz boat in a tube furnace under either an argon atmosphere, or a 5% H_2 in argon atmosphere by heating from room temperature to 550 ºC over 15 minutes, then held at 550 ºC for 30 minutes, and cooled to room temperature over a period of several hours to give black solids in yields ranging from 17 % to 31 %. The solid carbons were then characterized using IR spectroscopy and XPS.

The CO_2 adsorption experiments on the pyrolysed products were completed in a Perkin Elmer Pyris 1 TGA under continuous gas flow at ambient pressure. The powdered samples were dried in an oven at 140 ºC prior to analysis. The samples were first heated to 120 ºC under flow of nitrogen up to 15 minutes to remove any adsorbed water, or atmospheric gases, then cooled to 25 ºC. The samples were then exposed to a flow of dry CO_2 for 60 minutes and the % change in mass recorded, followed by returning the samples to a nitrogen atmosphere and further heating to liberate the adsorbed CO_2.

2.2.4. Computational Modelling

Quantum calculations were performed using the Gaussian 09 program assuming the ground state geometry in the gas phase.[39] Geometry optimization was performed at the B3LYP/CEP-31G level of theory and the optimized geometry was confirmed to be an energetic minimum by calculating the Hessian matrix and noticing an absence of imaginary frequencies.[40-45]

2.2.5 Photoluminescence Quantum Yield Determination

Quantum yields were determined using the relative quantum yield method of Williams *et al.* by plotting the integrated fluorescence intensity versus the absorbance of the samples over a range of A=0.0 through A=0.1.[44] Anthracene was chosen as an external standard because of the similarities in the range of emission wavelengths and also because at absorbs well at 356 nm, which is well under the absorption cut-off for acetone. The anthracene standards were prepared using ethanol as a solvent, and as such, the QY calculations required inclusion of refractive indices as in equation 1:

$$\Phi_x = \Phi_{st}\left(\frac{m_x}{m_{st}}\right)\left(\frac{n_x^2}{n_{st}^2}\right) \quad (1)$$

Where the subscript x refers to the sample and the subscript st refers to the standard, Φ is the quantum yield, m is the slope of the line, and n is the refractive index of the solvent or solvent mixture. For further information please see Appendix 1.

2.3. Results and Discussion

2.3.1. Synthesis and characterization of 1

A modified literature procedure derived from that used to prepare alkyl-substituted carbazole tetramers by Ostrauskaite *et al*. was employed to prepare **1** (See: Figure 2-1).[45] Briefly, 3,6-dibromocarbazole was coupled using Ni(Bpy)(COD) generated *in situ* to yield a crude product as an insoluble green solid. The target compound, **1**, was isolated and purified by soxhlet extraction of

the crude product with methanol and acetone. The NMR spectrum of the acetone extract in toluene-d8 prior to demetallation shows only a single absorption at 6.96 ppm, appearing as a singlet, following treatment of the acetone extract with a 3% solution of sodium dimethylglyoximate in ethanol resulted in the formation of a red precipitate of nickel dimethyl glyoximate (*i.e.*, $Ni(DMG)_2$) and the appearance of peaks at 8.63, 8.51 and 7.25 ppm. The NMR spectrum suggests that the proton appearing at 6.75 ppm corresponds to the N-H proton, and the absence of the protons associated with the polyparaphenyl backbone are the result of η- 6 type coordination of the aryl groups in the carbazole structure to the paramagnetic Ni(II) ions produced during polymerization (Figure 2-2 b). Following the removal of the nickel impurities the desired product was obtained as a glassy yellow solid in 67% yield.

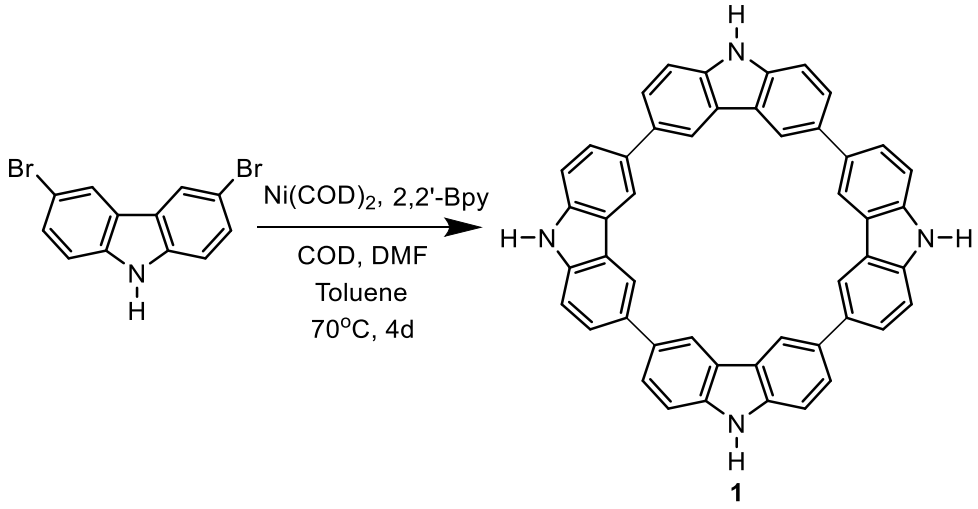

Figure 2-1. Synthesis of **1**

Purified **1** was evaluated using MALDI-TOF and showed a single high-intensity peak consistent with 4 linked monomers (Figure 2-2). Further analysis using high-resolution MALDI-FTICR (Figure 2-2 b) showed the fragment of

highest intensity occurred at m/z = 660.23084 with an isotopic distribution pattern corresponding to that predicted for the cyclic structure shown in Figure 2-1.

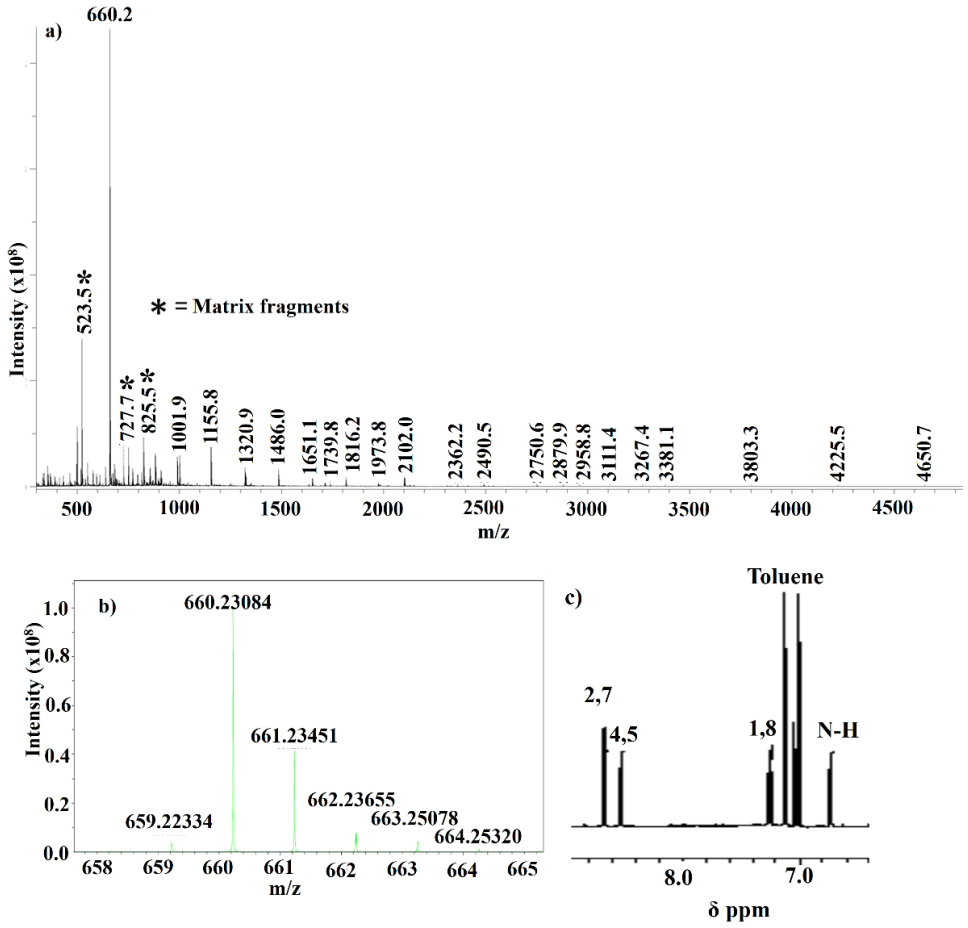

Figure 2-2. (a)Low resolution MALDI-TOF spectrum and (b) high resolution MALDI-FTICR trace of **1** showing the mass-to-charge ratio and isotopic distribution of the parent ion, and the aromatic region of the ^{1}H-NMR spectrum recorded in toluene-d_8 (c) including the proton NMR assignment.

Of important note, no evidence of linear tetramer was detected, by an absence of peaks centred at m/z= 662.2 (Figure 2-2 a). Consistent with the

present MS results, and the proposal of a cyclic structure the ^{1}H-NMR spectrum showed resonances readily assigned to protons in the 4 and 5 positions of the carbazole structural units that are shifted downfield to 8.51 ppm (Figure 2-2 c). Further discounting the presence of linear tetramer, no evidence of resonances at 8.04 ppm were detected at the sensitivity of ^{1}H-NMR technique.[46]

2.3.2. Switching from fiber to colloid- solubility considerations

Compound **1** exhibits limited solubility in most common solvents (*e.g.*, toluene) and is only slightly soluble in tetrahydrofuran (THF). At comparatively high concentrations (*i.e.*, 0.1 M), THF solutions of **1** form gels. SEM imaging of the resulting gels suggests there is some limited underlying fibrous structure within an apparent disordered matrix (Figure 2-3 a). The structure of the gels was further investigated using powder XRD which showed a single broad reflection spanning $10 < 2\theta < 35$ (Figure 2-3 b) consistent with a turbostratic carbon-like arrangement of molecules.[2, 47] The absence of extensive fiber structure is reasonably attributed to the absence of N-alkyl groups to help drive the face-on-face stacking of the macrocycles required to form 1D structures.[14]

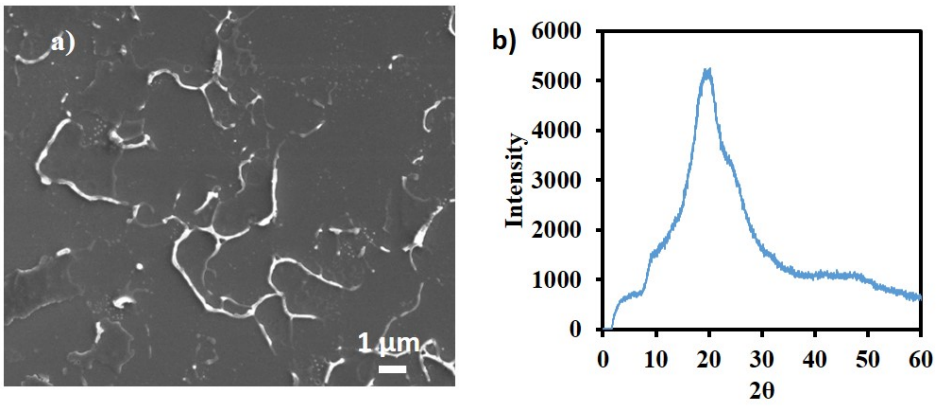

Figure 2-3. a) SEM image of the organogel prepared by dissolving **1** in THF **(1G)** and deposited by drop-casting onto Si wafer and b) the XRD trace of dried **1G**.

2.3.3. Formation of nanospheres in binary acetone/water solvent mixtures

Despite being poorly soluble in many neat solvents, binary solvent mixtures consisting of a polar aprotic organic solvent (e.g., toluene, THF, acetone) and hydrogen-bonding anti-solvent (e.g., methanol, water, ethanol) provide a medium in which stable colloids of **1** form following short periods of reflux. In this context, we investigated the solution dynamics of **1** in an acetone:water mixture where the mole fraction of water is X_{aq}. Slightly opalescent yellow colloidal suspensions were prepared by refluxing a 3 mM suspension of **1** in an acetone/water solution of given X_{aq} for 5 minutes followed by cooling to room temperature. Dynamic light scattering (DLS) revealed that the volume average hydrodynamic diameter of the particles produced depended upon the mole fraction of water in the solvent mixture (*i.e.,* X_{aq}). Particle dimensions increased from 72 ± 13 nm for X_{aq} = 0.0 to a maximum of 225 ± 37

nm where X_{aq} = 0.3 through the "low water regime". Upon entering the "high water regime", the hydrodynamic diameter decreased sharply to 60 ± 7 nm at X_{aq} = 0.5, and subsequently increased gradually to 81 ± 13 nm for X_{aq} = 0.6 through to 136 ± 22 nm at X_{aq} = 0.7 (Figure 2-4).

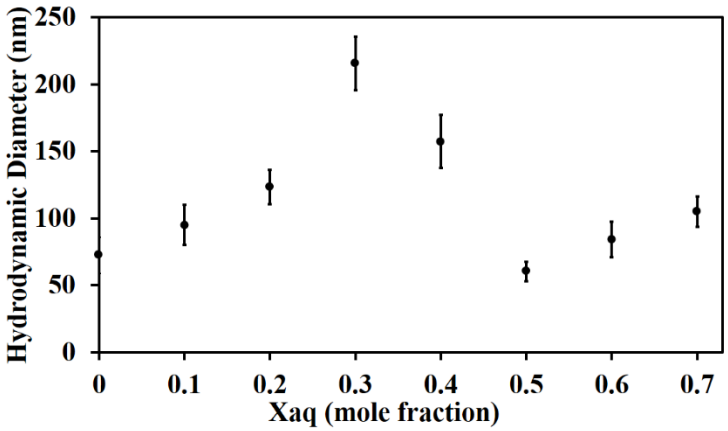

Figure 2-4. Volume average hydrodynamic diameter and corresponding standard deviations for the colloidal suspensions of **1** in solvent mixtures from X_{aq} = 0.0 through X_{aq} = 0.7 measured by DLS.

To further investigate the assembly of **1** in the solid state, suspensions were spin cast onto silicon wafers and secondary electron images were obtained using SEM (Figure 2-5 a-d). The images reveal that the samples are composed of particle morphologies and sizes that depend upon the solvent composition (*i.e.*, X_{aq}). When neat acetone was employed, spherical particles (d_{avg} = 224 ± 66 nm) with featureless surfaces formed (Figure 2-5 a). In addition, an underlying film was evident that presumably results from deposition of dissolved **1**.

The average dimension of the freestanding particles was clearly influenced by X_{aq}. Consistent with "low" and "high" water content regimes

observed in DLS measurements, SEM analysis shows a similar trend in particle size evolution with X_{aq} (see Figures 2-3 and 2-5 b). Furthermore, the SEM analysis also suggests these two categories of particles possess different surface morphologies; particles prepared between X_{aq} = 0.1 (d_{sphere} ~ 228 ± 61 nm) through X_{aq} = 0.3 (d_{sphere} = 290 ± 53 nm) were larger with porous surfaces (d_{holes} ~ 33 ± 12 nm), whereas particles prepared from X_{aq} = 0.5 (d_{sphere} = 151 ± 24 nm) through X_{aq} = 0.7 (d_{sphere} =182 ± 70 nm) were smaller, more monodisperse, and showed smooth surfaces (Figure 2-5 c-d, and Figure 2-6). TEM confirms that the particles obtained from all X_{aq} are solid, but appear slightly smaller than those observed in the SEM images (Figure 2-5 a-d). This observation appears to result from the flattening of the particles on the SEM substrate surface leading to an overestimation of the particle radii.

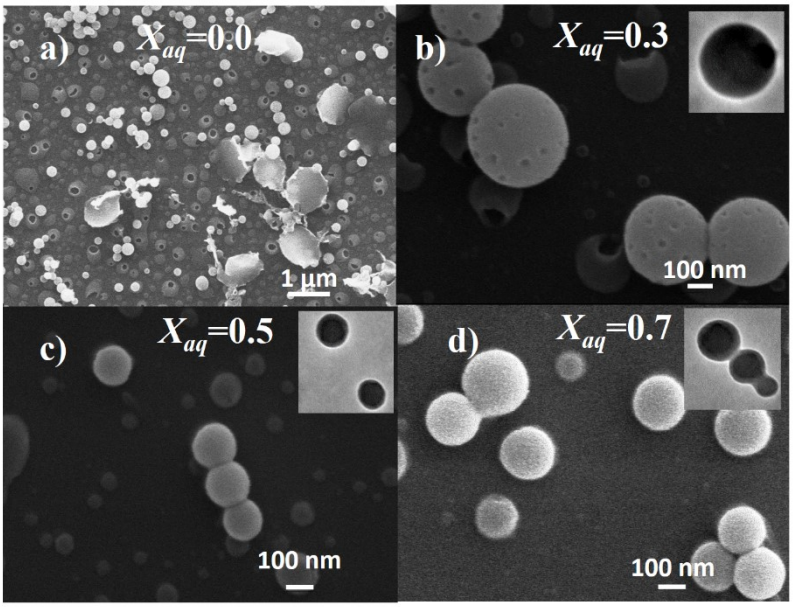

Figure 2-5. SEM images of colloidal suspensions of **1** prepared in acetone:water mixtures where a) X_{aq} = 0.0, b) X_{aq} = 0.3, c) X_{aq} = 0.5, and d) X_{aq} = 0.7.

To gain insight into the structure of the present nanoparticles, XRD was performed to probe the molecular ordering of **1** in the spheres as a function of X_{aq} (Figure 2-6). The XRD traces obtained of the dried colloids prepared at all X_{aq} are dominated by broad, featureless diffraction bands which cover a range of 2θ from 5 to 30 with a maximum intensity at ~20 which suggests that the morphology of **1** is primarily amorphous. The amorphous nature of the particles is most pronounced when prepared in acetone alone, where no well resolved diffraction peaks are observed, which suggests that no significant long range order is present in these particles. Increasing X_{aq} to 0.3 affords a single diffraction peak at 2θ = 32° consistent with a more ordered molecular assembly. Further increase of X_{aq} (*i.e.,* X_{aq}= 0.5 through X_{aq}= 0.7) results in an increase in the intensity of diffraction peaks suggesting a higher degree of ordering within the supramolecular structure. In the most extreme case, X_{aq}= 0.7, sharp diffraction peaks appear which correspond to d spacings varying from 6.6 Å through 2.5 Å which is consistent with the interplanar spacings observed in π-stacked molecules.[48] Another important observation for particles prepared within this "high water content" regime is the appearance of additional diffraction peaks that occur at successively smaller 2θ consistent with increasing separation between layers of molecules of **1**.

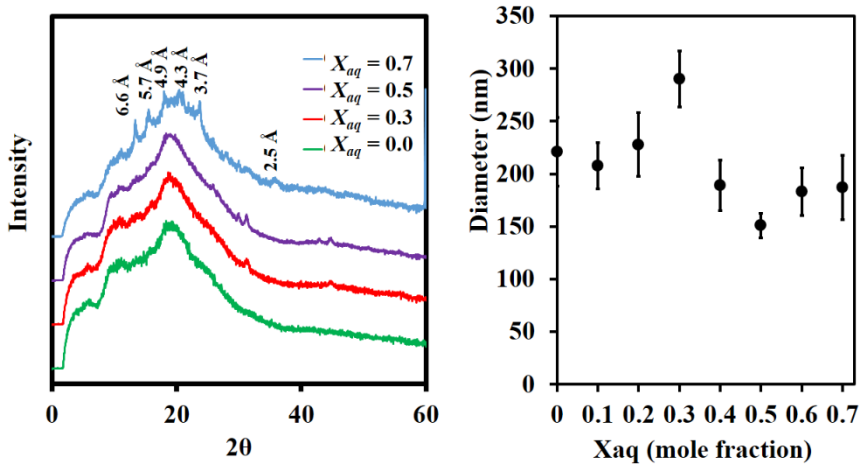

Figure 2-6 (left) Powder XRD traces of dried nanoparticles prepared using indicated water/acetone solvent mixtures and (right) size analysis as determined from SEM images.

2.3.4. Optical properties of the nanosphere suspensions

The optical properties of carbazole-based molecules and polymers are influenced by the interaction of adjacent carbazole structural units. Often such assemblies lead to the formation of exciplexes that render these materials poor solid state emitters; this process is known as aggregate induced quenching (AIQ).[49] Surprisingly, the solids spin and drop cast from the present particle suspensions of **1** show intense blue PL as well as intense luminescence observed in the colloidal suspensions (Figure 2-7).The PLE and PL spectra in π-conjugated materials, like the tetramer investigated here, are influenced by changes in electron delocalization arising from assembly induced geometric changes and/or the influences of molecular aggregation.[50] In particular, the Stokes shift (*i.e.*, the difference between the maximum PLE and PL

wavelengths) probes the vibrational freedom of molecules of **1** within a given assembly. A large Stokes shift occurs when molecules are undergoing significant geometric changes following photoexcitation (see Chapter 1 for a more in depth discussion).[51] For largely planar, macrocyclic compounds such as **1**, this increase in Stokes shift at high X_{aq} suggests that in the more aqueous environmnets, **1** experiences greater flexibility and enhanced molecular planarity.[51, 52]

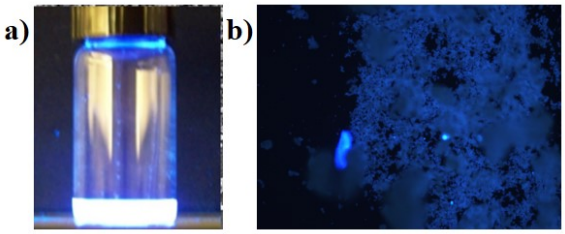

Figure 2-7. a) A photograph of a colloidal suspension of **1** prepared with X_{aq} = 0.7 under exposure to 365 nm light, and b) low magnification fluorescence microscopy images of drop-cast colloid, again where X_{aq} = 0.7, highlighting emission from clusters of nanospheres near the drop's edge.

Normalized PL and PLE spectra of the suspensions of **1** in water and acetone mixtures of X_{aq} = 0.0 through to X_{aq} = 0.8 are shown in Figure 2-8. Clearly, changing X_{aq} has little influence on the PL maximum, suggesting there are negligible changes in the nature of the vibrationally relaxed electronic excited state, or the radiative relaxation processes. The PLE spectra and Stokes shifts are independent of X_{aq} for particles prepared in the low water regime (*i.e.,* X_{aq} = 0.0 through 0.3); in all cases the PLE maximum occurs at *ca.* 370 nm, and the Stokes shift is *ca.* 40-50 nm. The consistent Stokes shift and similar broad, featureless PL and PLE spectra suggest the geometry of **1** in the spheres

prepared over this X_{aq} range remains consistent throughout these structures. For X_{aq} between 0.4 and 0.8, a slight red-shift (*i.e.,* 11 nm) in the PLE maximum occurs between X_{aq} = 0.3 and 0.4 (Figure 2-8) followed by a successive blue-shift with increasing X_{aq}, indicative of introduction of H-aggregates (*i.e.*, aggregates resulting from slipped-stack π-π stacking arrangement of molecules, as discussed in Chapter 1).[53] This shift in PLE maximum is accompanied by an increased Stokes shift suggesting higher X_{aq} favours ordering of the molecules of **1** into in a more planar geometry,[51] and is consistent with XRD analyses noted above.

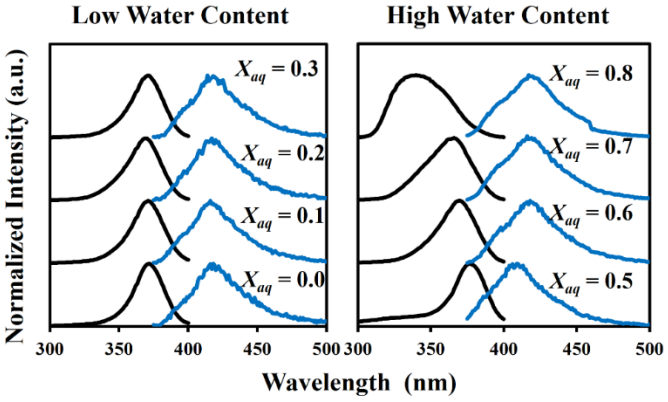

Figure 2-8 PLE spectra (black lines) of 3 mM suspensions of **1** formed in binary acetone/water mixtures of indicated mole fraction of water, X_{aq}, monitoring the intensity of emission at the emission maximum (*ca.* 420 nm). The PL spectra (blue lines) for the same suspensions were recorded using an excitation wavelength of 320 nm.

To investigate if the molecular ordering of **1** within the present nanospheres could be probed optically the PL intensities upon excitation at 320 nm were evaluated for particles prepared at different X_{aq} (Figure 2-9).

In the "low water" content regime (*i.e.*, X_{aq} = 0.0 to 0.3) comparatively small changes in the PL intensity at 420 nm were noted. These spectra are similar to those of the solvated macrocycle and are consistent with XRD and Stokes shift analyses that indicate molecules of **1** form an amorphous assembly. Samples prepared in the "high water" content regime show a 10-fold increase in PL intensity as X_{aq} is increased from 0.5 through 0.8. This observation is reasonably ascribed to AEE that would result from the ordering of **1** noted in the XRD and Stokes shift data obtained for these particles. This AIEE also serves as additional evidence that π-stacked H-aggregates are being formed, as this type of interaction between neighbouring molecules would limit the rotational freedom between neighbouring carbazole units in individual molecules of the tetramer **1** which may contribute to the emission enhancement observed at high X_{aq}.[54] From these results we conclude that at high X_{aq} AIEE is promoted by an increase in the structural rigidity of **1**, and the greater intermolecular spacing observed when X_{aq} is increased, which minimizes non-radiative losses through AIQ processes.[55]

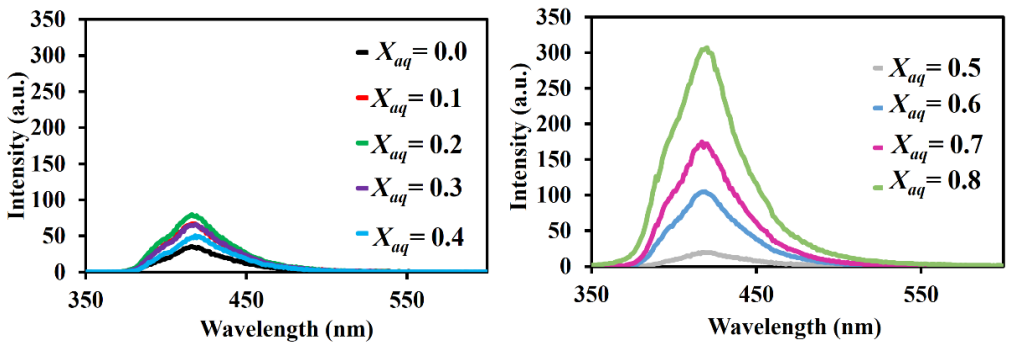

Figure 2-9. The PL spectra obtained for suspensions for X_{aq} = 0.0 to 0.4 (*i.e.*, "low water content" regime, left) and X_{aq} = 0.5 to 0.8 (*i.e.*, "high water" content regime, right).

The fluorescence lifetimes of the suspensions were recorded to determine if there is a change in the overall radiative processes as the solvent composition, and therefore the morphology of **1** within the samples, is changed. The decay transients were fit with a second order curve for all samples, suggesting two components to the radiative processes overall including a fast component, τ1, and a slow component described by τ2 (Figure 2-10 a). Inspection of both τ1 and τ2 as a function of X_{aq} suggests that there is a trend toward increasing lifetimes for both components as X_{aq} is increased from 0.3 to 0.7, but is accompanied by an anomalously long lifetime in the absence of water (Figure 2-10 b). The lifetimes as a function of wavelength were also determined for both emission components to help ascertain if the molecules obey Kasha's rule (*i.e.*, the fluorescence properties are independent from excitation wavelength),[56] or if **1** displays charge transfer character in either the high or low water content regimes (Figure 2-10 c-d).[57] No trend is observed in the lifetimes as the wavelength at

which the fluorescence lifetime is collected is increased for samples where X_{aq} =0.0 through 0.3, nor for the fully solvated molecule in dilute THF.

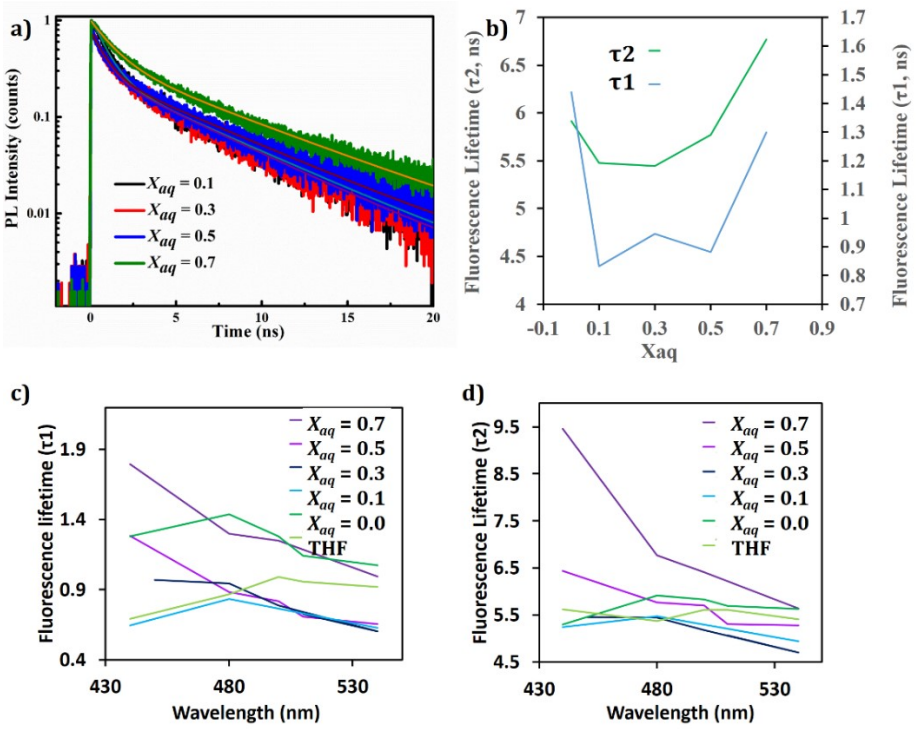

Figure 2-10. a) Fluorescence decay transients recorded from the nanoparticle suspensions with a collection wavelength of 480 nm following irradiation with a 440 nm laser. b) The relaxation time for the slow (green trace) and fast (blue trace) components of the relaxation of the colloidal suspensions, and the wavelength dependence of the fluorescence lifetime of c) the fast component and d) the slow component of the emission processes.

There is, however a trend to increasing lifetimes in both components as the wavelength at which the decay is monitored is decreased at higher X_{aq}. Figure 2-10 c and d show the evolution of τ1 and τ2 of **1** in different X_{aq} as the emission wavelength is varied from 440 nm to 540 nm. The overall change in τ1

and τ2 was observed in both X_{aq} = 0. 5, and X_{aq} = 0. 7 where τ1 changes from 0.654 ns to 1.283 ns and τ2 increases from 5.281 ns to 6.444 ns, and 0.7 where τ1 changes from 0.994 ns to 1.794 ns and τ2 increases from 5.645 ns to 9.462 ns respectively. This trend towards longer lifetimes shows that the introduction of a charge transfer state at large X_{aq} is likely, and may result from either hydrogen bonding to the solvent,[58] or the formation of intramolecular aggregates of **1** in these systems.[59] Since hydrogen bonding in carbazole containing molecules is always accompanied by a decrease in fluorescence intensity, and as previously discussed higher X_{aq} in suspensions of **1** yield more intense photoluminescence, the longer lifetimes observed here can be assigned to aggregates as opposed to changes in hydrogen bonding environment.[60]

2.3.5. Concentration dependence of optical properties- investigation into AIEE

In an effort to more effectively quantify the increase in absolute photoluminescence intensity as a function of growing X_{aq}, the PL quantum yields, Φ_{fl}, were calculated from the integrated fluorescence intensity and the absorption at 356 nm using anthracene as an external standard (Table 2-1). The trend observed in the quantum yields does not follow the same trend as the apparent trend observed in the emission spectra of the colloids prepared at a concentration 3.0 mM (see Figure 2-8). There is no clear difference between Φ_{fl} in spheres prepared in the high water content regime, or low water content regime (*i.e.*, X_{aq}= 0.7 through 0.5, and X_{aq}= 0.3 through 0.0), as was observed as would be predicted based on the AIEE suggested by the absolute PL intensities.

The only exception to the general similarities in Φ_{fl} observed for **1** in all X_{aq}, is the anomalously high Φ_{fl} for X_{aq} =0.6 where Φ_{fl} = 29.7% which is nearly a 3 fold increase from that observed where Φ_{fl} = 7.1- 12.1 observed in the samples with lower X_{aq}. We believe the difference between the observed change in intensity and the measured quantum yield is a result of the vastly different concentrations of **1** used to measure the quantum yields, and to prepare the suspensions. For example, the tetramer colloids samples were prepared at a concentration of 3 mM in **1** that yielded an absorption spectrum that was too intense to remain on scale. To record Φ_{fl} using the relative method of Williams *et al*. the maximum absorbance at the wavelength of excitation needs to be less than A = 0.1.[44] According to Beer's law this requires, at minimum, that the sphere samples be diluted by 2 orders of magnitude to record Φ_{fl}.

To confirm the proposed impact of changing the concentration on the optical properties of **1** in the low X_{aq} and high X_{aq} regimes, a range of colloid samples were prepared at various concentrations, and the excitation and emission monitored as a function of X_{aq} (Figure 2-11). At higher concentrations, with more aggregates of **1**, the same trend in PL maxima and intensities are observed as in the original concentrations, with no changes in fluorescence intensity throughout the low water content regime. However by decreasing the concentration by an order of magnitude, the trends in X_{aq} in either the low or high water content regimes is lost, and an anomalously high fluorescence intensity now observed in X_{aq} =0.6 similar to what was observed in the fluorescence quantum yields. We propose that with dilution, aggregates begin to

break apart, and greater solvation of **1** under intermediate X_{aq} (*i.e.*, X_{aq} =0.6) leads to higher quantum yields.

X_{aq}	Φ_{fl}	$\lambda_{em6.0}$	$\lambda_{em3.0}$	$\lambda_{ex3.0}$	$\lambda_{em0.3}$	$\lambda_{abs0.03}$
0.0	7.1	420	418	372	416	330
0.1	12.1	420	416	371	415	326
0.2	11	417	417	370	416	324
0.3	11.3	418	414	370	417	324
0.4	10.6	407	410	381	418	322
0.5	9.1	412	409	377	417	320
0.6	29.7	420	418	370	417	322
0.7	14.5	418	416	366	419	320

Table 2-1. A summary of the optical properties of the water:acetone suspensions of **1** at various concentrations. The emission maxima recorded at a concentration of 6.0 mM, 3.0 mM and 0.3 mM are denoted by $\lambda_{em6.0}$, $\lambda_{em3.0}$, and $\lambda_{em0.3}$ respectively. The excitation spectra recorded at a concentration of 3.0 mM appears under the heading of $\lambda_{ex3.0}$, and the absorption maxima recorded at very dilute concentrations (*i.e.*, 3.0 x 10^{-5} M) fall under $\lambda_{abs0.03}$. Wavelength values are all reported in nm.

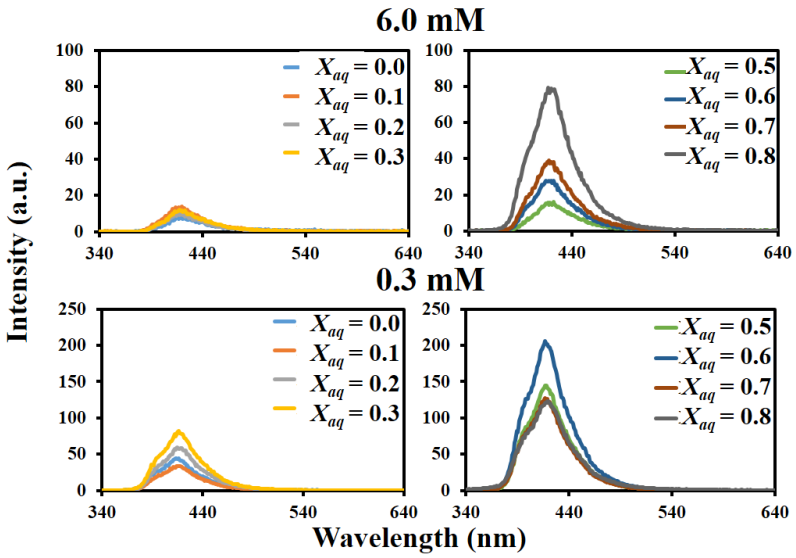

Figure 2-11. PL spectra recorded from the colloidal suspensions of **1** where X_{aq} is varied from 0.0 through 0.8 at higher (top) and lower (bottom) concentrations in the low water content (left) and high water content (right) regimes respectively.

2.3.6. The impact of nickel impurities on particle formation

The presence of nickel in the present samples is deleterious to both selectivity of the surface morphology and the dependence of size on water content of the samples prepared from fully demetallated macrocycle, **1** (Figure 2-12). The presence of nickel in the samples prior to demetallation was determined to be 3 atom % relative to carbon and nitrogen using X-ray photoelectron spectroscopy (XPS). Assuming all Ni ions are coordinated to tetramer molecules, the ratio of nickel atoms to tetramer molecules is *ca.* 3:2 molecules. It is reasonable the metal ions will be associated with the faces of the tetramers. In this context, the presence of the nickel impurities between the tetramer layers

would disrupt the regularity of intermolecular spacing in the assemblies of **1**, and would influence the self-assembly process, negating any influence that the solvent has on the geometry of the macrocycle.

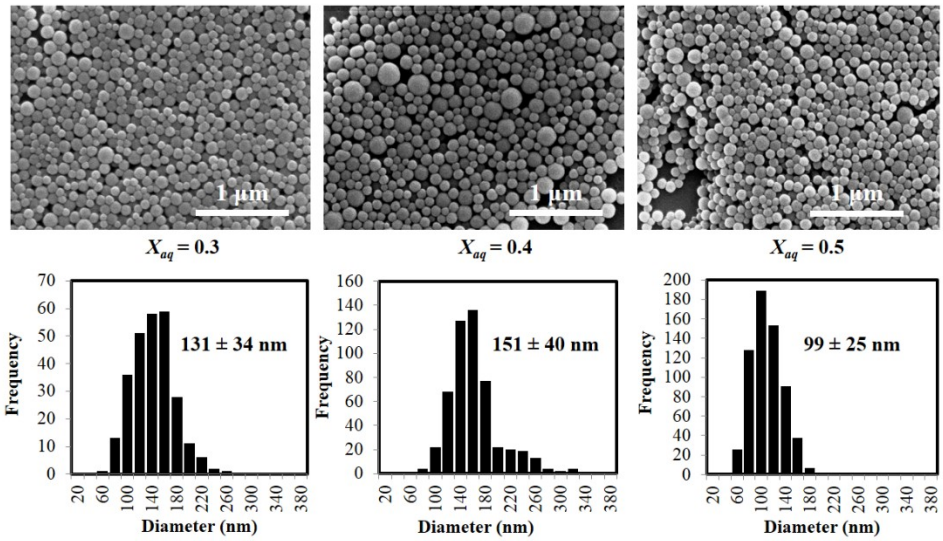

Figure 2-12. SEM images of drop-cast colloidal suspensions of **1** containing residual catalytic nickel.

2.3.7. Computational modelling and a proposed mechanism for nanoparticle formation

Seeking more insight into the molecular geometry of **1**, electronic structure calculations were performed at the B3LYP/CEP-31G level of theory (Figure 2-13 a-c). The modelled geometry indicates **1** will adopt a boat-type configuration (Figure 2-13 b). This non-planar structure arises as a result of the antiaromatic nature of the π-system of the HOMO (Figure 2-13 a). These calculations reveal that there is substantial electron density about the pyrrole ring of each subunit in the ground state that is absent in the LUMO (Figure 2-13 c). Given the predicted geometry and the spectroscopic evidence that **1** is not planar

in the present nanoparticle assemblies, in addition to suggestion of H-aggregates from the blue-shift in the excitation spectra at high X_{aq}, we propose that the molecules of **1** are interlocking in these assemblies and that the majority of the forces driving the molecules to form the spherical morphology are electrostatic H- bonding type interactions between the N-H protons on carbazole and the electron rich π-systems of the PPP backbone.

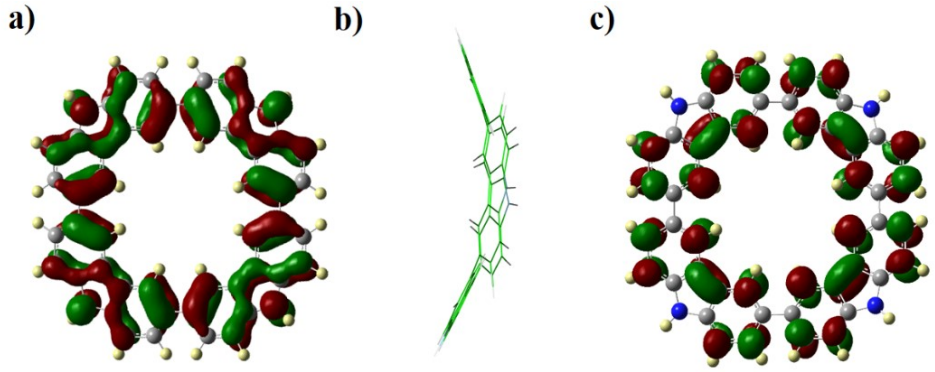

Figure 2-13. The a) HOMO, b) side view of the optimized geometry, and c) LUMO of **1** calculated at the B3LYP level of theory.

In this context, one reasonable mechanism for sphere formation involves interlocking of the carbazole subunits of the boat-shaped tetramer (*vide supra*). As X_{aq} is increased through the "low water" content regime, the assembly of **1** yields an amorphous solid, and particles form through a cooling induced precipitation process. For materials prepared from solvent mixtures in the high water content regime, colloids form result from a process, in which molecules assemble into more ordered structures,[61] likely resulting from water induced hydrogen bonding with the carbazole nitrogen.[62] Consistent with this proposed mechanism, the geometry of **1** impacts particle size – the more planar molecular geometry suggested by the trends observed in the PLE/PE Stokes shift results in

a larger radius of curvature at the surface of the particles yielding a particles with larger radii (Figure 2-14).

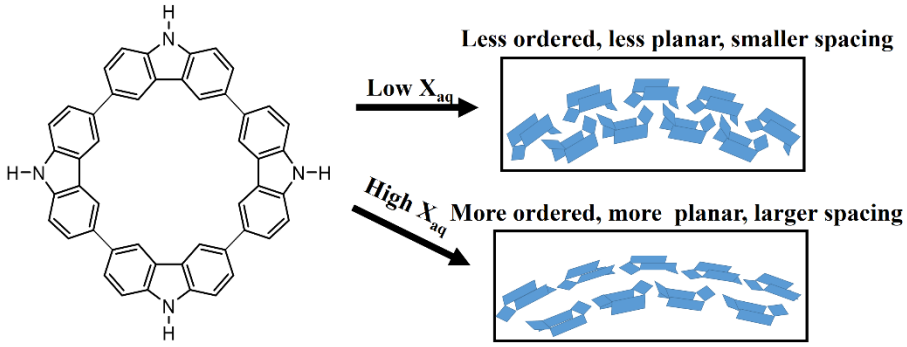

Figure 2-14. Proposed mechanism for the formation of the nanospheres of **1** in different X_{aq} regimes.

2.3.8. Carbonization and CO_2 adsorption

Recent literature reports suggest carbazole is an effective nitrogen source for the preparation of N-doped carbons suitable for application in CO_2 adsorption.[32, 33] In this regard, we endeavoured to prepare N-doped carbon nanomaterials *via* the carbonization of our nanomaterials made up of self-assembled **1**. An important aspect of this investigation aimed to evaluate whether the molecular ordering within the self-assembled structures would impact the nitrogen-environment and by extension the efficacy with which CO_2 is adsorbed by the resulting N-doped carbon.

Previous reports of carbonization of carbazole-based materials indicate that high temperatures (~1100 K) are preferred to achieve more complete oxidation; unfortunately, the resulting carbon products often suffer from significant N losses[63] which are deleterious to their application as CO_2

adsorbents.[64] To address this challenge and maintain particle morphology, it is ideal to employ the lowest possible carbonization temperature. For this reason, TGA of **1** was performed under an inert atmosphere and an onset of thermal decomposition was noted at 225 ºC, with a plateau occurring at 520 ºC corresponding to a total mass loss of 20% (Figure 2-15 a). Based upon these observations, 550 ºC was identified as the carbonization temperature of choice. To investigate if assemblies of **1** would melt under these conditions, DSC was performed (Figure 2-15 b) and indicated that no melting occurred between room temperature and the onset of thermal decomposition (*ca.* 225 ºC).

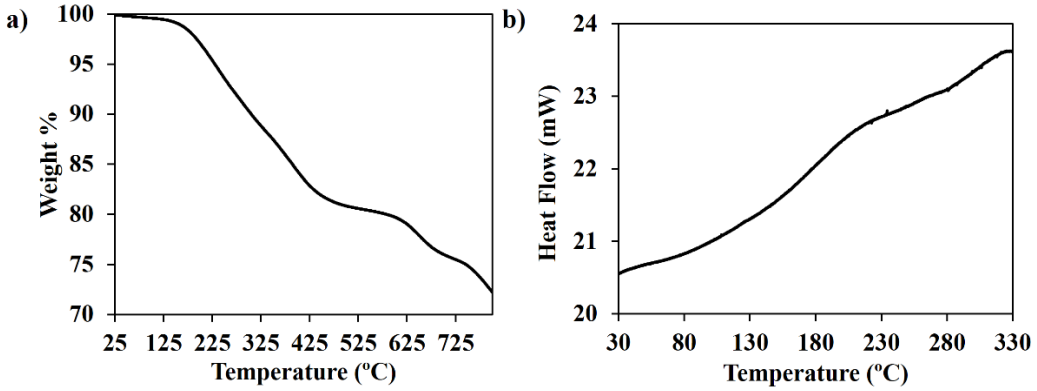

Figure 2-15. Thermogravimetric analysis recorded under nitrogen (a) and differential scanning calorimetry trace (b) of solid **1**.

Carbonization was performed in a flowing argon atmosphere at 550 ºC for 15 minutes. The resulting shiny black products obtained from the carbonization of the gel, and sphere samples prepared in solvent mixtures of X_{aq} = 0.3, 0.5 and 0.7, will be referred to as G-c, 3-c, 5-c, and 7-c, respectively. These carbonized products were mechanically ground using a mortar and pestle, dispersed in pentane and dropcast onto a silicon wafer. Substrates were

subsequently imaged using SEM (Figure 2-16). Generally, following carbonization nanospheres shrink by approximately 40-50 %. In addition, increasing X_{aq} (*i.e.,* increasing molecular ordering of **1** within the precursor particle) leads to loss of morphology following carbonization. The spherical morphology was most effectively retained in precursor spheres made up of amorphous assemblies of **1** (*i.e*., 3-c); fusing of nanoparticles was noted for 5-c, and a total loss of spherical morphology occurred in 7-c. All nanomorphology of the gel was lost upon carbonization.

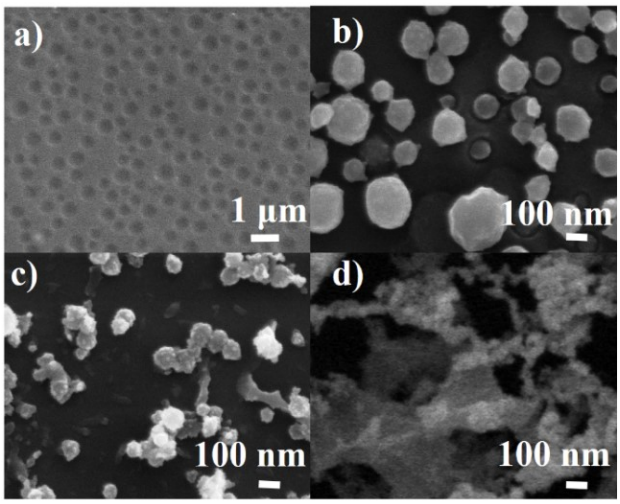

Figure 2-16. SEM images of the carbonized products of a) the gel, b) nanoparticles prepared by carbonization of colloids prepared in a solvent system where X_{aq}= 0.3 (3-c), c) X_{aq}= 0.5 (5-c) and d) X_{aq}= 0.7 (7-c).

To determine which morphologies better retain their nitrogen content throughout carbonization, the elemental composition (*i.e.*, nitrogen:carbon ratio) was determined using XPS (Table 2-2). The lowest relative nitrogen content was found for pre-carbonized **1**. Surprisingly, the carbonized products possessed

much higher relative nitrogen content (*i.e.*, nitrogen:carbon ratio = 0.052- 0.063) with the highest values corresponding to the amorphous spheres and gel (*i.e.,* 3-c and G-c, respectively). We also note the nitrogen:carbon ratio decreases with increased ordering of **1** in the parent material.

Sample	%N	%C	%N/%C	wt%$_{CO2}$ (25 ºC)
1	0.7	64.1	0.012	0.27
G-c	5.5	89.6	0.061	0.91
3-c	5.5	87.4	0.063	1.26
7-c	4.4	83.2	0.052	0.97
G-Hc	8.7	68.2	0.127	0.18
3-Hc	6.6	69.0	0.096	0.17

Table 2-2. Summary of relevant elemental analysis acquired from the XPS survey spectra for the samples under study and the wt% of CO_2 adsorbed by the samples at 298 K at 1 bar CO_2 pressure.

The oxidation state of the nitrogen species in N-doped carbons is of fundamental importance to their application.[64] The XPS spectra reveal that pre-carbonized **1** contains the greatest proportion of high oxidation state nitrogen species (See: yellow fitting trace in Figure 2-16 a). Most of the high oxidation state nitrogen is lost upon carbonization for all morphologies, but remains most prevalent in 3-c. The other two forms of nitrogen that dominate the N-doped carbons are pyrrole and pyridine moieties showing binding energies at 400.5,

and 398.9 eV, respectively.[37, 63] The most reduced nitrogen species (pyridine) is most dominant where **1** adopts the most ordered structure in the precursor (*i.e.*, 7-c). XPS also indicates that precursor morphology influences the nature of the N species following carbonization. For example, G-c retains the most carbazole-like structure as evidenced by an N 1s peak at 400 eV,[65] while carbonization of a precursor possessing nanosphere morphology (*i.e.,* 3-c, and 7-c) sees the loss of the carbazole functionality in favour of pyrrole (Figure 2-17).

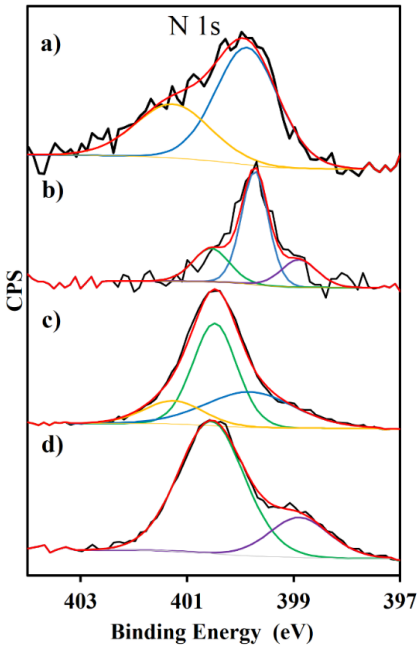

Figure 2-17 N 1s emission from the high-resolution XPS spectra of a) solid **1** and the solids obtained from carbonization of b) the gel and colloids prepared in c) X_{aq}= 0.3 and d) X_{aq}= 0.7. The black curves are the actual traces, the red lines represent the fitted curve, and the yellow, green, blue and violet traces represent the contributions to the overall spectrum from high oxidation state N, pyrrole, carbazole and pyridine, respectively.

From the above analysis, four categories of materials can be identified; i) amorphous solid **1** containing high oxidation state N, ii) N-doped carbon of ill-defined morphology containing N atoms in carbazole structural units (*i.e.,* G-c), iii) N-doped carbon of well-defined nanosphere morphology, with N atoms in pyridine structural units (*i.e.,* 3-c), and iv) N-doped carbon with micron-scale web morphology containing N atoms within pyridine and pyrrole structures (7-c) which is further confirmed by the IR spectra (Figure 2-18). The CO_2 adsorption capacities of these four materials were evaluated using TGA in an atmosphere of dry CO_2 at atmospheric pressure and 25 ºC (Table 1). The parent carbazole tetramer (*i.e.,* **1**) showed negligible CO_2 adsorption (*i.e.,* 0.27 wt %). Carbonization of the different morphologies of **1** increased the adsorption capacity to 0.91 - 1.26 wt%. This observation is reasonably ascribed to the increased nitrogen content and chemical reduction of high oxidation state nitrogen within in the carbonized materials relative to the non-carbonized **1**. G-c exhibits the lowest CO_2 adsorption capacity, presumably due to poor retention of its initial nanomorphology. The two samples prepared from nanosphere starting materials (3-c, and 7-c), displayed the greatest CO_2 adsorption capacity (*i.e.,* 1.26 and 0.97 wt%, respectively). While higher electron density on the nitrogen atoms of 7-c would be expected to lead to stronger interactions with CO_2,[34] our observations indicate the nanoscale morphology and higher nitrogen content of 3-c dominates the overall CO_2 adsorption capacity.

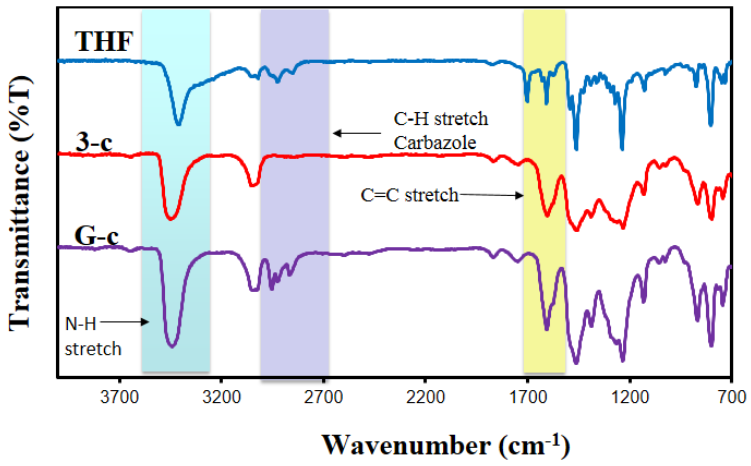

Figure 2-18. IR spectra of three of the materials prepared by self-assembly (THF) and carbonization (3-c and G-c) of **1**.

The CO_2 adsorption capacities of the samples carbonized under inert atmosphere measured above are not sufficient to render theses N-doped carbon materials competitive with other CO_2 adsorbents. For example, the CO_2 adsorption capacities of highly branched porous polycarbazole networks have recently been reported to nearly 12 % at 298 K.[33] In an attempt to boost the adsorption capacity of the carbons made using our method, in aiming to reduce N losses during carbonization, the carbonization was repeated under a slightly reducing atmosphere. Samples of **1** with X_{aq}= 0.3 and the gel product were carbonized under 5% H_2 in argon using the same heating cycle as the previously prepared carbons yielding visibly similar black powdered solids (3-Hc and G-Hc, respectively). To determine whether the carbonization atmosphere did have an impact on the nitrogen retention of the solids, the low resolution XPS spectra of the products were acquired. The XPS spectra of the solids showed a nearly

two-fold increase in nitrogen content on switching from an inert to a reducing atmosphere with %N/%C = 0.061 and 0.063 increasing to %N/%C= 0.127 and 0.096 for G-Hc and 3-Hc respectively (Table 2-2). Surprisingly, this increase in N content was not accompanied by an increase in the CO_2 adsorption capacity. The CO_2 adsorption capacities are were measured using an analogous TGA experiment as was performed on the carbons prepared under an inert atmosphere and are presented in Table 2-2. The resulting adsorption capacities of the carbons prepared under a reducing atmosphere are an order of magnitude than those prepared under an inert atmosphere with a $wt\%_{CO2}$ = 0.18 for G-Hc and $wt\%_{CO2}$ = 0.17 3-Hc.

To elucidate the source of the depressed adsorption capacities that resulted from performing the carbonization experiments under a reducing atmosphere, the high resolution XPS of the N 1s emission were consulted once again (Figure 2-19 a). The XPS N 1s spectra of 3-Hc and G-Hc are nearly identical, with over 80 % of the contribution to the overall emission arising from intact carbazole N species, with only minor amounts of N-atoms in the more electron poor pyrrole, and more electron rich pyridine forms.[66] This is in contrast to the significant contributions to the XPS N 1s peak observed in the spectra of 3-c and G-c from the more oxidized N species discussed above (Figure 2-19 b and c). The XPS results suggest that the presence of hydrogen during carbonization maintained the overall carbazole structural unit.

To confirm that this structural assignment is accurate, the IR spectra of the solids 3-Hc and G-Hc were recorded (Figure 2-19 b). Analysis of the IR

spectra again confirm that the structural characteristics of the N-doped carbons are comparable, with a large N-H stretch at c.a. 3400 cm^{-1}, and the broad featureless band in the C=C stretching region which is consistent with graphitic carbon, and is similar to the samples prepared under inert atmosphere that were discussed previously (see Figure 2-18). The near absence of peaks in the C-H stretching region of the IR spectra (c.a. 3000 cm^{-1}) suggests that carbonization was more complete, leaving less intact C-H bonds, and is indicative of a more dense post-carbonization carbon network, which is believed to be the source of the poor adsorption abilities of 3-Hc and G-Hc, relative to 3-c and G-c.

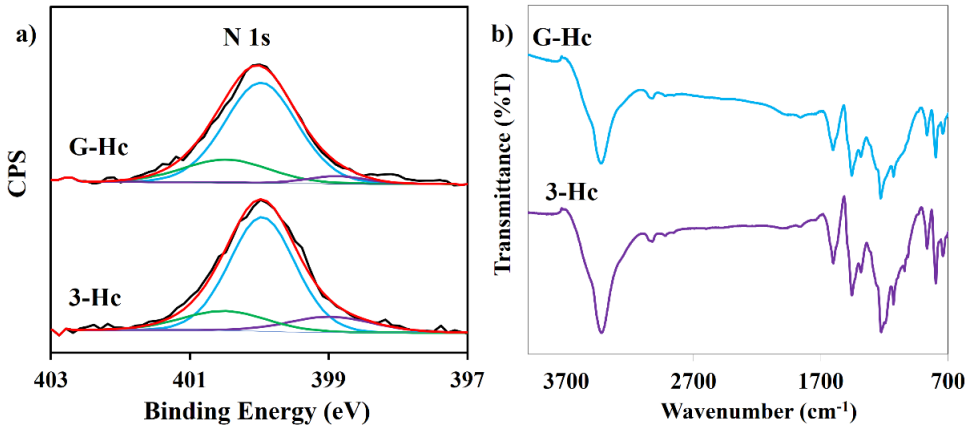

Figure 2-19 a) High-resolution XPS spectra showing the N 1s emission of the solids obtained from carbonization of the gel product (top) and X_{aq}=0.3 (bottom) under a slightly reducing atmosphere. The black curves are the actual traces, the red lines represent the fitted curve, and the green, blue and violet traces represent the contributions to the overall spectrum from pyrrole, carbazole and pyridine, respectively. b) The IR spectra of the products recorded as pressed pellets in KBr.

2.4. Conclusions

In conclusion, we have prepared an alkyl-free cyclic carbazole tetramer that forms well-defined nanostructures when precipitated from water/acetone solvent mixtures. Detailed analyses indicate defining the solvent mixture composition influences molecular geometry and assembly of **1** as well as the optical properties of the resulting nanomaterials. In the "low water" content regime (*i.e.,* a less polar environment) amorphous colloids bearing dimpled surfaces that exhibit optical properties equivalent to solvated **1** are formed. In contrast, in the "high water" content regime (*i.e.,* a more polar solvent environment) **1** adopts a more planar geometry that facilitates ordering within the resulting particles. This molecular ordering and the rigidity of **1** in the particles causes in an increase in PL intensity resulting from AEE – this property provides an indirect spectroscopic handle for tracking the molecular ordering within the self-assembled particles.

These carbazole-based materials provide convenient precursors for the preparation of macro, micro, and nanostructured nitrogen-doped carbon. Our studies show the morphology of the carbonized materials depends on the molecular ordering of **1**. Amorphous nanoparticles retain their morphology upon pyrolysis. Increasing the molecular ordering within the spheres results in a loss of the spherical morphology. We also find that the molecular ordering of **1** within the precursor particles influences the nitrogen environment in the pyrolyzed product and by extension their CO_2 adsorption capacity. Based upon the present investigations we conclude that while CO_2 adsorption capacity is

influenced by the identity of the nitrogen species and particle morphology, the later dominates for the present system.

2.5. References

(1) Li, H.; Kang, Z.; Liu, Y.; Lee, S.-T. *J. Mater. Chem.* **2012**, *22*, 24230.

(2) Sun, D.; Ban, R.; Zhang, P.-H.; Wu, G.-H.; Zhang, J.-R.; Zhu, J.-J. *Carbon* **2013**, *64*, 424.

(3) Schenning, A. P. H. J.; Meijer, E. W. *Chem. Commun*. **2005**, 3245.

(4) Xie, L.; Yang, S.; Lin, J.; Yi, M.; Huang, W. *Philos. Trans. R. Soc. London A* **2013**, *371*, 20120337.

(5) Jariwala, D.; Sangwan, V. K.; Lauhon, L. J.; Marks, T. J.; Hersam, M. C. *Chem. Soc. Rev.* **2013**, *42*, 2824.

(6) Ouyang, Y.; Shi, H.; Fu, R.; Wu, D. *Sci. Reports* **2013**, *3*, 1.

(7) Li, W.; Zhang, Z.; Kong, B.; Feng, S.; Wang, J.; Wang, L.; Yang, J.; Zhang, F.; Wu, P.; Zhao, D. *Angew. Chem. Int. Ed. Engl.* **2013**, *52*, 8151.

(8) Wang, Q.; Huang, X.; Long, Y.; Wang, X.; Zhang, H.; Zhu, R.; Liang, L.; Teng, P.; Zheng, H. *Carbon* **2013**, *59*, 192.

(9) Chen, S.; Li, Y.; Li, Y. *Polym. Chem.* **2013**, *4*, 5162.

(10) Coville, N. J.; Mhlanga, S. D.; Nxumalo, E. N.; Shaikjee, A. *S. Afr. J. Sci.* **2011**, *107*, 1.

(11) Cao, L.; Meziani, M. J.; Sahu, S.; Sun, Y.-P. *Acc. Chem. Res.* **2013**, *46*, 171.

(12) Baker, S. N.; Baker, G. A. *Angew. Chem. Int. Ed. Engl.* **2010**, *49*, 6726.

(13) Anilkumar, P.; Wang, X.; Cao, L.; Sahu, S.; Liu, J.-H.; Wang, P.; Korch, K.; Tackett, K. N.; Parenzan, A.; Sun, Y.-P. *Nanoscale* **2011**, *3*, 2023.

(14) Balakrishnan, K.; Datar, A.; Naddo, T.; Huang, J.; Oitker, R.; Yen, M.; Zhao, J.; Zang, L. *J. Am. Chem. Soc.* **2006**, *128*, 7390.

(15) Ke, D.; Zhan, C.; Xu, S.; Ding, X.; Peng, A.; Sun, J.; He, S.; Li, A. D. Q.; Yao, J. *J. Am. Chem. Soc.* **2011**, *133*, 11022.

(16) Huang, J.; Chen, P.; Yang, X.; Tang, R.; Wang, L.; Qin, J.; Li, Z. *Sci. China Chem.* **2013**, *56*, 1213.

(17) Zhao, Z.; Lam, J. W. Y.; Tang, B. Z. *Soft Matter* **2013***, 9*, 4564.

(18) Hoeben, F. J. M.; Jonkheijm, P.; Meijer, E. W.; Schenning, A. P. H. J. *Chem. Rev*. **2005**, *105*, 1491.

(19) Li, J.; Grimsdale, A. *Chem. Soc. Rev.* **2010**, *39*, 2399.

(20) Morin, J.-F.; Leclerc, M.; Adès, D.; Siove, A. *Macromol. Rapid Commun.* **2005**, *26*, 761.

(21) Park, K. S.; Salunkhe, S. M.; Lim, I.; Cho, C.-G.; Han, S.-H.; Sung, M. M. *Adv. Mater.* **2013**, *25*, 3351.

(22) Boudreault, P. T.; Blouin, N.; Leclerc, M. *Adv. Polym. Sci.* **2008**, *212*, 99.

(23) Huang, W.; Zhao, T.-Y.; Wen, M.-W.; Yang, Z.-Y.; Xu, W.; Yi, Y.-P.; Xu, L.-P.; Wang, Z.-X.; Gu, Z.-J. *J. Phys. Chem. C* **2014**, *118*, 6767.

(24) Balakrishnan, K.; Datar, A.; Zhang, W.; Yang, X.; Naddo, T.; Huang, J.; Zuo, J.; Yen, M.; Moore, J. S.; Zang, L. *J. Am. Chem. Soc.* **2006**, *128*, 6576.

(25) Finke, A. D.; Gross, D. E.; Han, A.; Moore, J. S. *J. Am. Chem. Soc.* **2011,** *133*, 14063.

(26) Che, Y.; Gross, D. E.; Huang, H.; Yang, D.; Yang, X.; Discekici, E.; Xue, Z.; Zhao, H.; Moore, J. S.; Zang, L. *J. Am. Chem. Soc.* **2012**, *134*, 4978.

(27) Yang, Z.; Chi, Z.; Xu, B.; Li, H.; Zhang, X.; Li, X.; Liu, S.; Zhang, Y.; Xu, J. *J. Mater. Chem.* **2010**, *20*, 7352.

(28) Dong, S.; Li, Z.; Qin, J. *J. Phys. Chem. B* **2009**, *113*, 434.

(29) Upamali, K. A. N.; Estrada, L. A.; De, P. K.; Cai, X.; Krause, J. A.; Neckers, D. C. *Langmuir* **2011**, *27*, 1573.

(30) Auttapornpitak, P.; Sukwattanasinitt, M.; Rashatasakhon, P. *Sensors Actuators B Chem.* **2013**, *178*, 296.

(31) Naddo, T.; Che, Y.; Zhang, W.; Balakrishnan, K.; Yang, X.; Yen, M.; Zhao, J.; Moore, J. S.; Zang, L. *J. Am. Chem. Soc.* **2007**, *129*, 6978.

(32) Chen, Q.; Luo, M.; Hammershøj, P.; Zhou, D.; Han, Y.; Laursen, B. W.; Yan, C.-G.; Han, B.-H. *J. Am. Chem. Soc*. **2012**, *134*, 6084.

(33) Zhu, X.; Mahurin, S. M.; An, S.-H.; Do-Thanh, C.-L.; Tian, C.; Li, Y.; Gill, L. W.; Hagaman, E. W.; Bian, Z.; Zhou, J.-H.; Hu, J.; Liu, H.; Dai, S. *Chem. Commun*. **2014**, *50*, 2.

(34) Casco, M. E.; Morelos-Gómez, A.; Vega-Díaz, S. M.; Cruz-Silva, R.; Tristán-López, F.; Muramatsu, H.; Hayashi, T.; Martínez-Escandell, M.; Terrones, M.; Endo, M.; Rodríguez-Reinoso, F.; Silvestre-Albero, J. *J. CO_2 Utiliz.* **2014***, 5*, 60.

(35) Drage, T. C.; Arenillas, A.; Smith, K.; Snape, C. E. *8th International Conference on Greenhouse Gas Technologies* **2006**, *19*.

(36) Arenillas, A.; Rubiera, F.; Parra, J. B.; Ania, C. O.; Pis, J. *J. Appl. Surf. Sci*. **2005**, *252*, 619.

(37) Arenillas, A.; Drage, T. C.; Smith, K.; Snape, C. E. *J. Anal. Appl. Pyrolysis* **2005**, *74*, 298.

(38) Xu, D.; Liu, X.; Lu, R.; Xue, P.; Zhang, X.; Zhou, H.; Jia, J. *Org. Biomol. Chem.* **2011**, *9*, 1523.

(39) Gaussian 09, Frisch, M. J.; Trucks, G. W.; Schlegel, H. B.; Scuseria, G. E.; Robb, M. A.; Cheeseman, J. R.; Scalmani, G.; Barone, V.; Mennucci, B.; Petersson, G. A.; Nakatsuji, H.; Caricato, M.; Li, X.; Hratchian, H. P.; Izmaylov, A. F.; Bloino, J.; Zheng, G.; Sonnenberg, J. L.; Hada, M.; Ehara, M.; Toyota, K.; Fukuda, R.; Hasegawa, J.; Ishida, M.; Nakajima, T.; Honda, Y.; Kitao, O.; Nakai, H.; Vreven, T.; Montgomery, Jr., J. A.; Peralta, J. E.; Ogliaro, F.; Bearpark, M.; Heyd, J. J.; Brothers, E.; Kudin, K. N.; Staroverov, V. N.; Kobayashi, R.; Normand, J.; Raghavachari, K.; Rendell, A.; Burant, J. C.; Iyengar, S. S.; Tomasi, J.; Cossi, M.; Rega, N.; Millam, N. J.; Klene, M.; Knox, J. E.; Cross, J. B.; Bakken, V.; Adamo, C.; Jaramillo, J.; Gomperts, R.; Stratmann, R. E.; Yazyev, O.; Austin, A. J.; Cammi, R.; Pomelli, C.; Ochterski, J. W.; Martin, R. L.; Morokuma, K.; Zakrzewski, V. G.; Voth, G. A.; Salvador, P.; Dannenberg, J. J.;

Dapprich, S.; Daniels, A. D.; Farkas, Ö.; Foresman, J. B.; Ortiz, J. V.; Cioslowski, J.; Fox, D. J. Gaussian, Inc., Wallingford CT, **2009**

(40) Becke, A. D. *J. Chem. Phys.* **1993**, 5648.

(41) Stevens, W. J.; Basch, H.; Krauss, M. *J. Chem. Phys*. **1984**, *81*, 6026.

(42) Stevens, W. J.; Krauss, M.; Basch, H.; Jasien, P. G. *Can. J. Chem.* **1992**, *70*, 612–630.

(43) Cundari, T. R.; Stevens, W. J. *J. Chem. Phys*. **1993**, *98*, 5555.

(44) Williams, A. T. R.; Winfield, S. A.; Miller, J. N. *Analyst* **1983**, *108*, 1067.

(45) Ostrauskaite, J.; Strohriegl, P. *Macromol*. *Chem*. *Phys*. **2003**, *204*, 1713.

(46) Raj, V.; Madheswari, D.; Ali, M. M. *J. Appl. Polym. Sci.* **2010**, *116*, 147.

(47) Li, Z. Q.; Lu, C. J.; Xia, Z. P.; Zhou, Y.; Luo, Z. *Carbon* **2007**, *45*, 1686.

(48) Sumrak, J. C.; Sokolov, A. N.; MacGillivray, L. R. In *Crystal Engineering Organic Semiconductors*; **2011**; pp. 1–19.

(49) Belletête, M.; Bouchard, J.; Leclerc, M.; Durocher, G. *Macromolecules* **2005**, *38*, 880.

(50) Martin, T. P.; Wise, A. J.; Busby, E.; Gao, J.; Roehling, J. D.; Ford, M. J.; Larsen, D. S.; Moule, A. J.; Grey, J. K. *J. Phys Chem. B* **2013**, *117*, 4478.

(51) Xu, B.; He, J.; Dong, Y.; Chen, F.; Yu, W.; Tian, W. *Chem. Commun.* **2011**, *47*, 6602.

(52) Yasutani, Y.; Honsho, Y.; Saeki, A.; Seki, S. *Synth. Met.* **2012**, *162*, 1713.

(53) Spano, F. C. *Acc. Chem. Res.* **2010**, *43*, 429.

(54) Gierschner, J.; Luer, L.; Milian-Medina, B.; Oelkrug, D.; Egelhaaf, H. J. *Phys. Chem. Lett.* **2013**, *4*, 2686.

(55) Wang, L.; Shen, Y.; Yang, M.; Zhang, X.; Xu, W.; Zhu, Q.; Wu, J.; Tian, Y.; Zhou, H. *Chem. Commun.* **2014**, *50*, 8723.

(56) Braslavsky, S. E. *Pure Appl. Chem.* **2007**, *79*, 293.

(57) Józefowicz, M.; Heldt, J. R. *J. Fluoresc.* **2011**, *21*, 239.

(58) Sarangi, M. K.; Mitra, A. K.; Sengupta, C.; Ghosh, S.; Chakraborty, S.; Saha, C.; Basu, S. *J. Phys. Chem. C* **2013**, *117*, 2166.

(59) Fita, P.; Fedoseeva, M.; Vauthey, E. *Langmuir* **2011**, *27*, 4645.

(60) Spencer, T. S. O'Donnell, C. M. *J. Am. Chem. Soc.* **1972**, *94,* 4846.

(61) Ma, L.; Wang, Q.; Lu, G.; Chen, R.; Sun, X. *Langmuir* **2010**, *26*, 6702.

(62) Bombach, R.; Honegger, E.; Leutwyler, S. *Chem. Phys. Lett.* **1985**, *118*, 449.

(63) Pels, J.; Kapteijn, F.; Moulijn, J.; Zhu, Q.; Thomas, K. *Carbon* **1995**, *33*, 1641.

(64) Hao, G.-P.; Li, W.-C.; Qian, D.; Lu, A.-H. *Adv. Mater.* **2010**, *22*, 853.

(65) Taoudi, H.; Bernede, J. C.; Bonnet, A.; Morsli, M.; Godoy, A. *Thin Solid Films* **1997**, *304*, 48.

Chapter 3:

Application of nanoparticle assemblies of cyclotetra(carbazol-3,6-diyl) as a fluorescence quenching sensor

3.1. Introduction

The environmental and biological impact of water-borne toxins have spurred widespread interest in the development of inexpensive, rapid and straightforward methods for detecting low concentrations of heavy metals and water-soluble organic compounds in aqueous environments.[1,2] A brief literature search yields thousands of reports of the deleterious impacts of contaminants including Pb ions leached from pipes and leaded glass,[3] Hg from consumer electronics,[4] as well as naphthenic acid residues from the processing of oil sands.[5,6] While continued efforts to limit environmental contaminants remain a priority, the growing global need for clean water demands rapid assessment of the purity of a sources.[2,7] Of the many methods under investigation for the detection of aqueous contaminants, fluorescence-based sensors are among the most attractive because they are rapid, portable, and do not require extensive instrumentation.[8]

Carbazole-based materials have emerged as potential candidates for sensing applications because the pyrrole nitrogen is available to coordinate to metal centres, and this binding process can influence the material optical properties.[9] One issue that has limited development of a carbazole-based sensor is the optical properties of these materials often depend upon how it is processed. In particular, aggregation induced quenching (AIQ) limits solid state luminescence in carbazole-based small molecules and homopolymers.[10] One strategy for addressing AIQ is to design small molecules that form highly emissive assemblies as a result of aggregation induced emission enhancement

(AIEE), in which aggregation forces the molecules into ordered morphologies that enhance the emission intensity. This strategy has seen carbazole derivatives form the active components in fluorescence-based sensors for heavy metals, nitroaromatic compounds,[11] acids,[12,13] caffeine,[14] and fluoride ions.[15] One limitation of existing methods is the sensing materials are generally dispersed in organic solvents; this presents obvious challenges when attempting to detect aqueous contaminants.

Naphthenic acids (NAs) are toxic to mammals and aquatic life;[6] they are the major water-soluble contaminant resulting from oil sands processing. NAs consist primarily of monocyclic and polycyclic aliphatic acids (Figure 3-1).[16] Because NAs are always present as complex mixtures, quantitative determination difficult.[5] Fluorescence detection is a popular alternative to quantitative analytical methods as detection can be performed quickly in the field without the need for heavy and expensive instruments. While fluorescence spectroscopy does offer a rapid, visible means for detecting NAs, these compound mixtures themselves are only weakly fluorescent, as such limits to detection are often well above the levels present in ground waters and tailings ponds close to oil-sands processing facilities. Unfortunately, NA quantification using its natural fluorescence is limited to high concentrations (*i.e.*, 25-400 mg/L)[17] and cannot compete with other methods (*e.g.*, high performance liquid chromatography and infrared spectroscopy) that have demonstrated limits of detection approaching 5 mg/L[18] and 1 mg/L, respectively.[19] As such, a

fluorescence-based detection method that amplifies or enhances NA fluorescence response would be attractive.[20]

The weakly basic nature of the pyrrole moiety in oligocarbazoles such as compound **1** provides a potential handle for fluorescence quenching in acidic media. More specifically, the luminescence of the oligocarbazole macrocycles should depend critically on pH, in which case acids such as NA should quench the luminescence in these all-carbazole materials.

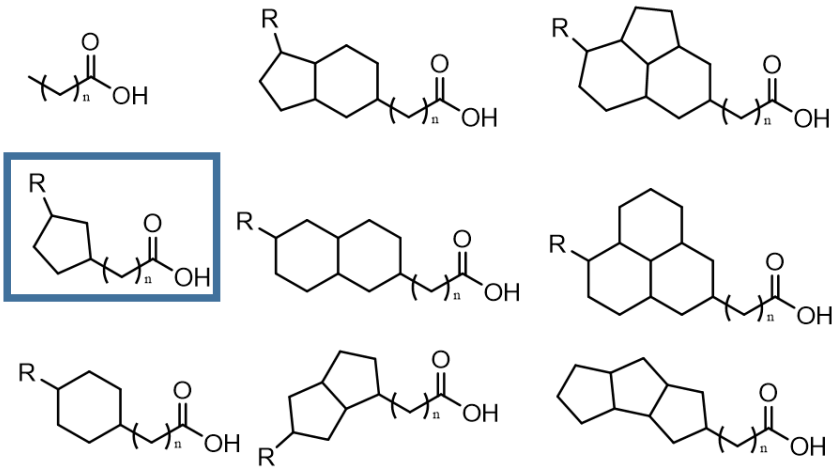

Figure 3-1. The structures of some of the components of naturally occurring naphthenic acids (NAs). Cyclopentanoic acid highlighted by a blue box is a primary component in natural NAs and is used here as a model NA compound.

In Chapter 2 the preparation of luminescent microspheres made up of an all-carbazole macrocyclic tetramer was reported. In the following section a preliminary investigation into the application of these materials to the fluorescent detection of metal ions (*i.e.*, Ni^{2+}, Cu^{2+}, and Co^{2+};) and NAs is reported.

3.2. Experimental

3.2.1. Materials and instrumentation

The synthetic procedure for preparing **1** (Figure 3-2, left) is described in Chapter 2 of the present thesis. Colloidal particles of **1** that were evaluated for sensing applications were prepared using the same methods outlined in Section 2.1.2.1 of this thesis, where X_{aq} = 0.7. These assemblies were chosen because they exhibited the greatest fluorescence response of studied herein. Particle suspensions were used as prepared. All water used in the present study was triply distilled prior to use and the acetone (HPLC grade, Sigma-Aldrich) was used as received. Cobalt acetate, nickel chloride, copper sulfate pentahydrate, zinc chloride, calcium chloride, magnesium sulfate and naphthenic acid (NA) were all purchased from Sigma-Aldrich and used as received. Photoluminescence (PL) spectra were recorded using a Varian Cary Eclipse fluorometer in quartz cuvettes at a scan rate of 2 nm per second with fixed excitation and emission slit widths of 2.5 nm and 5 nm, respectively and a λ_{ex} = 350 nm. To facilitate direct comparison between all spectra the emission filter was disabled for the present experiments.

3.2.2. Evaluation of external influences on the PL response of carbazole-tetramer assemblies

A survey of the influence of various analytes on the luminescent response of the tetramer spheres was performed by evaluating the PL spectra of a suspension of spherical assemblies of **1** prepared in a water/acetone co-solvent

mixture (0.9 mL) in which the mole fraction of water, X_{aq}, is 0.7 before and after addition 100 μL of 10^{-5} M aqueous solution of the target analyte; this procedure afforded a final analyte concentration of 1.0 x 10^{-6} M. The analytes evaluated included $Cu(NO_3)_2$, $NiCl_2$, $Co(CH_3CH_2COO)_2$, $Mg(SO_4)$, $CaCl_2$, and $ZnCl_2$. Stock solutions were prepared by dissolving the reagents in water followed by appropriate serial dilution to the desired concentration. Sensitivity to NAs was also evaluated by adding the potential quencher directly to the suspensions of **1**, which was used as received without further dilution. The control for these experiments consisted of a 0.9 mL sample of **1** which was diluted with 100 μL of water.

Additional evaluations of $Cu(NO_3)_2$, $NiCl_2$, and $Co(CH_3CH_2COO)_2$. Solutions of a predetermined concentration (*i.e.*, 0.011 M) were prepared and sequentially diluted to prepare solutions in the range of 0.0055 M through 5.5 × 10^{-6} M. The PL response of suspensions of **1** were determined by recording the PL of a 0.8 mL aliquot of 1 with X_{aq} = 0.7 prior to and following the addition of 200 μL of the target analyte solution.

3.3. Results and Discussion

3.3.1. Metal ion sensing in aqueous media

A colloidal suspension of **1** was prepared by adding the solid macrocycle to a water/acetone co-solvent mixture (X_{aq} = 0.7) followed by boiling for 5 minutes and cooled to room temperature. The procedure afforded a slightly cloudy, off-white suspension (Figure 3-2) made up of spherical assemblies of 1

(see Chapter 2). These suspensions are stable for weeks (*i.e.*, negligible settling upon standing). Secondary electron images of the colloidal particles show spheres with an average diameter of 340 ± 120 nm. Upon excitation at 365 nm the colloidal suspension shows blue PL that is obvious even with visible inspection and shows a PL maximum at *ca.* 420 nm.

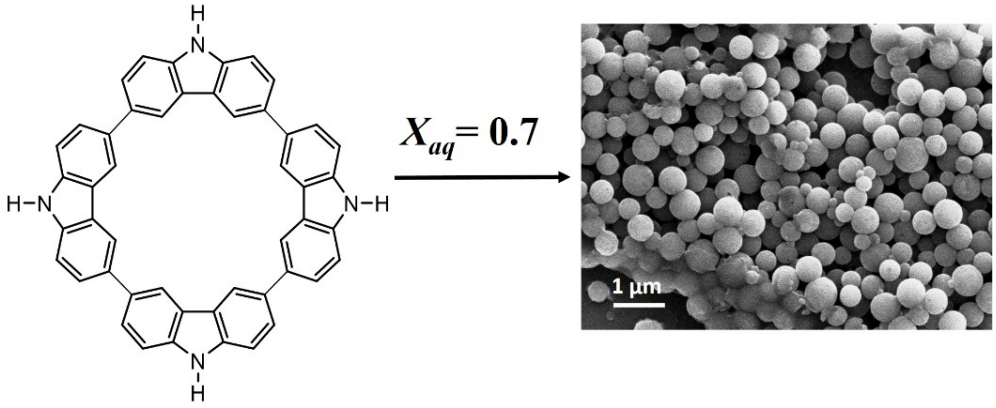

Figure 3-2. Structure of compound **1** (left) and SEM image of the colloid formed in a water/acetone mixture where X_{aq}= 0.7.

To evaluate the sensitivity of microsphere-based PL to exposure to aqueous metal ions, a series of target ions were screened and optical response was monitored. Aqueous metal ion solutions were prepared at a concentration of 1.0×10^{-5} M that were added to samples of colloids of **1** in water/acetone co-solvent where X_{aq}= 0.7. The final metal ion concentration after addition was 1.0×10^{-6} M. The PL spectra of the solutions were recorded before and after addition of the metal salts and the fraction of the original emission intensity that remained after exposure to the metal ions. Generally, the ratio of the integrated PL intensities remained close to unity at micromolar concentrations (Figure 3-3).

The ions that showed the greatest influence on the PL from colloidal assemblies of spheres made up of **1** were Ni^{2+}, Cu^{2+}, and Co^{2+}; these ions caused decrease in integrated PL (I/I_0) of 26 %, 24 % and 17 %.

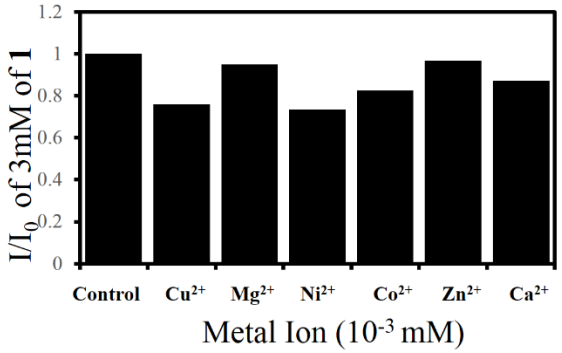

Figure 3-3. The change in integrated PL intensity (I/I_o) upon excitation (λ = 350 nm) of a colloidal suspension of spherical assemblies of **1** upon addition of indicated metal ions at a final concentration of 1.0 x 10^{-6} M. The control was prepared by the addition of water to the colloidal suspension alone to account for the dilution associated with the addition the metal ion solutions.

The decrease in PL response observed with the addition of Ni^{2+}, Cu^{2+}, and Co^{2+} were added to the colloids of **1** warranted investigation into the influence of higher metal ion concentrations; metal ion concentrations ranging from 1.0 mM to 1.0 μM were evaluated (Figure 3-4). The results of this study confirm the emissive suspensions of colloids derived from **1** are sensitive to Ni^{2+}, Cu^{2+}, and Co^{2+}. The magnitude of the influence of Ni^{2+} exposure is the largest noted for the ions investigated here and tracks with Ni^{2+} concentration (Figure 3-4 b).

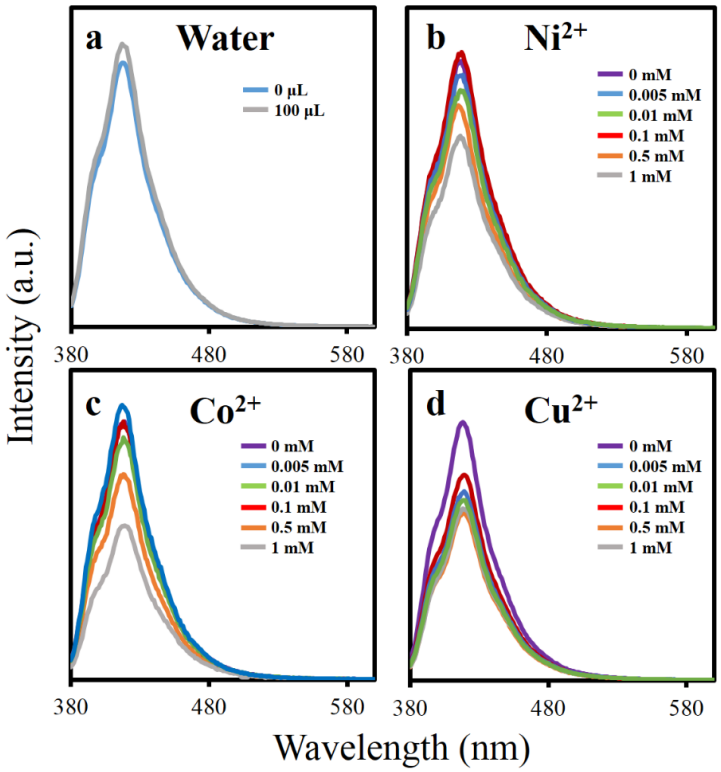

Figure 3-4. The evolution of the PL response of spherical colloids of 1 with upon addition of a) 200 µL of water, and addition of aqueous solutions of metal salts b) Ni^{2+}, c) Co^{2+}, and d) Cu^{2+}.

Exposing the colloids derived from **1** to Cu^{2+} and Co^{2+} impacts PL properties (Figure 3-4 c and d), however no clear relationship between the concentration of the metal ions and the magnitude of the PL quenching was noted. It is unclear why the behaviour of these metal ions differs from Ni^{2+}.

To better quantify the colloid PL response as a function of the concentration of the quencher ion, the magnitude of the quenching - taken as the ratio of the initial integrated fluorescence intensity and the fluorescence intensity in the presence of a quencher (*i.e.*, I_0/I) - is plotted against the concentration of the quencher.[21] For Ni^{2+}, presented in Figure 3-5, a linear relationship between

the concentration Ni^{2+} ions and the quenching the luminescence of the particles of **1** is observed. In contrast, similar plots for Cu^{2+} and Co^{2+} suggest no relationship between ion concentration and florescent response. The lack of correlation between PL intensity and Cu^{2+} and Co^{2+} ion concentrations combined with the limited quenching effect observed in the presence of Ni^{2+}, suggests that there is no statistical difference between the sensitivity of the colloid to the presence of any of the metal ions under study at any concentration investigated.

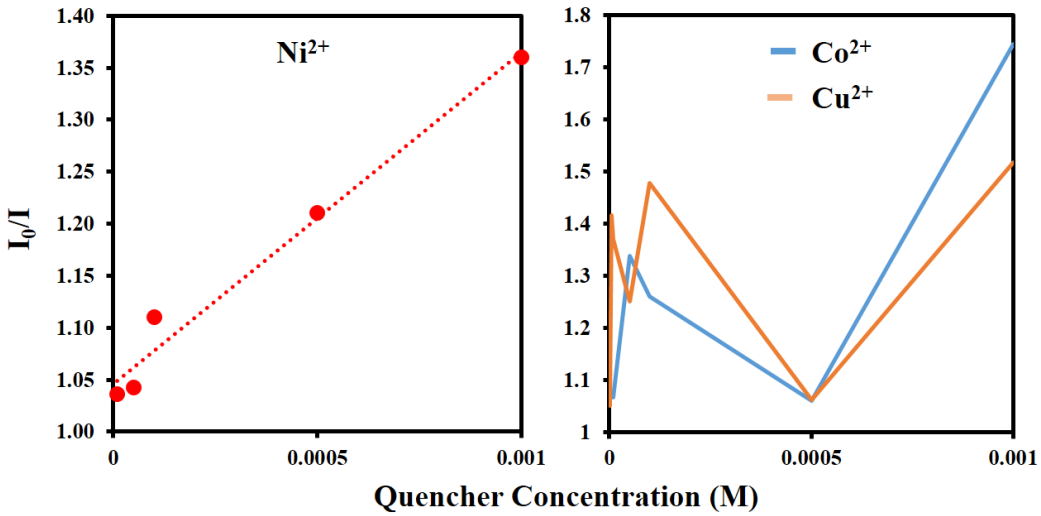

Figure 3-5. Stern-Volmer plots for the concentration dependent quenching by (left) Ni^{2+}, and (right) Co^{2+}, and Cu^{2+}.

While a small amount of PL quenching was observed on exposing the colloids of **1** to the studied metal ions, the observation of visible quenching requires very large concentrations, which limits their application. For example, other fluorescence-based sensing methods using dissolved conjugated polymers can rapidly detect Co^{2+}, Ni^{2+}, and Cu^{2+} ions at μM concentrations.[22, 23] One explanation for the limited quenching of the luminescence is molecules at the

interior of the spheres are not exposed to the quencher in a method similar to those at the interior of the film in thin film based sensors.[23] Unlike crystalline materials, electronic communication between molecules that compose the particles is not efficient, so the quenching at the interior of the particles does not occur.[24-27]

3.3.2. Naphthenic acid sensing in aqueous media

The influence of naphthenic acids on the PL response of colloids of **1** was evaluated by exposing colloids of **1** prepared as outlined in Chapter 2, and the experimental section of this Appendix. The PL spectra of 1.0 mL aliquots of the colloid suspensions were acquired. A predetermined quantity of NA was added with stirring and the PL was subsequently evaluated. The PL recorded following the addition of the NA was normalized to the intensity at the emission maximum of the initial PL spectrum for each sample. Using this method we obtained a series of relative PL intensities as a function of the amount of NA added (Figure 3-6).

The addition of small amounts of NA to the colloids of **1** resulted in negligible changes in the intensity of the PL spectra with PL intensity at the emission maximum remaining within 10 % of that recorded in the absence of NA (Figure 3-6). A visible decrease in the PL intensity began to occur at a NA content of 20 μL< V_{NA}< 30 μL where the measured PL intensity at the emission maximum decreased to 75 % and 64 % of that obtained in the absence of NA. The maximum quenching effect observed at V_{NA}= 40 μL, where the PL intensity was observed to decrease to 27 % of the intensity acquired from the original

colloidal suspension beyond this concentration an increase in PL intensity was observed presumably due to fluorescence arising from the NA itself.

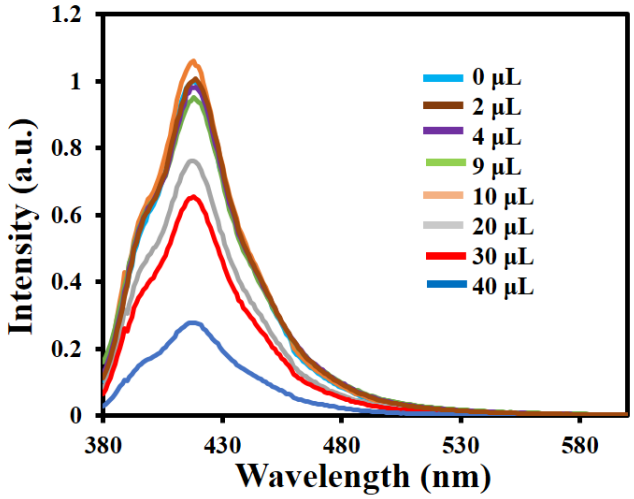

Figure 3-6. Dependence of the PL spectra of colloids based upon 1 upon exposure to the indicated concentrations of naphthenic acid in water.

While some quenching of the luminescence of the colloids was observed upon exposed to NAs, the effective range from between 20 µL and 40 µL corresponds to an overall concentration range of 20 ppm to 40 ppm, which is well above the 0.08 - 0.7 ppm observed in contaminated water run-off from natural crude oil deposits where this sensing method would be ideally suited.[16] Additionally, at concentrations above 40 ppm, no additional PL quenching is observed, which suggests any quantitative determination of NA concentrations in aqueous samples would not be possible, even at high concentrations. At high NA concentrations oxidation of molecules close to the surface of the particles could be responsible for the quenching of the PL. Unfortunately, the residual PL arising from the cores of the particles interferes with the quenching efficiency.[24-

[27] The effect may additionally limited by the high pK_a of naphthenic acid is 5-6, which is slightly weaker that acetic acid[28] this paired with the relatively low basicity of carbazole may limit the degree of protonation of the carbazole tetramer which would lead to PL quenching.[29]

3.4. Conclusions

The suggestion that the particles of **1** prepared at X_{aq}= 0.7 occur via a mechanism involving AIEE which leads to intense PL, infers that there is a possibility that these assemblies could undergo PL quenching in response to a number of external stimuli. Two of the properties of the carbazole subunit present in **1** that were investigated as quenching handles were their abilities to form transition metal complexes, and their sensitivity to acidic media. In this context, we exposed the microparticles of **1** to various metal salts, and the environmental toxin naphthenic acid.

The particles did show selective sensitivity to Ni^{2+}, Cu^{2+} and Co^{2+} ions over the other ions investigated, however there was no measurable dependence of the degree of quenching on the concentration of metal ions for Cu^{2+} and Co^{2+}. At relatively high Ni^{2+} concentrations (*i.e.*, 1.0 mM) the intensity of the luminescence from the solution decreases visibly, but at such high concentrations the added $NiCl_2$ solutions have a visibly green appearance from the dissolved nickel complex, which means simple colorimetric analysis is more practical, effective, and inexpensive.

As an alternative to metal sensing, exposure of the material to NA did result in visible quenching in the range of 20 to 40 ppm of added NA, which is a slight improvement over direct fluorescence detection for NAs. We believe the limitations to the quenching to be the product of residual luminescence from the large portion of embedded molecules of the macrocycle **1**, which are protected from oxidation by the added NA.

3.5. References

(1) Kokkali, V.; van Delft, W. *TrAC Trends Anal. Chem.* **2014**, *61*, 133.

(2) Jang, A.; Zou, Z.; Lee, K. K.; Ahn, C. H.; Bishop, P. L. *Meas. Sci. Technol*. **2011**, *22*, 032001.

(3) Yoshinaga, J. *Environ. Health Prev. Med.* **2012**, *17*, 433.

(4) Verma, R.; Gupta, B. D. *Food Chem.* **2015**, *166*, 568.

(5) Scott, A. C.; Mackinnon, M. D.; Fedorak, P. M. *Environ. Sci. Technol.* **2005**, *39*, 8388.

(6) Headley, J. V.; McMartin, D. W. *J. Environ. Sci. Heal. Part A* **2004**, *39*, 1989.

(7) Baruah, S.; Dutta, J. *Environ. Chem. Lett.* **2009**, *7*, 191.

(8) Zhang, D.; Cochrane, J. R.; Martinez, A.; Gao, G. *RSC Adv.* **2014**, *4*, 29735.

(9) Li, P.; Zhao, Y.; Yao, L.; Nie, H.; Zhang, M. *Sensors Actuators B Chem.* **2014**, *191*, 332.

(10) Catalan, J. *J. Phys. Chem. A* **2007**, *111*, 8774.

(11) Che, Y.; Gross, D. E.; Huang, H.; Yang, D.; Yang, X.; Discekici, E.; Xue, Z.; Zhao, H.; Moore, J. S.; Zang, L. *J. Am. Chem. Soc.* **2012**, *134*, 4978.

(12) Zhang, X.; Wu, Y.; Ji, S.; Guo, H.; Song, P.; Han, K.; Wu, W.; Wu, W.; James, T. D.; Zhao, J. *J. Org. Chem.* **2010**, *75*, 2578.

(13) Zhang, X.; Chi, L.; Ji, S.; Wu, Y.; Song, P.; Han, K.; Guo, H.; James, T. D.; Zhao, J. *J. Am. Chem. Soc.* **2009**, *131*, 17452.

(14) Mahapatra, A. K.; Roy, J.; Sahoo, P.; Mukhopadhyay, S. K.; Mukhopadhyay, A. R.; Mandal, D. *Bioorg. Med. Chem. Lett.* **2012**, *22*, 5379.

(15) Xu, D.; Liu, X.; Lu, R.; Xue, P.; Zhang, X.; Zhou, H.; Jia, *J. Org. Biomol. Chem.* **2011**, *9*, 1523.

(16) Grewer, D. M.; Young, R. F.; Whittal, R. M.; Fedorak, P. M. *Sci. Total Environ.* **2010**, *408*, 5997.

(17) Lu, W.; Ewanchuk, A.; Perez-Estrada, L.; Sego, D.; Ulrich, A. *J. Environ. Sci. Health. A. Tox. Hazard. Subst. Environ. Eng.* **2013**, *48*, 429.

(18) Yen, T.-W.; Marsh, W. P.; MacKinnon, M. D.; Fedorak, P. M. *J. Chromatogr. A* **2004**, *1033*, 83.

(19) Obtained from the RAMP monitoring activities; overview of 2008 activities.

(20) Ding, Z.; Zhao, Q.; Xing, R.; Wang, X.; Ding, J.; Wang, L.; Han, Y. *J. Mater. Chem. C* **2013**, *1*, 786.

(21) Suresh Kumar, H. M.; Kunabenchi, R. S.; Biradar, J. S.; Math, N. N.; Kadadevarmath, J. S.; Inamdar, S. R. *J. Lumin.* **2006**, *116*, 35.

(22) Murphy, C.; Zhang, Y.; Troxler, T. *J. Phys. Chem. B.* **2004**, *17*, 1537.

(23) Xing, C.; Yuan, H.; Xu, S.; An, H.; Niu, R.; Zhan, Y. *ACS Appl. Mater. Interfaces* **2014**, *6*, 9601.

(24) Li, Z.; Lu, J.; Li, S.; Qin, S.; Qin, Y. *Adv. Mater.* **2012**, *24*, 6053.

(25) McQuade, D. T.; Pullen, A. E.; Swager, T. M. *Chem. Rev.* **2000**, *100*, 2537.

(26) Toal, S. J.; Trogler, W. C. *J. Mater. Chem.* **2006**, *16*, 2871.

(27) Yang, J.; Swager, T. M. *J. Am. Chem. Soc.* **1998**, *78*, 5321.

(28) Kannel, P. R.; Gan, T. Y. *J. Environ. Sci. Health. A. Tox. Hazard. Subst. Environ. Eng.* **2012**, *47*, 1.

(29) Eicher, T.; Hauptmann, S.; Speicher, A. *The Chemistry of Heterocycles: Structure, Reactions, Synthesis, and Applications*; 3rd ed.; Wiley-VCH, **2012**; p. 118.

Chapter 4:

Preparation of a family of alkyl-substituted carbazole macrocycles and their self-assembly

4.1. Preparation of alkyl substituted carbazole macrocycles

4.1.1. Introduction

Macrocycles have been investigated as interesting intermediates between polymers and small molecules. From crown ethers,[1] to catenanes,[2] to aryl-based shape-persistent macrocycles (SPMs),[3] these molecules offer many of the same benefits of high molecular weight polymers such as good solution processability and consistent physical properties. Macrocycles also possess some of the beneficial properties of small molecules, for example their monodispersity promotes the possibility of predicting material properties,[4, 5] and ease characterization. One of the primary benefits of a macrocyclic system when compared to other small molecular scaffolds is cyclic systems can confine a large density of functional groups into the small region of space that the molecule occupies.[4] This functional group versatility, combined with the structural rigidity common to these molecules also allows control over directionality of the functional groups (as mentioned in Chapter 1).[4, 6] Together, these features can provide macrocycles with a propensity to form lock-in-key assemblies in which there is built-in dimensionality of self-assembly,[7, 8] dynamic response to changes in chemical environment,[9, 10] and even guest-host type assemblies.[10-12] Combining these properties has made macrocycles attractive targets for components in the construction of nanoscale motors,[13-15] and machines,[16] as well as sensors[17] and molecular switches.[18,19]

Historically macrocycle synthesis has been considered highly sensitive to experimental conditions; even under the most rigorous experimental control

preparations tend to generate moderate to low yields, and because of their similar properties the target products are difficult to isolate from linear contaminants.[8] Synthetic strategies that typically promote macrocycle synthesis include highly dilute conditions,[20] kinetic control over cyclization,[3] slow addition of the monomers to the reactant solution,[3, 21] and templated macrocycle formation.[22] All of these methods suffer from poor atom economy and require substantial "hands-on" time to achieve the desired product.

In efforts to improve the overall efficiency of macrocycle synthesis, much work has been focused on exploiting molecular structure (*e.g.*, bulky substituents and linkage isomerism) for the formation of small macrocycles; of particular note are reports of systems exhibiting shape persistent properties.[6, 23] Researchers working with phenyl-ethynyl and carbazyl-ethynyl monomers have made great strides forward using alkyne metathesis to realize macrocycles.[23-25] Generally, this methodology has afforded researchers exquisite control over macrocycle size and shape,[3] and has resulted in the development of a new family of compounds with intriguing solution dynamics,[26] and an inherent propensity for self-assembly when exposed to appropriate conditions.[27] While this relatively young family of materials has proven to be scientifically interesting, syntheses remain cumbersome, often involving multiple steps, and can result in very low overall yields.

A short report in 2003 noted that polymerization of an N-alkylated 3,6-dibromocarbazole yielded substantial quantities of cyclic oligomers when performed under dilute conditions and pointed to the potential of these types of

materials.[20] The authors suggested the optical and electronic properties of this macrocycle were similar to the parent linear polymer, however there was little to suggest the macrocycle was independently interesting from the parent linear polymer. Given recent interest in shape-persistent macrocycles and the relative simplicity with which both N-alkyl functionalization and C-C coupling can be performed to generate the cyclic structure, we have prepared a family of all-carbazole tetramers bearing N-alkyl functionalities of varied chain lengths and sizes with the intent of investigating their properties and self-assembly behaviour.

4.1.2. Experimental

4.1.2.1. Materials and Instrumentation

NMR spectroscopy was performed in an appropriate solvent using an Agilent/Varian Dual Cold Probe 500 MHz spectrometer. Low and high resolution mass spectra were acquired using an AB Sciex Voyager Elite MALDI-TOF spectrometer and Bruker 9.4T Apex-Qe MALDI-FTICR instrument, respectively using trans-2-[3-(4-tert-butylphenyl)-2-methyl-2-propenylidene]malononitrile (DCTB) matrix. All toluene used in the synthesis was distilled over Na/benzophenone immediately prior to use. Photoluminescence (PL) and excitation (PLE) spectra were recorded in a quartz cuvette using a Cary Eclipse fluorometer at a scan rate of 2 nm per second. 3,6-Dibromocarbazole, 2,2′-bipyridyl, 1,5-cyclooctadiene, alkyl bromides, and potassium carbonate were purchased from Sigma-Aldrich, bis(1,5-

cyclooctadiene)nickel(0) was purchased from Strem Chemicals, and all were used as received.

4.1.2.2. Monomer synthesis

Preparation of N-alkyl 3,6- dibromocarbazoles:

A general procedure is included for compound **2a**, **2b**-**2g** were prepared using identical procedures, as previously reported by Cui *et al.*,[28] with any differences in the syntheses noted in the individual subsection for that compound.

Representative synthesis of 3,6-dibromo-N-butyl carbazole (2a).[29] 3,6-Dibromocarbazole (2.0 g, 6.2 mmol), and potassium carbonate (0.94 g, 6.8 mmol) were dissolved in 20 mL DMF under ambient conditions forming an orange solution. 1-Bromobutane (0.74 ml, 6.8 mmol) was added to the solution resulting in an immediate colour change. The resulting pink solution was stirred at room temperature for 4 days, yielding a white solid on the inner surface of the flask. The solid and solution were poured into 400 mL of distilled water and a pink crude solid was isolated by vacuum filtration. The product was isolated from unreacted carbazole using column chromatography over silica gel (4:1 hexane:ethylacetate, R_F = 0.4) as 1.04 g white solid (44 % yield). ^{1}H-NMR ($CDCl_3$, 27 °C, 500 MHz); δ (ppm) = 8.13 (d, J_{HH}= 2.0 Hz, 2 H, Ar-H 2,7), 7.56 (dd, J_{HH}= 2.0 Hz, 8.5 Hz, 2 H, Ar-H 4,5), 7.26 (d, J_{HH}= 8.5 Hz, 2 H, Ar-H 1,8), 4.23 (t, J_{HH}= 7.5 Hz, 2 H, NC-H), 1.85-1.79 (m, 2 H, HC-H), 1.40- 1.35 (m, 2 H, HC-H), 0.96 (t, J_{HH}= 7.5, 3 H, H_2C-H). ^{13}C-NMR ($CDCl_3$, 27 °C, 125 MHz); δ (ppm) = 139.3 (C3, C6), 128.8 (C1′, C8′), 123.4 (C1, C8), 123.2 (C4, C5), 111.9

(C2, C7), 110.2 (C4′, C5′), 43.1 (N-CH_2), 31.0 (-CH_2-), 20.6 (-CH_2-), 14.1 (-CH_3). HRMS (m/z); $[M]^+$ calculated for $C_{16}H_{15}N^{79}Br_2$, 378.95712; found, 378.95740; error (ppm), -0.7. Elemental Analysis: calculated: 50.43 %C, 3.97 %H, and 3.68% N; found: 51.14 %C, 4.15 %H, and 3.79 %N.

3,6-dibromo-N-hexyl carbazole (2b).[30] 1-Bromohexane (0.91 mL, 6.5 mmol). Recrystallized from boiling ethanol. 0.92 g white solid (43 % yield). ^{1}H-NMR (toluene-d8, 27 °C, 500 MHz); δ (ppm) = 7.88 (d, J_{HH}= 1.5 Hz, 2 H, Ar-H 2,7), 7.43 (dd, J_{HH}= 1.5 Hz, 9 Hz, 2 H, Ar-H 4,5), 6.74 (d, J_{HH}= 9 Hz, 2 H, Ar-H 1,8), 3.57 (t, J_{HH}= 7.3 Hz, 2 H, NC-H), 1.38 (pentet, J_{HH}= 2.0 Hz, 2 H, HC-H), 1.15-1.00 (m, 6 H, HC-H), 0.83 (t, J_{HH}= 7.5 Hz, 3 H, H_2C-H). ^{13}C-NMR (toluene-d8, 27 °C, 125 MHz); δ (ppm) = 139.2 (C3, C6), 128.9 (C1′, C8′), 123.5 (C1, C8), 123.4 (C4′, C5′), 112.0 (C4, C5), 110.0 (C2, C7), 42.6 (N-CH_2), 31.4 (-CH_2-), 28.6 (-CH_2-), 26.7 (-CH_2-), 22.5 (-CH_2-), 13.8 (-CH_3). HRMS (m/z); $[M]^+$ calculated for $C_{18}H_{19}N^{79}Br_2$, 406.98843; found 406.98946; error (ppm), -1.2. Elemental Analysis: calculated: 52.84 %C, 4.68 %H, and 3.42 % N; found: 52.86 %C, 4.70 %H, and 3.43 %N.

3,6-dibromo-N-octyl carbazole (2c).[31] 1-Bromooctane (1.6 mL, 9.8 mmol).2:1 hexane: ethyl acetate, R_F = 0.8, 0.93 g white solid (41 % yield). ^{1}H-NMR, (acetone-d6, 27 °C, 500 MHz); δ (ppm) = 8.36 (d, J_{HH}= 2 Hz, 2 H, Ar-H 2,7), 7.59 (dd, J_{HH}= 2.0 Hz, 8.5 Hz, 2 H, Ar-H 4,5), 7.54 (d, J_{HH}= 8.5 Hz, 2 H, Ar-H 1,8), 4.40 (t, J_{HH}= 7.0 Hz, 2 H, NC-H), 1.84 (pentet, J_{HH}= 7 Hz, 2 H, HC-H), 1.36- 1.19 (m, 10 H, HC-H), 0.83 (t, J_{HH}= 7 Hz, 3 H, H_2C-H). ^{13}C-NMR, (acetone-d6, 27 °C, 125 MHz); δ (ppm) = 139.5 (C3, C6), 128.9 (C1′, C8′),

123.4 (C1, C8), 123.3 (C4′, C5′), 111.5 (C4, C5), 111.2 (C2, C7), 42.9 (N-CH_2), 31.6 (-CH_2-), 29.4 (-CH_2-), 29.0 (-CH_2-), 28.5 (-CH_2-), 26.8 (-CH_2-), 22.3 (-CH_2-), 13.4 (-CH_3). HRMS (m/z); $[M]^+$ calculated for $C_{20}H_{23}N^{79}Br_2$, 435.01971; found, $C_{20}H_{23}N^{79}Br_2$, 435.01882; error (ppm), 2.1. Elemental Analysis: calculated: 54.94 %C, 5.30 %H, and 3.20 % N; found: 54.91 %C, 5.30 %H, and 3.23 %N.

3,6-dibromo-N-decyl carbazole (2d).[29] 1-Bromodecane (1.4 mL, 6.7 mmol). Recrystallized from boiling ethanol, 0.529 g white solid (19 % yield). ^{1}H-NMR ($CDCl_3$, 27 °C, 500 MHz); δ (ppm) =: 8.17 (d, J_{HH}= 2.0 Hz, 2 H, Ar-H 2,7), 7.58 (dd, J_{HH}= 2.0 Hz, 8.5 Hz, 2 H, Ar-H 4,5), 7.30 (d, J_{HH}= 8.5, 2 H, Ar-H 1,8), 4.27 (t, J_{HH} = 6.0 Hz, 2 H, NC-H), 1.87-1.83 (m, 2 H, HC-H), 1.36-1.27 (m, 4 H, HC-H), 0.90 (t, J_{HH}= 7 Hz, 3 H, H_2C-H). ^{13}C-NMR ($CDCl_3$, 27 °C, 125 MHz); δ (ppm) = 139.3 (C3, C6), 129.0 (C1′, C8′), 123.5 (C1, C8), 123.3 (C4′, C5′), 112.0 (C4, C5), 110.4 (C2, C7), 43.4 (N-CH_2), 31.8 (-CH_2-), 29.5 (-CH_2-), 29.5 (-CH_2-), 29.3 (-CH_2-), 29.2 (-CH_2-), 28.9 (-CH_2-), 27.2 (-CH_2-), 22.7 (-CH_2-), 14.1 (-CH_3). HRMS (m/z); $[M]^+$ calculated for $C_{22}H_{27}N^{79}Br_2$, 463.05103; found, 463.05080; error (ppm), 0.5. Elemental Analysis: calculated: 56.79 %C, 5.85 %H, and 3.01 % N; found: 56.44 %C, 5.80 %H, and 3.06 %N.

3,6-dibromo-N-dodecyl carbazole (2e).[32] 1-Bromododecane (1.6 mL, 6.7 mmol). Recrystallized from boiling ethanol, 0.92 g white solid (30 % yield). ^{1}H-NMR ($CDCl_3$, 27 °C, 500 MHz); δ (ppm) = 8.16 (d, J_{HH}= 2.0 Hz, 2 H, Ar-H 2,7), 7.58 (dd, J_{HH}= 2.0 Hz, 8.5 Hz, 2 H, Ar-H 4,5), 7.29 (d, J_{HH}= 8.5 Hz, 2 H, Ar-H 1,8), 4.26 (t, J_{HH}= 7.0 Hz, 2 H, NC-H), 1.87-1.83 (m, 2 H, HC-H), 1.36-

1.27 (m, 6 H, HC-H), 0.90 (t, J_{HH}= 7.0 Hz, 3 H, H_2C-H). ^{13}C-NMR ($CDCl_3$, 27 °C, 125 MHz); δ (ppm) = 139.3 (C3, C6), 129.0 (C1′, C8′), 123.5 (C1, C8), 123.3 (C4′, C5′), 112.0 (C4, C5), 110.4 (C2, C7), 43.4 (N-CH_2), 31.9 (-CH_2-), 29.6 (-CH_2-), 29.5 (-CH_2-), 29.5 (-CH_2-), 29.3 (-CH_2-), 28.9 (-CH_2-), 27.2 (-CH_2-), 22.7 (-CH_2-), 14.1 (-CH_3). HRMS (m/z); $[M]^+$ calculated for $C_{24}H_{31}N^{79}Br_2$ 491.08234; found, 491.08220; error (ppm), 0.3. Elemental Analysis: calculated: 58.43 %C, 6.33 %H, and 2.84 % N; found: 58.45 %C, 6.30 %H, and 2.77 %N.

3,6-dibromo-N-isopropyl carbazole (2f). [28] 2-Bromopropane (2.3 mL, 24 mmol). 8:1 hexane:ethyl acetate, R_F= 0.7, 1.18 g white solid (52 % yield). ^{1}H-NMR (toluene-d8, 27 °C, 500 MHz); δ (ppm) = 7.88 (d, J_{HH}= 2.0 Hz, 2 H, Ar-H 2,7), 7.39 (dd, J_{HH}= 2.0 Hz, 8.5 Hz, 2 H, Ar-H 4,5), 6.82 (d, J_{HH}= 8.5 Hz, 2 H, Ar-H 1,8), 4.21 (septet, J_{HH}= 7.0 Hz, 1 H, NC-H), 1.14 (d, J_{HH}= 7.0 Hz, 6 H, H_2C-H). ^{13}C-NMR (toluene-d8, 27 °C, 125 MHz); δ (ppm) = 138.2 (C3, C6), 124.2 (C1′, C8′), 125.0 (C1, C8), 123.5 (C4′, C5′), 111.9 (C4, C5), 111.2 (C2, C7), 46.6 (N-CH-), 20.5 (-CH_3). HRMS (m/z); $[M]^+$ calculated for $C_{15}H_{13}N^{79}Br_2$, 368.93738; found, 368.93869; error (ppm), -1.4. Elemental Analysis: calculated: 49.08 %C, 3.57 %H, and 3.82 % N; found: 49.01 %C, 3.64 %H, and 3.71 %N.

3,6-dibromo-N-(2-ethylhexyl) carbazole (2g).[20] 1-Bromo-2-ethylhexane (2.2 mL, 12 mmol, KOH (0.71 g, 12 mmol). 11:1 hexane:ethyl acetate, R_F= 0.6, 0.89 g colourless gel (33 % yield). ^{1}H-NMR ($CDCl_3$, 27 °C, 500 MHz); δ (ppm) = 8.15 (d, J_{HH}= 2.0 Hz, 2 H, Ar-H 2,7), 7.56 (dd, J_{HH}= 2.0 Hz, 9.0 Hz, 2 H, Ar-H 4,5), 7.26 (d, J_{HH}= 9.0 Hz, 2 H, Ar-H 1,8), 4.11 (dd, J_{HH}= 3.0 Hz, 8.0 Hz, 2 H, NC-H), 2.03-1.99 (m, 1 H, C-H), 1.57-1.25 (m, 8 H, HC-H), 0.97- 0.87 (m, 6 H,

H_2C-H). ^{13}C-NMR ($CDCl_3$, 27 °C, 500 MHz); δ (ppm) = 140.X (C3, C6), 129.X (C1′, C8′), 123.X (C1, C8), 123.X (C4′, C5′), 112.X (C4, C5), 111.X (C2, C7), 48.X (N-CH_2), 39.X (-CH_2-), 31.X (-CH_2-), 30.X (-CH_2-), 24.X (-CH_2-), 23.X (-CH_2-), 14.X (-CH_2-), 11.X (-CH_3). HRMS (m/z); $[M]^+$ calculated for $C_{20}H_{23}N^{79}Br_2$, 435.01971; found, 435.01947; error (ppm), 0.6.

4.1.2.3. Tetramer syntheses

Preparation of cyclo-3,6-tetracarbazoles:

A general procedure is included for compound **3a**, **3b-3g** were prepared using identical procedures as developed by Ostrauskaite *et al.*, [20] with any differences in the syntheses noted in the individual subsection for that compound. All syntheses were performed using standard Schenck techniques unless otherwise noted.

Representative synthesis of cyclo-3,6- tetra-N-isopropylcarbazole (3f). In an oven-dried (140 – 200 °C) Schlenk flask under Ar atmosphere, 3,6-dibromo-N-isopropylcarbazole (0.361 g, 10.0 mmol) was dissolved in 50 mL of anhydrous DMF to form a clear colourless solution. The catalyst was prepared in a nitrogen filled glove box; a Schlenk flask was charged with bis(1,5- cyclooctadiene) nickel (0.60 g, 22 mmol), 2,2′-bipyridyl (0.34 g, 22 mmol), 1,5-cyclooctadiene (0.28 mL, 22 mmol) and 60 mL toluene. The catalyst mixture was removed from the glovebox, attached to a double manifold and stirred in an Ar atmosphere at 80 °C for 30 minutes, after which the monomer solution was added to the flask containing the catalyst mixture via canula transfer. The resulting purple/black

solution was stirred at 70 °C for 4 days then poured into 300 mL of a 1:1:1 mixture of methanol, acetone and 1M HCl. The crude tetramer was extracted into toluene, washed with water, then brine, and dried over $MgSO_4$ and filtered to remove the solid. The filtrate was evaporated on a Rotovap and the solid was dissolved in a minimum volume of THF then precipitated upon addition of 200 mL methanol. The tetramer was isolated upon extraction into hot acetone followed by gravity filtration. The acetone was evaporated from the filtrate to yield the tetramer as a beige solid (0.104 g; 51 % yield). ^{1}H-NMR (toluene-d8, 27 °C, 500 MHz); δ (ppm) = 8.96 (d, J_{HH}= 1.5 Hz, 8 H, Ar-H 2,7), 8.05 (dd, J_{HH}= 1.5 Hz, 8.5 Hz, 8 H, Ar-H 4,5), 7.49 (d, J_{HH}= 8.5 Hz, 8 H, Ar-H 1,8), 4.70 (septet, J_{HH}= 7.0 Hz, 8 H, NC-H), 1.51 (d, J_{HH}= 7.0 Hz, 24 H, H_2C-H). ^{13}C-NMR (toluene-d8, 27 °C, 125 MHz); δ (ppm) = 145.2 (C1′, C8′), 135.1(C1, C8), 132.9 (C3, C6), 119.6 (C4′, C5′), 119.4 (C4, C5), 110.2 (C2, C7), 46.8 (N-CH-), 25.5 (-CH_3). HRMS (m/z); $[M]^+$ calculated for $C_{60}H_{52}N_4$, 828.419, found, 828.418; error (ppm),-0.5. Elemental Analysis: calculated: 86.92 %C, 6.32 %H, and 6.76 % N; found: 84.86 %C, 7.07 %H, and 5.93 %N.

Cyclo-3,6- tetra-N-butyl carbazole (3a). 3,6-Dibromo-N-butyl carbazole (0.190 g, 5.0 mmol), bis(1,5-cyclooctadiene) nickel (0.300 g, 11 mmol), 2,2′-bipyridyl (0.170 g, 11 mmol), 1,5-cyclooctadiene (0.14 mL, 11 mmol) and 25 mL DMF, 30 mL toluene. 0.097 g beige solid (47 % yield). ^{1}H NMR ($CDCl_3$, 27 °C, 500 MHz); δ (ppm) = 8.58 (m, 8H, Ar-H 2,7), 7.88 (m, 8H, Ar-H 4,5), 7.50 (m, 8H, Ar-H 1,8), 4.37 (m, 8H, NC-H), 1.97-1.81 (m, 8H, HC-H), 1.50-1.37 (m, 8H, HC-H), 1.01-0.86 (m, 12H, H_2C-H) . ^{13}C NMR (CD_2Cl_2, 27 °C, 125 MHz);

δ (ppm) = 135.3 (C1′, C8′), 132.2 (C1, C8), 128.9 (C3, C6), 125.3 (C4′, C5′), 114.8 (C4, C5), 105.1 (C2, C7), 37.6 (N-CH_2), 26.3 (-CH_2-), 10.1 (-CH_3). .HRMS (m/z); $[M]^+$ calculated for $C_{64}H_{60}N_4$; 884.48180, found; 884.47940; error (ppm), -0.40. Elemental Analysis: calculated: 86.84 %C, 6.83 %H, and 6.33 % N; found: 83.25 %C, 6.62 %H, and 6.10 %N.

Cyclo-3,6-tetra-N-hexylcarbazole (3b). 3,6-Dibromo-N-hexylcarbazole (0.405 g, 1.0 mmol), 0.134 g beige solid (54 % yield). ^{1}H NMR (CD_2Cl_2, 27 °C, 500 MHz); δ (ppm) = 8.96 (s, 8 H, Ar-H 2,7), 7.94 (d, J_{HH}= 8 Hz, 8 H, Ar-H 4,5), 7.55 (d, J_{HH}= 8. Hz, 8 H, Ar-H 1,8), 4.34 (s, 8 H, NC-H), 1.97 (m, 16 H, HC-H), 1.41- 1.38 (m, 40 H, HC-H), 0.97- 0.93 (m, 12 H, H_2C-H). ^{13}C NMR (CD_2Cl_2, 27 °C, 125 MHz); δ (ppm) = 140.4 (C1′, C8′), 134.4 (C1, C8), 127.5 (C3, C6), 123.7 (C4′, C5′), 119.3 (C4, C5), 109.4 (C2, C7), 43.7 (N-CH_2), 32.0 (-CH_2-), 30.5 (-CH_2-), 29.5 (-CH_2-), 27.4 (-CH_2-), 23.0 (-CH_2-), 14.2 (-CH_3). HRMS (m/z); $[M]^+$ calculated for $C_{72}H_{76}N_4$; 996.60699, found, 996.60619; error (ppm), 0.26. Elemental Analysis: calculated: 86.70 %C, 7.68 %H, 5.62 % N; found: 85.75 %C, 7.69 %H, and 5.47 %N.

Cyclo-3,6-tetra-N-octylcarbazole (3c). 3,6-Dibromo-N-octylcarbazole (0.433 g, 1.0 mmol), 0.176 g beige solid (63 % yield). ^{1}H NMR (toluene-d8, 27 °C, 500 MHz); δ (ppm) = 8.99 (d, J_{HH}= 2.0 Hz, 8 H, Ar-H 2,7), 8.08 (dd, J_{HH}= 2.0 Hz, 8.5 Hz, 8 H, Ar-H 4,5), 7.42 (d, J_{HH}= 8.5 Hz, 8 H, Ar-H 1,8), 4.07-4.01 (m, 8 H, NC-H), 1.80- 1.72 (m, 16 H, HC-H), 1.29- 1.16 (m, 48 H, HC-H), 0.93- 0.88 (m, 12 H, H_2C-H). ^{13}C NMR (toluene-d8, 27 °C, 125 MHz); δ (ppm) = 140.4 (C1′, C8′), 133.1 (C1, C8), 128.9 (C3, C6), 127.8 (C4′, C5′), 119.6 (C4, C5), 108.9

(C2, C7), 43.0 (N-CH_2), 31.9 (-CH_2-), 29.5 (-CH_2-), 29.3 (-CH_2-), 29.0 (-CH_2-), 27.3 (-CH_2-), 22.7 (-CH_2-), 14.0 (-CH_3). HRMS (m/z); $[M]^+$ calculated for $C_{80}H_{92}N_4$; 1108.73220, found; 1108.73108; error (ppm), 0.51. Elemental Analysis: calculated: 86.594 %C, 8.357 %H, 5.049 % N; found: 83.8333 %C, 8.2712 %H, 4.8237 %N.

Cyclo-3,6-tetra-N-decylcarbazole (3d). 3,6-Dibromo-N-decylcarbazole (0.464, 1.0 mmol), 0.219 g beige solid (72 % yield). ^{1}H NMR (CD_2Cl_2, 27 °C, 500 MHz); δ (ppm) = 8.85 (s, 8 H, Ar-H 2,7), 7.92 (d, J_{HH}= 3.5 Hz, 8 H, Ar-H 4,5), 7.53 (d, J_{HH}= 3.5 Hz, 8 H, Ar-H 1,8), 4.38 (t, J_{HH}= 7.0 Hz, 8 H, NC-H), 1.98-1.93 (m, 8 H, HC-H), 1.48-1.34 (m, 32 H, HC-H),1.27 (m, 32 H, HC-H), 0.84 (t, J_{HH}= 7.0 Hz, 12 H, H_2C-H),. ^{13}C NMR (CD_2Cl_2, 27 °C, 125 MHz); δ (ppm) = 140.6 (C1', C8'), 132.9 (C1, C8), 124.8 (C3, C6), 124.3 (C4', C5'), 119.0 (C4, C5), 109.6 (C2, C7), 43.8 (N-CH_2), 32.3 (-CH_2-), 30.1 (-CH_2-), 30.0 (-CH_2-), 29.9 (-CH_2-), 29.8 (-CH_2-), 29.5 (-CH_2-), 27.7 (-CH_2-), 23.1 (-CH_2-), 14.3 (-CH_3). HRMS (m/z); $[M]^+$ calculated for $C_{88}H_{108}N_4$, 1220.85740; found, 1220.85685; error (ppm), 1.24. Elemental Analysis: calculated: 86.51 %C, 8.91 %H, 4.58 % N; found: 85.69 %C, 8.86 %H, and 4.57 %N.

Cyclo-3,6-tetra-N-dodecylcarbazole (3e). 3,6-Dibromo-N-dodecylcarbazole (0.488 g, 1.0 mmol), 0.197 g beige solid (60 % yield). ^{1}H NMR (CD_2Cl_2, 27 °C, 500 MHz); δ (ppm) = 8.86 (d, J_{HH}= 1.5 Hz, 8 H, Ar-H 2,7), 7.93 (dd, J_{HH}= 1.5 Hz, 8.5 Hz, 8 H, Ar-H 4,5), 7.54 (d, J_{HH}= 8.5 Hz, 8 H, Ar-H 1,8), 4.40-4.36 (m, 16 H, NC-H),1.93-1.98 (m, 16 H, HC-H), 1.48-1.17 (m, 64 H, HC-H), 0.91-0.86 (m, 12 H, H_2C-H). ^{13}C NMR (CD_2Cl_2, 27 °C, 125 MHz); δ (ppm) = 140.6 (C1′,

C8′), 132.9 (C1, C8), 124.8 (C3, C6), 124.3 (C4′, C5′), 119.0 (C4, C5), 109.6 (C2, C7), 43.8 (N-CH_2), 32.3 (-CH_2-), 30.0 (-CH_2-), 30.0 (-CH_2-), 29.9 (-CH_2-), 29.8 (-CH_2-), 29.7 (-CH_2-), 29.5 (-CH_2-), 29.4 (-CH_2-), 27.7 (-CH_2-), 23.1 (-CH_2-), 14.3 (-CH_3). HRMS (m/z); $[M]^+$ calculated for $C_{96}H_{124}N_4$, 1332.98260 ; found, 1332.96205; error (ppm), -1.49. Elemental Analysis: calculated: 86.43 %C, 9.37 %H, and 4.20 % N; found: 85.67 %C, 9.45 %H, and 4.18 %N.

Cyclo-3,6-tetra-N-2-ethylhexylcarbazole (3g). 3,6-Dibromo-N-2-ethylhexyl carbazole (0.433 g, 1.0 mmol), bis(1,5- cyclooctadiene)Nickel (0) (0.300 g, 2.18 mmol), 2,2'-bipyridyl (0.170 g, 2.18 mmol), 1,5-cyclooctadiene (0.14 mL, 2.18 mmol) and 25 mL DMF, 30 mL toluene. 0.107 g beige solid (47 % yield). ^{1}H NMR (CD_2Cl_2, 27 °C, 500 MHz); δ (ppm) = 8.53 (s, 8H, Ar-H 2,7), 7.86 (s, 8H, Ar-H 4,5), 7.40 (s, 8H, Ar-H 1,8), 4.03 (s, 8H, NC-H), 2.06 (s, 4H, HC-H), 1.32 (s, 32H, HC-H), 0.85 (s, 24H, H_2C-H) . ^{13}C NMR (CD_2Cl_2, 27 °C, 125 MHz); δ (ppm) = 139.3 (C1′, C8′), 132.0 (C1, C8), 124.3 (C3, C6), 122.6 (C4′, C5′), 117.7 (C4, C5), 108.2 (C2, C7), 46.3 (N-CH_2), 38.4 (-CH_2-), 29.9 (-CH_2-), 27.8 (-CH_2-), 23.3 (-CH_2-), 22.1 (-CH_2-), 13.1 (-CH_2-), 9.9 (-CH_3). HRMS (m/z); $[M]^+$ calculated for $C_{80}H_{92}N_4$; 1108.73220, found; 1108.73093; error (ppm), 0.19.

4.1.2.4. Evaluation of Photoluminescence Quantum Yields

Photoluminescence quantum yields were determined as discussed in Chapter 2 using the method of Williams *et al.*. Briefly, the integrated fluorescence intensity was plotted against the absorbance of the tetramers in THF.[33] Anthracene was chosen as an appropriate standard given the similarities

in the range of emission and absorption wavelengths to all of the tetramer samples under study. Standard solutions of anthracene were prepared using ethanol as a solvent, and as such, the refractive indices (η) were included in the calculation of the quantum yields as in equation (1):

$$\Phi_x = \Phi_{st}\left(\frac{m_x}{m_{st}}\right)\left(\frac{\eta_x^2}{\eta_{st}^2}\right) \quad (1)$$

Where the subscripts *x* and *st* refer to the sample and standard, respectively. Other parameters include: quantum yield (Φ), *m* is the slope of the line of best fit found from plotting the integral of the fluorescence spectra versus the absorption at 356 nm, and η is the refractive index of solvent. The quantum yield of anthracene used, Φ_{st}, was the value of 0.27 reported by Melhuish *et al.*, and the refractive indices for ethanol, η_{st} is 1.359 and for THF is 1.405,[34-36] for an example of this calculation please refer to Appendix 1.

4.1.3. Results and discussion

4.1.3.1. Preparation of monomers and oligomers

Alkylated carbazole monomers (**2a-g**) were prepared through deprotonation of the amine under basic conditions at room temperature. The corresponding alkyl halides were then employed as electrophiles to produce N-alkylated 3,6-dibromocarbazoles with alkyl groups ranging from 3 to 8 carbons in length (Scheme 3-1, and Table 3-1) in moderate yield. The alkylated products

were isolated from unreacted carbazole *via* column chromatography with the exception of compounds **2e** and **2f** that were recrystallized.

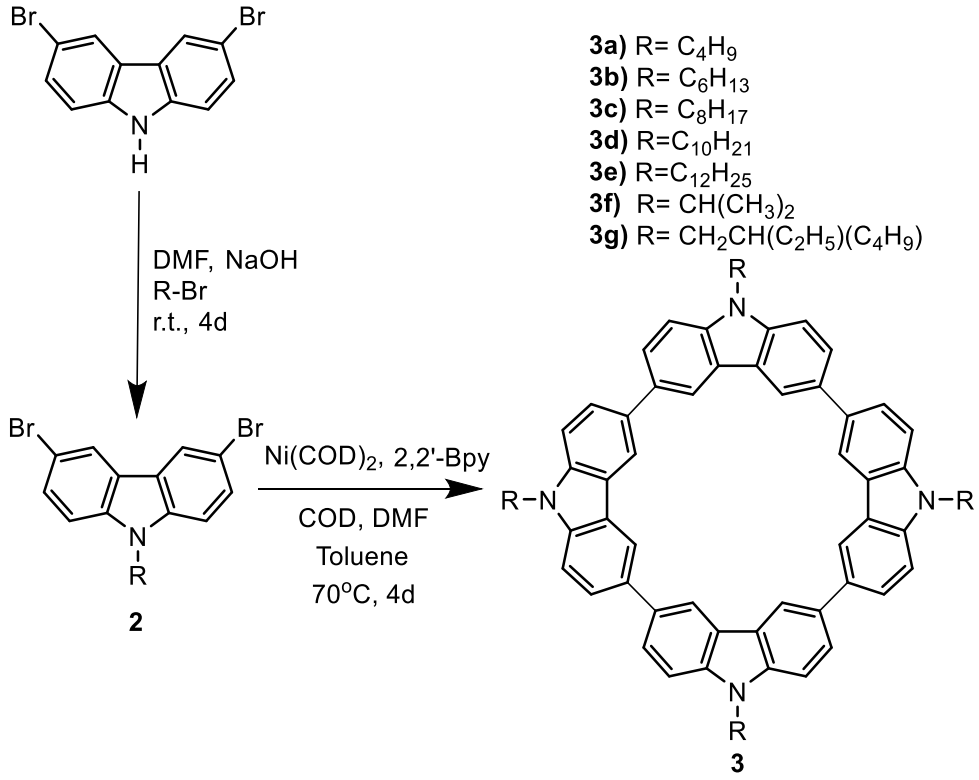

Figure 4-1. Synthetic methodology used to prepare compounds **2a**-**g** and **3a**-**g**.

Functionalization of the carbazole structural unit was confirmed using ^{1}H-NMR and IR spectroscopies; the absence of the characteristic signal from a carbazole N-H proton at 8.05 ppm, and amine N-H stretching *ca.* 3200 cm^{-1} are consistent with no remaining unreacted **1**. The presence of the alkyl substituents was confirmed by characteristic resonances in the upfield region of the ^{1}H-NMR spectra (*i.e.*, 2.0-0.8 ppm) as well as a shift of the resonance attributed to protons bonded to C9′ of the alkyl substituent (Figure 4-1) from *ca.* 3.4 ppm for bromoalkanes to *ca.* 4.2 ppm following formation of the C-N bond (See Appendix 2 for further details). Functionalization of the N-position with t-butyl

bromide was likely unsuccessful because N-alkylations proceed through an S_N2 mechanism, which involves nucleophilic attack on the alkyl bromide through the C-Br antibonding orbital, which in the case of tBu-Br is sterically hindered.[37]

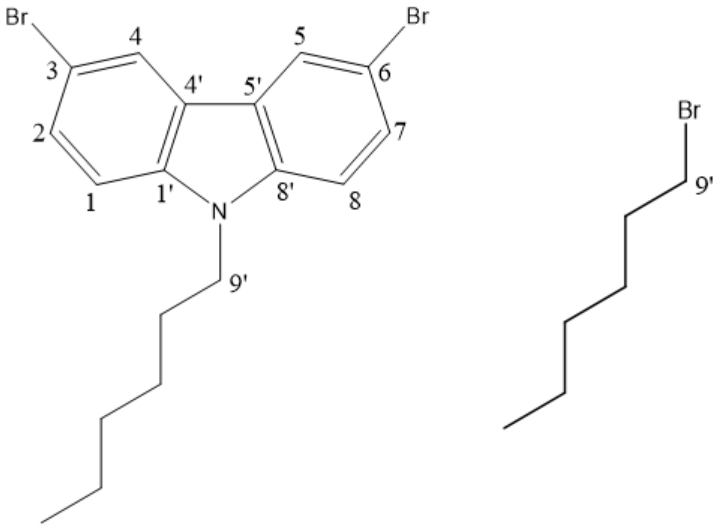

Figure 4-2. Numbering convention for the N-alkylated carbazole monomers prepared (left) and their parent alkyl bromides (right) using **2b** as an example.

Compounds **2a-2g** were subsequently coupled to form tetramers using Ni(Bpy)(COD) in an inert atmosphere; the crude product consisting of linear and cyclic oligomers was isolated as a solid upon addition of methanol.[20] The product was purified upon extraction with methanol acetone and HCl followed by isolation of the tetramer upon extraction with hot acetone, which was evaporated to yield yellow/beige solid on a 100-200 mg scale. The extracts were confirmed to be cyclic tetramers (**3a-3g**, Table 3-1) using MALDI-TOF spectrometry which reveals single high intensity peaks at m/z that correspond to the molecular ion [M^+] of the target cyclic tetramer for **3a-g** (see Appendix 2).

High resolution MALDI-FTICR was employed on the fragments of interest and confirmed that the m/z ratio was consistent with the molecular formula of compounds **3a-g** (see Appendix 2).

R	Monomer	% Yield	Tetramer	% Yield
C_4H_9	**2a**	44	**3a**	47
C_6H_{13}	**2b**	43	**3b**	54
C_8H_{17}	**2c**	41	**3c**	63
$C_{10}H_{21}$	**2d**	19	**3d**	72
$C_{12}H_{25}$	**2e**	30	**3e**	60
$CH(CH_3)_2$	**2f**	52	**3f**	51
$CH_2CH(C_2H_5)C_4H_9$	**2g**	33	**3g**	47

Table 4-1. Outline of the compounds prepared and their yields.

^{1}H-NMR also confirmed the cyclic tetrameric structure of (See discussion of **3a** in Chapter 2 of this thesis). Figure 3-3 shows spectra of the dodecyl functionalized monomer, **2e** (Figure 4-3 c) and the product of oligomerization producing the tetramer **3e** (Figure 4-3 d). The spectrum of the mixed product contains a mixture of 2 products in a 1:4 ratio - neither component has the identical chemical shifts of the monomer which rules out the presence of unreacted monomer asa source for the impurity detected in the NMR spectrum. Similarly to the discussion of the NMR spectra for **1** which was discussed in detail in Chapter 2, analogous changes in chemical shifts attributed to the influences of ring currents are observed in the peaks corresponding to the

aryl protons of compounds **3a-3g** and confirm a closed, fully conjugated macrocycle structure as the major product (see Appendix 2 for complete spectra). The resonances attributed to the major product (*i.e.*, at 8.86 and 7.58 ppm) are narrower than those ascribed to the minor product which lie upfield from the major product at *ca*. 7.7 and 8.4 ppm (Figure 4-3 d, blue stars). This observation is consistent with a discrete, monodisperse macrocycle as opposed to the broad resonances characteristic of a mixture of linear oligomers.[38]

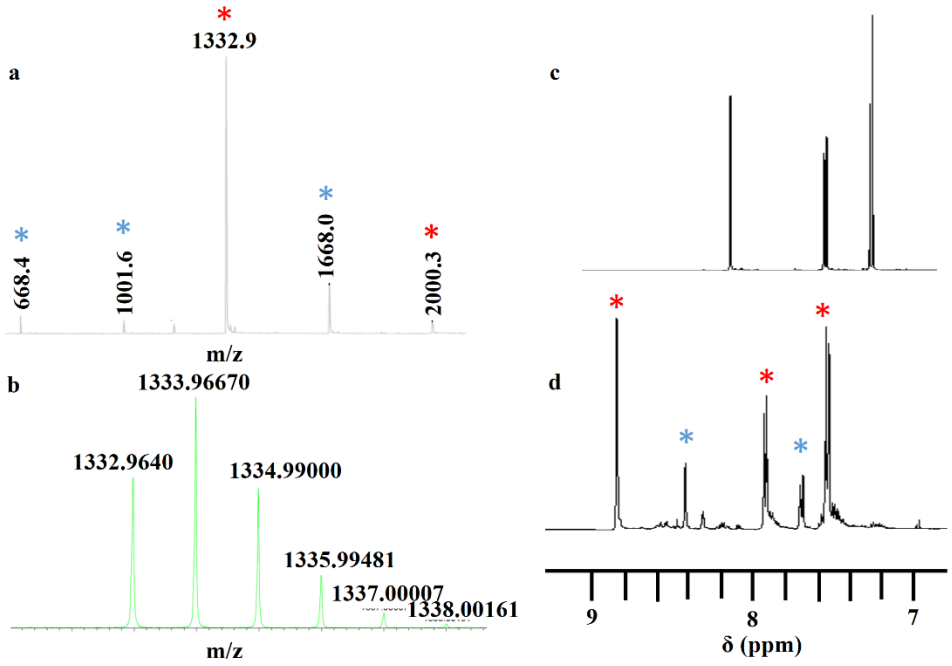

Figure 4-3. ^{1}H-NMR spectra recorded in CD_2Cl_2 (left) and MALDI-TOF mass spectra (right) of a) **2e**, b) the crude product following polymerization, and c) **3e** illustrating which peaks in the NMR spectra correspond to linear polymer (*) and tetramer (*).

The mass spectrum of the isolated tetramer product shows a single high intensity peak corresponding to the cyclic tetramer at m/z = 1332.9 (Figure 4-3 a

and b). This species is accompanied by fragments corresponding to linear and cyclic oligomers made up of 2, 3, 5 and 6 repeat units (Figure 4-3 a). These results suggest signals in the ^{1}H-NMR spectrum may be attributed to small quantities of linear oligomers.

Employing this combined synthetic/purification approach the yield of isolated alkyl-substituted tetramer increases with the length of the alkyl substituent up to a maximum chain length of 10 alkyl units. For example, the yield of tetramer isolated from the crude mixture of products is 47 % for the n-butyl substituted **3a** the yield then increases linearly to a maximum yield of 72 % for the decyl substituted **3d**. The increase in yield which accompanies the increase in alkyl chain length is likely due the transmetallation step during the Yamamoto coupling process[39] in which ring closure would minimize steric repulsions between the spatially demanding alkyl groups, and the bulky BPy groups appended to the catalyst (see Figure 4-4). In contrast the branched **3f** and **3g** deviate from the trend presumably as a result of their very different solubilities, and differences in purification methods as discussed above in the experimental section.

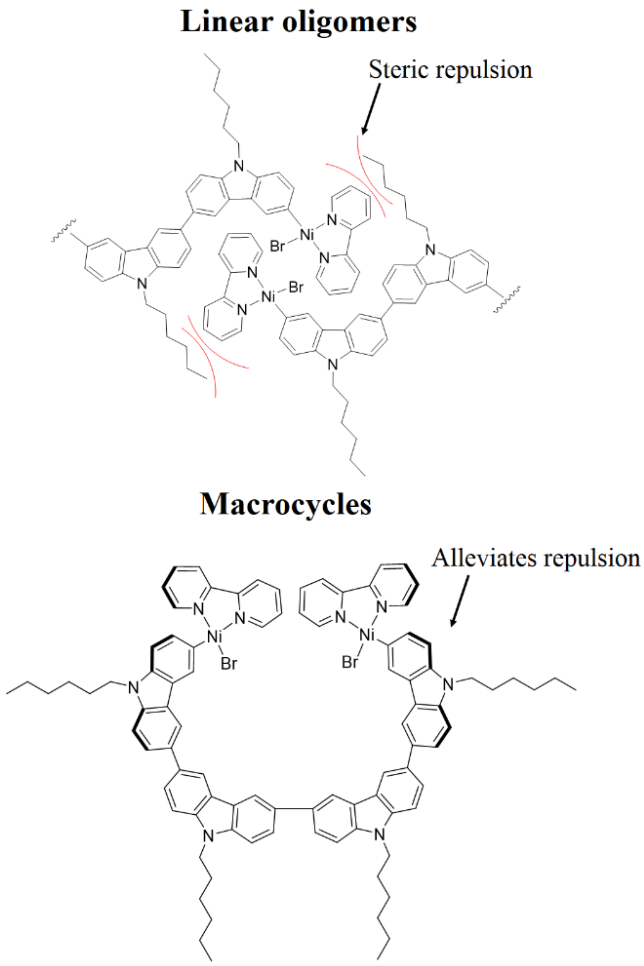

Figure 4-4. Proposed influence of steric repulsions on the formation of macrocycles during transmetallation.

4.1.3.2. Optical properties of the solvated tetramers

Given the importance of material optical properties in many applications of carbazole-based materials (see Chapter 1), the excitation (PLE) and emission (PL) spectra of the compounds **3a-3g** were evaluated. THF was solvent of choice given its compatibility with carbazole-based materials and widespread use in the preparation of thin films for optoelectronic applications. Furthermore, the association of π-conjugated materials in solution often translates to the solid

state,[40] and can vary greatly depending on the solubility of a given molecule in a solvent;[41] this can lead to PL enhancement,[42] quenching,[43] and variations in the absorption and emission maxima.[44] Compounds **3a – 3g** were dissolved in THF to form transparent, yellow, 3 mM solutions, and their excitation and emission spectra were recorded (Figure 4-5). Inspection of the spectra revealed two trends; one relating to the length of alkyl chains in samples with linear R groups (Figure 4-5, left), and a second relating to the length of the pendant group in samples prepared with branched R groups (Figure 4-5, right).

For those samples with linear R groups (*i.e.*, **3a – 3e**), little difference is observed between the compounds where the length of the alkyl chain exceeds 4 carbons in length; the PLE and PL maxima are near identical, and the amount of vibronic definition in the emission spectra are comparable. These observations are consistent with **3b** – **3e** experiencing similar chemical environments when dissolved in THF. **1** and **3a** show broader excitation and emission spectra than the other tetramers, with negligible vibronic detail. As discussed in Chapter 1, these optical characteristics are common to aggregated π-conjugated molecules. This observation is believed to be the result of molecular aggregation manifesting in the formation of solvated sandwich-dimers,[45,46] which is not unexpected given the large cyclic π-conjugated skeleton and limited solubilizing effects of short alkyl chains, and may be the source of the large fluorescence quantum yield (Φ_{fl},Table 4-2).[47] This situation will lead to broad spectral signatures arising from stronger intermolecular interactions within ordered aggregates in solution.[48] Surprisingly, tetramers bearing branched alkyl chains,

did not exhibit broader emission spectra with the increased alkyl group size.

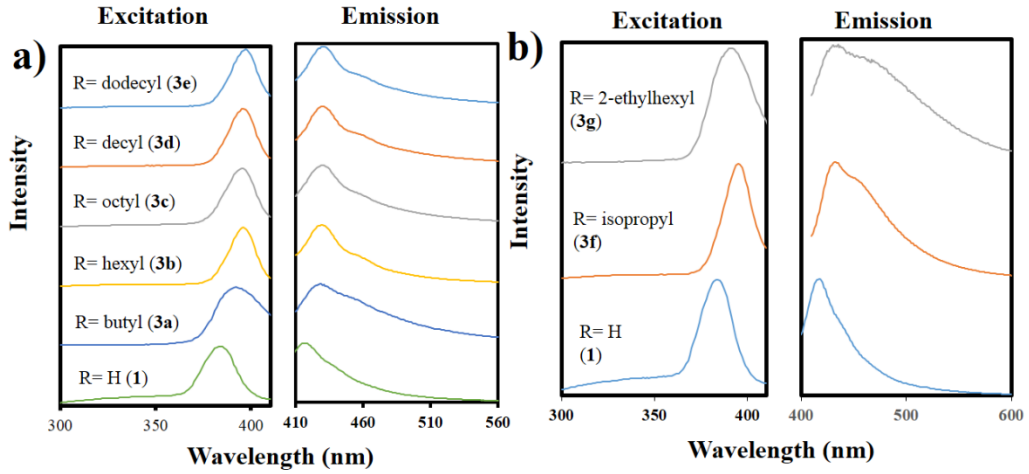

Figure 4-5. PL and PLE spectra of the tetramers **1** and **3a-g** recoded in THF solution for tetramers with linear R groups (left) and branched R groups (right).

While the limitations to solubility in **3a** and **3b** can easily be ascribed to the short butyl and hexyl functional groups, the broad nature of the PL of **3g** in THF, which is functionalized with the more sterically demanding, and highly solubilizing 2-ethylhexyl group, is unexpected.[48] To ascertain the origin of the broader PL spectrum of **3g** (*i.e.*, the 2-ethylhexyl substituted tetramer), the Stokes shifts and photoluminescent quantum yields (*i.e.*, Φ_{fl}) of all tetramers were evaluated (Table 4-2).

The Stokes shift noted for **3g** (*i.e.*, 39 nm) is the largest of all of the compounds, which means that it undergoes the greatest conformational change as the geometry relaxes from that corresponding to the vertically excited state to that of the vibrationally relaxed excited state.[49] Considering the featureless nature

of the excitation spectrum which coincides with a flexible, bent molecular geometry, and the greater vibronic structure in the emission spectrum, it is reasonable to conclude that **3g** assumes a more planar geometry in THF than the other compounds.[49]

Compound	R	λ_{ex} (nm)	λ_{em} (nm)	Stokes shift (nm)	Φ_{fl}
1	H	384	417	33	15
3a	C_4H_9	392	428	36	13
3b	C_6H_{13}	396	430	34	47
3c	C_8H_{17}	395	430	35	11
3d	$C_{10}H_{21}$	396	430	34	12
3e	$C_{12}H_{25}$	397	431	34	12
3f	$CH(CH_3)_2$	395	432	37	12
3g	$CH_2CH(C_2H_5)C_4H_9$	391	430	39	21

Table 4-2. Relevant optical properties of the tetramers **1** and **3a** – **3g** determined in THF. λ_{ex} and λ_{em} are the maximum PL and PLE wavelength, respectively.

Additionally, Φ_{fl} for **3g** is *ca.* 21% greater than the majority of the alkyl substituted compounds, and more in line with those observed for macrocycles with shorter alkyl chains. The branched 2-ethylhexyl group not only increases the steric demand at the N-position, but the non-polar nature of this group is occasionally observed to inhibit solubility through strong self-association.[50] It is likely that this influence is driving these relatively large pendant groups to aggregate, resulting in the large Stokes shift and enhanced quantum yield when

dissolved in THF. The complicated solubility of these materials has two very important consequences 1) obtaining crystal structures of the materials is very difficult, 2) the solvent environment could potentially be tailored to induce self-assembly into interesting morphologies.

4.1.4. Conclusions

A family of carbazole-based macrocycles bearing pendant alkyl chains of varying length and tethered to the pyrrole nitrogen have been prepared by straightforward coupling of the corresponding 3,6-dibromocarbazole via Yamamoto coupling using Ni(Bpy)(COD). The tetramers were readily extracted from a matrix of partially linear byproducts using acetone and obtained in comparatively high yields relative to other methods used for preparing related aromatic shape-persistent macrocycles. We also note, reactions involving larger R groups provided greater yields of macrocyclic tetramers than those performed with smaller N-alkyl groups suggesting that the formation of macrocycles is facilitated by that steric constraints of the pendant alkyl chains.

Evaluation of the tetramer optical properties suggest the emission spectra of the presented carbazole macrocycles depend upon on the nature of the substituent at the N-position. The solvophobic nature of the ring π-system leads to ready aggregation in solution, however this can be mitigated by introducing the solubilizing linear alkyl pendant groups. Surprisingly, in contrast to the impact of linear substituents, branched pendant groups induce broad, red-shifted emission spectra. These changes in the PL spectra are accompanied by anomalously high quantum yields relartive to other oligocarbazoles,[51] which are

reasonably ascribed to aggregates formed in the THF solvent that likely result from self-association of the 2-ethylhexyl side chains.

4.2. Preparation of self-assembled "soft" carbon micromaterials from alkyl-substituted carbazole-based macrocycles

4.2.1. Introduction

Micro- and nano-scale structures formed through the self-assembly of small molecules represent an interesting class of materials. Inspired by the intricacy and functionality of self-assembled biomolecules such as, phospholipids, fatty acids and proteins,[52, 53] this rapidly growing field of research now reaches beyond biologically significant molecules and their derivatives, and includes molecular assemblies with diverse applications in materials sciences including drug delivery, [54,55] catalysis,[56] sensing,[57] separations, [58] electronics,[59, 60] and templates for the preparation of inorganic nano- and micro-materials.[61, 62]

More specifically, self-assembled organic materials based upon π-conjugated organic semiconductors,[63] such as porphyrins,[64-66] perylenediimides,[67-69] and oligomers of common functional polymers (*e.g.*, polyfluorene,[70-72] polythiophene,[73-76] and poly(p-phenylenevinylene) [77,78]) are receiving attention. As discussed in Chapter 1, carbazole-based materials have a long history of applications ranging from electrochromic devices,[79-84] to organic light-emitting diodes,[85-87] and most recently have been applied in organic photovoltaics.[28, 88-92] Due to their planar structure,[6] exposed π-systems,[63] and favorable optoelectronic properties,[93] carbazole-based macrocycles are also emerging as popular scaffolds for new families of shape persistent macrocycles (SPMs) that form useful micro- and nano-structures that retain the desirable

electronic and optical properties of the carbazole species from which they are derived.[63,94]

Carbazole-based SPMs are attractive because their predictable π-π stacking behaviour and ease of functionalization provide access to pendant functionalities ranging from non-polar aliphatic chains to hydrogen bond-forming structure directing groups.[72,95,96] A range of morphologies have been realized including microcrystals,[24] and nano-fibers,[96,97] that are typically prepared by slow precipitation from solvent/antisolvent mixtures. It is challenging to design more complex morphologies because of complexities associated with the molecular assembly processes. For example, π-π stacking interactions are weak (*ca.* 1.8 to 2.8 kcal/mol)[98] compared to hydrogen bonds (3.4 to 12.1 kcal/mol)[99] and a C-C single bonds (82 kcal/mol).[100] Additionally, π-π stacking interactions result from weak electrostatic interactions between quadrupolar π-systems, and as such lack the inherent directionality of other stronger bonding arrangements.[101] This combination of the weak bonding and ill-defined orientation of the participating molecules means the stacking is not limited to a sandwich-type orientation of molecules (such as in H-aggregates) – it can also manifest in indirect slip-stacked and T-shaped arrangements of π-systems (See Chapter 1).[101]

Consequently, the assembly of low molecular weight molecules depends on the nature of the functional groups pendent to the aryl-based core of the molecule. For example, aliphatic chain solubilizing groups offer a wide range of possibilities for tailoring the self-assembly process (See Chapters 1 and 2). The

number of carbon atoms,[102] branching,[67] and stereocenters[103] of the pendent chain all influence the self-assembly process. For example, the morphology of assemblies of carbazole-ethynyl macrocyclic tetramers can be interchanged between 0D to 1D nanostructures and the molecular ordering within these assemblies can be altered by defining the length of N-bonded alkyl functionalities.[97]

The sensitivity of particle morphology to the nature to the structure of the pendent group arises because the aliphatic groups associate through even weaker interactions than π-π stacking (*i.e.*, van der Waals and dispersion forces and solvophobic effects). The result of the concerted contributions of these weak interactions result in a delicate balance between the electrostatics that drive the 1D π-π stacking interaction and the solvophobic interactions that drive assembly in lateral directions. Consequently, despite the propensity of the presented π-systems to self-associate, the development of appropriate conditions to induce this self-assembly into supramolecular morphology is often a reversible and kinetically controlled process. Thus, the formation of specific morphologies is largely achieved through iterative investigations.[104]

Chapter 2 outlined the preparation of an all-carbazole alkyl-free macrocycle (**1**) that self-assembled into nanospheres, and was followed by the expansion of the synthetic protocol used to make **1** to prepare a series of tetramers bearing alkyl chains of varying length and steric bulk in the first section of this chapter (Compounds **3a**-**3g**, Figure 4-6). In this Chapter, the discussion is expanded to include an investigation of how this rational variation

of the N-bonded substituents influences the formation of self-assembled micromaterials.

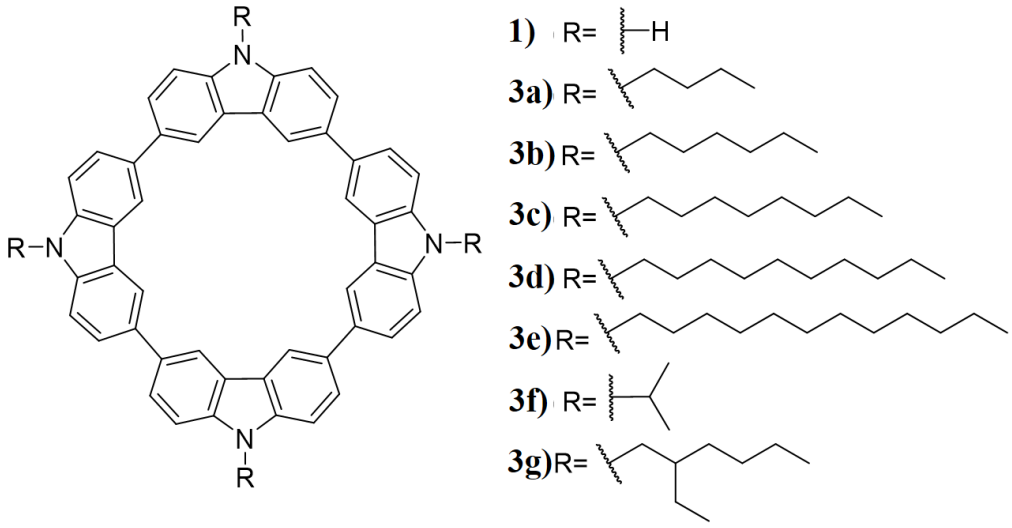

Figure 4-6. Structures of the molecules investigated for self-assembly.

4.2.2. Experimental

4.2.2.1. General

All THF was distilled over Na/benzophenone immediately prior to use, and the water used was triple distilled. Compounds **1** and **3a** through **3g** were prepared as outlined in Chapters 2 and Section 4.1.

Scanning electron microscopy (SEM) samples were prepared by dispersing the solid in pentane and drop-casting the suspensions onto silicon wafers (See Section 4.2.2 for further details). The samples were sputtered with 8-10 Å of chromium, and SEM imaging was performed using a JEOL 6301F Field Emission Scanning Electron Microscope with a 5 KV beam. Circular dichroism was performed on a Olis DSM 17 Circular Dichroism spectrometer using

samples in a THF/water solution with a mole fraction of water X_{aq} = 0.3, 0.4, and 0.6 and tetramer concentration of 0.9 mM

4.2.2.2. Nanostructure preparation.

Self-assembled nanostructures of macrocycles **1** and **3a-3g** were prepared using the following general procedure. A known quantity of macrocycle necessary to achieve a 3 mM solution was added to THF and placed in a bath sonicator for 5 minutes to yield clear yellow/orange solutions; the colour of the solution depended upon the macrocycle used; from tan for **1** to pale yellow for **3a-3c**, **3f** and orange for **3d**, **3e**, **3g**. Self-assembly was induced by adding a predetermined quantity of water using a micropipette to achieve the target X_{aq}. For **1-3c**, **3f** an X_{aq} = 0.6 was chosen; **3d-e,** X_{aq} = 0.8 ; **3g**, X_{aq} = 0.9.

"Fast addition" of the water was performed over *ca.* 30 seconds by adding the water dropwise from a syringe followed by gentle swirling. To qualitatively evaluate the impact of addition rate on the self-assembly process of **3c**, water was also added over 20, 40, 60 minutes, 2 hours, and 16 hours followed by gentle swirling. Addition was performed using a micropipette by adding 25 μL at intervals of 40 seconds over a period of 20 minutes, 80 seconds over a period of 40 minutes, 2 minutes over a period of 60 minutes, 4 minutes over a period of 2 hours, and every 32 minutes over a period of 16 hours. The addition of water to THF solutions of the various macrocycles yielded cloudy suspensions.

The optical properties of the suspensions were evaluated by diluting the original suspensions with THF/water cosolvent at X_{aq} = 0.6 without further purification of the assemblies. To prepare the samples of the assemblies for XRD and SEM analysis, self-assembled precipitates were isolated by 3 methods depending upon the precursor tetramer. Centrifugation was used to isolate the particles from the THF/water mixture used to prepare the colloids of **1**. Assemblies of **3a-d, 3g** were isolated by slow settling from the THF/water solution for a minimum of 10 hours. Assemblies of **3e** and **3f** were isolated by allowing the solid material to settle for *ca.* 5 minutes and decanting the solvent mixture immediately following particle formation.

The supernatant solutions were removed from each sample using a pipette and the precipitate was resuspended in pentane.

4.2.2.3. Photoluminescence and excitation

Photoluminescence (PL) and excitation (PLE) spectra were recorded in a quartz cuvette using a Cary Eclipse fluorometer at a scan rate of 2 nm per second. All spectra were recorded with an excitation slit width of 2.5 nm and emission slit width of 5 nm; this allowed direct comparison of the spectra. All PL spectra were recorded using an excitation wavelength of 380 nm unless otherwise noted.

4.2.3. Results and discussion

4.2.3.1. Nano- and micro-material preparation

Solution-phase self-assembly of carbazole-based tetramers bearing N-bonded pendant groups *(i.e.*, **3a-3g**) was investigated. Assembly was induced by changing the polarity of the solvent medium upon rapid addition of known quantities of water to achieve target mole fractions of water (X_{aq} = 0.6 for **3a-3d** and **3f**, X_{aq} = 0.8 for **3d-e**, and X_{aq} = 0.9 for **3g**); in all cases this procedure yielded suspensions of white precipitates.

Qualitatively, suspensions prepared using tetramers having comparatively small N-bonded R groups, **3f**, **3b** and **3c**, rapidly form large precipitates that settle from the assembly media. Precipitation/assembly of tetramers bearing larger N-bonded R groups (*i.e.*, **3d**, **3e**, and **3g**) necessitated the addition of additional water because longer N-bonded substituents increased the solubility of thse tetramers in THF.[102,106] Cloudy mixtures obtained from **1-3c** and **3f-g** contained solids that maintained their morphology for weeks (or longer), however structures prepared prepared from tetramers bearing long R groups (*i.e.*, **3d** and **3e**) were stable for only < 12-16 hours after which oils were obtained. As a result, it was necessary perform solution-based analyses immediately following preparation.

4.2.3.2. The influence of steric bulk at N on self-assembly

Chapter 2 outlined the unsubstituted all-carbazole tetramer, **1**, self-assembled from solutions in hot acetone/water solvent mixtures at large X_{aq} to form spherical colloids that exhibited aggregation induced emission enhancement. The results of B3LYP calculations suggested the tetramer assumes a boat-type geometry. This, along with optical data indicating the molecules

undergo structural distortion as X_{aq} was increased, suggests flattening of **1** was responsible for the large particle sizes observed at high X_{aq}. Further analysis of the colloids using XRD indicated the increase in X_{aq} was accompanied by the appearance of sharp diffraction peaks at 2θ = 13.4 - 35.8° corresponding to d-spacings in the range of 2.7 - 6.6 Å that are consistent with π-stacked macrocycles.[106] From this, we proposed the formation of spherical particles resulted from macrocycles interlocking to form a curved particle surface with a radius of curvature that changes in response to the planarity of the macrocycle.

Macrocycles bearing long aliphatic pendant groups generally self-assemble to form sheets[60,107] and fibres;[97] it has been proposed this directed assembly is driven by hydrophobic effects between non-polar pendant groups and polar solvent media.[107] In this context, we questioned if substituting tetramer **1** at the carbazole nitrogen sites with short alkyl groups could sufficiently disrupt macrocycle stacking responsible for spherical morphology and induce different particle morphologies. Hence, the morphologies of the precipitates formed through the precipitation of the macrocycles **1**, **3a** and **3f** from THF and water where X_{aq} = 0.6 were evaluated.

Scanning electron microscopy is a powerful method that provides information regarding the morphology of the assemblies on a sub-micron scale. Specifically, secondary electron images offer topographical information.[108] SEM images of precipitates isolated from water induced assembly of **1** from THF (Figure 4-2) show hollow, spherical particles with an average diameter of d_{avg} = 260 ± 50 nm and shell thickness of T_{avg} = 32 ± 9 nm. This coincides well with

the spherical particles formed upon precipitation from acetone and water mixtures of X_{aq} = 0.6 presented in Chapter 2 (Figure 4-2 a).

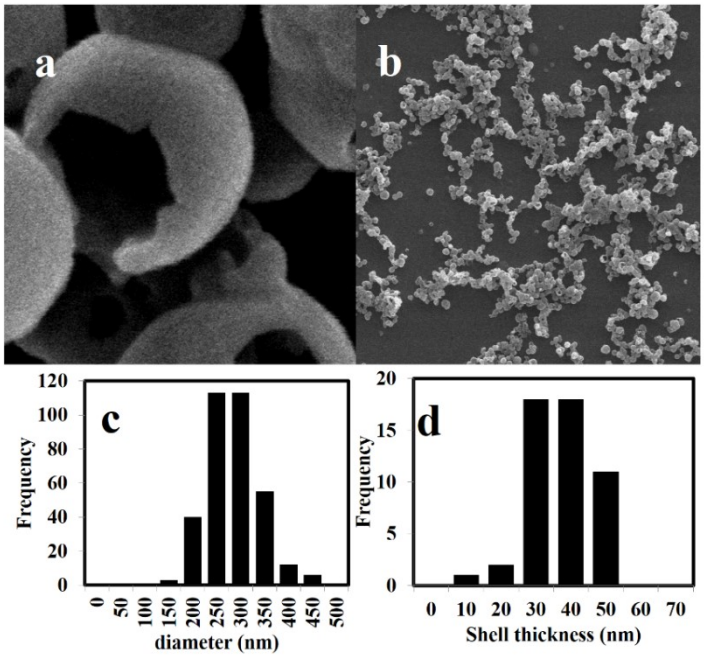

Figure 4-7. Secondary electron SEM images of hollow nanoparticles obtained from the precipitation of **1** from THF through rapid addition of water at a) high magnification, and b) low magnification, and histograms for (c) the diameter and (d) the thickness of the shells.

SEM analysis of assemblies obtained from THF/water mixtures of **3f** show very different particle morphologies. Appending isopropyl groups to the tetramer N-positions resulted in the formation of particles exhibiting a general ribbon-type morphology suggesting the assembly is dominated by lateral 2D interactions (Figure 4-3 a and b).[110] The network of interconnected ribbons shows an average width (W_{avg}) of 140 ± 30 nm (Figure 4-3 c and d) and average

thicknesses (T_{avg}) of 42 ± 11 nm that is similar to that of the assemblies formed from both **1** and **3f**; the origin of this similarity is currently unclear.

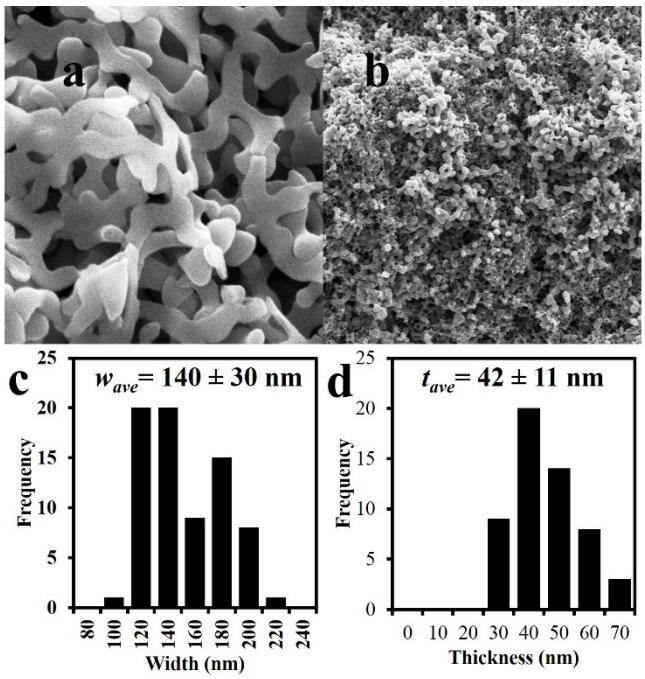

Figure 4-8. Secondary electron SEM images of interconnected nanoribbons obtained from the precipitation of 3f from THF upon rapid addition of water at a) high magnification, and b) low magnification. Histograms showing the distribution of the width (c) and thickness (d) of the ribbons

Assemblies obtained from the n-butyl substituted tetramer, **3a**, contained a polydisperse mixture of flat islands and spheres with sizes exceeding 1 μm (Figure 4-4 c). Similar island structures have been observed elsewhere in the assembly in other small molecules and have been attributed to uncontrolled self-assembly.[67,110] It is reasonable that the comparatively long n-butyl groups at the N positions of the carbazole tetramer limit controlled assembly. The additional

bulk of the n-butyl substituents may also hinder the π-π stacking responsible for the formation of the spheres and ribbons.

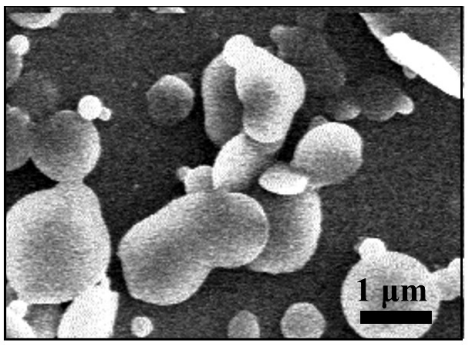

Figure 4-9. Secondary electron SEM image of micro-structures obtained from the precipitation induced upon adding water (X_{aq} = 0.6) to a THF solution of **3a**.

While electron microscopy provides information regarding particle morphology, it cannot give insight into the internal ordering of the constituent molecules within these structures. The optical properties of conjugated molecules can give insight into the electronic structure of a molecule within an aggregate and are dependent on their conformational structure (see Chapters 1 and 2).[111] In the context of the assemblies discussed herein, the excitation and emission spectra can be used to monitor changes in molecular conformation that result from the assembly process.[112]

Changes in the normalized PLE and PL spectra of the macrocycle assemblies (Figure 4-5, dashed traces) compared to their fully solvated counterparts (Figure 4-5, solid traces) can be reasonably attributed to variations in the effective conjugation length, and give insight into molecular planarity (See Chapter 1).[113] The PL spectra of solvated tetramers (Figure 4-6, blue solid lines)

and tetramer assemblies (Figure 4-5, blue dashed lines) show near identical PL maxima, $\lambda_{EM,}$.

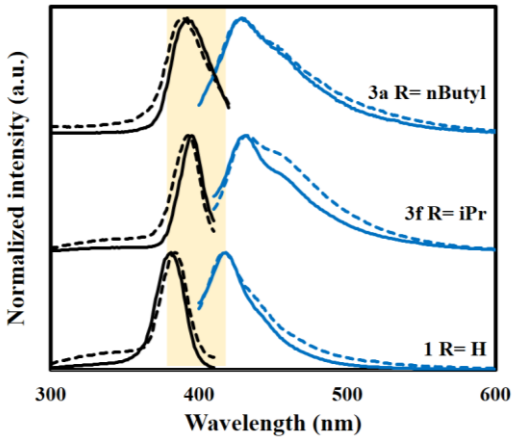

Figure 4-10. Normalized PLE spectra (black traces) and PL spectra (blue traces) of compounds **1** (bottom), **3f** (middle) and **3a** (top) at a concentration of 3 mM recorded in solution in THF (solid lines) and as a suspension in THF/Water at X_{aq} = 0.6 (dashed lines). The yellow band highlights the PL and PLE maxima compound **1** to assist in visualizing the spectral shifts.

The PL maximum of the cyclic carbazole tetramers red-shifts from λ_{EM} = 417 nm for alkyl free **1** to 432 and 429 nm for **3f** and **3a** (*i.e.,* R= isopropyl and n-butyl), respectively. This result suggests the effective conjugation length increases upon substitution at the N-position (Figure 4-5, blue traces).[48] However, as discussed in Chapter 3, the shape of the emission profile changes with R for the dissolved tetramers – these changes are even more pronounced for the self-assembled structures. For example, self-assembly **3f** results in an enhancement of the lowest energy vibronic feature at *ca.* 450 nm leading to peak broadening through the low energy region of the spectrum. The increased

intensity of this vibronic feature is consistent greater structural rigidity and suggests a more planar conformation than in the precipitates of **1** and **3a**.[48]

In addition to the structural information that can be extracted from the PL spectra, PLE spectra provide useful insight into the π-stacking within the assemblies (See Chapter 1).[112] The relative orientation of the π-systems can lead to aggregate formation that induces a spectral red-shifted if they adopt a slip-stacked J-aggregate orientation, or a blue-shift if a face-on-face stacked H-aggregate is preferred.[114] To investigate aggregate formation in the present assemblies the PLE spectra were evaluated (black traces in Figure 4-5) before (solid line) and after (dashed line) self-assembly of **1**, **3a** and **3f**. While there is negligible change in the PLE maximum following self-assembly, the general shape of the PLE spectra for **1**, **3a** and **3f** changes (Figure 4-5, black dashed lines). Assembly is accompanied by an increase in PLE intensity between 300 and 370 nm (*i.e.*, at higher energies), suggesting H-aggregate formation.[115] The intensity of the PLE in this high-energy region after assembly is least pronounced in **3a,** and increases through **3f** with a maximum increase in higher-energy PLE occurring in the assemblies of **1**. Based upon these observations, we contend that the introduction of N-alkyl substituents disrupts the formation of H-aggregates.

The concept of aggregation-induced emission enhancement (AIEE) was introduced in Chapter 1 and results from the self-assembly of π-conjugated molecules and the formation of aggregates that enhance the PL efficiency.[116] In Chapter 2, colloids of **1** that formed in acetone and water mixtures displayed

AIEE because the packing of the macrocycles lead to formation of H-aggregates. With this in mind, the PL and PLE spectra of **1**, **3a** and **3f** in THF/water solvent media of varying X_{aq} were investigated for AIEE. Figure 4-6 shows the PLE (left) and PL (right) spectra of the tetramers with short R group at a concentration of 3 mM in THF (blue traces) and as water is gradually added up to a final water concentration of X_{aq} = 0.6 (brown traces).

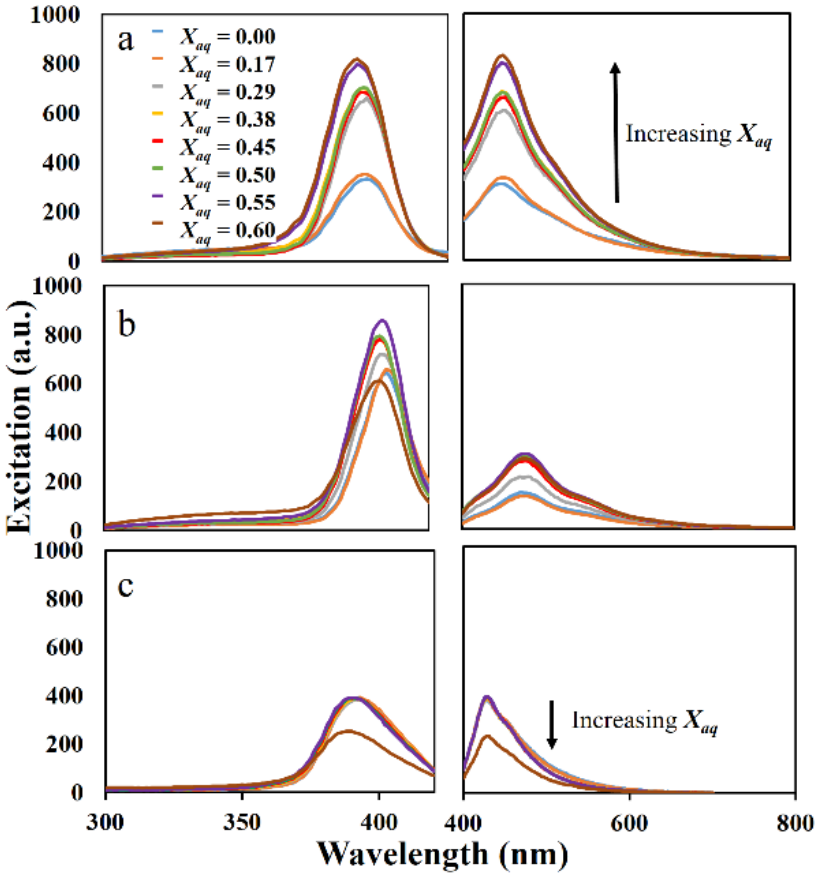

Figure 4-11. Excitation and emission spectra of 3 mM solutions of a) **1**, b) **3f**, and c) **3a** in THF as water is gradually added at to the stated X_{aq}.

The PLE and PL intensity of alkyl-free **1** increases as the mole fraction of water is increased up to a final X_{aq} = 0.6 (Figure 4-6 a). The introduction of the

isopropyl groups at the N-positions results in a smaller increase in PL (Figure 4-6 b). Further increasing the R group length to n-butyl did not induce any increase in the PL and PLE intensity (Figure 4-6 c) - in fact, increasing the water content to X_{aq} = 0.6 *decreased* the PL and PLE intensity (Figure 4-6 c, brown traces). These results suggest that aggregates obtained from **3a** exhibit AIQ processes commonly observed for other homocarbazoles rather than the AIEE observed in **1** and **3f** (see Chapter 1).[117]

We propose the formation mechanism for the present hollow sphere and ribbon morphologies formed from **1** and **3f** is similar to that proposed for the formation of spheres in Chapter 2. In the absence of an alkyl substituent at the N-positions, the interlocking semi-planar macrocycles curve to form a sphere. Introducing substituents at the N-positions increase the interplanar spacing and the lamellar structure remains flat. Surprisingly, despite having slightly longer substituents **3a** does not self-assemble in the same way - apparently the added bulk of the n-butyl substituents influences π-stacking interactions that guide the assembly of **1** and **3f**.

4.2.3.3. Microrod formation from macrocycles

As discussed in Chapters 1 and 2, microrods are commonly formed by SPMs bearing long aliphatic pendant groups.[118] This morphology is favored because the long aliphatic chains experience non-specific, entropy driven solvophobic interactions that promote the π-π stacking interactions dominating and directing the structure direction.[119] In an effort to evaluate if long aliphatic groups (*i.e.*, decyl, dodecyl and 2-ethylhexyl groups) tethered to the N sites on

the present tetramers would induce rod or fiber morphology, suspensions of **3d**, **3e** and **3g** were prepared in THF and assemblies were prepared upon rapid addition of water at X_{aq} = 0.8 for **3d** and **3e**, and X_{aq} = 0.9 for **3g**. The resultant solids were then drop cast onto silicon wafers and evaluated using SEM.

SEM analyses indicated that at X_{aq} = 0.8 **3d** and **3e** assembled into a microrods with average diameters of d_{avg} = 400 ± 100 nm and 500 ± 200 nm, respectively (Figure 4-7 a and b). Increasing the the length of the R group from R= $C_{10}H_{21}$ in **3d** to R= $C_{12}H_{25}$ in **3e** does not induce a statistically significant change in the rod diameter. Conversely, introduction of a 2-ethylhexyl group (*i.e.*, **3g**) yielded narrower rods with d_{avg} = 190 ± 50 nm (Figure 4-7 c). It is reasonable the 2-ethylhexyl functionality inhibits pendant group agglomeration and the associated long range lateral self-assembly this would limit the microrod diameter.[60]

The pendant alkyl groups also influence the length of the observed rode structures. Decyl groups (*i.e.*, **3d)** guide the assembly to form long rods (*i.e.,* l_{avg} = 18 ± 12 μm; Figure 4-7 a), whereas the microrods prepared from **3g** at X_{aq} = 0.6 are short and polydisperse with l_{avg} = 0.6 ± 0.3 μm (Figure 4-7 c). This observation is consistent with stericly demanding pendant groups disrupting the π-stacking and inhibiting the formation of long wires.[67] Surprisingly, dodecyl groups (*i.e.*, **3e)** do not produce longer rods; instead, the resulting rods are intermediate in length (l_{avg} = 7 ± 5 μm; Figure 4-7b) between those obtained from assembly of tetramers bearing decyl and 2-ethylhexyl functionalities (*vide*

infra). This suggests the conformation of the dodecyl groups adopts a greater *effective* steric bulk than the decyl groups under the same conditions.[120]

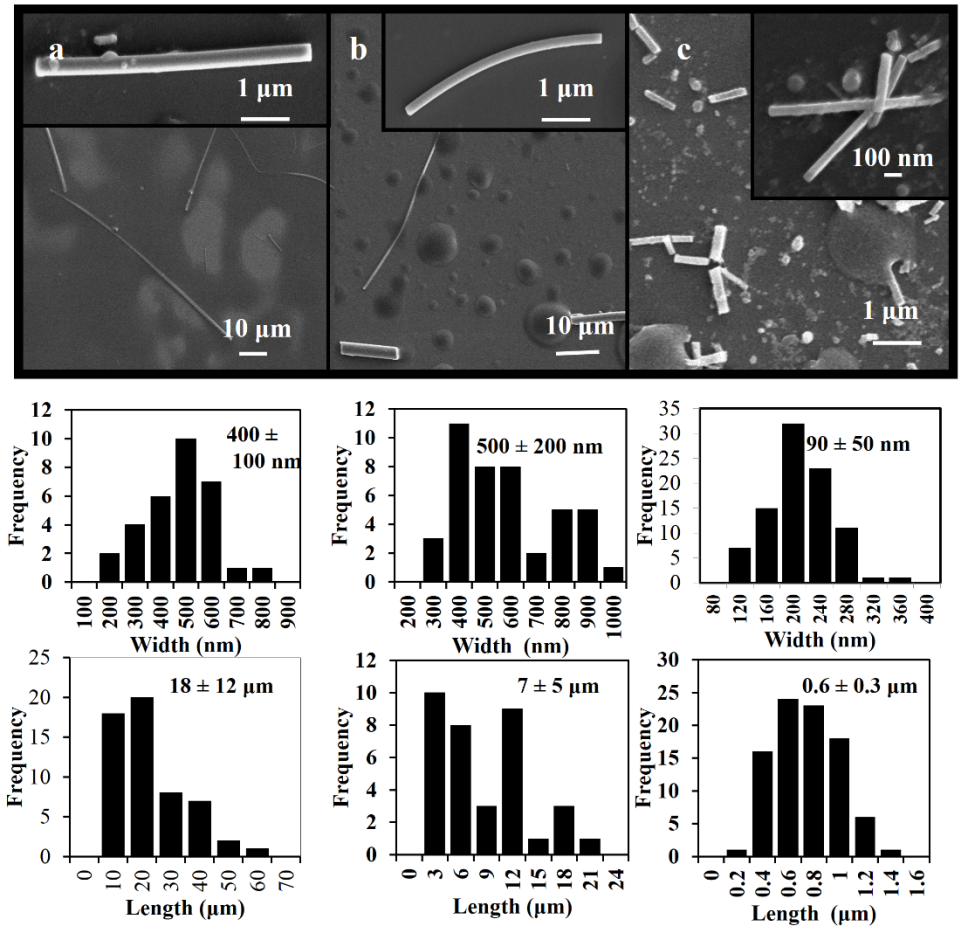

Figure 4-12. SEM images of microrods formed from self-assembly of a) **3d**, b) **3e**, c) **3g**.

The formation of 1D structures similar to those noted here for **3d**, **3e**, and **3g** is often observed as a manifestation of two structural characteristics in shape persistent macrocycles: i) the length of the pendant alkyl chain, and ii) the planarity of the macrocycle core.[121] As discussed previously, the optical properties of these emissive macrocycles can be useful in determining how the

conformation of the macrocycles changes as a result of the self-assembly process.[122] In this context, the PL and PLE properties of the microrods were evaluated (Table 4-1).

The Stokes shift gives insight into the relative planarity of an SPM (see Chapter 1).[3] To determine the Stokes shifts of the molecules in solution, the PLE and PL spectra of **3d**, **3e** and **3g** were recorded at a series of X_{aq} (Table 4-1). The Stokes' shifts were then determined for THF solutions (Δ_{THF}), and as water was added in increments of $X_{aq} \approx 0.1$ to a final concentration of with $X_{aq} = 0.6$ (Table 4-1). The Stokes shifts for **3d**, **3e** and **3g** all follow the same general dependence on X_{aq}. Based upon these observations, each experiences the same restriction to rotational motion following self-assembly.

Compound	$\lambda_{ex\ THF}$ (nm)	$\lambda_{em\ THF}$ (nm)	Δ_{THF} (nm)	$\lambda_{ex\ H_2O}$ (nm)	λ_{emH_2O} (nm)	Δ_{H_2O} (nm)
3d	396	430	34	391	431	40
3e	397	431	34	392	430	38
3g	391	430	39	388	432	44

Table 4-3. Summary of the relevant optical data acquired from the tetramers dissolved in THF ($\lambda_{ex\ THF}$, $\lambda_{em\ THF}$, Δ_{THF}) and following addition of water up to $X_{aq} = 0.6$ ($\lambda_{ex\ H_2O}$, λ_{emH_2O}, Δ_{H_2O}).

In addition to Stokes' shifts, the shape, and relative positions of the PL and PLE spectra give qualitative insight into the molecular geometry, and degree of molecular aggregation in solution or assemblies.[111] The PL and PLE spectra of **3g**, **3d** and **3e** acquired in THF (Figure 4-8, solid lines) and in THF/H_2O mixtures X_{aq} = 0.6 (Figure 4-8, dashed lines) were compared. The PLE and PL maxima in THF (*i.e.*, $\lambda_{ex\ THF}$ and $\lambda_{em\ THF}$ respectively) of the different tetramers did not depend on the tetramer structure; furthermore, no changes in the position of the emission maximum following the addition of water, λ_{emH_2O} at the resolution of the spectrometer were noted (see Table 4-1). However, the shape of the emission spectra does depend on tetramer structure. An increase in the 0-1 vibronic transition in the emission spectrum of **3g** is noted following self-assembly (Figure 4-8, blue dashed lines) suggesting the conformation of **3g** is more rigid than that of **3d** and **3e**.[123] Additionally, the appearance of a new PLE transition at *ca.* 350 nm in the assemblies of **3d** and **3e** suggests the formation of H-aggregates when X_{aq} = 0.6. When considered in combination with the Stokes' shift data discussed above, it can be concluded that the 2-ethylhexyl appended **3g** forms tighter aggregates, however these aggregates poorly ordered when compared to assemblies derived from **3d** and **3e** that show evidence of ordered face-to-face stacking in the form of H-aggregates. As such, we propose disordered aggregation of **3g** contributes to the formation of smaller microrods.

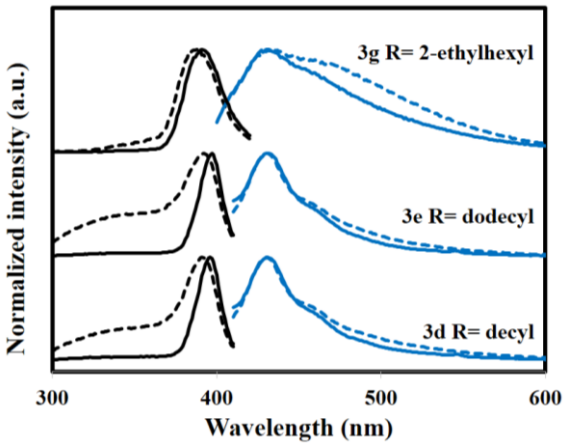

Figure 4-13. Normalized PLE spectra (black traces) and PL spectra (blue traces) of **3d**, **3e**, and **3g** dissolved in THF (3 mM; solid lines) and corresponding suspensions in THF/Water (X_{aq} = 0.6; dashed lines).

4.2.3.4. Self-assembled structures from other tetramers

The discussion thus far in this Chapter has focused on how carbazole SPMs N-functionalized bearing comparatively small functional groups preferred lateral self-assembly into hollow spheres and ribbons, while larger substituents guided the formation of microrods of varied length and diameters. The remaining tetrameric carbazole macrocycles, **3b** and **3c** bear R groups that can be considered intermediate length (*i.e.,* R= hexyl and octyl, respectively). Few examples of SPMs with pendant alkyl chains of intermediate length appear in the literature.[3] Hence, an investigation of the self-assembly of **3b** and **3c** might provide a means for the preparation of unique SPM-based morphologies. As discussed above, assemblies were prepared by dissolving **3b** and **3c** in THF, followed by precipitation by the addition of water up to X_{aq} = 0.6. The off-white

solids were isolated, dispersed in pentane and dropcast onto Si wafers for morphological analysis using SEM (Figure 4-9).

Substitution of the macrocycle with hexyl groups (**3b**) resulted in assemblies composed entirely of entwined fibres with average diameters of t_{avg}= 41 ± 20 nm, and lengths exceeding 10 μm (Figure 4-9 a). Increasing the length of R by 2 carbons (*i.e.*, octyl groups; **3c**) saw the dominant morphology become one that resembles a spoked wheel with lamellar paddles of an average length of l_{avg} = 13 ± 7 μm, average width of T_{avg} = 350 ± 100 nm (Figure 4-9 b). The blades are fused to a central axis and radiate in a staggered fashion from the axis to form an overall spoked-wheel geometry. The stark morphological change induced by the introduction of only 2 additional carbon atoms on the pendant groups suggests the associated self-assembly process differs substantially from the straightforward ordering invoked previously to describe formation of spheres, ribbons, and rods.

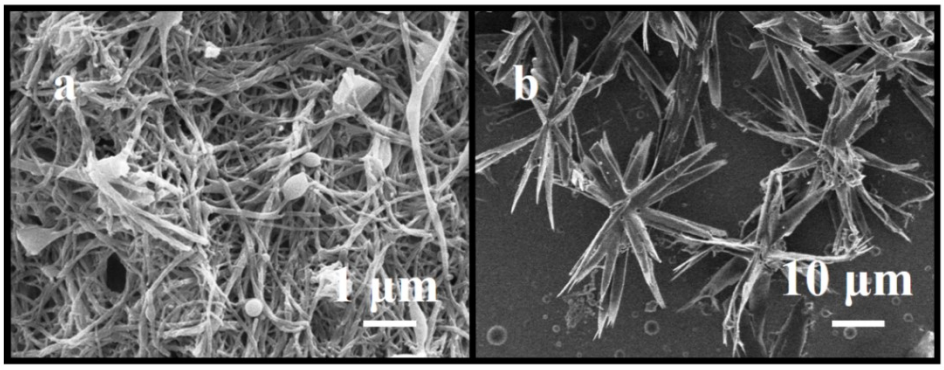

Figure 4-14. SEM images of the nano- and micro-structures produced upon addition of water to THF solutions of a) **3b**, and b) **3c** where X_{aq} = 0.6.

As is the case for other SPM assemblies studied here, optical properties of (*i.e.,* PL and PLE spectra and the Stokes' shift) can provide information about the relative geometries and orientations of the molecules within the chosen assemblies.[112] So, again we turn to a comparison of the optical properties of the solvated molecules and their assemblies. The PL and PLE spectra were recorded for both **3b** and **3c** and presented in Figure 4-10, where the solid lines represent the spectra recorded in solution in THF, and the dashed lines represent the spectra acquired of the suspensions formed in X_{aq} = 0.6. The PLE spectra of the alkyl-substituted tetramers are similar when dissolved in THF (*i.e.,* λ_{ex} = 396 nm for **3b**; λ_{ex} = 395 nm for **3c**). Following self-assembly, the excitation maxima blue-shift (*i.e.,* λ_{ex} = 392 nm for **3b**; λ_{ex}= 390 nm for **3c**)**.** These shifts are accompanied by increases in PLE intensity in the region of 300 - 360 nm that have previously been attributed to H-aggregate formation,[124] the intensity of these features increases with longer R (Figure 4-10, black traces).

Surprisingly, there is negligible change in the PL spectrum of **3b** upon assembly (*i.e.*, λ_{em} = 430 nm in THF, and λ_{em} = 432 nm at X_{aq} = 0.6). This suggests molecules of **3b** remain in similar geometries when dissolved and in self-assembled structures. This differs from our observations for the octyl-substituted **3c** which shows a shift in the 0-2 vibronic transition from λ_{em} = 430 nm in THF to λ_{em} = 439 nm following assembly indicating a change in molecular geometry as it transitions from a dissolved state, to the spoked wheel assemblies observed at X_{aq} = 0.6 (Figure 4-10, blue traces).

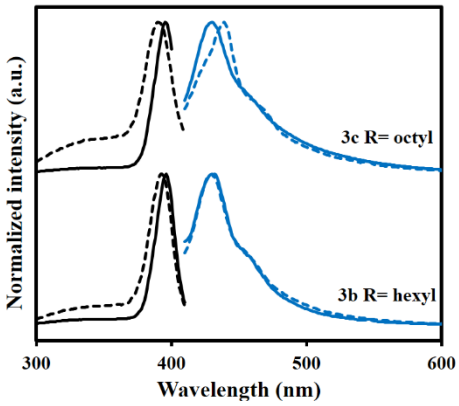

Figure 4-15. Normalized PLE spectra (black traces) and PL spectra (blue traces) of **3b** (bottom) and **3c** (top) at a concentration of 3 mM recorded in solution in THF (solid lines) and as a suspension in THF/Water at X_{aq} = 0.6 (dashed lines).

To identify the water concentration at which the change in **3c** PL occurs**,** the PL and PLE spectra were evaluated as a function of the water concentration in THF (Figure 4-11). Unlike the AIEE observed with **1** (*vide supra*), both **3b** and **3c** show decreased PL intensity as water is added to X_{aq} = 0.6 (Figure 4-11, right). Both see loss of PL response when water content exceeds X_{aq} = 0.3 (Figure 4-11, yellow traces). The accompanying shift in PL maximum from λ_{em} = 430 nm to λ_{em} = 439 nm does not occur until X_{aq} = 0.50. We propose these observations result from **3b** and **3c** being electronically and structurally similar until a certain threshold X_{aq} (*i.e.*, X_{aq} = 0.40) is reached afterwhich **3c** follows a different assembly pathway.

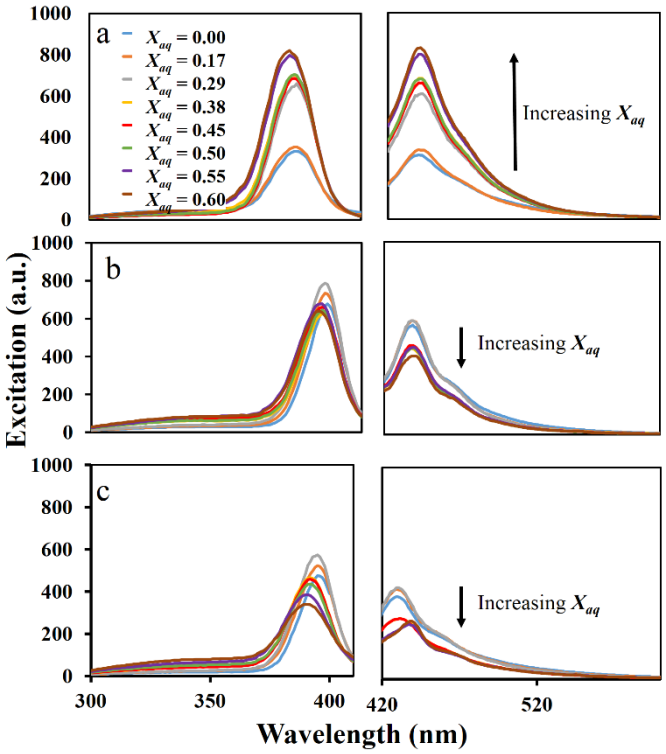

Figure 4-16. Excitation and emission spectra of 3 mM solutions of a) **1,** b) **3b**, and c) **3c** in THF as water is to the given X_{aq}.

4.2.3.5. Investigation of the self-assembly mechanisms - fibers and micro-spoked wheels

The observations that the both **3b** and **3c** display very similar electronic properties up to a certain threshold water concentration and that the morphologies they assume in their assembled states differ substantially suggests the formation of the spoked wheel geometry from **3c** may be hierarchical. To investigate this possibility, we first aimed to determine how fibers of **3b** form, and identify the impact of different concentrations of water. Close examination of the SEM images of the fibers reveals the assemblies produced from the

addition of water to THF solutions containing **3b** forms large agglomerates of fibers with diameters of 41 ± 20 nm (Figure 4-12 a).

Higher magnification SEM images of the fibers reveal the assemblies consist of a twisted-coil (Figure 4-12b). Morphologies of this type are commonly seen for self-assembly of π-conjugated SPMs and is generally believed to arise from hierarchical fibre assembly.[125] This mechanism is further supported by the diameters of the fibres measured by the SEM images which cut off sharply at 20 nm, and then follow a stepwise distribution of diameters up to over 100 nm (Figure 4-12c).[126]

Investigations performed on the formation of fibers from similar macrocycles suggest that SPM assembly involves a dynamic process of assembly/disassembly at low antisolvent concentrations. It is not until the concentration of the antisolvent becomes great enough, that the assemblies become trapped in metastable geometries.[127] Consequently, parameters such as handedness in twisted coils depend on the initial morphologies of the seed fibres.[128,129] To gain further insight into the mechanism for the formation of coiled fibers in the self-assembly of **3b**, the evolution of the assemblies was tracked using SEM as water was gradually added (Figure 4-13).

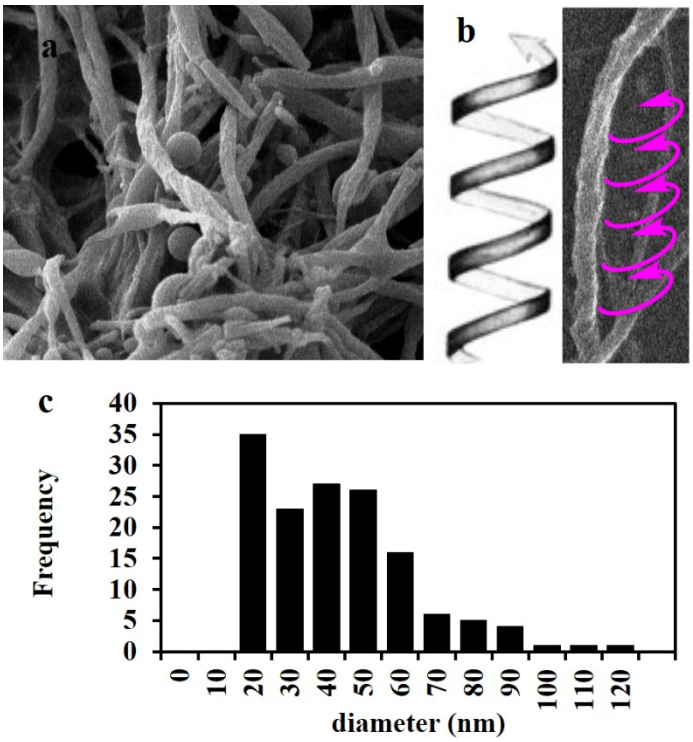

Figure 4-17. a) SEM image of the precipitate formed by **3b** in THF and water where X_{aq} = 0.6 illustrating the twisted coil morphology of the fibers, b) an illustration of the proposed right-handed twist of the fibers, and c) the distribution of sizes of the fibers obtained from the self-assembly of **3b** in THF and water where X_{aq} = 0.6.

Even at very low water concentrations (*i.e.*, X_{aq} = 0.2) the hexyl functionalized tetramer, **3b**, assumes a fibrous morphology with lengths less than 1 μm, and diameters of d_{avg} = 17 ± 6 nm (Figure 4-13 a). The diameters of these seed fibers is similar to those of the smallest fibers observed in the SEM images of the assemblies prepared where X_{aq} = 0.6. Adding more water (*i.e.*, X_{aq} = 0.4) coincides with the appearance of longer fibers and coiled superstructures (Figure 4-13 b). Beyond X_{aq} = 0.4 there is no change in the overall morphology or size of

the twisted coils. Instead, the increased water concentrations are accompanied by greater agglomeration of the fibers (Figure 4-13 c). These results are consistent with a transition occuring over the range of X_{aq} = 0.2 to 0.4 that leads to the onset of coiling of the short, 20 nm diameter fibers to form longer, wider coils observed in the SEM at higher X_{aq}.

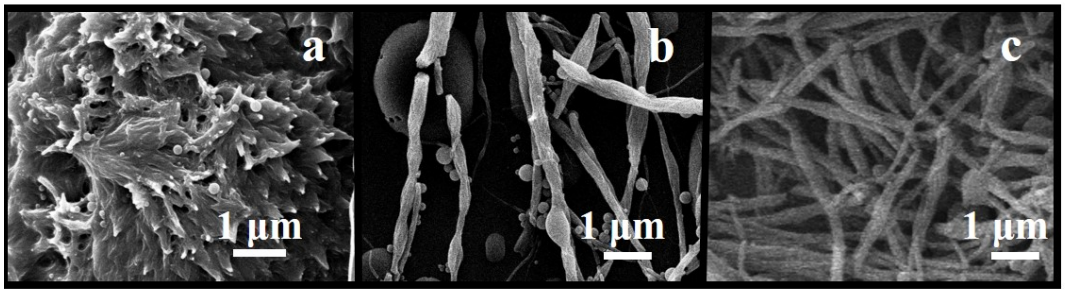

Figure 4-18. SEM images of the evolution of the fibers as water is gradually added to a solution of **3b** in THF where X_{aq} is: a) 0.2, b) 0.4 and c) 0.45.

The optical studies discussed in Section 4.3.3 show that the shift in the PL spectrum of **3c**, and the onset of hierarchical assembly suggested by the SEM results for **3b** occur at X_{aq} = 0.4. This result suggests there may be a relationship between the radial nature of the spines in the assemblies seen for **3c** and the coil morphology observed in the assemblies of **3b**. The evolution of the morphology of assemblies of **3c** at the onset of self-assembly was probed using a similar experimental method to that employed for **3b** discussed above. As the onset of the formation of the fibers of **3b** occurred at X_{aq} = 0.2, and their subsequent assembly into the coiled morphology occurred at X_{aq} = 0.4, assemblies of **3c** were prepared at these X_{aq} and their morphology probed using SEM (Figure 4-14, a-c). At X_{aq} = 0.2, there is evidence of assembly of **3c** into a twisted rod

geometry with no obvious preferred handedness to the twist of the rods observed in the SEM images (Figure 4-14 a). Increasing the water content to X_{aq} = 0.4 saw the appearance of a spiked morphology (Figure 4-14 b). The spikes are stacked and overlaped, with a rotational shift between each successive layer (Figure 4-14 b). Under higher magnification, the edge-wise overlap of the spikes at the central axis is more obvious suggesting the spikes grow radially from the twisted rods observed at X_{aq} = 0.2 (Figure 4-15, c, e, and f).

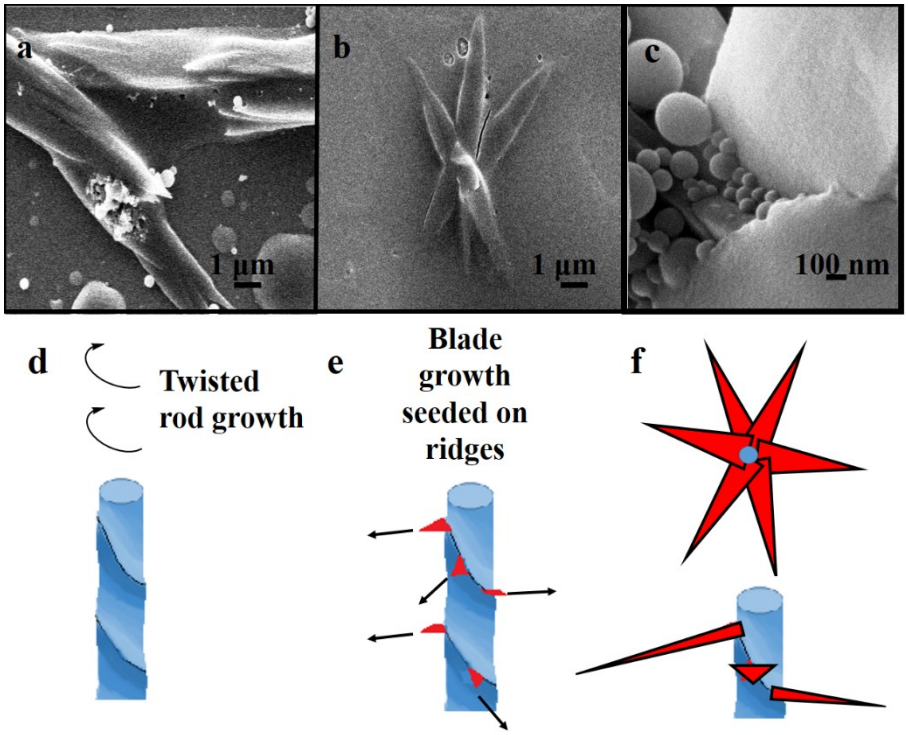

Figure 4-19. SEM images of suspensions of **3c** (a-c) summarizing the morphological evolution as the water content is increased from (a) X_{aq} = 0.2, to (b and c) X_{aq}= 0.4 along with schematic diagram of how hierarchical assembly evolves at d) X_{aq} = 0.2, e) X_{aq} = 0.3, and f) X_{aq} = 0.4.

The observation that the spikes of the spoked wheel follow the same rotational pattern as the twisting of ridges on the surface of the assembled microrods at X_{aq} = 0.2, suggests the ridges may be nucleation sites for the growth of the spiked geometries that are observed at X_{aq} = 0.4 (Figure 4-14). To investigate whether the number of nucleation sites could be modified by controlling the water addition rate **3c** was precipitated from THF by addition of water over a range of time intervals (*i.e.*, 30 seconds through 16 hours) to a final water concentration of X_{aq} = 0.6 (Figure 4-15). The morphology assumed by the assemblies of **3c** formed through rapid precipitation (*i.e.,* 30 second addition, Figure 4-15 a) is a mixture of short, poorly aligned spoked wheel structures, however in reducing the water addition rate two observations emerge.

First the lengths of the spine features increased from 13 ± 7 μm when water was added rapidly (Figure 4-15 a), to a maximum of 22 ± 7 μm for samples prepared upon slow addition of water over 16 hours (Figure 4-15 f). Additionally, when the water addition rate was decreased the number of spines also decreased. This decrease in the number of spines is accompanied by an increase in spine diameter from 340 ± 100 nm under rapid addition (Figure 4-15 a) to a maximum average spine thickness of 760 ± 260 nm when the water is added over a 16 hour time period (Figure 4-15 f). The sensitivity of the morphology to the water addition rates further supports that the formation spoked wheel like structures is kinetically controlled and that the twisted rod geometry is gradually dominated by the metastable stable spine geometry as the water content becomes large.

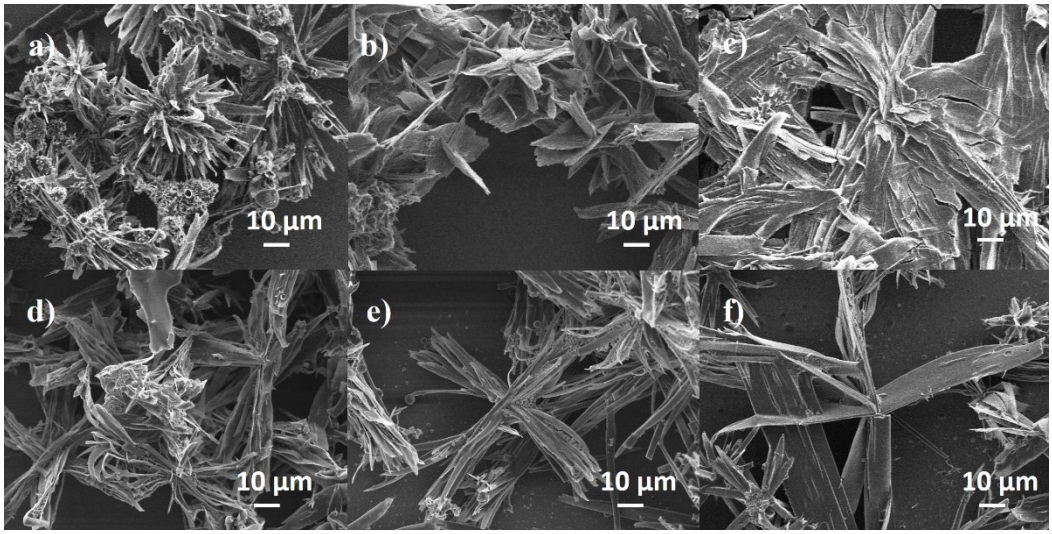

Figure 4-20. SEM images of assemblies of **3c** outlining the evolution of the morphology as the water addition rate is changed from a) 30 seconds to b) 20 minutes, c) 40 minutes, d) 1 hour, e) 2 hours, and f) 16 hours.

We propose that the formation of these two interesting structures observed from the self-assembly of compounds **3b** and **3c** occurs in a stepwise fashion. It starts with the directed assembly of the kinetic product- twisted fibers, and twisted rods that assemble in a 1D fashion. The second stage of the assembly process involves the formation of the thermodynamically stable product, involving the growth of the lateral aggregates in the form of coiled assemblies of fibers in the case of the hexyl substituted **3b** and in the form of paddles from the twisted rods of the octyl substituted **3c**.

4.2.4. Conclusions

In this section the influence of the length and steric bulk of the N-alkyl pendant groups on the self-assembly of carbazole based macrocycles was investigated. Three observations emerged based on the size and nature of the R-

group. First, the presence of steric bulk at the N-position disrupts formation of face-on π-stacked assemblies of macrocycles. This manifests in the promotion of short-range lateral assembly at the expense of significant 1D assembly where R is short and bulky, and prohibition of both lateral and 1D growth where R is bulky and long.

The second observation emerges from the tetramers that are functionalized with linear R groups, and suggests R that are too short (as in **3a**) are incapable of directing self-assembly. When the R groups are long linear alkyl chains, 1D and lateral growth are promoted resulting in the formation of microrods with fixed lengths and widths. This trend is only observed to hold until R group reaches a threshold length (*i.e.*, R= dodecyl) where the folding in of the R group becomes as deleterious to the self-assembly process as the addition of steric bulk.

The final observation is perhaps the most interesting, and involves the previously poorly studied R groups of intermediate length, where R is in the range of 6 to 8 carbons. Here morphologies are obtained through the hierarchical self-assembly of the macrocycles into 1D twisted morphologies. These morphologies then serve as nucleation sites for the growth of their secondary structure; coiled wires in the case of **3b** and spoked wheels for **3c**. The wide range of structures accessible to this family of compounds through self-assembly in simple binary solvent mixtures, in combination with their interesting optical and electronic properties suggests that these materials would be good candidates for application in various organic electronics.

4.3. References

(1) Pedersen, C. J. *Angew. Chem. Int. Ed. Engl.***1988**, *100*, 1053.

(2) Xue, W.; Li, Z.; Liu, G.; Chen, X.; Li, T.; Liu, S. H.; Yin, J. *Org. Biomol. Chem.* **2014**, *12*, 4862.

(3) Zhang, W.; Moore, J. S. *Angew. Chem. Int. Ed.* **2006**, *45*, 4416.

(4) Vehoff, T.; Kirkpatrick, J.; Kremer, K.; Andrienko, D. *Phys. Status Solidi* **2008**, *245*, 839.

(5) Vehoff, T.; Baumeier, B.; Andrienko, D. *J. Chem. Phys.* **2010**, *133*, 134901.

(6) Höger, S. *Chemistry* **2004**, *10*, 1320.

(7) Yang, Y.; Feng, W.; Hu, J.; Zou, S.; Gao, R.; Yamato, K.; Kline, M.; Cai, Z.; Gao, Y.; Wang, Y.; Li, Y.; Yang, Y.; Yuan, L.; Zeng, X. C.; Gong, B. *J. Am. Chem. Soc.* **2011**, *133*, 18590.

(8) Iyoda, M.; Yamakawa, J.; Rahman, M. J. *Angew. Chem. Int. Ed.* **2011**, *50*, 10522.

(9) Canevet, D.; Emilio, M. P.; Mart, N. *Organic Nanomaterials: Synthesis, Characterization, and Device Applications*; Torres, T.; Botlari, G., Eds.; John Wiley and Sons, **2013**; pp. 147–162.

(10) Dsouza, R. N.; Pischel, U.; Nau, W. M. *Chem. Rev.* **2011**, *111*, 7941.

(11) Kong, Q.; Qian, H.; Bo, H.; Zhang, C.; Liu, K.; Zhang, X.; Wang, J.; Li, J.; Gao, G. *Synth. Met.* **2011**, *161*, 2361.

(12) Schmaltz, B.; Rouhanipour, A.; Räder, H. J.; Pisula, W.; Müllen, K. *Angew. Chem. Int. Ed.* **2009**, *48*, 720.

(13) Baroncini, M.; Gao, C.; Carboni, V.; Credi, A.; Previtera, E.; Semeraro, M.; Venturi, M.; Silvi, S. *Chemistry* **2014**, *20*, 10737.

(14) Li, H.; Cheng, C.; Mcgonigal, P. R.; Fahrenbach, A. C.; Frasconi, M.; Liu, W.; Zhu, Z.; Zhao, Y.; Ke, C.; Lei, J.; Young, R. M.; Dyar, S. M.; Co, D. T.; Yang, Y.; Botros, Y. Y.; Goddard, W. A.; Wasielewski, M. R.; Astumian, R. D.; Stoddart, J. F. *J. Am. Chem. Soc.* **2014**, *136*, 10.

(15) Jena, N. K.; Murugan, N. A. *J. Phys. Chem. C* **2013**, *117*, 25059.

(16) Bruns, C. J.; Stoddart, J. F. *Acc. Chem. Res.* **2014**, *47*, 2186.

(17) Ghale, G.; Nau, W. M. *Acc. Chem. Res.* **2014**, *47*, 2150.

(18) Lan, J.; Zheng, X. H.; Hao, H.; Wang, X. L.; Shi, X. Q.; Zeng, Z. *J. Appl. Phys.* **2014**, *115*, 013702.

(19) Kallweit, C.; Haberhauer, G.; Woitschetzki, S. *Chemistry* **2014**, *20*, 6358.

(20) Ostrauskaite, J.; Strohriegl, P. *Macromol. Chem. Phys.* **2003**, *204*, 1713.

(21) Zhao, D.; Moore, J. S. *ChemInform* **2003**, *34*, 807.

(22) Laughrey, Z. R.; Gibb, B. C. *Top. Curr. Chem.* **2005**, *249*, 67.

(23) Sisco, S. W.; Larson, B. M.; Moore, J. S. *Macromolecules* **2014**, *47*, 3829.

(24) Finke, A. D.; Gross, D. E.; Han, A.; Moore, J. S. *J. Am. Chem. Soc.* **2011**, *133*, 14063.

(25) Jin, Y.; Wang, Q.; Taynton, P.; Zhang, W. *Acc. Chem. Res.* **2014**, *47*, 1575.

(26) Tobe, Y.; Utsumi, N.; Kawabata, K.; Nagano, A.; Adachi, K.; Araki, S.; Sonoda, M.; Hirose, K.; Naemura, K. *J. Am. Chem. Soc.* **2002**, *124*, 5350.

(27) Balakrishnan, K.; Datar, A.; Zhang, W.; Yang, X.; Naddo, T.; Huang, J.; Zuo, J.; Yen, M.; Moore, J. S.; Zang, L. *J. Am. Chem. Soc.* **2006**, *128*, 6576.

(28) Park, M.; Buck, J.; Rizzo, C. *Tetrahedron* **1998**, *54*, 12707.

(29) Cabaj, J.; Idzik, K.; Sołoducho, J.; Chyla, A. *Tetrahedron* **2006**, *62*, 758.

(30) Ludwiczak, M.; Majchrzak, M.; Bayda, M.; Marciniak, B.; Kubicki, M.; Marciniec, B. *J. Organomet. Chem.* **2014**, *750*, 150.

(31) Dong, W.; Fei, T.; Palma-Cando, A.; Scherf, U. *Polym. Chem.* **2014**, *5*, 4048.

(32) Pansay, S.; Prachumrak, N.; Jungsuttiwong, S.; Keawin, T.; Sudyoadsuk, T.; Promarak, V. *Tetrahedron Lett.* **2012**, *53*, 4568.

(33) Williams, A. T. R.; Winfield, S. A.; Miller, J. N. *Analyst* **1983**, *108*, 1067.

(34) Scott, T. A. J. *J. Phys. Chem.* **1946**, 406.

(35) Wankhede, D. S. *Int. J. Chem. Res.* **2011**, *2*, 23.

(36) Melhuish, W. H. *J. Phys. Chem.* **1961**, *97*, 229.

(37) Wothers, P.; Greeves, N.; Warren, S.; Clayden, J. *Organic Chemistry*; Oxford University Press, **2001**; pp. 437–438.

(38) Maruyama, S.; Hokari, H.; Wada, T.; Sasabe, H. *Synthesis* **2001**, *12*, 1794.

(39) Yamamoto, T.; Wakabayashi, S.; Osakada, K. *J. Organomet. Chem.* **1992**, *428*, 223.

(40) Shi, Y.; Liu, J.; Yang, Y. *J. Appl. Phys.* **2000**, *87*, 4254.

(41) Ruelle, P.; Sarraf, E.; Kesselring, U. W. *Int. J. Pharm.* **1994**, *104*, 125.

(42) Xu, B.; He, J.; Dong, Y.; Chen, F.; Yu, W.; Tian, W. *Chem. Commun.* **2011**, *47*, 6602.

(43) Zhai, Z.; Lam, J.; Tang, B. Z. *Soft Matter* **2013**, *9*, 4564.

(44) Hong, Y.; Lam, J. W. Y.; Tang, B. Z. *Chem. Commun.* **2009**, *45*, 4332.

(45) Dutta, A. *Langmuir* **1996**, *12*, 5909.

(46) Höger, S.; Bonrad, K.; Mourran, A.; Beginn, U.; Möller, M. *J. Am. Chem. Soc.* **2001**, *123*, 5651.

(47) Liu, X.; Xu, D.; Lu, R.; Li, B.; Qian, C.; Xue, P.; Zhang, X.; Zhou, H. *Chem. Eur. J.* **2011**, *17*, 1660.

(48) Belletête, M.; Bouchard, J.; Leclerc, M.; Durocher, G. *Macromolecules* **2005**, *38*, 880.

(49) Tirapattur, S.; Belletête, M.; Drolet, N.; Leclerc, M.; Durocher, G. *Chem. Phys. Lett.* **2003**, *370*, 799.

(50) Yagai, S.; Iwashima, T.; Kishikawa, K.; Nakahara, S.; Karatsu, T.; Kitamura, A. *Chemistry* **2006**, *12*, 3984.

(51) Huang, J.; Li, Q.; Li, Z. *Aggregation Inducced Emission: Fundamentals.* First Ed. **2013**, John Wiley and Sons.

(52) Tomasini, C.; Castellucci, N. *Chem. Soc. Rev.* **2013**, *42*, 156.

(53) Avinash, M. B.; Govindaraju, T. *Nanoscale* **2014**, *6*, 13348.

(54) Sagiri, S. S.; Behera, B.; Rafanan, R. R.; Bhattacharya, C.; Pal, K.; Banerjee, I.; Rousseau, D. *Soft Mater*. **2014**, *12*, 47.

(55) Vintiloiu, A.; Leroux, J.-C. *J. Control. Release* **2008**, *125*, 179.

(56) Díaz Díaz, D.; Kühbeck, D.; Koopmans, R. *J. Chem. Soc. Rev.* **2011**, *40*, 427.

(57) Li, Y.; Liu, T.; Liu, H.; Tian, M.-Z.; Li, Y. *Acc. Chem. Res.* **2014**, *47*, 1186.

(58) Schenning, A. P. H. J.; Meijer, E. W. *Chem. Commun.* **2005**, *41*, 3245.

(59) Delclos, T.; Aimé, C.; Pouget, E.; Brizard, A.; Huc, I.; Delviles, M.; Oda, R. *Nano Lett.* **2008**, *8*, 1929.

(60) Banerjee, S.; Das, R. K.; Maitra, U. *J. Mater. Chem.* **2009**, *19*, 6649.

(61) Zhao, Z.; Lam, J. W. Y.; Tang, B. Z. *Soft Matter* **2013**, *9*, 4564.

(62) Shelnutt, J.; Medforth, C. In *Organic Nanomaterials: Synthesis, Characterization, and Device Applications*; **2013**; First Edit, p.103-130.

(63) Wang, Z.; Medforth, C. J.; Shelnutt, J. A. *J. Am. Chem. Soc.* **2004**, *126*, 15954.

(64) Wang, Z.; Ho, K. J.; Medforth, C. J.; Shelnutt, J. A. *Adv. Mater.* **2006**, *18*, 2557.

(65) Balakrishnan, K.; Datar, A.; Naddo, T.; Huang, J.; Oitker, R.; Yen, M.; Zhao, J.; Zang, L. *J. Am. Chem. Soc.* **2006**, *128*, 7390.

(66) Zhang, Z.; Zhan, C.; Zhang, X.; Zhang, S.; Huang, J.; Li, A. D. Q.; Yao, J. *Chemistry* **2012**, *18*, 12305.

(67) Ma, L.; Wang, Q.; Lu, G.; Chen, R.; Sun, X. *Langmuir* **2010**, *26*, 6702.

(68) Xie, L.; Yang, S.; Lin, J.; Yi, M.; Huang, W. *Philos. Trans. R. Soc. London A* **2013**, *371*, 20120337.

(69) Surin, M.; Sonar, P.; Grimsdale, A. C.; Müllen, K.; De Feyter, S.; Habuchi, S.; Sarzi, S.; Braeken, E.; Ver Heyen, A.; Van der Auweraer, M.; De Schryver, F. C.; Cavallini, M.; Moulin, J.-F.; Biscarini, F.; Femoni, C.; Lazzaroni, R.; Leclére, P. *J. Mater. Chem.* **2007**, *17*, 728.

(70) Maggini, L.; Bonifazi, D. *Chem. Soc. Rev.* **2012**, *41*, 211.

(71) Tsai, W.-W.; Tevis, I. D.; Tayi, A. S.; Cui, H.; Stupp, S. I. *J. Phys. Chem. B* **2010**, *114*, 14778.

(72) Gentili, D.; Di Maria, F.; Liscio, F.; Ferlauto, L.; Leonardi, F.; Maini, L.; Gazzano, M.; Milita, S.; Barbarella, G.; Cavallini, M. *J. Mater. Chem.* **2012**, *22*, 20852.

(73) Di Maria, F.; Olivelli, P.; Gazzano, M.; Zanelli, A.; Biasiucci, M.; Gigli, G.; Gentili, D.; D'Angelo, P.; Cavallini, M.; Barbarella, G. *J. Am. Chem. Soc.* **2011**, *133*, 8654.

(74) Tevis, I. D.; Palmer, L. C.; Herman, D. J.; Murray, I. P.; Stone, D. A.; Stupp, S. I. *J. Am. Chem. Soc.* **2011**, *133*, 16486.

(75) Korevaar, P. A.; Schaefer, C.; de Greef, T. F. A.; Meijer, E. W. *J. Am. Chem. Soc.* **2012**, *134*, 13482.

(76) Schenning, A. P. H. J.; Jonkheijm, P.; Peeters, E.; Meijer, E. W. *J. Am. Chem. Soc.* **2001**, *123*, 409.

(77) Beaujuge, P. M.; Reynolds, J. R. *Chem. Rev.* **2010**, *110*, 268.

(78) Hu, B.; Lv, X.; Sun, J.; Bian, G.; Ouyang, M.; Fu, Z.; Wang, P.; Zhang, C. *Org. Electron.* **2013**, *14*, 1521.

(79) Baycan Koyuncu, F.; Koyuncu, S.; Ozdemir, E. *Org. Electron.* **2011**, *12*, 1701.

(80) Verghese, M.; Ram, M.; Vardhan, H. *Polymer* **1997**, *38*, 1625.

(81) Verghese, M. M.; Ram, M. K.; Vardhan, H.; Ashrafb, S. M.; Malhotra, B. D. *Adv. Mater. Opt. Electron.* **1996**, *6*, 399.

(82) Tran-van, F.; Vancaeyzeele, C.; Henri, T.; Gazulevivius, J. V.; Chevrot, C. *Mater. Res. Soc. Symp. Proc.* **2002**, *708*, 1.

(83) Hu, B.; Yang, Z.; Karasz, F. E. *J. Appl. Phys.* **1994**, *76*, 2419.

(84) Qian, Y.; Cao, F.; Guo, W. *Tetrahedron* **2013**, *69*, 4169.

(85) Wang, Y.; Hou, L.; Yang, K.; Chen, J.; Wang, F.; Cao, Y. *Macromol. Chem. Phys.* **2005**, *206*, 2190.

(86) Boudreault, P. T.; Blouin, N.; Leclerc, M. *Adv. Polym. Sci.* **2008**, *212*, 99.

(87) Xu, X.; Cai, W.; Chen, J.; Cao, Y. *J. Polym. Sci. Part A Polym. Chem.* **2011**, *49*, 1263.

(88) Casey, A.; Ashraf, R. S.; Fei, Z.; Heeney, M. *Macromolecules* **2014,** *47,* 2279.

(89) Lek, J. Y.; Lam, Y. M.; Niziol, J.; Marzec, M. *Nanotechnology* **2012**, *23*, 315401.

(90) Xie, H.; Zhang, K.; Duan, C.; Liu, S.; Huang, F.; Cao, Y. *Polymer* **2012**, *53*, 5675.

(91) El-Shafei, A.; Hussain, M.; Atiq, A.; Islam, A.; Han, L. *J. Mater. Chem.* **2012**, *22*, 24048.

(92) Zheng, C.; Tao, Y.; Cao, J.-Z.; Chen, R.-F.; Zhao, P.; Wu, X.-J.; Huang, W. *J. Mol. Model.* **2012**, *18*, 4929.

(93) Zhao, T.; Liu, Z.; Song, Y.; Xu, W.; Zhang, D.; Zhu, D. *J. Org. Chem.* **2006**, *71*, 7422.

(94) Che, Y.; Gross, D. E.; Huang, H.; Yang, D.; Yang, X.; Discekici, E.; Xue, Z.; Zhao, H.; Moore, J. S.; Zang, L. *J. Am. Chem. Soc.* **2012**, *134*, 4978.

(95) Yang, Y.; Xue, M.; Marshall, L. J.; de Mendoza, J. *Org. Lett.* **2011**, *13*, 3186.

(96) Jung, S.-H.; Pisula, W.; Rouhanipour, A.; Räder, H. J.; Jacob, J.; Müllen, K. *Angew. Chem. Int. Ed*. **2006**, *45*, 4685.

(97) Upamali, K. A. N.; Estrada, L. A.; De, P. K.; Cai, X.; Krause, J. A.; Neckers, D. C. *Langmuir* **2011**, *27*, 1573.

(98) Sinnokrot, M. O.; Valéev, E. F.; Sherrill, C. D. *J. Am. Chem. Soc.* **2002**, *124*, 10887.

(99) Ayoub, A. T.; Tuszynski, J.; Klobukowski, M. Theor. *Chem. Acc.* **2014**, *133*, 1520.

(100) Zumdahl, S. S. *Chemistry*; 5th ed.; p. 373.

(101) Martinez, C. R.; Iverson, B. L. *Chem. Sci.* **2012**, *3*, 2191.

(102) Palmans, A. R. A; Meijer, E. W. *Angew. Chem. Int. Ed.* **2007**, *46*, 8948.

(103) Raeburn, J.; Zamith Cardoso, A.; Adams, D. *J. Chem. Soc. Rev.* **2013**, *42*, 5143.

(104) Wunsch, B. H.; Rumi, M.; Tummala, N. R.; Risko, C.; Kang, D.-Y.; Steirer, K. X.; Gantz, J.; Said, M.; Armstrong, N. R.; Brédas, J.-L.; Bucknall, D.; Marder, S. R. *J. Mater. Chem. C* **2013**, *1*, 5250.

(105) Sumrak, J. C.; Sokolov, A. N.; MacGillivray, L. R. In *Crystal Engineering Organic Semiconductors*; **2011**; pp. 1–19.

(106) Kastler, M.; Pisula, W.; Wasserfallen, D.; Pakula, T.; Müllen, K. *J. Am. Chem. Soc.* **2005**, *127*, 4286.

(107) Höger, S.; Bonrad, K.; Mourran, A.; Beginn, U.; Möller, M. *J. Am. Chem. Soc.* **2001**, *123*, 5651.

(108) Yu, G.; Yan, X.; Han, C.; Huang, F. *Chem. Soc. Rev.* **2013**, *42*, 6697.

(109) Yagai, S.; Gushiken, M.; Karatsu, T.; Kitamura, A.; Kikkawa, Y. *Chem. Commun.* **2011**, *47*, 454.

(110) Canevet, D.; Pérez del Pino, Á.; Amabilino, D. B.; Sallé, M. *J. Mater. Chem.* **2011**, *21*, 1428.

(111) Spano, F. C.; Silva, C. *Annu. Rev. Phys. Chem.* **2014**, *65*, 477.

(112) Brédas, J. L.; Cornil, J.; Beljonne, D.; Dos Santos, D.; Shuai, Z. G. *Acc. Chem. Res.* **1999**, *32*, 267.

(113) Chochos, C. L.; Choulis, S. A. *Prog. Polym. Sci.* **2011**, *36*, 1326.

(114) Siddiqui, S.; Spano, F. C. *Chem. Phys. Lett.* **1999**, *308*, 99.

(115) Yamagata, H.; Spano, F. C. *J. Chem. Phys.* **2012**, *136*, 184901.

(116) Dong, S.; Li, Z.; Qin, J. *J. Phys. Chem. B* **2009**, *113*, 434.

(117) Lin, H.; Zheng, M.; Yang, J.; Bai, F. *Chinese Sci. Bull.* **2013**, *48*, 637.

(118) Spectus, C. O. N.; Palmer, L.; Stupp, S. *Acc. Chem. Res.* **2008**, *41*, 1674.

(119) Kim, F. S.; Ren, G.; Jenekhe, S. A. *Chem. Mater.* **2011**, *23*, 682.

(120) Zang, L.; Che, Y.; Moore, J. S. *Acc. Chem. Res.* **2008**, *41*, 1596.

(121) Estroff, L. A.; Hamilton, A. D. *Chem. Rev.* **2004**, *104*, 1201.

(122) Meylemans, H. A.; Damrauer, N. H. *Inorg. Chem.* **2009**, *48*, 11161.

(123) Heeger, A. J. *Chem. Soc. Rev.* **2010**, *39*, 2354.

(124) Beckers, E. H. A.; Meskers, S. C. J.; Schenning, A. P. H. J.; Chen, Z.; Würthner, F.; Marsal, P.; Beljonne, D.; Cornil, J.; Janssen, R. A. J. *J. Am. Chem. Soc.* **2006**, *128*, 649.

(125) Amabilino, D. B. In *Organic Nanomaterials: Synthesis, Characterization, and Device Applications*; **2013**; First Edit, pp. 59–77.

(126) George, S. J.; Ajayaghosh, A.; Jonkheijm, P.; Schenning, A. P. H. J.; Meijer, E. W. *Angew. Chemie. Int. Ed.* **2004**, *43*, 3422.

(127) Ruiz, L.; Keten, S. J. *Phys. Chem. Lett.* **2014**, *5*, 2021.

(128) Korevaar, P. A.; de Greef, T. F. A.; Meijer, E. W. *Chem. Mater.* **2014**, *26*, 576-586.

(129) Jonkheijm, P.; van der Schoot, P.; Schenning, A. P. H. J.; Meijer, E. W. *Science* **2006**, *313*, 80.

Chapter 5:

A computational investigation into the effects of substituting the spiro-bridging atom in spirobifluorene-based molecules influences charge-transfer

5.1. Introduction

Polyfluorene (PF)-based materials have long been explored as active systems in blue light-emitting diodes;[1,2] most recently they have garnered attention as wide band-gap materials for polymer solar cells (PSCs).[3] The substantial research and development of PFs has been spurred by their high luminescent quantum efficiencies, straightforward preparation, and solution processability that allows for low cost device production.[4,5] While attractive, the instability of the quaternary carbon in the 9-position has limited their large-scale application.[6-8] One strategy employed to improve the stability of PFs has been to replace the carbon in the 9-position with a heavier silicon atom.[9] Studies of alternating copolymers containing 9,9′- dialkylfluorene, 9,9′-dialkyldibenzosilole,[9,10] and 9,9′-dialkyldibenzogermole[11] blocks with various fluorophores have facilitated tuning of the luminescent maximum (see Figure 5-1).[9,12,13] In addition, these same materials have been used as hosts in electro-phosphorescent organic light-emitting diodes, and their absorbance maximum may also be tuned to produce improve absorbers for use in PSCs.[4,9,13-16]

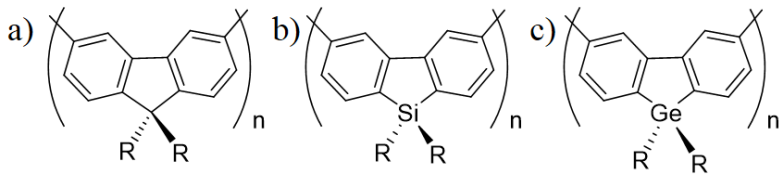

Figure 5-1. General structures of a) 9,9′- dialkylfluorene, b) 9,9′-dialkyldibenzosilole, and c) 9,9′-dialkyldibenzogermole.

A subclass of PF materials containing spirobifluorene (SBF, Figure 5-2) residues has become very popular because the steric bulk offered by the off-chain moieties, that are held rigidly perpendicular to the main chain, inhibits close approach of neighboring polymer chains and minimize red-shifted excimer-based emission.[17] Excimer-based defects are electron traps that inhibit carrier mobility in PFs and limit exciton diffusion lengths.[18] Investigations of the complex photophysics of SBFs unearthed discoveries that they exhibit two-photon absorption,[19] polaron absorption,[20] and upon introduction of electron donating pendant groups, polarization of charge in the excited state across the quaternary spiro-centre *via* a mechanism known as spiro-conjugation.[21]

As a direct consequence of spiroconjugation, SBF homopolymers exhibit enhanced carrier mobilities and form mixed charge transfer (CT) excited states that may reside at lower energy than the lowest energy singlet state.[22,23] Weak photoluminescence at the nanosecond timescale has been attributed to charge transfer states involving symmetry forbidden, yet vibronically allowed spiro-conjugation between the polyfluorene backbone, and a terminal spiro-sidegroup.[21]

It is useful to recall that the PF structural unit consists of a cyclopentadiene (Cp) moiety flanked by two aromatic rings (Figure 5-2). Materials based upon a Cp scaffold exhibit narrower band-gaps and increased conductivity through the incorporation of silole functionality.[24] The origin of this property has been attributed to the subtle differences in the electronic structure of the heavier metallole.[25] It has been suggested the higher electron mobilities result

from σ*-π* conjugation between Si-C σ*-orbitals and the π*-system of the conjugated diene.[26] The overall effect of the introduction of this heteroatom is a reduction in the energy of the lowest unoccupied molecular orbital (LUMO). [25] Further studies of Cp derivatives incorporating heavier Group 14 elements show the impact of these elements on the LUMO is insignificant due to increased C-M bond lengths.[27,28] Still, there remains great interest in the Ge and Sn SBF analogues because of the increased three dimensional conduction exhibited by these materials.[11,29]

The nature of the atom at the 9-position has little influence on the optical properties of the dibenzometallole core, but it does have a positive influence on the redox potentials of these molecules.[26] However, redox potentials are not the only properties that point to increasing the size of the spiro-centre in these systems as a means toward influencing device performance. The inclusion of silole functionalities into a fluorene skeleton allows for more efficient interchain packing relative to carbon based analogues, leading to more efficient PSCs.[30] Enhanced carrier mobilities in the conjugated polymer within bulk heterojunction PSC significantly impact the overall device performance; higher carrier mobilities reduce bimolecular recombinative losses and faciliate the production of devices with thicker photoactive layers which increases the fill factor and therefore overall device efficiency.[31]

Here, we present the results of a computational study of monomers (Figure 5-2, **4a**-**4d**) and trimers (Figure 5-2, **5a**-**5d**) based upon a 2,7-oligo-spirobifluorene skeleton. Our investigation tracks the impact of changing the

identity of the spiro atom (*i.e.*, 9-position, Figure 5-2) to Si, Ge, and Sn. Recent research has shown that many functionals used in density functional theory (DFT) are inaccurate when applied to the calculation of charge transfer transitions in π-conjugated molecules due to over-estimation of electron correlation.[32] To investigate the impact of functional choice on spiroconjugation, the off-chain CT was approximated by modelling the excited states of the molecules at the time dependent DFT (TD-DFT) level of theory using three combinations of functional and basis set. Our aim is to investigate whether this substitution changes the CT mechanism responsible for the weak spiroconjugation effects in the carbon only **5a**, to σ*-π* conjugation involving the heavier more polarisable elements, which may help design better materials for PSCs. Our results show that prediction of CT in spiroconjugated systems is more sensitive to functional choice (*i.e.*, through long-range correction) than to augmentation of the basis set using polarization functions.

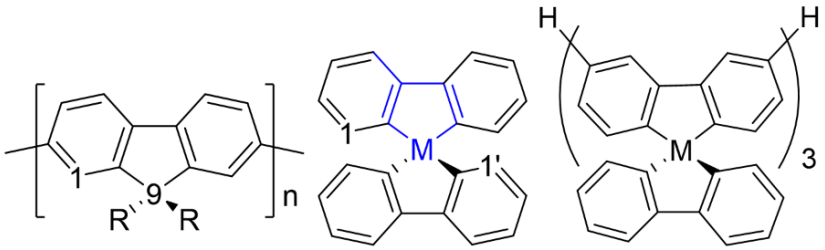

Figure 5-2. General structures of polyfluorene skeleton (left) and structures of the SBF based monomers (centre) and trimers (right) investigated here, with the metallole unit highlighted in blue.

5.2. Experimental

5.2.1. Computational methods

Calculations were performed using the Gaussian 09 program[33] at the DFT level of theory employing the compact effective potentials of Stevens, Basch, and Krauss [51, 34] the B3LYP hybrid exchange-correlation functional. The B3LYP functiona was used due to its lack of sensitivity to basis set selection in achieving accurate descriptions of charge transfer in spiro-type systems.[35] Simulated singlet excitons were calculated using TD-DFT methods including the first six excited states. Calculations of vertical excitations were performed using TD-DFT methods in the absence of excited state geometry optimization. All optimized geometries were confirmed to be energetic minima on the potential energy surface by calculating the Hessian matrix, and noticing the absence of imaginary vibrational frequencies.

To investigate the impact of long-range corrected functionals on the prediction of charge transfer properties in this system, the calculations were repeated using the short-range generalized gradient approximation based functional of Perdew-Burke-Ernzerhof, [36] with the long range correction of Vydrov *et al.* (LC-ωPBE).[37, 38] In the final calculations, a long-range corrected functional functional was again employed, using a special basis set based on a 3-21g basis with added d-type polarization functions to heavy atoms (*i.e.*, C, Si, Ge and Sn).[38-40]

All bond distances and angles were determined using the MOLDEN molecular visualization program using the optimized geometries of calculated at the given levels of theory. Visualization of the molecular orbitals discussed in this chapter was performed using the Gaussview 5 Suite provided by the University of Alberta through the Numerical and Statistical Server.

5.2.2. Calculation of energies

The spiro splitting energy, $\Delta E_{SPIRO,}$ is calculated as the energy difference between the highest occupied molecular orbital (HOMO) and HOMO-1. This calculation treats the molecules as a Class II spiro molecule as defined by Simmons *et al.* where an equivalent, even number of π-bonds exist on both orthogonal spiro-moieties. The spiro splitting energy is presented as a measure of the gain in delocalization which occurs by adopting the spiro arrangement when compared to the parent metallole.[41] The energy difference between the highest occupied molecular orbital (HOMO) and lowest unoccupied molecular orbital (LUMO) is presented as the HOMO/LUMO gap, E_g. The vertical excitation energy, ΔE_{TD} is the energy corresponding to the lowest energy singlet excited state as calculated using TD-DFT methods. For TD calculations the percentage of contribution of the stated transitions to the overall excited state results from taking the square of the expansion coefficients and appears in brackets next to the transitions tabulated below. The predicted relative intensity of each excited state is given by the oscillator strength (f), which is a unitless quanity.

5. 3. Results and discussion

5.3.2. Monomer and trimer calculations with minimal basis set: B3LYP/CEP-31G level of theory

Geometry optimization yielded structures with bond angles (θ_{spiro}) and lengths of the delocalized phenyl bonds (d_{PH}), and the σ-bond to the spiro-centre ($d_{C\text{-}M}$) that agree with values determined experimentally for **4a** (Figure 5-3).[42] As expected, introducing heavier 14 elements at the spiro centre leads to a linear increase in the calculated C-M bond lengths from 1.551 Å for **4a**, to a maximum of 2.125 Å for **4d**; this also resulted in deviation of the C-M-C angles from the ideal 109.5° in **4b-4d** (see Table 5-1). Analysis of the trimers (Table 5-2) revealed the biphenyl bridging bond length (d_{BB}), also increased resulting in an overall expansion of the metallole ring with heavier M.

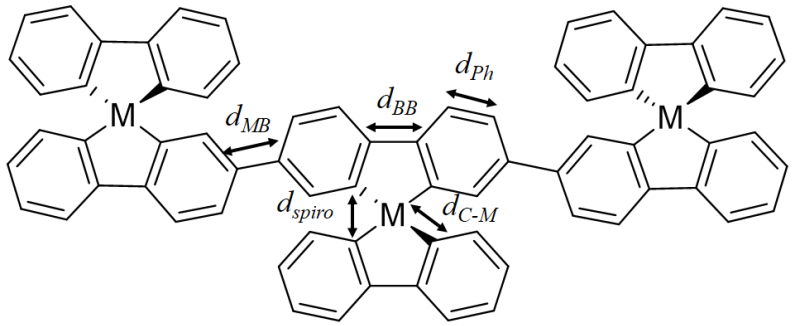

Figure 5-3. General structure of spiro trimers investigated in the present study. Key geometrical parameters used to assess material properties are shown.

This structural reorganization arising from changes at the spiro site is also manifested in the degree of spiroconjugation. The distance between mutually perpendicular π-systems (d_{spiro}) is commonly measured as the distance

between C_1 and $C_{1'}$ (Figure 5-2) through analysis of the optimized structures.[43] The values increase monotonically from **4a** (2.259 Å) to **4d** (3.732 Å) as summarized in Table 5-1. The impact of this expansion of the interfluorene space with larger M is manifested in a reduction of favorable overlap between adjacent π-systems.

Compound	d_{Ph} (Å)	d_{BB} (Å)	d_{MB} (Å)	$d_{C\text{-}M}$ (Å)	d_{spiro} (Å)	θ_{spiro} (°)
4a	1.424	1.491	-	1.551	2.259	97.34
4b	1.426	1.510	-	1.905	3.288	91.28
4c	1.410	1.512	-	1.939	3.381	89.97
4d	1.427	1.519	-	2.125	3.732	85.12
5a	1.409	1.427	1.503	1.540	-	-
5b	1.427	1.506	1.502	1.906	-	-
5c	1.412	1.507	1.499	1.939	-	-
5d	1.413	1.515	1.499	2.111	-	-

Table 5-1. Structural parameters for d_{Ph}, d_{BB}, d_{MB}, and $d_{C\text{-}M}$ for **4a-4d** and **5a-5d**.

The frontier orbitals of **4a-d** are shown pictorially in Figure 5-4. In all cases the HOMOs exhibit π-symmetry with the electron density distributed equally over the mutually perpendicular fluorene moieties. The LUMOs possess density that is localized primarily on a single fluorene moiety, however they

differ in how the density is distributed about the spiro-dibenzometallole center. For **4a**, the electron density resides primarily on one of the two fluorene units.

As the size of the atom at the spiro-center increases from **4a** to **4d** (*i.e.*, C → Si → Ge → Sn) the amount of electron density residing in the inter-fluorene space increases because of partial occupation of σ*-orbitals localized about the spiro center. For **4c**, substantial electron density is shared between perpendicular biphenyl moieties. Surprisingly, the less electron density located about the spiro-center in the interfluorene space in **4d**, indicating poor communication between orthogonal fluorene units. It is reasonable that this observation results from poorer shielding from d-orbitals, a net contraction of electron density about heavy atoms due to relativistic effects, and a reduction in effective overlap in the metallole unit leading to a limited σ*-contribution to the excited state of **4d**.[52]

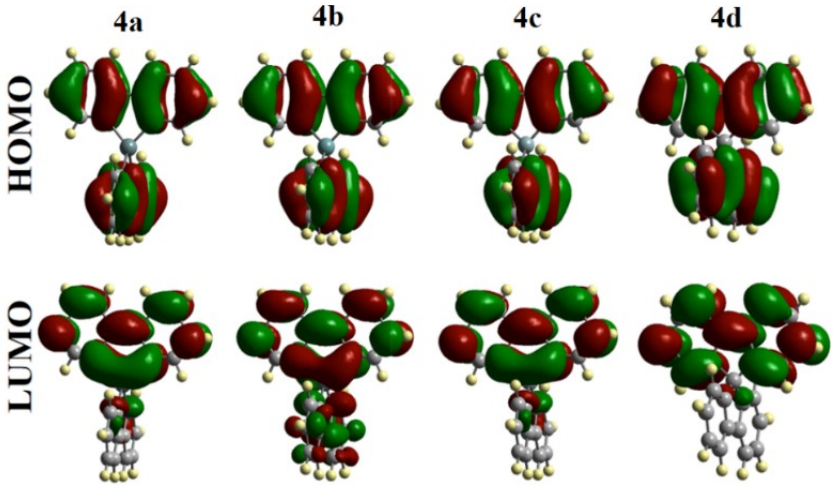

Figure 5-4. A depiction of the HOMO and LUMO orbitals for **4a**, **4b**, **4c**, and **4d** calculated at the B3LYP/CEP-31G level of theory.

To obtain a better understanding of the impact of increased occupation of the interfluorene space would have on an extended π-system, we expanded our

study to include trimers, (see Figure 5-2). The calculated HOMO-LUMO gaps (*i.e.*, E_g) for the trimers are inversely related to the atomic number of the atom at the spiro-position (*i.e.*, E_g decrease as heavier spiro-atoms; see Table 5-2). Again, the E_g determined for **5c** deviates from the trend of decreasing E_g observed as M is changed from C, for **5a** in which E_g = 3.684 eV, to the heavier Si and Sn derivatives where **5b** has E_g = 3.607 eV, and **5c** has E_g = 3.610 eV. This anomalously large value of 3.634 eV arises because of the anomalously high electronegativity of Ge.[45]

Compound Number	ε_{HOMO-1}	ε_{HOMO}	ε_{LUMO}	ΔE_{SPIRO}	E_g	ΔE_{TD}
4a	-6.051	-5.747	-1.018	0.142	4.729	-
4b	-6.070	-5.921	-1.281	0.089	4.640	-
4c	-6.069	-5.943	-1.254	0.063	4.690	-
4d	-6.055	-5.961	-1.308	0.027	4.653	-
5a	-	-5.276	-1.592	-	3.684	3.2756
5b	-	-5.36	-1.753	-	3.607	3.1914
5c	-	-5.378	-1.744	-	3.634	3.2188
5d	-	-5.387	-1.777	-	3.610	3.1925

Table 5-2. Calculated energies (in eV) of frontier orbitals and HOMO-LUMO (E_g) and spiro splitting energies.

The present results reflect narrower E_g values than those determined by Chen *et al*. for hydrogen functionalized heterofluorene trimers (*i.e.*, E_g = 3.848, 3.769, and 3.786 eV for C, Si and Ge, respectively).[25] This difference presumably results from a contraction of the oligofluorene skeleton, and is manifested in the degree of bond length alternation between the biphenyl bond, d_{BB}, and adjacent phenyl double bonds, d_{Ph}, which is lower in the spirobifluorene derived **5a-5d** than those calculated for the hydrogenated derivatives studied by Chen (Table 5-2, and Figure 5-5).[46-48] Another factor that may contribute to narrowing of E_g is the extension of the π-system through neighbouring backbone fluorenes; [49] this is apparent from the decrease in length of the C-C bonds bridging adjacent monomers, $d_{MB,}$ in **5c** and **5d** relative to **5a** and **5b** (Table 5-1).

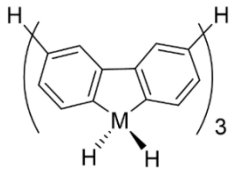

M = C, Si, Ge and Sn

Figure 5-5. The structures of the dibenzometalloles studied by Chen *et al*.[25]

As the size of the spiro-atom is increased, we also note the majority of the lengthening of the C-M bond is manifested in an overall elongation of the backbone. The optimized geometry for **5a** exhibits alternating orientations of the spiro-moiety relative to the plane of the backbone that deviate from mirror symmetry by a rotational angle denoted by θ_{dh} (see Figure 5-6). This semi-helical structure reflects the conformation common to α-phase polyfluorene in solution and can influence the charge transfer through increases in states wherein electron

density is localized on the backbone relative to the states in which the density is confined to the off-chain spiro moieties.[50]

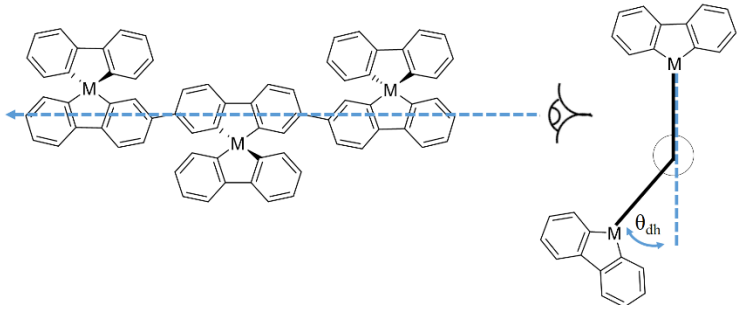

Figure 5-6. Illustration of the meaning of the backbone dihedral angle, θ_{dh}.

The measurable impact of the large dihedral angles on the properties of **5a**-**5d** is their direct influence on E_g through limitation of the effective conjugation length.[51] This arises because the effective conjugation length of the target metallo-SBF polymers depends on the length of d_{ME} and the deviation of the backbone from planarity, as reflected in the dihedral angles θ_{dh}.[51] The dihedral angle observed in **5a** is 34°, notably smaller than the result of 41° obtained by Franco *et al.* who performed similar calculations involving α-phase polyfluorene.[52] The introduction of the heavier, electron-rich centers (*i.e.*, Si, Ge, Sn) is expected to introduce greater electronic repulsions, which drive an overall loss in planarity of the trimers and will certainly influence charge polarization of the system.[53] To investigate the combined impact of the loss of planarity and expanding metallole units on the optical properties of the present model systems TDDFT calculations were performed.

The occurrence and likelihood of occupation of CT states in the trimers **5a**, **5b**, **5c** and **5d** were evaluated using TD-DFT methods. Observation of the

frontier orbitals belonging to the trimers highlights their electronic similarities. In all cases the HOMO and LUMO (see Figure 5-7) consist of the electron density residing along the main chain. Excitations from the HOMO to LUMO in all trimers are calculated to be the most probable, with oscillator strengths of 1.9615 for **5a**, and decreasing to 1.8179, 1.8745, and 1.8366 for **5b**, **5c**, and **5d**, respectively (Table 5-4).

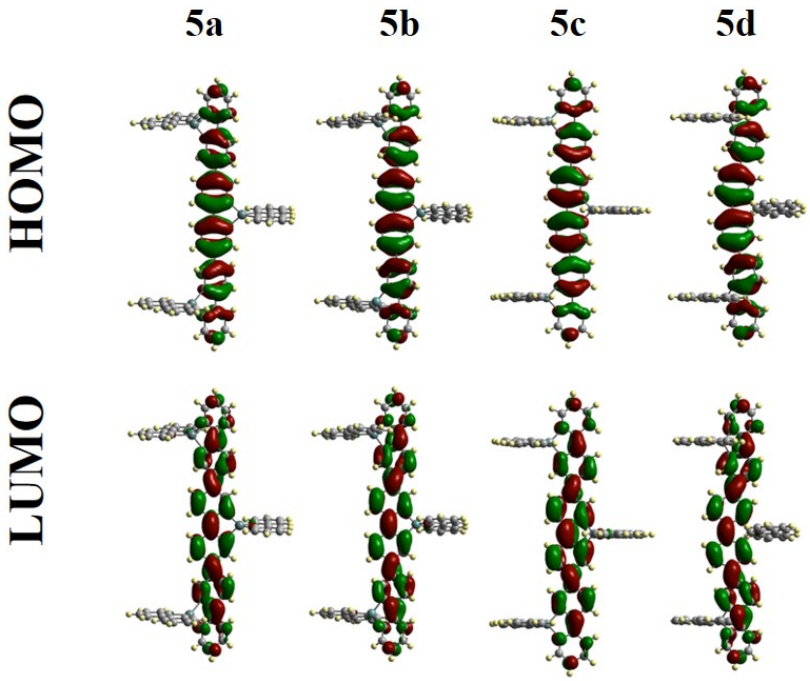

Figure 5-7. The HOMO and LUMO orbitals for **5a**, **5b**, **5c**, and **5d** calculated at the B3LYP/CEP-31G level of theory.

Visualization of higher order molecular orbitals in **5a-5d** revealed the three orbitals of lowest energy with significant off-chain charge polarization are the LUMO+2, LUMO+3 and LUMO+4, with density residing on the single central, two peripheral, and three pendant groups, respectively (Figure 5-8). From the perspective of designing materials for PPVs, all of these states would

be equally attractive; they are close in energy and the electron density resides off-chain in each CT state. This localization of electron density onto pendant fluorene groups renders the excited-state electrons more accessible to a neighboring electron acceptor,[54] and within a less structurally hindered environment that could allow for better overlap of the MOs with neighbouring chains and lead to faster, more efficient charge separation.[55]

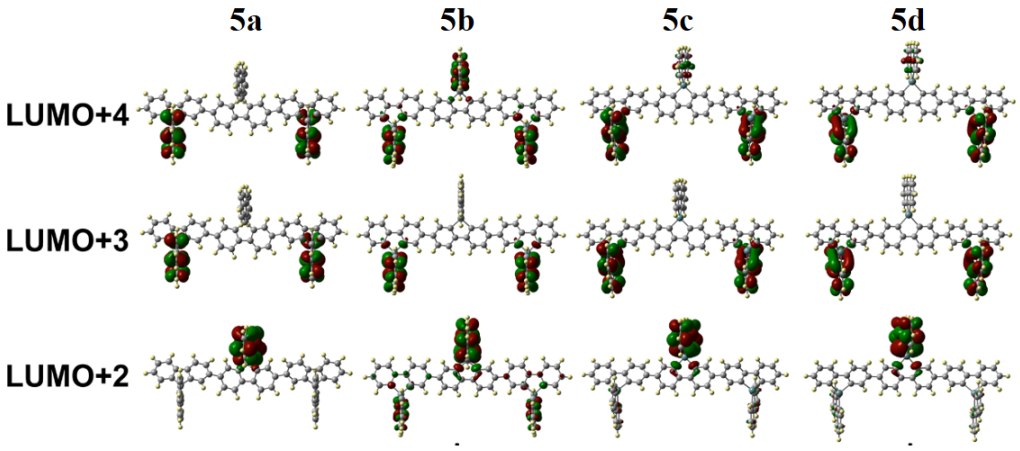

Figure 5-8. LUMO+2, LUMO+3 and LUMO+4 orbitals as well as a view down the axis of the backbone for **5a**- **5d** calculated at the B3LYP/CEP-31G level of theory.

Spontaneous charge polarization in **5a**, and polySBFs in general is limited by the nature of the electronic states localized to the π-systems. Efficient charge transfer states require the HOMO of the donor be antisymmetric with respect to the LUMO of the acceptor; this is not the case for **5a**.[56] Only singlet excited states 2 and 4 (*i.e.*, E_{S2} and E_{S4}, respectively) possess significant contributions from the LUMO+2 and LUMO+3 (see Table 5-4) with oscillator

strengths of *ca.* 10^{-3} and high excitation energies of 3.786 eV and 3.869 eV, respectively.

With the introduction of a more polarisable Si atom at the 9-position of the spirobifluorene unit the oscillator strengths for transitions involving charge polarization increase five-fold, and the number of excitations with off-chain CT contributions doubles. Introducing Ge and Sn (*i.e.*, **5c** and **5d**) sees an overall increase in the oscillator strengths of the 4^{th} and 6^{th} excitation to one order of magnitude greater than that observed in **5a**, and continued increases in the number of accessible CT states for the first 6 singlet vertical excitations.

Compound Number	E_{S1} (eV)	E_{S2} (eV)	E_{S3} (eV)	E_{S4} (eV)	E_{S5} (eV)	E_{S6} (eV)
5a	3.276	3.742	3.776	3.786	3.843	3.869
5b	3.191	3.604	3.661	3.684	3.701	3.704
5c	3.219	3.664	3.705	3.751	3.754	3.766
5d	3.193	3.630	3.658	3.715	3.720	3.730

Table 5-3. The energies of the first six singlet excitations of **5a-5d**.

The energies of the first six singlet excitations in the trimers (*i.e.,* **5a-5d**) show a non-linear decrease in the energies of the first singlet excitation, E_{S1}, with an increase in atomic number of the spiro-bridging atom (Table 5-4). Because the majority of CT character corresponds to higher order transitions, the disproportionate lowering of the energies relative to **5a** of the heavier analogues

Molecule	Excited State	Transition	E_S (eV)	f
5a	4	HOMO →LUMO+2 (48.3 %)	3.786	0.0027
	6	HOMO →LUMO+3 (44.6 %)	3.869	0.0015
5b	2	HOMO →LUMO+2 (24.6 %) HOMO →LUMO+4 (5.2 %)	3.604	0.0012
	3	HOMO →LUMO+2 (14.8 %)	3.661	0.0058
	5	HOMO→LUMO+2(8.4%) HOMO→LUMO+4 (37.3 %)	3.701	0.0004
	6	HOMO →LUMO+3 (38.5 %)	3.704	0.0018
5c	2	HOMO →LUMO+2 (46.4 %)	3.664	0.0004
	4	HOMO →LUMO+4 (33.3 %)	3.751	0.0102
	5	HOMO →LUMO+3 (45.1 %)	3.754	0.0003
	6	HOMO →LUMO+4 (10.3 %)	3.765	0.0151
5d	2	HOMO →LUMO+2 (46.6 %)	3.630	0.0003
	4	HOMO →LUMO+4 (30.3 %)	3.715	0.0152
	5	HOMO →LUMO+3 (45.9 %)	3.720	0.0004
	6	HOMO →LUMO+4 (13.9 %)	3.730	0.0174

Table 5-4. Charge-transfer contributions to the first six vertical singlet excitations calculated at the TD-DFT/B3LYP level of theory for **5a-5d**, their oscillator strengths (f) and energies (Es).

is of interest. For **5a** the dominant excitations which contribute to the CT transitions correspond to E_{S4} and E_{S6} with energies of 3.786 eV and 3.869 eV, respectively. Compound **5b** shows the most promising excitation energy characteristics for PPV applications because the number of calculated singlet CT states is greater and they require the longest wavelength of light for excitation. However, the calculated oscillator strengths suggest the likelihood of occupying these states is limited compared to the Ge and Sn derivatives.

5.3.3. The impact of functional choice and basis set on the charge-transfer character

While the results of the calculations discussed above are promising, recent research suggests that common functionals used in DFT calculations are optimized for short-range interactions are poor models for calculating charge transfer transitions in π-conjugated molecules.[32] This poor performance arises from their treatment of electron-correlation, and is a manifestation of self-interaction error.[57] As such, we sought to investigate the charge transfer character of **5a-5d** using a newer functional designed to more accurately model the electronic characteristics of large π-conjugated molecules to see if the results could be reproduced at a more advanced level of theory. Recent research suggests the electronic properties in π-conjugated polymers are best modelled using long-range corrected functionals. These functionals introduce long range separation into the exchange component which has yielded results that are in better agreement with experimental data.[58] The LC-ωPBE functional in particular, in which the short-range exchange component is replaced by a

Hartree-Fock based component, is particularly useful for investigations of CT transitions in π-conjugated molecules such as tetrathiafulvalene-diquinone, anthraquinone, and polymethine systems.[37,59,60] In this context, the LC-ωPBE functional was chosen to calculate the optimized geometry and excited state dynamics of trimers **5a - 5d**.

The qualitative appearance of the orbitals calculated using the LC-ωPBE functional was equivalent to those modeled at the B3LYP level; the majority of the electron density in the HOMO and HOMO-1 resides on the trimer backbone, and the orbitals possessing primarily off-chain density are the LUMO +2, LUMO +3, LUMO+4, LUMO +8, LUMO +9, and LUMO +10.

To evaluate the reliability of the results of the TDDFT calculations the vertical excitation energies were compared to the absorption spectra of select model compounds. The carbon-based trimer (*i.e.*, **5a**) exhibits an absorption maximum at 310 nm (4.0 eV) which is in good agreement with the lowest energy singlet transition (*i.e.*, E_{S1} = 4.158 eV).[61] Consistent with other reports, calculations performed using the B3LYP functional above underestimated the excitation energy by *ca.* 0.7 eV.[62,63] The trends in E_{S1} calculated using LC-ωPBE are as expected, with direct relationship between E_g and electronegativity of M (Table 5-5). Given the accuracy with which the absorption characteristics were calculated for **5a** using the LC-ωPBE functional, it is reasonable the predicted CT properties obtained using this method are expected to be more accurate.

Compound Number	E_{S1}	E_{S2}	E_{S3}	E_{S4}	E_{S5}	E_{S6}
5a	4.1583	4.6598	4.7499	4.8692	4.8786	4.9219
5b	4.0788	4.4949	4.5358	4.7029	4.7064	4.7109
5c	4.1074	4.5387	4.5934	4.7385	4.7625	4.7638
5d	4.0837	4.4984	4.5685	4.7177	4.7199	4.7261

Table 5-5. Energies of the first six singlet excitations of the trimers (in eV) calculated at the LC-PBE level of theory.

As we are interested in charge transfer processes in **5a-5d** the transitions that contribute to their singlet excited states, their relative proportions, and the corresponding oscillator strengths were calculated. As expected, there is a significant difference in the number and percent contribution of the CT excitations to the overall excitation profiles of **5a-5d** on switching from the short range B3LYP to the long range corrected LC-ωPBE. Examination of the transitions contributing to each excited state shows only five accessible CT transitions from the S1 through S6 states of all four model compounds, with most being very high energy transitions (*e.g.*, E_{S6} = 4.9219 for **5a**). This relative energy increase is accompanied by a decrease in the percent contribution of these CT states to the overall singlet excitations compared to those calculated using the B3LYP functional (Table 5-6 for LC-ωPBE results; Table 5-4 for B3LYP). The three CT transitions contributing to the **5a** S6 transition contribute between 1.1 and 2.4 % to the excited state - an order of magnitude smaller than those

calculated at the B3LYP level of theory. We also note that the B3LYP calculations predicted an increase in CT character as the spiro-atom was substituted by larger elements; the opposite clear when the LC-ωPBE method is used suggesting that the trend noted in the results of the B3LYP calculations may be a manifestation of inappropriate functional choice.

Molecule	Excited State	Transition	E_S (eV)	f
5a	6	HOMO →LUMO+2 (1.7 %) HOMO →LUMO+3 (1.1 %) HOMO →LUMO+3 (2.4 %)	4.9219	0.0023
5c	5	HOMO-9 →LUMO+3 (1.1 %)	4.7625	0.0801
5d	2	HOMO-14 →LUMO+8 (1.3 %)	4.7177	0.0687

Table 5-6. Charge-transfer contributions to the first six vertical singlet excitations calculated at the TD-DFT/LC-PB0E level of theory for **5a-5d**, their oscillator strengths (f) and energies (Es).

To assist in rebuilding the CT character observed using the B3LYP functional, the long-range corrected calculations were performed again employing polarization functions as a part of the basis set used for geometry optimization and calculation of the Kohn-Sham orbitals. As the diffusion of electron density across the spiro center is of interest, it is believed that the incorporation of more diffuse d-orbitals to the bridge-head element (*i.e.*, C (**5a**),

Si (**5b**), Ge (**5c**) and Sn (**5d**)) could improve the spiro-conjugation effects that led to the CT states. Incorporation of polarization functions only yielded small increases in the predicted CT character of the first six singlet excitations (see Tables 5-6 and 5-7).

Again, it is the higher energy singlet transitions (*i.e.*, S4, S5 and S6) that possess CT character; the energies of these transitions are E_{S4} = 4.956 eV, E_{S5} = 4.978 eV, and E_{S6} = 4.983 eV. These energies, which correspond to wavelengths well outside of the visible region of the solar spectrum, and would not be ideal for PPV applications. It is also interesting that CT is only observed for **5a** and **b** (Table 5-7); in contrast, the Ge and Sn species were the most promising using B3LYP methods.

These increases in the number of CT states in **5a** and **5b** are accompanied by an increase in the oscillator strengths for those transitions. For example, when **5a** is modeled using LC-ωPBE calculations is shows 3 CT transitions which all contributed to the S6 transition with an oscillator strength of 0.0023. This is in stark contrast to the calculations performed with polarization functions that afford an oscillator strength of 0.1408 for the same transition – nearly 2 orders of magnitude increase. Unfortunately, the CI^2 associated with any of the CT contributions calculated at this level of theory suggest that they would be negligible.

Compound	Excited State	Transition[a]	E_S	f
5a	4	HOMO →LUMO+8 (1.5 %)	4.960	0.0003
		HOMO →LUMO+10 (1.3 %)		
	5	HOMO-1→LUMO+4 (3.6 %)	4.978	0.0028
		HOMO→LUMO+2 (1.2 %)		
	6	HOMO →LUMO+2 (1.0 %)	4.983	0.1408
		HOMO →LUMO+2 (7.6 %)		
5b	5	HOMO→LUMO+4 (1.9 %)	4.718	0.0004
	6	HOMO →LUMO+3 (1.4 %)	4.719	0.0018

Table 5-7. Charge-transfer contributions to the first six vertical singlet excitations calculated at the TD-DFT/ LC-ωPBE level of theory with polarization functions for the trimers, their oscillator strengths (f) and energies (Es).

5.4. Conclusions

We report a computational investigation of the CT characteristics of a series of candidate polymers based upon a polyspirobifluorene scaffold and the associated influence of incorporating Si, Ge, and Sn at the spirocenter. This study was performed in the context of these materials being candidate systems for PSCs. In symmetric monomers, an increase in electronic communication between perpendicular fluorenes is expected based upon the observation of increased occupation of the spatial region about the spiro center as the spiro

carbon is replaced with heavier and more polarisable Si, Ge, and Sn. By changing the 9-atom from C through Sn down Group 14, it was shown that vertical excitations are expected to exhibit greater CT character per excitation and larger oscillator strengths when calculated using the B3LYP functional. The underestimation of the HOMO-LUMO gap energy calculated using this method is commonly attributed to poor treatment of electron-correlation and indicated that the CT results may not be representative.

Attempts to repeat the calculations employing the more suitable, long-range, LC-ωPBE functional yielded vertical transition energies for the S1 transition of **5a** that were in good agreement with absorption data obtained for oligo-SBF. This improvement over than the underestimation of the E_g calculated using the B3LYP functional suggested that the LC-ωPBE functional better approximates the electronic characteristics of the trimers. The CT character calculated using the LC-ωPBE functional was negligible, and while modifying the basis sets to incorporate more polarization did increase the number of accessible CT contributions for **5a** and **5b,** the energies required to induce these transitions are too large for practical application in PSCs.

5.5. References

(1) Su, H.-J.; Wu, F.-I.; Shu, C.-F. *Macromolecules* **2004**, *37*, 7197.

(2) Neher, D. *Macromol. Rapid Commun.* **2001**, *22*, 1365.

(3) Loi, M. A.; Toffanin, S.; Muccini, M.; Forster, M.; Scherf, U.; Scharber, M. *Adv. Funct. Mater.* **2007**, *17*, 2111.

(4) Abbel, R.; Schenning, A. P. H. J.; Meijer, E. W. *J. Polym. Sci. Part A Polym. Chem.* **2009**, *47*, 4215.

(5) Pei, Q.; Yang, Y. *J. Am. Chem. Soc.* **1996**, *118*, 7416.

(6) Tseng, Y.; Shih, P.; Chien, C.; Dixit, A. K.; Shu, C.; Liu, Y.; Lee, G. *Macromolecules* **2005**, *38*, 10055.

(7) Lee, J.; Klaerner, G.; Miller, R. *Chem. Mater.* **1999**, *11*, 1083.

(8) Romaner, L.; Pogantsch, A.; Scandiucci de Freitas, P.; Scherf, U.; Gaal, M.; Zojer, E.; List, E. J. W. *Adv. Funct. Mater.* **2003**, *13*, 597.

(9) Wong, W.; Hooper, J.; Holmes, A. *Aust. J. Chem.* **2009**, *62*, 393.

(10) Lee, S. H.; Jang, B.-B.; Kafafi, Z. H. *J. Am. Chem. Soc.* **2005**, *127*, 9071.

(11) Lucht, B.; Buretea, M.; Tilley, T. *Organometallics* **2000**, *19*, 3469.

(12) Ego, C.; Marsitzky, D.; Becker, S.; Zhang, J.; Grimsdale, A. C.; Müllen, K.; MacKenzie, J. D.; Silva, C.; Friend, R. H. *J. Am. Chem. Soc.* **2003**, *125*, 437.

(13) Chen, R.; Zhu, R.; Zheng, C.; Liu, S.; Fan, Q.; Huang, W. *Sci. China Ser. B Chem.* **2009**, *52*, 212.

(14) Allard, N.; Aïch, R. B.; Gendron, D.; Boudreault, P.-L. T.; Tessier, C.; Alem, S.; Tse, S.-C.; Tao, Y.; Leclerc, M. *Macromolecules* **2010**, *43*, 2328.

(15) Yin, J.; Zhang, S.-L.; Chen, R.-F.; Ling, Q.-D.; Huang, W. *Phys. Chem. Chem. Phys.* **2010**, *12*, 15448.

(16) Ponomarenko, S.; Kirchmeyer, S. *Adv. Polym. Sci.* **2011**, *48*, 33.

(17) Pudzich, R.; Fuhrmann-Lieker, J.; Salbeck, J. *Adv. Polym. Sci.* **2006**, *199*, 83.

(18) Lee, J.-I. L.; Lee, V. Y. L.; Miller, R. D. M. *ETRI J.* **2002**, *24*, 409.

(19) Grisanti, L.; Terenziani, F.; Sissa, C.; Cavazzini, M.; Rizzo, F.; Orlandi, S.; Painelli, A. *J. Phys. Chem. B* **2011**, *115*, 11420.

(20) Rabe, T.; Görrn, P.; Lehnhardt, M.; Tilgner, M.; Riedl, T.; Kowalsky, W. *Phys. Rev. Lett.* **2009**, *102*, 137401.

(21) Hintschich, S. I.; Rothe, C.; King, S. M.; Clark, S. J.; Monkman, A. P. *J. Phys. Chem. B* **2008**, *112*, 16300.

(22) King, S. M.; Hintschich, S. I.; Dai, D.; Rothe, C.; Monkman, A. P. *J. Phys. Chem. C* **2007**, *111*, 18759.

(23) Wu, C.-C.; Liu, W.-G.; Hung, W.-Y.; Liu, T.-L.; Lin, Y.-T.; Lin, H.-W.; Wong, K.-T.; Chien, Y.-Y.; Chen, R.-T.; Hung, T.-H.; Chao, T.-C.; Chen, Y.-M. *Appl. Phys. Lett.* **2005**, *87*, 052103.

(24) Chen, J.; Cao, Y. *Macromol. Rapid Commun.* **2007**, *28*, 1714.

(25) Yamaguchi, S.; Tamao, K. *Bull. Chem. Soc. Jpn.* **1996**, *69*, 2327.

(26) Zhan, X.; Barlow, S.; Marder, S. R. *Chem. Commun.* **2009**, 1948.

(27) Yamaguchi, S.; Itami, Y.; Tamao, K. *Organometallics* **1998**, *17*, 4910.

(28) Khabashesku, V. N.; Boganov, S. E.; Antic, D.; Nefedov, O. M.; Michl, J. *Organometallics* **1996**, *15*, 4714.

(29) Hissler, M.; Dyer, P. W.; Réau, R. *Coord. Chem. Rev.* **2003**, *244*, 1.

(30) Chen, H.-Y.; Hou, J.; Hayden, A. E.; Yang, H.; Houk, K. N.; Yang, Y. *Adv. Mater.* **2010**, *22*, 371.

(31) Chochos, C. L.; Choulis, S. A. *Prog. Polym. Sci.* **2011**, *36*, 1326.

(32) Reimers, J. R.; Cai, Z.-L.; Bilić, A.; Hush, N. S. *Ann. N. Y. Acad. Sci.* **2003**, ***1006***, 235.

(33) Gaussian 09, Frisch, M. J.; Trucks, G. W.; Schlegel, H. B.; Scuseria, G. E.; Robb, M. A.; Cheeseman, J. R.; Scalmani, G.; Barone, V.; Mennucci, B.; Petersson, G. A.; Nakatsuji, H.; Caricato, M.; Li, X.; Hratchian, H. P.; Izmaylov, A. F.; Bloino, J.; Zheng, G.; Sonnenberg, J. L.; Hada, M.; Ehara, M.; Toyota, K.; Fukuda, R.; Hasegawa, J.; Ishida, M.; Nakajima, T.; Honda, Y.; Kitao, O.; Nakai, H.; Vreven, T.; Montgomery, Jr., J. A.; Peralta, J. E.; Ogliaro, F.; Bearpark, M.; Heyd, J. J.; Brothers, E.; Kudin, K. N.; Staroverov, V. N.; Kobayashi, R.; Normand, J.; Raghavachari, K.; Rendell, A.; Burant, J. C.; Iyengar, S. S.; Tomasi, J.; Cossi, M.; Rega, N.; Millam, N. J.; Klene, M.; Knox, J. E.; Cross, J. B.; Bakken, V.; Adamo, C.; Jaramillo, J.; Gomperts, R.; Stratmann, R. E.; Yazyev, O.; Austin, A. J.; Cammi, R.; Pomelli, C.; Ochterski, J. W.; Martin, R. L.; Morokuma, K.; Zakrzewski, V. G.; Voth, G. A.; Salvador, P.; Dannenberg, J. J.; Dapprich, S.; Daniels, A. D.; Farkas, Ö.; Foresman, J. B.; Ortiz, J. V.; Cioslowski, J.; Fox, D. J. Gaussian, Inc., Wallingford CT, **2009**

(34) Stevens, W. J.; Basch, H.; Krauss, M. *J. Chem. Phys.* **1984**, *81*, 6026.

(35) Glaesemann, K.; Govind, N.; Krishnamoorthy, S.; Kowalski, K. *J. Phys. Chem. A* **2010**, *114*, 8764.

(36) Perdew, J. P.; Burke, K.; Ernzerhof, M. *Phys. Rev. Lett.* **1996**, *77*, 3865.

(37) Vydrov, O. A.; Scuseria, G. E.; Perdew, J. P. *J. Chem. Phys.* **2007**, *126*, 154109.

(38) Vydrov, O. A.; Scuseria, G. E. *J. Chem. Phys.* **2006**, *125*, 234109.

(39) Gordon, M. S.; Binkley, J. S.; Pople, J. A.; Pietro, I. W. J.; Hehre, W. J. *J. Am. Chem. Soc.* **1982**, *104*, 2797.

(40) Pietro, W. J.; Francl, M. M.; Hehre, I. W. J.; Defrees, D. J.; Pople, I. J. A.; Binkley, J. S. *J. Am. Chem. Soc.* **1982**, *104*, 5039.

(41) Simmons, H. E.; Fukunaga, T. *J. Am. Chem. Soc.* **1967**, *89*, 5208.

(42) Schenk, H. *Acta Crystallogr. Sect. B* **1972**, *28*, 625.

(43) Semmelhack, M.; Foos, J.; Katz, S. *J. Am. Chem. Soc.* **1973**, *95*, 7325.

(44) Cui, Z. H.; Guo, X. X. *J. Power Sources* **2014**, *267*, 20.

(45) Allred, A.; Rochow, E. *J. Inorg. Nucl. Chem.* **1958**, *5*, 269.

(46) Chen, R.-F.; Zheng, C.; Fan, Q.-L.; Huang, W. *J. Comput. Chem.* **2007**, *28*, 2091.

(47) Roncali, J. *Chem. Rev.* **1997**, *97*, 173.

(48) Salzner, U.; Lagowski, J.; Pickup, P.; Poirier, R. *Synth. Met.* **1998**, *96*, 177.

(49) Teetsov, J.; Fox, M. A. *J. Mater. Chem.* **1999**, *9*, 2117.

(50) Knaapila, M.; Garamus, V.; Dias, F. *Macromolecules* **2006**, *39*, 6505.

(51) Wang, J.; Feng, J.; Ren, A.; Liu, X.; Ma, Y. *Macromolecules* **2004**, *37*, 3451.

(52) Franco, I.; Tretiak, S. *J. Am. Chem. Soc.* **2004**, *126*, 12130.

(53) Chen, R.-F.; Liu, L.-Y.; Fu, H.; Zheng, C.; Xu, H.; Fan, Q.-L.; Huang, W. *J. Phys. Chem. B* **2011**, *115*, 242.

(54) Heeger, A. J. *Adv. Mater.* **2014**, *26*, 10.

(55) Goldsmith, R. H.; DeLeon, O.; Wilson, T. M.; Finkelstein-Shapiro, D.; Ratner, M. A; Wasielewski, M. R. *J. Phys. Chem. A* **2008**, *112*, 4410.

(56) Maslak, P.; Chopra, A.; Moylan, C. R.; Wortmann, R.; Lebus, S.; Rheingold, A. L.; Yap, G. P. A. *J. Am. Chem. Soc.* **1996**, *118*, 1471.

(57) Perdew, J.; Zunger, A. *Phys. Rev. B* **1981**, *23*, 5048.

(58) McCormick, T. M.; Bridges, C. R.; Carrera, E. I.; Dicarmine, P. M.; Gibson, G. L.; Hollinger, J.; Kozycz, L. M.; Seferos, D. S. *Macromolecules* **2013**, *46*, 3879.

(59) Gieseking, R. L.; Mukhopadhyay, S.; Risko, C.; Marder, S. R.; Brédas, J.-L. *Adv. Mater.* **2014**, *26*, 68.

(60) Hahn, T.; Liebing, S.; Kortus, J. *Nanoscale* **2014**, *6*, 14508.

(61) Saragi, T. P. I.; Spehr, T.; Siebert, A.; Fuhrmann-Lieker, T.; Salbeck, J. *Chem. Rev.* **2007**, *107*, 1011.

(62) Jacquemin, D.; Femenias, A.; Chermette, H.; Ciofini, I.; Adamo, C.; André, J.-M.; Perpète, E. A. *J. Phys. Chem. A* **2006**, *110*, 5952.

(63) Marsman, M.; Paier, J.; Stroppa, A.; Kresse, G. *J. Phys. Condens. Matter* **2008**, *20*, 064201.

Chapter 6:

Thesis summary and future research directions

6.1. Carbazole-based tetramers (Chapters 2-4)

6.1.1. Summary and Conclusions

The $Ni(COD)_2$ catalyzed polymerization of 3,6-dibromocarbazole has long been considered ineffective in the preparation of high molecular weight polycarbazole because the position of the C-Br bonds on the monomers promotes ring closure during transmetallation, and favours the formation of cyclic oligomers – however, these ring systems are interesting in their own rite. In this thesis, research exploiting macrocycle formation and a synthetic methodology for the preparation of a family of all-carbazole shape persistent macrocycles (SPMs) are described.

In contrast to many methods for the preparation of SPMs ,some of the benefits of the synthetic methodology presented here include it requires only a single synthetic step, material purification is straightforward, it is possible to vary the N-pendant group widely, and (in most cases) the reaction is moderate to high yielding. This strategy was successfully applied in the preparation of tetramers with intact N-H bonds as well as a variety of pendant N-alkyl groups of sizes ranging from 3-12 carbons.

In Chapter 2, discussion centered around the preparation, characterization and properties of the alkyl-free tetramer cyclo-3,6-tetra(carbazole) (**1**) from the coupling of 3,6-dibromocarbazole over $Ni(COD)_2$. The macrocycle was obtained in 67% yield following the removal of Ni(II) impurities using dimethylglyoximate, and was confirmed to be the cyclic structure by both high

resolution mass spectrometry and ^{1}H NMR. The solid state morphology of **1** was sensitive to the solvent environment, allowing the preparation of semi-fibrous gels, porous colloids and solid spheres depending on the solvents employed, and the solvent/antisolvent ratio. Additionally, the particles prepared under more aqueous conditions were observed to undergo aggregation induced emission enhancement (AIEE), which coincided with an increase in molecular order within the colloids. It was proposed that the planarization of the macrocycles was responsible for the formation of ordered aggregates, which were the source of the increase in size of the particles and the AIEE respectively. The resulting nano and micromaterials of **1** were exposed to further thermal processing to induce carbonization with the goal of determining whether the morphology could be maintained through carbonization to produce functional N-doped carbon nanomaterials without the need for post processing purification or chemical modification. Using this strategy, N-doped carbons were successfully prepared at 550 °C under inert atmosphere. The resulting chars maintained their nanomorphology when porous spheres were used as a precursor, unfortunately their application to CO_2 adsorption was insufficiently efficient for commercial application.

In Chapter 3, a preliminary series of experiments were discussed which investigated the sensing capabilities of the colloids prepared in Chapter 2. The luminescence intensity of colloidal assemblies of compound **1** in acetone/water mixture of X_{aq} = 0.7 were investigated as a function of added aqueous contaminants. Unfortunately, preliminary quenching results by exposing

thecolloids to a variety of dissolved metal salts and naphthenic acids did not produce favourable results.

In Chapter 4, the discussion shifted to the preparation, purification and characterization of N-alkyl substituted carbazole macrocycles. A series of 3,6-dibromo(N-alkylcarbazole) monomers were prepared via nucleophilic substitution of the deprotonated 3,6-dibromocarbazole on the corresponding alkyl halide. These precursors were then used to prepare cyclic tetramer products using the same methodology used to prepare **1**. Preliminary evaluation of the optical properties of the tetramers showed that the presence of an alkyl substituent at the N-position caused a blue-shift in photoemission relative to the alkyl-free **1**. The emission (PL) spectra showed varying amounts of vibronic structure, and spectral broadening depending on the identity of the N-alkyl chain. It was noted that the molecular conformation, and degree of aggregation in solution is sensitive to the size of the N-alkyl group, and suggests that precipitation of the macrocycles from solution through the addition of an antisolvent might produce a variety of morphologies.

The precipitation/self-assembly of the macrocycles was also discussed in Chapter 4. An investigation into the morphology of the precipitates using scanning electron microscopy (SEM) showed that both the length and steric bulk of the N-alkyl group have an influence on the self-assembly behaviour of the macrocycles. Using this methodology materials were prepared with morphologies that varied from well-defined hollow spheres where R= H (*i.e.*, **1**), through microrods where R is large (*i.e.*, R= $C_{12}H_{25}$). Of particular interest were

the assemblies of macrocycles with N-alkyl chains of intermediate length (*i.e.* R= C_6H_{13} and C_8H_{17}), where the molecules assumed twisted nanocoil and micro-paddlewheel geometries respectively. Investigations into the evolution of these assemblies as the proportion of water was increased suggested that the assembly occurred in a hierarchical fashion.

In conducting the body of research associated with the work described in Chapters 2 through 4 we have begun to answer the question posed in Chapter 1 of this thesis; can varying the length of the alkyl substituent appended to carbazole SPMs can be used to tailor the morphology of the assemblies formed through precipitation of the molecules from solution? The simple answer to this question is: yes. However, in answering this question a new host of questions arise that can lead to future work.

6.1.2. Future Work

6.1.2.1. Optimizing the most promising structures for application

The chiral assemblies formed from **3c** are of particular interest for further investigation as such self-assembled organic chiral fibers have potential in applications such as chiroptical switching, sensing of chiral analytes, and asymmetric catalysis (Figure 6-5).[1]To investigate the potential of these assemblies, the overall handedness, as well as the hierarchy in the structures would need to be better controlled.

The preparation of chiral fibers from achiral precursors depends on the occurrence of a chiral induction event that often involves twisting motions arising from a change in the relative orientation of alkyl side-groups on adjacent, interacting macrocycles.[2] The subtleties of these events often require very specific conditions, or changes in conditions for any preferred handedness to be assumed by the bulk of the assembly.[3] As such, to optimize the utility of the twisted fires of **3c** and the micropaddlewheels of **3d** for any application, a more thorough investigation into the chiral induction events would be necessary. As a preliminary strategy, electron microscopy and complementary circular dichroism CD could be used to track changes in the morphology and chirality of the assemblies as a function of temperature, and concentration, in addition to solvent choice.

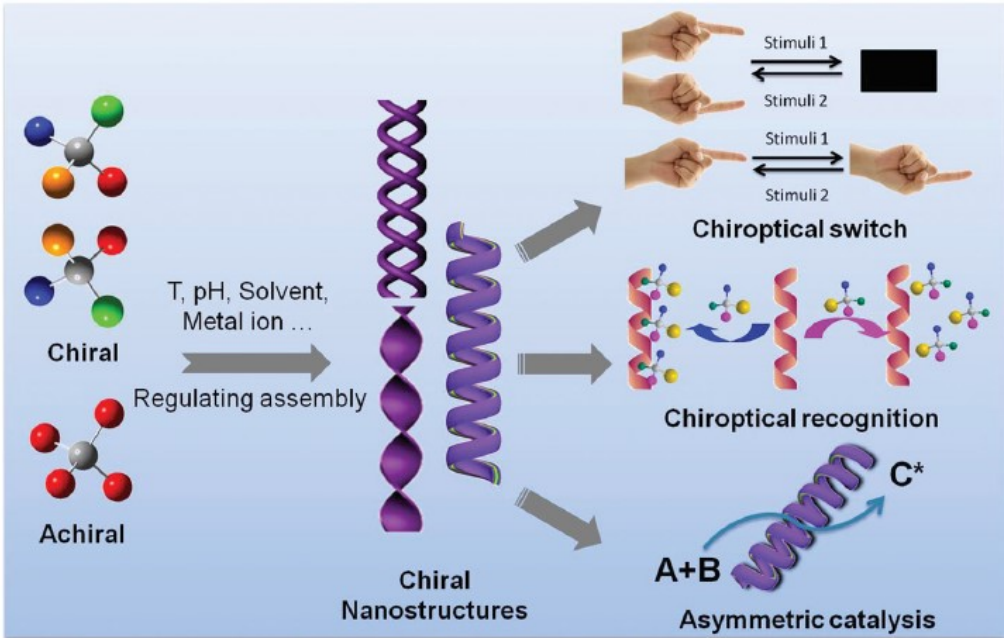

Figure 6-1. Outline of some common application for chiral fibers formed from both chiral and achiral precursors (Reprinted with permission from Ref 2).

6.1.2.2. Amphiphilic macrocycles for sensing applications.

Recently, the importance of "green" methods in chemistry have led to growing interest in developing novel chemical and materials systems that perform well in aqueous environments. Likewise, in response to the push in SPM research towards sensing of biologically relevant molecules, assemblies need to have surfaces that are stable (*i.e.*, resistant towards aggregation) in aqueous, or buffered media.[4] In this context, methods to render the carbazole SPMs prepared in Chapter 2 of this thesis amphiphilic would be attractive for sensing, separations, and catalysis in aqueous environments. We propose that the poor sensing capabilities of the colloids discussed in Chapter is the result of difficulty in maintaining colloid stability as the ionic strengths and water/acetone ratios

change throughout the experiment. Preparing assemblies with a surface that is more stable in ionic and aqueous media will assist in making more stable colloids for this purpose.

Typically, two strategies are employed to render aryl-based molecules and polymers amphiphilic; these methods include functionalization with a charged hydrophilic head-group, or the preparation of bioconjugates which impart their existing hydrophilicity to the structures. From these strategies a number of possible methodologies are available for the preparation of amphiphilic carbazole-based SPMs. For example, appending alkylsulfonate,[5] alkylcarbonate,[6] and alkylammonium[7] salts at the N-position would provide a simple means for increasing the hydrophilicity of the macrocycle side chains (Figure 6-3). Alternatively, to optimize the assembly of the novel macrocycle structures into chiral structures,[8] existing chiral biomolecules such as sugars and amino acids could easily be appended to the N- position.

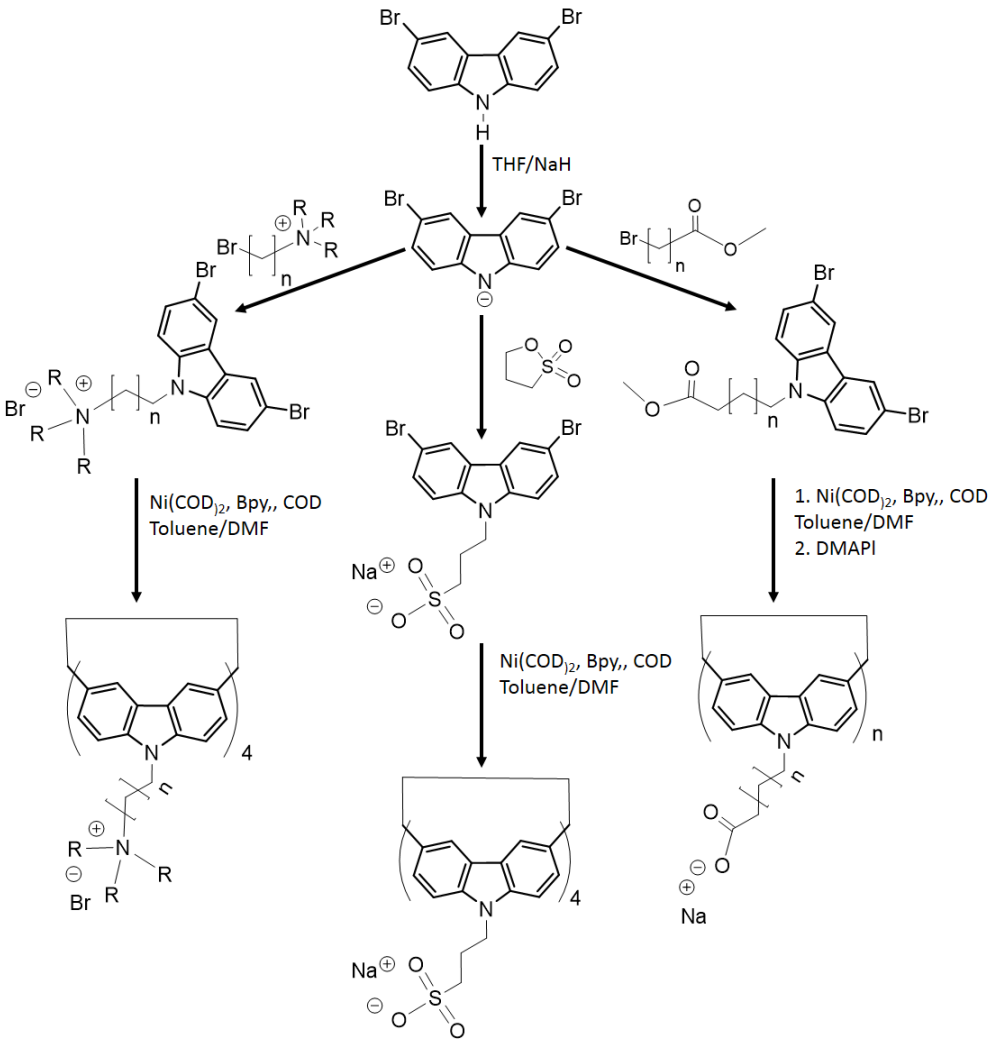

Figure 6-2. Synthetic strategies for the preparation of amphiphilic tetramers.

6.1.2.3. Applications in heterogenous organic catalysis.

A second potential future direction for these materials would be in the field of organic catalysis. While the field of all-organic catalysis is rapidly expanding, optimizing the solubility of these large organic catalysts in aqueous media for homogeneous catalysis is challenging. As such heterogenous catalysts with surface bound urea catalysts have become attractive alternatives for

catalysts in reactions such as Friedel-Crafts alkylation[9] and Michael addition.[10] The known assembly-directing capabilities of urea groups[11] suggests that functionalizing the N-position of the tetramer with urea-derived functional groups, could not only introduce a reactivity center for catalysis, but also help guide the formation of nanomaterials in partially aqueous media as proposed in Figure 6-4. The poor solubility of the π-systems in the tetramers would help to insure that the assemblies, with surface bound catalytically active groups, remained heterogeneous in aqueous reaction media.

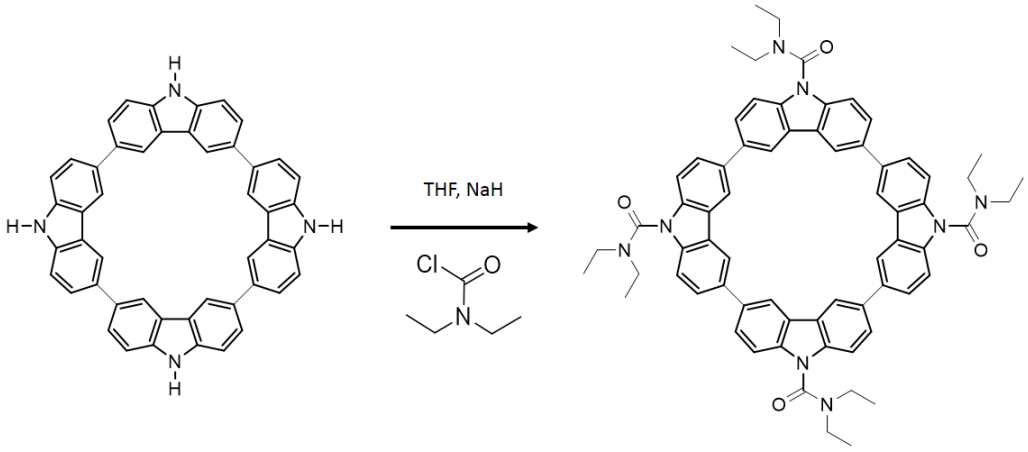

Figure 6-3. Proposed synthetic route for obtaining a representative urea-based catalytic organic material.

6.1.2.4. Carbazole assemblies as supports for nickel and nickel oxide nanoparticles.

The last potential research direction that may promote successful application of the tetramers and their assemblies prepared in Chapters 2 through 4 of this thesis is as a support for metal nanoparticles. Early success in the use of

organic materials such as block-copolymers,[12] conducting polymers,[13] and polycarbazole[14,15] as templates to help assemble metal nanoparticles and enhance the properties/reactivity of either component of the hybrid, have helped inspire a new generation of research into the decoration of carbon nanomaterials with metal nanoparticles. Using this methodology a small but promising family of hybrid materials has been prepared by attaching Au, MnO, Ni_xCo_{x-1} and NiO nanoparticles to the surface of both hard and soft carbon nanomaterials for application in sensing,[16,17] batteries,[18] and catalysis.[19-21] Given the affinity of the tetramers for Ni (as discussed in Chapter 2 of this thesis), we propose using the tetramer assemblies as water stable templates for Ni, and NiO nanoparticles that could be employed as high surface area cathode/catalyst networks in catalytic C-C coupling, and water oxidation respectively. The scope of the work could then be expanded by tailoring the functional groups appended to the N-alkyl group to bind to specific nanoparticles for other applications.

6.2. Group 14 element bridged-spirobifluorene derivatives (Chapter 5)

6.2.1. Summary and Conclusions

In Chapter 5 of this thesis, we discussed a theoretical investigation into the charge transfer characteristics of a series monomers and trimers based on a polyspirobifluorene structural units wherein the identity of the spiro-bridgehead atom was changed from carbon through Si, Ge and Sn (see Figure 6-5). The intended influence of incorporating heavier elements at the spirocenter was to promote spontaneous charge transfer across the interfluorene space by occupation of the void with virtual density arising from the d-orbitals on the heavier elements. The trimer based-calculations were initially performed at the B3LYP level of theory and predicted that contributions to the overall excited state of the molecules with heavier spiro atoms that exhibited charge transfer character were both greater in number and more intense than in the C-centred derivative.

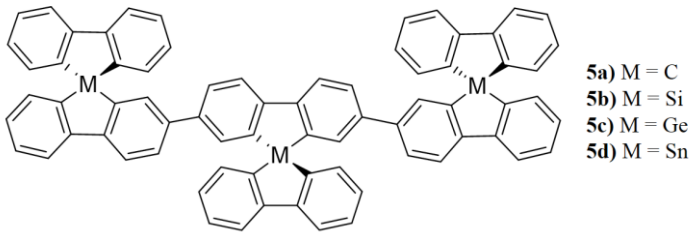

Figure 6-4. Structures of the compounds studied computationally in Chapter 5.

The calculations were then repeated with the more suitable, long-range corrected LC-ωPBE functional which yielded values in vertical excitation data

that were more consistent with the experimental absorption data obtained for the carbon-centered derivative. This result suggested a better approximation of electronic characteristics of the trimers using this functional over B3LYP. Unfortunately, switching to the LC-ωPBE functional had a deleterious impact on the predicted charge transfer. In particular, the number of charge transfer states contributing to the overall excited states of the molecules with large spiro-centers (*e.g.* Si, Ge, and Sn) were negligible. Modification of the basis sets to incorporate more polarization did increase the number of accessible CT contributions for the C and Si derivatives relative to the LC-ωPBE calculations discussed above**,** however the energies required to induce these transitions are too large for application in solar cell devices. In Chapter 1, I asked whether or not substituting the spirobifluorene trimer with heavier Group 14 elements can be predicted to promote charge transfer states in this system using computational methods? Based on the results discussed above, the answer to this question is no.

6.2.2. Future Work

Initially, the plan for the group-14 bridged spirobifluorene projects was to produce a large series of materials with a variety of substituents across the spiro-center form the backbone. As a novice researcher fresh out of undergraduate studies, I lacked the practical experience required to judge how difficult these multistep syntheses would be. As such many of the structures that I intended to investigate were never prepared.

As a complement to this research, a series of theoretical investigations were also performed into the predicted charge transfer behavior of the similar spirobifluorene based materials in which the off-chain substituent was changed to include more electron withdrawing substituents, and the end-groups of the oligofluorene backbone was modified with electron donating groups to help drive charge transfer, but these calculations were unsuccessful (see Figure 6-6). I do still believe that investigation of some of these structures may yield interesting materials, though not for photovoltaic applications. For example, the presence of heavier elements within the fluorene structure would be expected to improving 3D conductivity. As a result, these materials may be better suited to electronic applications in high conductivities would be an asset such as host materials in phosphorescent light emitting diodes. Additionally, compounds with a carbon based spiro-center (*i.e.*, that exploit spiroconjugation) have been successfully employed in dye sensitized solar with moderate success. It may be worth investigating the heavier analogues for this purpose.

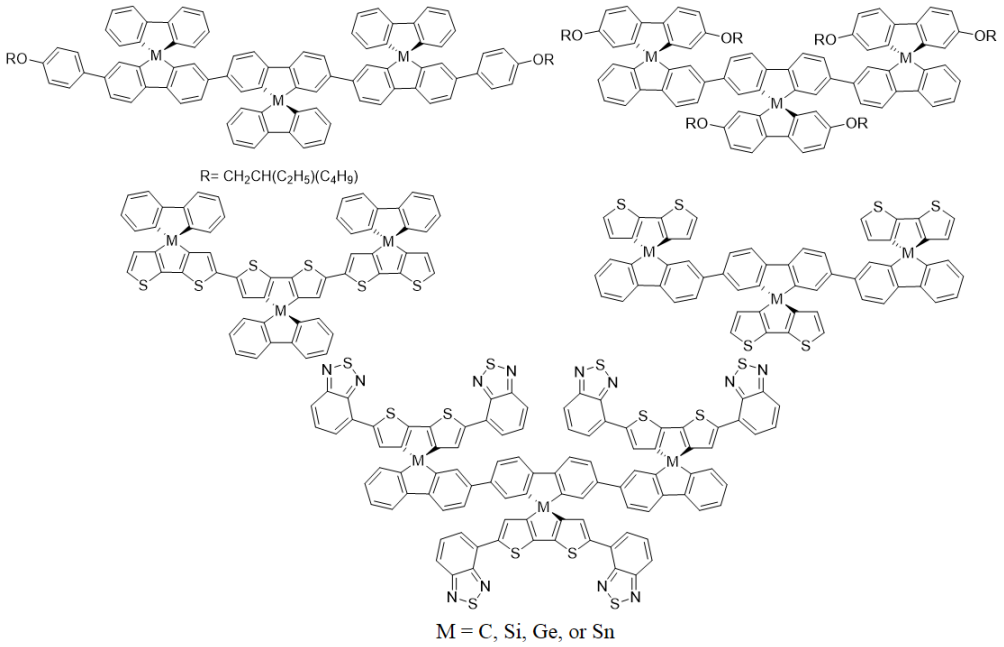

Figure 6-5. Structures of the compounds that were the subject of unsuccessful theoretical study into CT character.

6.3 References

(1) Zhang, L.; Qin, L.; Wang, X.; Cao, H.; Liu, M. *Adv. Mater.* **2014**, *26*, 6959.

(2) Romeo, A.; Castriciano, M. A.; Occhiuto, I.; Zagami, R.; Pasternack, R. F.; Scolaro, L. M. *J. Am. Chem. Soc*. **2014,** *136,* 40.

(3) Das, R. K.; Kandanelli, R.; Linnanto, J.; Bose, K.; Maitra, U. *Langmuir* **2010**, *26*, 16141.

(4) Nandi, N.; Vollhardt, D. *Acc. Chem. Res.* **2007**, *40*, 351.

(5) Wang, Z.; Ma, K.; Xu, B.; Li, X.; Tian, W. *Sci. China Chem.* **2013**, *56*, 1234.

(6) Rogers, M. A.; Weiss, R. G. *New J. Chem*. **2014**.

(7) Palmer, L. C.; Leung, C.; Kewalramani, S.; Kumthekar, R.; Newcomb, C. J.; Olvera, M.; Cruz, D.; Bedzyk, M. J.; Stupp, S. I. *J. Am. Chem. Soc.* **2014**, *136*, 14377.

(8) Yang, Y.; Zhang, Y.; Wei, Z. *Adv. Mater.* **2013**, *25*, 6039.

(9) Dong, X.-W.; Liu, T.; Hu, Y.-Z.; Liu, X.-Y.; Che, C.-M. *Chem. Commun.* **2013**, *49*, 7681.

(10) Sohtome, Y.; Tanatani, A.; Hashimoto, Y.; Nagasawa, K. *Chem. Pharm. Bull*. **2004**, *52*, 477.

(11) Estroff, L. A.; Hamilton, A. D. *Chem. Rev.* **2004**, *104*, 1201.

(12) Kao, J.; Thorkelsson, K.; Bai, P.; Rancatore, B. J.; Xu, T. *Chem. Soc. Rev.* **2013**, *42*, 2654.

(13) Janáky, C.; Visy, C. *Anal. Bioanal. Chem.* **2013**, *405*, 3489.

(14) Gupta, B.; Joshi, L.; Prakash, R. *Macromol. Chem. Phys.* **2011**, *212*, 1692.

(15) Zhou, W.; Xu, J.; Du, Y.; Yang, P. *Int. J. Hydrogen Energy* **2011**, *36*, 1903.

(16) Briseno, A. L.; Mannsfeld, S. C. B.; Formo, E.; Xiong, Y.; Lu, X.; Bao, Z.; Jenekhe, S. A..; Xia, Y. *J. Mater. Chem.* **2008**, *18*, 5395.

(17) Leghrib, R.; Dufour, T.; Demoisson, F.; Claessens, N.; Reniers, F.; Llobet, E. *Sensors Actuators B Chem.* **2011**, *160*, 974.

(18) Cui, Z. H.; Guo, X. X. *J. Power Sources* **2014**, *267*, 20.

(19) Kim, F. S.; Ren, G.; Jenekhe, S. A. *Chem. Mater.* **2011**, *23*, 682.

(20) Barakat, N. a. M.; Motlak, M.; Kim, B.-S.; El-Deen, A. G.; Al-Deyab, S. S.; Hamza, a. M. *J. Mol. Catal. A Chem.* **2014**, *394*, 177.

(21) Li, X.-H.; Antonietti, M. *Chem. Soc. Rev.* **2013**, *42*, 6593.

Bibliography

Chapter 1

(1) Kroto, H. W.; Heath, J. R.; O'Brien, S. S.; Curl, R. F.; Smalley, R. E. *Nature* **1985**, *318*, 162.

(2) Shirakawa, H.; Jouis, E. J.; MacDiarmid, A. G.; Chiang, C. K.; Heeger, A. J. *J. Chem. Soc. Chem. Commun.* **1977**, 578.

(3) Nobel Media, A. The Nobel Prize in Physics 2010 <http://www.nobelprize.org/nobel_prizes/physics/laureates/2010/>.

(4) Yang, L.; Zhao, Y.; Chen, S.; Wu, Q.; Wang, X.; Hu, Z. *Chinese J. Catal.* **2013**, *34*, 1986.

(5) Ye, N.; Shi, P. *Sep. Purif. Rev*. **2014**, *44*, 183.

(6) Wang, Q.; Huang, X.; Long, Y.; Wang, X.; Zhang, H.; Zhu, R.; Liang, L.; Teng, P.; Zheng, H. *Carbon* **2013**, *59*, 192.

(7) Zhang, R.; Chen, W. *Biosens. Bioelectron.* **2014**, *55*, 83.

(8) Arenillas, A.; Drage, T. C.; Smith, K.; Snape, C. E. *J. Anal. Appl. Pyrolysis* **2005**, *74*, 298.

(9) Paraknowitsch, J. P.; Thomas, A. *Energy Environ. Sci.* **2013**, *6*, 2839.

(10) Chung, D. D. L. *J. Mater. Sci.* **2004**, *39*, 2645.

(11) Shenderova, O. A.; Zhirnov, V. V.; Brenner, D. W. *Crit. Rev. Solid State Mater. Sci.* **2002**, *27*, 227.

(12) Dresselhaus, M. S. *Annu. Rev. Mater. Sci.* **1997**, *27*, 1.

(13) Cullers, R. L. Carbon (C). *Salem Press Encyclopedia of Science*, **2013**.

(14) Stwertka, A. *A Guide to the Elements*; **2012**; p. 191.

(15) Dubey, N.; Leclerc, M. *J. Polym. Sci. Part B Polym. Phys.* **2011**, *49*, 467.

(16) Li, W.; Zhang, Z.; Kong, B.; Feng, S.; Wang, J.; Wang, L.; Yang, J.; Zhang, F.; Wu, P.; Zhao, D. *Angew. Chem. Int. Ed. Engl.* **2013**, *52*, 8151.

(17) Coville, N. J.; Mhlanga, S. D.; Nxumalo, E. N.; Shaikjee, A. *S. Afr. J. Sci.* **2011**, *107*, 1.

(18) Barford, W. *Electronic and Optical Properties of Conjugated Polymers*; Birman, J.; Edwards, S. F.; Friend, R.; Rees, M.; Sherrington, D.; Veneziano, G., Eds.; Oxford University Press, **2005**; pp. 1–25.

(19) Clayden, J.; Greeves, N.; Warren, S.; Wothers, P. *Organic Chemistry*; **2001**; Vol. 40, pp. 1990–1992.

(20) Housecroft, C. E.; Sharpe, A. C. *Inorganic Chemistry*; **2005**; pp. 338–384.

(21) Erlandsson, R.; Salaneck, W. R.; Lundström, I. *Mater. Des.* **1986**, *7*, 246.

(22) Moliton, A.; Hiorns, R. C. *Polym. Int.* **2004**, *53*, 1397.

(23) Hoffmann, R.; Janiak, C.; Kollmar, C. *Macromolecules* **1991**, *24*, 3725.

(24) Heeger, A. J. *Chem. Soc. Rev.* **2010**, *39*, 2354.

(25) Soos, Z. G.; Hayden, G. W.; Ramaseshan, S. *Solid State Ionics* **1989**, *32/33*, 567.

(26) Meier, H.; Stalmach, U.; Kolshorn, H. *Acta Polym*. **1997**, *48*, 379.

(27) Chen, R.-F.; Liu, L.-Y.; Fu, H.; Zheng, C.; Xu, H.; Fan, Q.-L.; Huang, W. *J. Phys. Chem. B* **2011**, *115*, 242.

(28) Garnier, F. *Acc. Chem. Res.* **1999**, *32*, 209.

(29) Rossi, G.; Chance, R. R.; Silbey, R. J. *Chem. Phys.* **1989**, *90*, 7594.

(30) Hutten, P. F. V. A. N.; Krasnikov, V. V; Hadziioannou, G. *Acc. Chem. Res.* **1999**, *32*, 257.

(31) Van Bolhuis, F.; Wynberg, H.; Havinga, E. E.; Meijer, E. W.; Staring, E. G. J. *Synth. Met.* **1989**, *30*, 381.

(32) Hotta, S.; Waragai, K. *J. Mater. Chem.* **1991**, *1*, 835.

(33) Gieseking, R. L.; Mukhopadhyay, S.; Risko, C.; Marder, S. R.; Brédas, J.-L. *Adv. Mater.* **2014**, *26*, 68.

(34) Brédas, J. L. *J. Chem. Phys.* **1985**, *82*, 3808.

(35) Karl, N. *Synth. Met.* **2003**, *133-134*, 649.

(36) Beaujuge, P. M.; Reynolds, J. R. *Chem. Rev.* **2010**, *110*, 268.

(37) Kushmerick, J. G.; Holt, D. B.; Pollack, S. K.; Ratner, M. A.; Yang, J. C.; Schull, T. L.; Naciri, J.; Moore, M. H.; Shashidhar, R. *J. Am. Chem. Soc.* **2002**, *124*, 10654.

(38) Bässler, H.; Köhler, A. *Chem. Rev*. **2012**, *312*, 1.

(39) Tiago, M.; Rohlfing, M.; Louie, S. *Phys. Rev. B* **2004**, *70*, 193204.

(40) Bolinger, J. C.; Traub, M. C.; Brazard, J.; Adachi, T.; Barbara, P. F.; vanden Bout, D. A. *Acc. Chem. Res.* **2012**, *45*, 1992.

(41) Fischer, F. S. U.; Tremel, K.; Link, S.; Kayunkid, N.; Brinkmann, M.; Delgado, M. C. R.; Ludwigs, S. *Macromolecules* **2013**, *46*, 4924.

(42) Karabunarliev, S.; Baumgarten, M.; Bittner, E. R.; Müllen, K. *J. Chem. Phys*. **2000**, *113*, 11372.

(43) Saragi, T. P. I.; Spehr, T.; Siebert, A.; Fuhrmann-Lieker, T.; Salbeck, J. *Chem. Rev.* **2007**, *107*, 1011.

(44) Oliveira, F. A. C.; Cury, L. A.; Righi, A.; Moreira, R. L.; Guimarães, P. S. S.; Matinaga, F. M.; Pimenta, M. A.; Nogueira, R. A. *J. Chem. Phys.* **2003**, *119*, 9777.

(45) Brédas, J. L.; Cornil, J.; Heeger, A. J.; Briidas, B. J. *Adv. Mater.* **1996**, *8*, 447.

(46) Liu, X.; Xu, D.; Lu, R.; Li, B.; Qian, C.; Xue, P.; Zhang, X.; Zhou, H. *Chem. Eur. J.* **2011**, *17*, 1660.

(47) Hagler, T. W.; Pakbaz, K.; Voss, K. F.; Heeger, A. J. *Phys. Rev. B* **1991**, *44*, 8652.

(48) Coropceanu, V.; André, J. M.; Malagoli, M.; Brédas, J. L. *Theor. Chem. Accounts Theory, Comput. Model.* **2003**, *110*, 59.

(49) Maus, M.; Rettig, W.; Bonafoux, D.; Lapouyade, R. *J. Phys. Chem. A* **1999**, *103*, 3388.

(50) Zhang, Z.; Zhan, C.; Zhang, X.; Zhang, S.; Huang, J.; Li, A. D. Q.; Yao, J. *Chem. Eur. J.* **2012**, *18*, 12305.

(51) Beckers, E. H. A.; Meskers, S. C. J.; Schenning, A. P. H. J.; Chen, Z.; Würthner, F.; Marsal, P.; Beljonne, D.; Cornil, J.; Janssen, R. A. J. *J. Am. Chem. Soc.* **2006**, *128*, 649.

(52) Spano, F. C. *Acc. Chem. Res*. **2010**, *43*, 429.

(53) Wang, W.; Li, L.-S.; Helms, G.; Zhou, H.-H.; Li, A. D. Q. *J. Am. Chem. Soc.* **2003**, *125*, 1120.

(54) Meskers, S. C. J.; Janssen, R. A. J.; Haverkort, J. E. M.; Wolter, J. H. *Chem. Phys.* **2000**, *260*, 415.

(55) Wang, C.; Dong, H.; Hu, W.; Liu, Y.; Zhu, D. *Chem. Rev.* **2012**, *112*, 2208.

(56) Patil, A. O.; Heeger, A. J.; Wudl, F. *Chem. Rev.* **1988**, *88*, 183.

(57) Henson, Z. B.; Müllen, K.; Bazan, G. C. *Nat. Chem.* **2012**, *4*, 699.

(58) Grimsdale, A. C.; Müllen, K. *Adv. Polym. Sci.* **2006**, *199*, 1.

(59) Jansen, M.; Baldus, H. P.; Patent, U. S.; Jaschek, R.; Russel, C.; Solids, J. N.; Grimme, B. J.; Kreyenschmidt, M.; Uckert, F.; Müllen, K.; Scherf, U. *Adv. Mater.* **1995**, *292*, 292.

(60) Neher, D. *Macromol. Rapid Commun.* **2001**, *22*, 1365.

(61) Xie, L.; Yang, S.; Lin, J.; Yi, M.; Huang, W. *Philos. Trans. R. Soc. London A* **2013**, *371*, 20120337.

(62) Li, Z.; Dong, Y. Q.; Lam, J. W. Y.; Sun, J.; Qin, A.; Häubler, M.; Dong, Y. P.; Sung, H. H. Y.; Williams, I. D.; Kwok, H. S.; Tang, B. Z. *Adv. Funct. Mater*. **2009**, *19*, 905.

(63) Ferman, J.; Kakareka, J. P.; Klooster, W. T.; Mullin, J. L.; Quattrucci, J.; Ricci, J. S.; Tracy, H. J.; Vining, W. J.; Wallace, S. *Inorg. Chem.* **1999**, *38*, 2464.

(64) Geramita, K.; Mcbee, J.; Tilley, T. D. *J. Org. Chem.* **2009**, *74*, 820.

(65) Yin, J.; Zhang, S.-L.; Chen, R.-F.; Ling, Q.-D.; Huang, W. *Phys. Chem. Chem. Phys.* **2010**, *12*, 15448.

(66) Geramita, K.; Tao, Y.; Segalman, R. A.; Tilley, T. D. *J. Org. Chem*. **2010**, *75*, 1871.

(67) Zheng, C.; Tao, Y.; Cao, J.-Z.; Chen, R.-F.; Zhao, P.; Wu, X.-J.; Huang, W. *J. Mol. Model.* **2012**, *18*, 4929.

(68) Pujari, B. S.; Gusarov, S.; Brett, M.; Kovalenko, A. *Electr. Chem. Soc. Trans.* **2011**, *41*, 129.

(69) Duan, C.; Cai, W.; Huang, F.; Zhang, J.; Wang, M.; Yang, T.; Zhong, C.; Gong, X.; Cao, Y. *Macromolecules* **2010**, *43*, 5262.

(70) Gendron, D.; Leclerc, M. *Energy Environ. Sci.* **2011**, *4*, 1225.

(71) Ahmad, A.; Durocher, G. *Photochem. Photobiol.* **1981**, *34*, 573.

(72) Martin, M. M.; Brohoret, E. *J. Phys. Chem.* **1982**, *177*, 107.

(73) Morin, J.-F.; Leclerc, M.; Adès, D.; Siove, A. *Macromol. Rapid Commun.* **2005**, *26*, 761.

(74) Kodali, H. K.; Ganapathysubramanian, B. *Comput. Methods Appl. Mech. Eng.* **2012**, *247-248*, 113.

(75) Shi, Q.; Chen, H. *Sci. China Chem*. **2013**, *56*, 1271.

(76) Xue, F.; Jiang, S. *Polymers* **2014**, *6*, 2116.

(77) Shi, Y.; Liu, J.; Yang, Y. *J. Appl. Phys.* **2000**, *87*, 4254.

(78) Schwartz, B. J. *Annu. Rev. Phys. Chem*. **2003**, *54*, 141.

(79) Liu, J.; Shi, Y.; Yang, Y. *Adv. Funct. Mater.* **2001**, *11*, 420.

(80) Vehoff, T.; Baumeier, B.; Andrienko, D. *J. Chem. Phys.* **2010**, *133*, 134901.

(81) Gupta, D.; Hong, Y. *Org. Electron.* **2010**, *11*, 127.

(82) Malliaras, G.; Friend, R. *Phys. Today* **2005**, *58*, 53.

(83) Balakrishnan, K.; Datar, A.; Naddo, T.; Huang, J.; Oitker, R.; Yen, M.; Zhao, J.; Zang, L. *J. Am. Chem. Soc.* **2006**, *128*, 7390.

(84) Huser, T.; Yan, M.; Rothberg, L. J. *Proc. Natl. Acad. Sci. U. S. A.* **2000**, *97*, 11187.

(85) O'Reilly, J. M. *Crit. Rev. Solid State Mater. Sci.* **1987**, *13*, 259.

(86) Facchetti, A. *Chem. Mater.* **2011**, *23*, 733.

(87) Grimsdale, A. C.; Mullen, K. *Adv. Polym. Sci.* **2008**, *212*, 1.

(88) Nguyen, T.-Q.; Yee, R. Y.; Schwartz, B. J. *J. Photochem. Photobiol. A Chem.* **2001**, *144*, 21.

(89) Kumar, B.; Kaushik, B. K.; Negi, Y. S. *Polym. Rev.* **2014**, *54*, 33.

(90) Huser, T.; Yan, M. *J. Photochem. Photobiol. A Chem.* **2001**, *144*, 43.

(91) Street, R.; Northrup, J.; Salleo, A. *Phys. Rev. B* **2005**, *71*, 165202.

(92) Brédas, J.-L.; Cornil, J.; Beljonne, D.; Dos Santos, D. A.; Shuai, Z.; *Acc. Chem. Res.* **1999**, *32*, 267.

(93) Newman, C. R.; Frisbie, C. D.; Da Silva Filho, D. A.; Brédas, J.-L.;Ewbank, P. C.;Mann, K. R. *Chem. Mater.* **2004**, *16*, 4436.

(94) Zang, L.; Che, Y.; Moore, J. S. *Acc. Chem. Res.* **2008**, *41*, 1596.

(95) Mas-Torrent, M.; Rovira, C. *Chem. Soc. Rev.* **2008**, *37*, 827.

(96) Shirota, Y.; Kageyama, H. *Chem. Rev.* **2007**, *107*, 953.

(97) Jenkins, A. D.; Kratochvil, P.; Stepto, R. F. T.; Suter, U. W. *Pure Appl. Chem.* **1996**, *68*, 2287.

(98) Whitesides, G. M.; Grzybowski, B. *Science* **2002**, *295*, 2418.

(99) Ding, Z.; Xing, R.; Sun, Y.; Zheng, L.; Wang, X.; Ding, J.; Wang, L.; Han, Y. *RSC Adv.* **2013**, *3*, 8037.

(100) Kim, F. S.; Ren, G.; Jenekhe, S. A. *Chem. Mater.* **2011**, *23*, 682.

(101) Korevaar, P. A.; de Greef, T. F. A.; Meijer, E. W. *Chem. Mater.* **2014**, *26*, 576.

(102) Ruiz, L.; Keten, S. *J. Phys. Chem. Lett.* **2014**, *5*, 2021.

(103) Tambara, K.; Olsen, J.-C.; Hansen, D. E.; Pantoş, G. D. *Org. Biomol. Chem.* **2014**, *12*, 607.

(104) Hu, X.-D.; Jenkins, S. E.; Min, B. G.; Polk, M. B.; Kumar, S. *Macromol. Mater. Eng.* **2003**, *288*, 823.

(105) He, C.; Wu, D.; Zhang, F.; Xue, M.; Zhuang, X.; Qiu, F.; Feng, X. *Chem physchem* **2013**, *14*, 2954.

(106) Zhang, K.-D.; Tian, J.; Hanifi, D.; Zhang, Y.; Sue, A. C.-H.; Zhou, T.-Y.; Zhang, L.; Zhao, X.; Liu, Y.; Li, Z.-T. J. *Am. Chem. Soc.* **2013***, 135*, 17913.

(107) Mes, T.; Smulders, M. M. J.; Palmans, A. R. A.; Meijer, E. W. *Macromolecules* **2010**, *43*, 1981.

(108) Chakrabarty, R.; Mukherjee, P. S.; Stang, P. J. *Chem. Rev.* **2011**, *111*, 6810.

(109) Chen, L.-J.; Zhao, G.-Z.; Jiang, B.; Sun, B.; Wang, M.; Xu, L.; He, J.; Abliz, Z.; Tan, H.; Li, X.; Yang, H.-B. *J. Am. Chem. Soc.* **2014**, *136*, 5993.

(110) Wang, Z.; Medforth, C. J.; Shelnutt, J. A. *J. Am. Chem. Soc.* **2004**, *126*, 15954.

(111) Che, Y.; Gross, D. E.; Huang, H.; Yang, D.; Yang, X.; Discekici, E.; Xue, Z.; Zhao, H.; Moore, J. S.; Zang, L. *J. Am. Chem. Soc.* **2012**, *134*, 4978.

(112) Dong, Z.; Luo, Q.; Liu, J. *Chem. Soc. Rev.* **2012**, *41*, 7890.

(113) Li, Y.; Liu, T.; Liu, H.; Tian, M.-Z.; Li, Y. *Acc. Chem. Res.* **2014**, *47*, 1186.

(114) Schenning, A. P. H. J.; Meijer, E. W. *Chem. Commun*. **2005**, *41*, 3245.

(115) Brunner, K.; van Dijken, A.; Börner, H.; Bastiaansen, J. J. A. M.; Kiggen, N. M. M.; Langeveld, B. M. W. *J. Am. Chem. Soc.* **2004**, *126*, 6035.

(116) Beaujuge, P. M.; Fréchet, J. M. J. *J. Am. Chem. Soc.* **2011**, *133*, 20009.

(117) Sun, Y.; Welch, G. C.; Leong, W. L.; Takacs, C. J.; Bazan, G. C.; Heeger, A. J. *Nat. Mater.* **2012**, *11*, 44.

(118) Jonkheijm, P.; van der Schoot, P.; Schenning, A. P. H. J.; Meijer, E. W. *Science* **2006**, *313*, 80.

(119) Stolnik, S.; Illum, L.; Davis, S. S. *Adv. Drug Deliv. Rev.* **2012**, *64*, 290.

(120) Korevaar, P. A.; Schaefer, C.; de Greef, T. F.A.; Meijer, E. W. *J. Am. Chem. Soc.* **2012**, *134*, 13482.

(121) Dong, J.; Yin, C.; Zhang, Y.; Zhang, Q. *J. Polym. Sci. Part B Polym. Phys.* **2014**, *52*, 450.

(122) Zhao, Y. S.; Fu, H.; Peng, A.; Ma, Y.; Xiao, D.; Yao, *J. Adv. Mater.* **2008**, *20*, 2859.

(123) Zhao, T.; Liu, Z.; Song, Y.; Xu, W.; Zhang, D.; Zhu, D. *J. Org. Chem.* **2006**, *71*, 7422.

(124) Höger, S. *Chemistry* **2004**, *10*, 1320.

(125) Finke, A. D.; Gross, D. E.; Han, A.; Moore, J. S. *J. Am. Chem. Soc.* **2011**, *133*, 14063.

(126) Balakrishnan, K.; Datar, A.; Zhang, W.; Yang, X.; Naddo, T.; Huang, J.; Zuo, J.; Yen, M.; Moore, J. S.; Zang, L. *J. Am. Chem. Soc.* **2006**, *128*, 6576.

(127) Aggarwal, a V.; Jester, S.-S.; Taheri, S. M.; Förster, S.; Höger, S. *Chemistry* **2013**, *19*, 4480.

(128) Yang, Y.; Feng, W.; Hu, J.; Zou, S.; Gao, R.; Yamato, K.; Kline, M.; Cai, Z.; Gao, Y.; Wang, Y.; Li, Y.; Yuan, L.; Zeng, X. C.; Gong, B. *J. Am. Chem. Soc.* **2011**, *133*, 18590.

(129) Pan, G.; Cheng, X. J.; Höger, S.; Freyland, W. *J. Am. Chem. Soc.* **2006**, *128*, 4218.

(130) Huang, W.; Zhao, T.-Y.; Wen, M.-W.; Yang, Z.-Y.; Xu, W.; Yi, Y.-P.; Xu, L.-P.; Wang, Z.-X.; Gu, Z.-J. *J. Phys. Chem. C* **2014**, *118*, 6767.

(131) Kong, Q.; Qian, H.; Bo, H.; Zhang, C.; Liu, K.; Zhang, X.; Wang, J.; Li, J.; Gao, G. *Synth. Met.* **2011**, *161*, 2361.

(132) Jung, S.-H.; Pisula, W.; Rouhanipour, A.; Räder, H. J.; Jacob, J.; Müllen, K. *Angew. Chem. Int. Ed.* **2006**, *45*, 4685.

(133) Li, T.; Yue, K.; Yan, Q.; Huang, H.; Wu, H.; Zhu, N.; Zhao, D. *Soft Matter* **2012**, *8*, 2405.

(134) Heimel, G.; Brédas, J.-L. *Nat. Nanotechnol.* **2013**, *8*, 230.

(135) Di Maria, F.; Olivelli, P.; Gazzano, M.; Zanelli, A.; Biasiucci, M.; Gigli, G.; Gentili, D.; D'Angelo, P.; Cavallini, M.; Barbarella, G. *J. Am. Chem. Soc.* **2011**, *133*, 8654.

(136) Zhao, D.; Moore, J. *Chem. Commun.* **2003**, *34*, 807.

(137) Catalan, J. *J. Phys. Chem. A* **2007**, *111*, 8774.

(138) Sinnokrot, M. O.; Valéev, E. F.; Sherrill, C. D. *J. Am. Chem. Soc.* **2002**, *124*, 10887.

(139) Martinez, C. R.; Iverson, B. L. *Chem. Sci.* **2012**, *3*, 2191.

(140) Spano, F. C. *Annu. Rev. Phys. Chem.* **2006**, *57*, 217.

(141) Lim, J. M.; Kim, P.; Yoon, M.-C.; Sung, J.; Dehm, V.; Chen, Z.; Würthner, F.; Kim, D. *Chem. Sci.* **2013**, *4*, 388.

(142) Yamagata, H.; Pochas, C. M.; Spano, F. C. *J. Phys. Chem. B* **2012**, *116*, 14494.

(143) Spano, F. C.; Silva, C. *Annu. Rev. Phys. Chem.* **2014**, *65*, 477.

(144) Yamagata, H.; Spano, F. C. *J. Chem. Phys.* **2012**, *136*, 184901.

(145) Gierschner, J.; Luer, L.; Milian-Medina, B.; Oelkrug, D.; Egelhaaf, H. *J. Phys. Chem. Lett.* **2013**, *4*, 2686.

(146) Hong, Y.; Lam, J. W. Y.; Tang, B. Z. *Chem. Commun.* **2009**, *45*, 4332.

(147) Belletête, M.; Bouchard, J.; Leclerc, M.; Durocher, G. *Macromolecules* **2005**, *38*, 880.

(148) Xu, B.; He, J.; Dong, Y.; Chen, F.; Yu, W.; Tian, W. *Chem. Commun.* **2011**, *47*, 6602.

(149) Eisfeld, A..; Briggs, J. S. *Chem. Phys.* **2006**, *324*, 376.

(150) Li, Z.; Dong, Y. Q.; Lam, J. W. Y.; Sun, J.; Qin, A.; Häubler, M.; Dong, Y. P.; Sung, H. H. Y.; Williams, I. D.; Kwok, H. S.; Tang, B. Z. *Advanced Functional Materials*, **2009**, *19*, 905.

(151) Wu, W.; Ye, S.; Huang, L.; Xiao, L.; Fu, Y.; Huang, Q.; Yu, G.; Liu, Y.; Qin, J.; Li, Q.; Li, Z. *J. Mater. Chem.* **2012**, *22*, 6374.

(152) Busseron, E.; Ruff, Y.; Moulin, E.; Giuseppone, N. *Nanoscale* **2013**, *5*, 7098.

(153) Huang, C.; Wen, L.; Liu, H.; Li, Y.; Liu, X.; Yuan, M.; Zhai, J.; Jiang, L.; Zhu, D. *Adv. Mater.* **2009**, *21*, 1721.

(154) Guo, S.; Wang, E. *Acc. Chem. Res.* **2011**, *44*, 491.

(155) Deng, R.; Liang, F.; Li, W.; Yang, Z.; Zhu, J. *Macromolecules* **2013**, *46*, 7012.

(156) Tao, J.; Yang, M.; Gao, H.; Yu, J.; Wang, G. *Colloids Surf. A* **2014**, *451*, 117.

(157) Sacanna, S.; Pine, D. J.; Yi, G.-R. *Soft Matter* **2013**, *9*, 8096.

(158) Kosa, T.; Sukhomlinova, L.; Su, L.; Taheri, B.; White, T. J.; Bunning, T. J. *Nature* **2012**, *485*, 347.

(159) Ke, D.; Zhan, C.; Xu, S.; Ding, X.; Peng, A.; Sun, J.; He, S.; Li, A. D. Q.; Yao, J. *J. Am. Chem. Soc.* **2011**, *133*, 11022.

(160) Wang, Y.; Wang, Y.; Zheng, X.; Yi, G.-R.; Sacanna, S.; Pine, D. J.; Weck, M. *J. Am. Chem. Soc.* **2014**, *136*, 6866.

Chapter 2

(1) Li, H.; Kang, Z.; Liu, Y.; Lee, S.-T. *J. Mater. Chem.* **2012**, *22*, 24230.

(2) Sun, D.; Ban, R.; Zhang, P.-H.; Wu, G.-H.; Zhang, J.-R.; Zhu, J.-J. *Carbon* **2013**, *64*, 424.

(3) Schenning, A. P. H. J.; Meijer, E. W. *Chem. Commun*. **2005**, 3245.

(4) Xie, L.; Yang, S.; Lin, J.; Yi, M.; Huang, W. *Philos. Trans. R. Soc. London A* **2013**, *371*, 20120337.

(5) Jariwala, D.; Sangwan, V. K.; Lauhon, L. J.; Marks, T. J.; Hersam, M. C. *Chem. Soc. Rev.* **2013**, *42*, 2824.

(6) Ouyang, Y.; Shi, H.; Fu, R.; Wu, D. *Sci. Reports* **2013**, *3*, 1.

(7) Li, W.; Zhang, Z.; Kong, B.; Feng, S.; Wang, J.; Wang, L.; Yang, J.; Zhang, F.; Wu, P.; Zhao, D. *Angew. Chem. Int. Ed. Engl.* **2013**, *52*, 8151.

(8) Wang, Q.; Huang, X.; Long, Y.; Wang, X.; Zhang, H.; Zhu, R.; Liang, L.; Teng, P.; Zheng, H. *Carbon* **2013**, *59*, 192.

(9) Chen, S.; Li, Y.; Li, Y. *Polym. Chem.* **2013**, *4*, 5162.

(10) Coville, N. J.; Mhlanga, S. D.; Nxumalo, E. N.; Shaikjee, A. *S. Afr. J. Sci.* **2011**, *107*, 1.

(11) Cao, L.; Meziani, M. J.; Sahu, S.; Sun, Y.-P. *Acc. Chem. Res.* **2013**, *46*, 171.

(12) Baker, S. N.; Baker, G. A. *Angew. Chem. Int. Ed. Engl.* **2010**, *49*, 6726.

(13) Anilkumar, P.; Wang, X.; Cao, L.; Sahu, S.; Liu, J.-H.; Wang, P.; Korch, K.; Tackett, K. N.; Parenzan, A.; Sun, Y.-P. *Nanoscale* **2011**, *3*, 2023.

(14) Balakrishnan, K.; Datar, A.; Naddo, T.; Huang, J.; Oitker, R.; Yen, M.; Zhao, J.; Zang, L. *J. Am. Chem. Soc.* **2006**, *128*, 7390.

(15) Ke, D.; Zhan, C.; Xu, S.; Ding, X.; Peng, A.; Sun, J.; He, S.; Li, A. D. Q.; Yao, J. *J. Am. Chem. Soc.* **2011**, *133*, 11022.

(16) Huang, J.; Chen, P.; Yang, X.; Tang, R.; Wang, L.; Qin, J.; Li, Z. *Sci. China Chem.* **2013**, *56*, 1213.

(17) Zhao, Z.; Lam, J. W. Y.; Tang, B. Z. *Soft Matter* **2013***, 9*, 4564.

(18) Hoeben, F. J. M.; Jonkheijm, P.; Meijer, E. W.; Schenning, A. P. H. J. *Chem. Rev*. **2005**, *105*, 1491.

(19) Li, J.; Grimsdale, A. *Chem. Soc. Rev.* **2010**, *39*, 2399.

(20) Morin, J.-F.; Leclerc, M.; Adès, D.; Siove, A. *Macromol. Rapid Commun.* **2005**, *26*, 761.

(21) Park, K. S.; Salunkhe, S. M.; Lim, I.; Cho, C.-G.; Han, S.-H.; Sung, M. M. *Adv. Mater.* **2013**, *25*, 3351.

(22) Boudreault, P. T.; Blouin, N.; Leclerc, M. *Adv. Polym. Sci.* **2008**, *212*, 99.

(23) Huang, W.; Zhao, T.-Y.; Wen, M.-W.; Yang, Z.-Y.; Xu, W.; Yi, Y.-P.; Xu, L.-P.; Wang, Z.-X.; Gu, Z.-J. *J. Phys. Chem. C* **2014**, *118*, 6767.

(24) Balakrishnan, K.; Datar, A.; Zhang, W.; Yang, X.; Naddo, T.; Huang, J.; Zuo, J.; Yen, M.; Moore, J. S.; Zang, L. *J. Am. Chem. Soc.* **2006**, *128*, 6576.

(25) Finke, A. D.; Gross, D. E.; Han, A.; Moore, J. S. *J. Am. Chem. Soc.* **2011,** *133*, 14063.

(26) Che, Y.; Gross, D. E.; Huang, H.; Yang, D.; Yang, X.; Discekici, E.; Xue, Z.; Zhao, H.; Moore, J. S.; Zang, L. *J. Am. Chem. Soc.* **2012**, *134*, 4978.

(27) Yang, Z.; Chi, Z.; Xu, B.; Li, H.; Zhang, X.; Li, X.; Liu, S.; Zhang, Y.; Xu, J. *J. Mater. Chem.* **2010**, *20*, 7352.

(28) Dong, S.; Li, Z.; Qin, J. *J. Phys. Chem. B* **2009**, *113*, 434.

(29) Upamali, K. A. N.; Estrada, L. A.; De, P. K.; Cai, X.; Krause, J. A.; Neckers, D. C. *Langmuir* **2011**, *27*, 1573.

(30) Auttapornpitak, P.; Sukwattanasinitt, M.; Rashatasakhon, P. *Sensors Actuators B Chem.* **2013**, *178*, 296.

(31) Naddo, T.; Che, Y.; Zhang, W.; Balakrishnan, K.; Yang, X.; Yen, M.; Zhao, J.; Moore, J. S.; Zang, L. *J. Am. Chem. Soc.* **2007**, *129*, 6978.

(32) Chen, Q.; Luo, M.; Hammershøj, P.; Zhou, D.; Han, Y.; Laursen, B. W.; Yan, C.-G.; Han, B.-H. *J. Am. Chem. Soc*. **2012**, *134*, 6084.

(33) Zhu, X.; Mahurin, S. M.; An, S.-H.; Do-Thanh, C.-L.; Tian, C.; Li, Y.; Gill, L. W.; Hagaman, E. W.; Bian, Z.; Zhou, J.-H.; Hu, J.; Liu, H.; Dai, S. *Chem. Commun*. **2014**, *50*, 2.

(34) Casco, M. E.; Morelos-Gómez, A.; Vega-Díaz, S. M.; Cruz-Silva, R.; Tristán-López, F.; Muramatsu, H.; Hayashi, T.; Martínez-Escandell, M.;

Terrones, M.; Endo, M.; Rodríguez-Reinoso, F.; Silvestre-Albero, J. *J. CO_2 Utiliz.* **2014**, *5*, 60.

(35) Drage, T. C.; Arenillas, A.; Smith, K.; Snape, C. E. *8th International Conference on Greenhouse Gas Technologies* **2006**, *19*.

(36) Arenillas, A.; Rubiera, F.; Parra, J. B.; Ania, C. O.; Pis, J. *J. Appl. Surf. Sci*. **2005**, *252*, 619.

(37) Arenillas, A.; Drage, T. C.; Smith, K.; Snape, C. E. *J. Anal. Appl. Pyrolysis* **2005**, *74*, 298.

(38) Xu, D.; Liu, X.; Lu, R.; Xue, P.; Zhang, X.; Zhou, H.; Jia, J. *Org. Biomol. Chem.* **2011**, *9*, 1523.

(39) Gaussian 09, Frisch, M. J.; Trucks, G. W.; Schlegel, H. B.; Scuseria, G. E.; Robb, M. A.; Cheeseman, J. R.; Scalmani, G.; Barone, V.; Mennucci, B.; Petersson, G. A.; Nakatsuji, H.; Caricato, M.; Li, X.; Hratchian, H. P.; Izmaylov, A. F.; Bloino, J.; Zheng, G.; Sonnenberg, J. L.; Hada, M.; Ehara, M.; Toyota, K.; Fukuda, R.; Hasegawa, J.; Ishida, M.; Nakajima, T.; Honda, Y.; Kitao, O.; Nakai, H.; Vreven, T.; Montgomery, Jr., J. A.; Peralta, J. E.; Ogliaro, F.; Bearpark, M.; Heyd, J. J.; Brothers, E.; Kudin, K. N.; Staroverov, V. N.; Kobayashi, R.; Normand, J.; Raghavachari, K.; Rendell, A.; Burant, J. C.; Iyengar, S. S.; Tomasi, J.; Cossi, M.; Rega, N.; Millam, N. J.; Klene, M.; Knox, J. E.; Cross, J. B.; Bakken, V.; Adamo, C.; Jaramillo, J.; Gomperts, R.; Stratmann, R. E.; Yazyev, O.; Austin, A. J.; Cammi, R.; Pomelli, C.; Ochterski, J. W.; Martin, R. L.; Morokuma, K.; Zakrzewski, V. G.; Voth, G. A.; Salvador, P.; Dannenberg, J. J.; Dapprich, S.; Daniels, A. D.; Farkas, Ö.; Foresman, J. B.; Ortiz, J. V.; Cioslowski, J.; Fox, D. J. Gaussian, Inc., Wallingford CT, **2009**

(40) Becke, A. D. *J. Chem. Phys.* **1993**, 5648.

(41) Stevens, W. J.; Basch, H.; Krauss, M. *J. Chem. Phys*. **1984**, *81*, 6026.

(42) Stevens, W. J.; Krauss, M.; Basch, H.; Jasien, P. G. *Can. J. Chem.* **1992**, *70*, 612–630.

(43) Cundari, T. R.; Stevens, W. J. *J. Chem. Phys*. **1993**, *98*, 5555.

(44) Williams, A. T. R.; Winfield, S. A.; Miller, J. N. *Analyst* **1983**, *108*, 1067.

(45) Ostrauskaite, J.; Strohriegl, P. *Macromol. Chem. Phys.* **2003**, *204*, 1713.

(46) Raj, V.; Madheswari, D.; Ali, M. M. *J. Appl. Polym. Sci.* **2010**, *116*, 147.

(47) Li, Z. Q.; Lu, C. J.; Xia, Z. P.; Zhou, Y.; Luo, Z. *Carbon* **2007**, *45*, 1686.

(48) Sumrak, J. C.; Sokolov, A. N.; MacGillivray, L. R. In *Crystal Engineering Organic Semiconductors*; **2011**; pp. 1–19.

(49) Belletête, M.; Bouchard, J.; Leclerc, M.; Durocher, G. *Macromolecules* **2005**, *38*, 880.

(50) Martin, T. P.; Wise, A. J.; Busby, E.; Gao, J.; Roehling, J. D.; Ford, M. J.; Larsen, D. S.; Moule, A. J.; Grey, J. K. *J. Phys Chem. B* **2013**, *117*, 4478.

(51) Xu, B.; He, J.; Dong, Y.; Chen, F.; Yu, W.; Tian, W. *Chem. Commun.* **2011**, *47*, 6602.

(52) Yasutani, Y.; Honsho, Y.; Saeki, A.; Seki, S. *Synth. Met.* **2012**, *162*, 1713.

(53) Spano, F. C. *Acc. Chem. Res.* **2010**, *43*, 429.

(54) Gierschner, J.; Luer, L.; Milian-Medina, B.; Oelkrug, D.; Egelhaaf, H. J. *Phys. Chem. Lett.* **2013**, *4*, 2686.

(55) Wang, L.; Shen, Y.; Yang, M.; Zhang, X.; Xu, W.; Zhu, Q.; Wu, J.; Tian, Y.; Zhou, H. *Chem. Commun.* **2014**, *50*, 8723.

(56) Braslavsky, S. E. *Pure Appl. Chem.* **2007**, *79*, 293.

(57) Józefowicz, M.; Heldt, J. R. *J. Fluoresc.* **2011**, *21*, 239.

(58) Sarangi, M. K.; Mitra, A. K.; Sengupta, C.; Ghosh, S.; Chakraborty, S.; Saha, C.; Basu, S. *J. Phys. Chem. C* **2013**, *117*, 2166.

(59) Fita, P.; Fedoseeva, M.; Vauthey, E. *Langmuir* **2011**, *27*, 4645.

(60) Spencer, T. S. O'Donnell, C. M. *J. Am. Chem. Soc.* **1972**, *94,* 4846.

(61) Ma, L.; Wang, Q.; Lu, G.; Chen, R.; Sun, X. *Langmuir* **2010**, *26*, 6702.

(62) Bombach, R.; Honegger, E.; Leutwyler, S. *Chem. Phys. Lett.* **1985**, *118*, 449.

(63) Pels, J.; Kapteijn, F.; Moulijn, J.; Zhu, Q.; Thomas, K. *Carbon* **1995**, *33*, 1641.

(64) Hao, G.-P.; Li, W.-C.; Qian, D.; Lu, A.-H. *Adv. Mater.* **2010**, *22*, 853.

(65) Taoudi, H.; Bernede, J. C.; Bonnet, A.; Morsli, M.; Godoy, A. *Thin Solid Films* **1997**, *304*, 48.

Chapter 3

(1) Kokkali, V.; van Delft, W. *TrAC Trends Anal. Chem.* **2014**, *61*, 133.

(2) Jang, A.; Zou, Z.; Lee, K. K.; Ahn, C. H.; Bishop, P. L. *Meas. Sci. Technol*. **2011**, *22*, 032001.

(3) Yoshinaga, J. *Environ. Health Prev. Med.* **2012**, *17*, 433.

(4) Verma, R.; Gupta, B. D. *Food Chem.* **2015**, *166*, 568.

(5) Scott, A. C.; Mackinnon, M. D.; Fedorak, P. M. *Environ. Sci. Technol.* **2005**, *39*, 8388.

(6) Headley, J. V.; McMartin, D. W. *J. Environ. Sci. Heal. Part A* **2004**, *39*, 1989.

(7) Baruah, S.; Dutta, J. *Environ. Chem. Lett.* **2009**, *7*, 191.

(8) Zhang, D.; Cochrane, J. R.; Martinez, A.; Gao, G. *RSC Adv.* **2014**, *4*, 29735.

(9) Li, P.; Zhao, Y.; Yao, L.; Nie, H.; Zhang, M. *Sensors Actuators B Chem.* **2014**, *191*, 332.

(10) Catalan, J. *J. Phys. Chem. A* **2007**, *111*, 8774.

(11) Che, Y.; Gross, D. E.; Huang, H.; Yang, D.; Yang, X.; Discekici, E.; Xue, Z.; Zhao, H.; Moore, J. S.; Zang, L. *J. Am. Chem. Soc.* **2012**, *134*, 4978.

(12) Zhang, X.; Wu, Y.; Ji, S.; Guo, H.; Song, P.; Han, K.; Wu, W.; Wu, W.; James, T. D.; Zhao, J. *J. Org. Chem.* **2010**, *75*, 2578.

(13) Zhang, X.; Chi, L.; Ji, S.; Wu, Y.; Song, P.; Han, K.; Guo, H.; James, T. D.; Zhao, J. *J. Am. Chem. Soc.* **2009**, *131*, 17452.

(14) Mahapatra, A. K.; Roy, J.; Sahoo, P.; Mukhopadhyay, S. K.; Mukhopadhyay, A. R.; Mandal, D. *Bioorg. Med. Chem. Lett.* **2012**, *22*, 5379.

(15) Xu, D.; Liu, X.; Lu, R.; Xue, P.; Zhang, X.; Zhou, H.; Jia, *J. Org. Biomol. Chem.* **2011**, *9*, 1523.

(16) Grewer, D. M.; Young, R. F.; Whittal, R. M.; Fedorak, P. M. *Sci. Total Environ.* **2010**, *408*, 5997.

(17) Lu, W.; Ewanchuk, A.; Perez-Estrada, L.; Sego, D.; Ulrich, A. *J. Environ. Sci. Health. A. Tox. Hazard. Subst. Environ. Eng.* **2013**, *48*, 429.

(18) Yen, T.-W.; Marsh, W. P.; MacKinnon, M. D.; Fedorak, P. M. *J. Chromatogr. A* **2004**, *1033*, 83.

(19) Obtained from the RAMP monitoring activities; overview of 2008 activities.

(20) Ding, Z.; Zhao, Q.; Xing, R.; Wang, X.; Ding, J.; Wang, L.; Han, Y. *J. Mater. Chem. C* **2013**, *1*, 786.

(21) Suresh Kumar, H. M.; Kunabenchi, R. S.; Biradar, J. S.; Math, N. N.; Kadadevarmath, J. S.; Inamdar, S. R. *J. Lumin.* **2006**, *116*, 35.

(22) Murphy, C.; Zhang, Y.; Troxler, T. *J. Phys. Chem. B.* **2004**, *17*, 1537.

(23) Xing, C.; Yuan, H.; Xu, S.; An, H.; Niu, R.; Zhan, Y. *ACS Appl. Mater. Interfaces* **2014**, *6*, 9601.

(24) Li, Z.; Lu, J.; Li, S.; Qin, S.; Qin, Y. *Adv. Mater.* **2012**, *24*, 6053.

(25) McQuade, D. T.; Pullen, A. E.; Swager, T. M. *Chem. Rev.* **2000**, *100*, 2537.

(26) Toal, S. J.; Trogler, W. C. *J. Mater. Chem.* **2006**, *16*, 2871.

(27) Yang, J.; Swager, T. M. *J. Am. Chem. Soc.* **1998**, *78*, 5321.

(28) Kannel, P. R.; Gan, T. Y. *J. Environ. Sci. Health. A. Tox. Hazard. Subst. Environ. Eng.* **2012**, *47*, 1.

(29) Eicher, T.; Hauptmann, S.; Speicher, A. *The Chemistry of Heterocycles: structure, reactions, synthesis, and applications*; 3rd ed.; Wiley-VCH, **2012**; p. 118.

Chapter 4

(1) Pedersen, C. J. *Angew. Chem. Int. Ed. Engl.***1988**, *100*, 1053.

(2) Xue, W.; Li, Z.; Liu, G.; Chen, X.; Li, T.; Liu, S. H.; Yin, J. *Org. Biomol. Chem.* **2014**, *12*, 4862.

(3) Zhang, W.; Moore, J. S. *Angew. Chem. Int. Ed.* **2006**, *45*, 4416.

(4) Vehoff, T.; Kirkpatrick, J.; Kremer, K.; Andrienko, D. *Phys. Status Solidi* **2008**, *245*, 839.

(5) Vehoff, T.; Baumeier, B.; Andrienko, D. *J. Chem. Phys.* **2010**, *133*, 134901.

(6) Höger, S. *Chemistry* **2004**, *10*, 1320.

(7) Yang, Y.; Feng, W.; Hu, J.; Zou, S.; Gao, R.; Yamato, K.; Kline, M.; Cai, Z.; Gao, Y.; Wang, Y.; Li, Y.; Yang, Y.; Yuan, L.; Zeng, X. C.; Gong, B. *J. Am. Chem. Soc.* **2011**, *133*, 18590.

(8) Iyoda, M.; Yamakawa, J.; Rahman, M. J. *Angew. Chem. Int. Ed.* **2011**, *50*, 10522.

(9) Canevet, D.; Emilio, M. P.; Mart, N. *Organic Nanomaterials: Synthesis, Characterization, and Device Applications*; Torres, T.; Botlari, G., Eds.; John Wiley and Sons, **2013**; pp. 147–162.

(10) Dsouza, R. N.; Pischel, U.; Nau, W. M. *Chem. Rev.* **2011**, *111*, 7941.

(11) Kong, Q.; Qian, H.; Bo, H.; Zhang, C.; Liu, K.; Zhang, X.; Wang, J.; Li, J.; Gao, G. *Synth. Met.* **2011**, *161*, 2361.

(12) Schmaltz, B.; Rouhanipour, A.; Räder, H. J.; Pisula, W.; Müllen, K. *Angew. Chem. Int. Ed.* **2009**, *48*, 720.

(13) Baroncini, M.; Gao, C.; Carboni, V.; Credi, A.; Previtera, E.; Semeraro, M.; Venturi, M.; Silvi, S. *Chemistry* **2014**, *20*, 10737.

(14) Li, H.; Cheng, C.; Mcgonigal, P. R.; Fahrenbach, A. C.; Frasconi, M.; Liu, W.; Zhu, Z.; Zhao, Y.; Ke, C.; Lei, J.; Young, R. M.; Dyar, S. M.; Co, D. T.; Yang, Y.; Botros, Y. Y.; Goddard, W. A.; Wasielewski, M. R.; Astumian, R. D.; Stoddart, J. F. *J. Am. Chem. Soc.* **2014**, *136*, 10.

(15) Jena, N. K.; Murugan, N. A. *J. Phys. Chem. C* **2013**, *117*, 25059.

(16) Bruns, C. J.; Stoddart, J. F. *Acc. Chem. Res.* **2014**, *47*, 2186.

(17) Ghale, G.; Nau, W. M. *Acc. Chem. Res.* **2014**, *47*, 2150.

(18) Lan, J.; Zheng, X. H.; Hao, H.; Wang, X. L.; Shi, X. Q.; Zeng, Z. *J. Appl. Phys.* **2014**, *115*, 013702.

(19) Kallweit, C.; Haberhauer, G.; Woitschetzki, S. *Chemistry* **2014**, *20*, 6358.

(20) Ostrauskaite, J.; Strohriegl, P. *Macromol. Chem. Phys.* **2003**, *204*, 1713.

(21) Zhao, D.; Moore, J. S. *ChemInform* **2003**, *34*, 807.

(22) Laughrey, Z. R.; Gibb, B. C. *Top. Curr. Chem.* **2005**, *249*, 67.

(23) Sisco, S. W.; Larson, B. M.; Moore, J. S. *Macromolecules* **2014**, *47*, 3829.

(24) Finke, A. D.; Gross, D. E.; Han, A.; Moore, J. S. *J. Am. Chem. Soc.* **2011**, *133*, 14063.

(25) Jin, Y.; Wang, Q.; Taynton, P.; Zhang, W. *Acc. Chem. Res.* **2014**, *47*, 1575.

(26) Tobe, Y.; Utsumi, N.; Kawabata, K.; Nagano, A.; Adachi, K.; Araki, S.; Sonoda, M.; Hirose, K.; Naemura, K. *J. Am. Chem. Soc.* **2002**, *124*, 5350.

(27) Balakrishnan, K.; Datar, A.; Zhang, W.; Yang, X.; Naddo, T.; Huang, J.; Zuo, J.; Yen, M.; Moore, J. S.; Zang, L. *J. Am. Chem. Soc.* **2006**, *128*, 6576.

(28) Park, M.; Buck, J.; Rizzo, C. *Tetrahedron* **1998**, *54*, 12707.

(29) Cabaj, J.; Idzik, K.; Sołoducho, J.; Chyla, A. *Tetrahedron* **2006**, *62*, 758.

(30) Ludwiczak, M.; Majchrzak, M.; Bayda, M.; Marciniak, B.; Kubicki, M.; Marciniec, B. *J. Organomet. Chem.* **2014**, *750*, 150.

(31) Dong, W.; Fei, T.; Palma-Cando, A.; Scherf, U. *Polym. Chem.* **2014**, *5*, 4048.

(32) Pansay, S.; Prachumrak, N.; Jungsuttiwong, S.; Keawin, T.; Sudyoadsuk, T.; Promarak, V. *Tetrahedron Lett.* **2012**, *53*, 4568.

(33) Williams, A. T. R.; Winfield, S. A.; Miller, J. N. *Analyst* **1983**, *108*, 1067.

(34) Scott, T. A. J. *J. Phys. Chem.* **1946**, 406.

(35) Wankhede, D. S. *Int. J. Chem. Res.* **2011**, *2*, 23.

(36) Melhuish, W. H. *J. Phys. Chem.* **1961**, *97*, 229.

(37) Wothers, P.; Greeves, N.; Warren, S.; Clayden, J. *Organic Chemistry*; Oxford University Press, **2001**; pp. 437–438.

(38) Maruyama, S.; Hokari, H.; Wada, T.; Sasabe, H. *Synthesis* **2001**, *12*, 1794.

(39) Yamamoto, T.; Wakabayashi, S.; Osakada, K. *J. Organomet. Chem.* **1992**, *428*, 223.

(40) Shi, Y.; Liu, J.; Yang, Y. *J. Appl. Phys.* **2000**, *87*, 4254.

(41) Ruelle, P.; Sarraf, E.; Kesselring, U. W. *Int. J. Pharm.* **1994**, *104*, 125.

(42) Xu, B.; He, J.; Dong, Y.; Chen, F.; Yu, W.; Tian, W. *Chem. Commun.* **2011**, *47*, 6602.

(43) Zhai, Z.; Lam, J.; Tang, B. Z. *Soft Matter* **2013**, *9*, 4564.

(44) Hong, Y.; Lam, J. W. Y.; Tang, B. Z. *Chem. Commun.* **2009**, *45*, 4332.

(45) Dutta, A. *Langmuir* **1996**, *12*, 5909.

(46) Höger, S.; Bonrad, K.; Mourran, A.; Beginn, U.; Möller, M. *J. Am. Chem. Soc.* **2001**, *123*, 5651.

(47) Liu, X.; Xu, D.; Lu, R.; Li, B.; Qian, C.; Xue, P.; Zhang, X.; Zhou, H. *Chem. Eur. J.* **2011**, *17*, 1660.

(48) Belletête, M.; Bouchard, J.; Leclerc, M.; Durocher, G. *Macromolecules* **2005**, *38*, 880.

(49) Tirapattur, S.; Belletête, M.; Drolet, N.; Leclerc, M.; Durocher, G. *Chem. Phys. Lett.* **2003**, *370*, 799.

(50) Yagai, S.; Iwashima, T.; Kishikawa, K.; Nakahara, S.; Karatsu, T.; Kitamura, A. *Chemistry* **2006**, *12*, 3984.

(51) Huang, J.; Li, Q.; Li, Z. *Aggregation Inducced Emission: Fundamentals.* First Ed. **2013**, John Wiley and Sons.

(52) Tomasini, C.; Castellucci, N. *Chem. Soc. Rev.* **2013**, *42*, 156.

(53) Avinash, M. B.; Govindaraju, T. *Nanoscale* **2014**, *6*, 13348.

(54) Sagiri, S. S.; Behera, B.; Rafanan, R. R.; Bhattacharya, C.; Pal, K.; Banerjee, I.; Rousseau, D. *Soft Mater*. **2014**, *12*, 47.

(55) Vintiloiu, A.; Leroux, J.-C. *J. Control. Release* **2008**, *125*, 179.

(56) Díaz Díaz, D.; Kühbeck, D.; Koopmans, R. *J. Chem. Soc. Rev.* **2011**, *40*, 427.

(57) Li, Y.; Liu, T.; Liu, H.; Tian, M.-Z.; Li, Y. *Acc. Chem. Res.* **2014**, *47*, 1186.

(58) Schenning, A. P. H. J.; Meijer, E. W. *Chem. Commun.* **2005**, *41*, 3245.

(59) Delclos, T.; Aimé, C.; Pouget, E.; Brizard, A.; Huc, I.; Delviles, M.; Oda, R. *Nano Lett.* **2008**, *8*, 1929.

(60) Banerjee, S.; Das, R. K.; Maitra, U. *J. Mater. Chem.* **2009**, *19*, 6649.

(61) Zhao, Z.; Lam, J. W. Y.; Tang, B. Z. *Soft Matter* **2013**, *9*, 4564.

(62) Shelnutt, J.; Medforth, C. In *Organic Nanomaterials: Synthesis, Characterization, and Device Applications*; **2013**; First Edit, p.103-130.

(63) Wang, Z.; Medforth, C. J.; Shelnutt, J. A. *J. Am. Chem. Soc.* **2004**, *126*, 15954.

(64) Wang, Z.; Ho, K. J.; Medforth, C. J.; Shelnutt, J. A. *Adv. Mater.* **2006**, *18*, 2557.

(65) Balakrishnan, K.; Datar, A.; Naddo, T.; Huang, J.; Oitker, R.; Yen, M.; Zhao, J.; Zang, L. *J. Am. Chem. Soc.* **2006**, *128*, 7390.

(66) Zhang, Z.; Zhan, C.; Zhang, X.; Zhang, S.; Huang, J.; Li, A. D. Q.; Yao, J. *Chemistry* **2012**, *18*, 12305.

(67) Ma, L.; Wang, Q.; Lu, G.; Chen, R.; Sun, X. *Langmuir* **2010**, *26*, 6702.

(68) Xie, L.; Yang, S.; Lin, J.; Yi, M.; Huang, W. *Philos. Trans. R. Soc. London A* **2013**, *371*, 20120337.

(69) Surin, M.; Sonar, P.; Grimsdale, A. C.; Müllen, K.; De Feyter, S.; Habuchi, S.; Sarzi, S.; Braeken, E.; Ver Heyen, A.; Van der Auweraer, M.; De Schryver, F. C.; Cavallini, M.; Moulin, J.-F.; Biscarini, F.; Femoni, C.; Lazzaroni, R.; Leclére, P. *J. Mater. Chem.* **2007**, *17*, 728.

(70) Maggini, L.; Bonifazi, D. *Chem. Soc. Rev.* **2012**, *41*, 211.

(71) Tsai, W.-W.; Tevis, I. D.; Tayi, A. S.; Cui, H.; Stupp, S. I. *J. Phys. Chem. B* **2010**, *114*, 14778.

(72) Gentili, D.; Di Maria, F.; Liscio, F.; Ferlauto, L.; Leonardi, F.; Maini, L.; Gazzano, M.; Milita, S.; Barbarella, G.; Cavallini, M. *J. Mater. Chem.* **2012**, *22*, 20852.

(73) Di Maria, F.; Olivelli, P.; Gazzano, M.; Zanelli, A.; Biasiucci, M.; Gigli, G.; Gentili, D.; D'Angelo, P.; Cavallini, M.; Barbarella, G. *J. Am. Chem. Soc.* **2011**, *133*, 8654.

(74) Tevis, I. D.; Palmer, L. C.; Herman, D. J.; Murray, I. P.; Stone, D. A.; Stupp, S. I. *J. Am. Chem. Soc.* **2011**, *133*, 16486.

(75) Korevaar, P. A.; Schaefer, C.; de Greef, T. F. A.; Meijer, E. W. *J. Am. Chem. Soc.* **2012**, *134*, 13482.

(76) Schenning, A. P. H. J.; Jonkheijm, P.; Peeters, E.; Meijer, E. W. *J. Am. Chem. Soc.* **2001**, *123*, 409.

(77) Beaujuge, P. M.; Reynolds, J. R. *Chem. Rev.* **2010**, *110*, 268.

(78) Hu, B.; Lv, X.; Sun, J.; Bian, G.; Ouyang, M.; Fu, Z.; Wang, P.; Zhang, C. *Org. Electron.* **2013**, *14*, 1521.

(79) Baycan Koyuncu, F.; Koyuncu, S.; Ozdemir, E. *Org. Electron.* **2011**, *12*, 1701.

(80) Verghese, M.; Ram, M.; Vardhan, H. *Polymer* **1997**, *38*, 1625.

(81) Verghese, M. M.; Ram, M. K.; Vardhan, H.; Ashrafb, S. M.; Malhotra, B. D. *Adv. Mater. Opt. Electron.* **1996**, *6*, 399.

(82) Tran-van, F.; Vancaeyzeele, C.; Henri, T.; Gazulevivius, J. V.; Chevrot, C. *Mater. Res. Soc. Symp. Proc.* **2002**, *708*, 1.

(83) Hu, B.; Yang, Z.; Karasz, F. E. *J. Appl. Phys.* **1994**, *76*, 2419.

(84) Qian, Y.; Cao, F.; Guo, W. *Tetrahedron* **2013**, *69*, 4169.

(85) Wang, Y.; Hou, L.; Yang, K.; Chen, J.; Wang, F.; Cao, Y. *Macromol. Chem. Phys.* **2005**, *206*, 2190.

(86) Boudreault, P. T.; Blouin, N.; Leclerc, M. *Adv. Polym. Sci.* **2008**, *212*, 99.

(87) Xu, X.; Cai, W.; Chen, J.; Cao, Y. *J. Polym. Sci. Part A Polym. Chem.* **2011**, *49*, 1263.

(88) Casey, A.; Ashraf, R. S.; Fei, Z.; Heeney, M. *Macromolecules* **2014,** *47,* 2279.

(89) Lek, J. Y.; Lam, Y. M.; Niziol, J.; Marzec, M. *Nanotechnology* **2012**, *23*, 315401.

(90) Xie, H.; Zhang, K.; Duan, C.; Liu, S.; Huang, F.; Cao, Y. *Polymer* **2012**, *53*, 5675.

(91) El-Shafei, A.; Hussain, M.; Atiq, A.; Islam, A.; Han, L. *J. Mater. Chem.* **2012**, *22*, 24048.

(92) Zheng, C.; Tao, Y.; Cao, J.-Z.; Chen, R.-F.; Zhao, P.; Wu, X.-J.; Huang, W. *J. Mol. Model.* **2012**, *18*, 4929.

(93) Zhao, T.; Liu, Z.; Song, Y.; Xu, W.; Zhang, D.; Zhu, D. *J. Org. Chem.* **2006**, *71*, 7422.

(94) Che, Y.; Gross, D. E.; Huang, H.; Yang, D.; Yang, X.; Discekici, E.; Xue, Z.; Zhao, H.; Moore, J. S.; Zang, L. *J. Am. Chem. Soc.* **2012**, *134*, 4978.

(95) Yang, Y.; Xue, M.; Marshall, L. J.; de Mendoza, J. *Org. Lett.* **2011**, *13*, 3186.

(96) Jung, S.-H.; Pisula, W.; Rouhanipour, A.; Räder, H. J.; Jacob, J.; Müllen, K. *Angew. Chem. Int. Ed*. **2006**, *45*, 4685.

(97) Upamali, K. A. N.; Estrada, L. A.; De, P. K.; Cai, X.; Krause, J. A.; Neckers, D. C. *Langmuir* **2011**, *27*, 1573.

(98) Sinnokrot, M. O.; Valéev, E. F.; Sherrill, C. D. *J. Am. Chem. Soc.* **2002**, *124*, 10887.

(99) Ayoub, A. T.; Tuszynski, J.; Klobukowski, M. Theor. *Chem. Acc.* **2014**, *133*, 1520.

(100) Zumdahl, S. S. *Chemistry*; 5th ed.; p. 373.

(101) Martinez, C. R.; Iverson, B. L. *Chem. Sci.* **2012**, *3*, 2191.

(102) Palmans, A. R. A; Meijer, E. W. *Angew. Chem. Int. Ed.* **2007**, *46*, 8948.

(103) Raeburn, J.; Zamith Cardoso, A.; Adams, D. *J. Chem. Soc. Rev.* **2013**, *42*, 5143.

(104) Wunsch, B. H.; Rumi, M.; Tummala, N. R.; Risko, C.; Kang, D.-Y.; Steirer, K. X.; Gantz, J.; Said, M.; Armstrong, N. R.; Brédas, J.-L.; Bucknall, D.; Marder, S. R. *J. Mater. Chem. C* **2013**, *1*, 5250.

(105) Sumrak, J. C.; Sokolov, A. N.; MacGillivray, L. R. In *Crystal Engineering Organic Semiconductors*; **2011**; pp. 1–19.

(106) Kastler, M.; Pisula, W.; Wasserfallen, D.; Pakula, T.; Müllen, K. *J. Am. Chem. Soc.* **2005**, *127*, 4286.

(107) Höger, S.; Bonrad, K.; Mourran, A.; Beginn, U.; Möller, M. *J. Am. Chem. Soc.* **2001**, *123*, 5651.

(108) Yu, G.; Yan, X.; Han, C.; Huang, F. *Chem. Soc. Rev.* **2013**, *42*, 6697.

(109) Yagai, S.; Gushiken, M.; Karatsu, T.; Kitamura, A.; Kikkawa, Y. *Chem. Commun.* **2011**, *47*, 454.

(110) Canevet, D.; Pérez del Pino, Á.; Amabilino, D. B.; Sallé, M. *J. Mater. Chem.* **2011**, *21*, 1428.

(111) Spano, F. C.; Silva, C. *Annu. Rev. Phys. Chem.* **2014**, *65*, 477.

(112) Brédas, J. L.; Cornil, J.; Beljonne, D.; Dos Santos, D.; Shuai, Z. G. *Acc. Chem. Res.* **1999**, *32*, 267.

(113) Chochos, C. L.; Choulis, S. A. *Prog. Polym. Sci.* **2011**, *36*, 1326.

(114) Siddiqui, S.; Spano, F. C. *Chem. Phys. Lett.* **1999**, *308*, 99.

(115) Yamagata, H.; Spano, F. C. *J. Chem. Phys.* **2012**, *136*, 184901.

(116) Dong, S.; Li, Z.; Qin, J. *J. Phys. Chem. B* **2009**, *113*, 434.

(117) Lin, H.; Zheng, M.; Yang, J.; Bai, F. *Chinese Sci. Bull.* **2013**, *48*, 637.

(118) Spectus, C. O. N.; Palmer, L.; Stupp, S. *Acc. Chem. Res.* **2008**, *41*, 1674.

(119) Kim, F. S.; Ren, G.; Jenekhe, S. A. *Chem. Mater.* **2011**, *23*, 682.

(120) Zang, L.; Che, Y.; Moore, J. S. *Acc. Chem. Res.* **2008**, *41*, 1596.

(121) Estroff, L. A.; Hamilton, A. D. *Chem. Rev.* **2004**, *104*, 1201.

(122) Meylemans, H. A.; Damrauer, N. H. *Inorg. Chem.* **2009**, *48*, 11161.

(123) Heeger, A. J. *Chem. Soc. Rev.* **2010**, *39*, 2354.

(124) Beckers, E. H. A.; Meskers, S. C. J.; Schenning, A. P. H. J.; Chen, Z.; Würthner, F.; Marsal, P.; Beljonne, D.; Cornil, J.; Janssen, R. A. J. *J. Am. Chem. Soc.* **2006**, *128*, 649.

(125) Amabilino, D. B. In *Organic Nanomaterials: Synthesis, Characterization, and Device Applications*; **2013**; First Edit, pp. 59–77.

(126) George, S. J.; Ajayaghosh, A.; Jonkheijm, P.; Schenning, A. P. H. J.; Meijer, E. W. *Angew. Chemie. Int. Ed.* **2004**, *43*, 3422.

(127) Ruiz, L.; Keten, S. J. *Phys. Chem. Lett.* **2014**, *5*, 2021.

(128) Korevaar, P. A.; de Greef, T. F. A.; Meijer, E. W. *Chem. Mater.* **2014**, *26*, 576-586.

(129) Jonkheijm, P.; van der Schoot, P.; Schenning, A. P. H. J.; Meijer, E. W. *Science* **2006**, *313*, 80.

Chapter 5

(1) Su, H.-J.; Wu, F.-I.; Shu, C.-F. *Macromolecules* **2004**, *37*, 7197.

(2) Neher, D. *Macromol. Rapid Commun.* **2001**, *22*, 1365.

(3) Loi, M. A.; Toffanin, S.; Muccini, M.; Forster, M.; Scherf, U.; Scharber, M. *Adv. Funct. Mater.* **2007**, *17*, 2111.

(4) Abbel, R.; Schenning, A. P. H. J.; Meijer, E. W. *J. Polym. Sci. Part A Polym. Chem.* **2009**, *47*, 4215.

(5) Pei, Q.; Yang, Y. *J. Am. Chem. Soc.* **1996**, *118*, 7416.

(6) Tseng, Y.; Shih, P.; Chien, C.; Dixit, A. K.; Shu, C.; Liu, Y.; Lee, G. *Macromolecules* **2005**, *38*, 10055.

(7) Lee, J.; Klaerner, G.; Miller, R. *Chem. Mater.* **1999**, *11*, 1083.

(8) Romaner, L.; Pogantsch, A.; Scandiucci de Freitas, P.; Scherf, U.; Gaal, M.; Zojer, E.; List, E. J. W. *Adv. Funct. Mater.* **2003**, *13*, 597.

(9) Wong, W.; Hooper, J.; Holmes, A. *Aust. J. Chem.* **2009**, *62*, 393.

(10) Lee, S. H.; Jang, B.-B.; Kafafi, Z. H. *J. Am. Chem. Soc.* **2005**, *127*, 9071.

(11) Lucht, B.; Buretea, M.; Tilley, T. *Organometallics* **2000**, *19*, 3469.

(12) Ego, C.; Marsitzky, D.; Becker, S.; Zhang, J.; Grimsdale, A. C.; Müllen, K.; MacKenzie, J. D.; Silva, C.; Friend, R. H. *J. Am. Chem. Soc.* **2003**, *125*, 437.

(13) Chen, R.; Zhu, R.; Zheng, C.; Liu, S.; Fan, Q.; Huang, W. *Sci. China Ser. B Chem.* **2009**, *52*, 212.

(14) Allard, N.; Aïch, R. B.; Gendron, D.; Boudreault, P.-L. T.; Tessier, C.; Alem, S.; Tse, S.-C.; Tao, Y.; Leclerc, M. *Macromolecules* **2010**, *43*, 2328.

(15) Yin, J.; Zhang, S.-L.; Chen, R.-F.; Ling, Q.-D.; Huang, W. *Phys. Chem. Chem. Phys.* **2010**, *12*, 15448.

(16) Ponomarenko, S.; Kirchmeyer, S. *Adv. Polym. Sci.* **2011**, *48*, 33.

(17) Pudzich, R.; Fuhrmann-Lieker, J.; Salbeck, J. *Adv. Polym. Sci.* **2006**, *199*, 83.

(18) Lee, J.-I. L.; Lee, V. Y. L.; Miller, R. D. M. *ETRI J.* **2002**, *24*, 409.

(19) Grisanti, L.; Terenziani, F.; Sissa, C.; Cavazzini, M.; Rizzo, F.; Orlandi, S.; Painelli, A. *J. Phys. Chem. B* **2011**, *115*, 11420.

(20) Rabe, T.; Görrn, P.; Lehnhardt, M.; Tilgner, M.; Riedl, T.; Kowalsky, W. *Phys. Rev. Lett.* **2009**, *102*, 137401.

(21) Hintschich, S. I.; Rothe, C.; King, S. M.; Clark, S. J.; Monkman, A. P. *J. Phys. Chem. B* **2008**, *112*, 16300.

(22) King, S. M.; Hintschich, S. I.; Dai, D.; Rothe, C.; Monkman, A. P. *J. Phys. Chem. C* **2007**, *111*, 18759.

(23) Wu, C.-C.; Liu, W.-G.; Hung, W.-Y.; Liu, T.-L.; Lin, Y.-T.; Lin, H.-W.; Wong, K.-T.; Chien, Y.-Y.; Chen, R.-T.; Hung, T.-H.; Chao, T.-C.; Chen, Y.-M. *Appl. Phys. Lett.* **2005**, *87*, 052103.

(24) Chen, J.; Cao, Y. *Macromol. Rapid Commun.* **2007**, *28*, 1714.

(25) Yamaguchi, S.; Tamao, K. *Bull. Chem. Soc. Jpn.* **1996**, *69*, 2327.

(26) Zhan, X.; Barlow, S.; Marder, S. R. *Chem. Commun.* **2009**, 1948.

(27) Yamaguchi, S.; Itami, Y.; Tamao, K. *Organometallics* **1998**, *17*, 4910.

(28) Khabashesku, V. N.; Boganov, S. E.; Antic, D.; Nefedov, O. M.; Michl, J. *Organometallics* **1996**, *15*, 4714.

(29) Hissler, M.; Dyer, P. W.; Réau, R. *Coord. Chem. Rev.* **2003**, *244*, 1.

(30) Chen, H.-Y.; Hou, J.; Hayden, A. E.; Yang, H.; Houk, K. N.; Yang, Y. *Adv. Mater.* **2010**, *22*, 371.

(31) Chochos, C. L.; Choulis, S. A. *Prog. Polym. Sci.* **2011**, *36*, 1326.

(32) Reimers, J. R.; Cai, Z.-L.; Bilić, A.; Hush, N. S. *Ann. N. Y. Acad. Sci.* **2003**, ***1006***, 235.

(33) Gaussian 09, Frisch, M. J.; Trucks, G. W.; Schlegel, H. B.; Scuseria, G. E.; Robb, M. A.; Cheeseman, J. R.; Scalmani, G.; Barone, V.; Mennucci,

B.; Petersson, G. A.; Nakatsuji, H.; Caricato, M.; Li, X.; Hratchian, H. P.; Izmaylov, A. F.; Bloino, J.; Zheng, G.; Sonnenberg, J. L.; Hada, M.; Ehara, M.; Toyota, K.; Fukuda, R.; Hasegawa, J.; Ishida, M.; Nakajima, T.; Honda, Y.; Kitao, O.; Nakai, H.; Vreven, T.; Montgomery, Jr., J. A.; Peralta, J. E.; Ogliaro, F.; Bearpark, M.; Heyd, J. J.; Brothers, E.; Kudin, K. N.; Staroverov, V. N.; Kobayashi, R.; Normand, J.; Raghavachari, K.; Rendell, A.; Burant, J. C.; Iyengar, S. S.; Tomasi, J.; Cossi, M.; Rega, N.; Millam, N. J.; Klene, M.; Knox, J. E.; Cross, J. B.; Bakken, V.; Adamo, C.; Jaramillo, J.; Gomperts, R.; Stratmann, R. E.; Yazyev, O.; Austin, A. J.; Cammi, R.; Pomelli, C.; Ochterski, J. W.; Martin, R. L.; Morokuma, K.; Zakrzewski, V. G.; Voth, G. A.; Salvador, P.; Dannenberg, J. J.; Dapprich, S.; Daniels, A. D.; Farkas, Ö.; Foresman, J. B.; Ortiz, J. V.; Cioslowski, J.; Fox, D. J. Gaussian, Inc., Wallingford CT, **2009**

(34) Stevens, W. J.; Basch, H.; Krauss, M. *J. Chem. Phys.* **1984**, *81*, 6026.

(35) Glaesemann, K.; Govind, N.; Krishnamoorthy, S.; Kowalski, K. *J. Phys. Chem. A* **2010**, *114*, 8764.

(36) Perdew, J. P.; Burke, K.; Ernzerhof, M. *Phys. Rev. Lett.* **1996**, *77*, 3865.

(37) Vydrov, O. A.; Scuseria, G. E.; Perdew, J. P. *J. Chem. Phys.* **2007**, *126*, 154109.

(38) Vydrov, O. A.; Scuseria, G. E. *J. Chem. Phys.* **2006**, *125*, 234109.

(39) Gordon, M. S.; Binkley, J. S.; Pople, J. A.; Pietro, I. W. J.; Hehre, W. J. *J. Am. Chem. Soc.* **1982**, *104*, 2797.

(40) Pietro, W. J.; Francl, M. M.; Hehre, I. W. J.; Defrees, D. J.; Pople, I. J. A.; Binkley, J. S. *J. Am. Chem. Soc.* **1982**, *104*, 5039.

(41) Simmons, H. E.; Fukunaga, T. *J. Am. Chem. Soc.* **1967**, *89*, 5208.

(42) Schenk, H. *Acta Crystallogr. Sect. B* **1972**, *28*, 625.

(43) Semmelhack, M.; Foos, J.; Katz, S. *J. Am. Chem. Soc.* **1973**, *95*, 7325.

(44) Cui, Z. H.; Guo, X. X. *J. Power Sources* **2014**, *267*, 20.

(45) Allred, A.; Rochow, E. *J. Inorg. Nucl. Chem.* **1958**, *5*, 269.

(46) Chen, R.-F.; Zheng, C.; Fan, Q.-L.; Huang, W. *J. Comput. Chem.* **2007**, *28*, 2091.

(47) Roncali, J. *Chem. Rev.* **1997**, *97*, 173.

(48) Salzner, U.; Lagowski, J.; Pickup, P.; Poirier, R. *Synth. Met.* **1998**, *96*, 177.

(49) Teetsov, J.; Fox, M. A. *J. Mater. Chem.* **1999**, *9*, 2117.

(50) Knaapila, M.; Garamus, V.; Dias, F. *Macromolecules* **2006**, *39*, 6505.

(51) Wang, J.; Feng, J.; Ren, A.; Liu, X.; Ma, Y. *Macromolecules* **2004**, *37*, 3451.

(52) Franco, I.; Tretiak, S. *J. Am. Chem. Soc.* **2004**, *126*, 12130.

(53) Chen, R.-F.; Liu, L.-Y.; Fu, H.; Zheng, C.; Xu, H.; Fan, Q.-L.; Huang, W. *J. Phys. Chem. B* **2011**, *115*, 242.

(54) Heeger, A. J. *Adv. Mater.* **2014**, *26*, 10.

(55) Goldsmith, R. H.; DeLeon, O.; Wilson, T. M.; Finkelstein-Shapiro, D.; Ratner, M. A; Wasielewski, M. R. *J. Phys. Chem. A* **2008**, *112*, 4410.

(56) Maslak, P.; Chopra, A.; Moylan, C. R.; Wortmann, R.; Lebus, S.; Rheingold, A. L.; Yap, G. P. A. *J. Am. Chem. Soc.* **1996**, *118*, 1471.

(57) Perdew, J.; Zunger, A. *Phys. Rev. B* **1981**, *23*, 5048.

(58) McCormick, T. M.; Bridges, C. R.; Carrera, E. I.; Dicarmine, P. M.; Gibson, G. L.; Hollinger, J.; Kozycz, L. M.; Seferos, D. S. *Macromolecules* **2013**, *46*, 3879.

(59) Gieseking, R. L.; Mukhopadhyay, S.; Risko, C.; Marder, S. R.; Brédas, J.-L. *Adv. Mater.* **2014**, *26*, 68.

(60) Hahn, T.; Liebing, S.; Kortus, J. *Nanoscale* **2014**, *6*, 14508.

(61) Saragi, T. P. I.; Spehr, T.; Siebert, A.; Fuhrmann-Lieker, T.; Salbeck, J. *Chem. Rev.* **2007**, *107*, 1011.

(62) Jacquemin, D.; Femenias, A.; Chermette, H.; Ciofini, I.; Adamo, C.; André, J.-M.; Perpète, E. A. *J. Phys. Chem. A* **2006**, *110*, 5952.

(63) Marsman, M.; Paier, J.; Stroppa, A.; Kresse, G. *J. Phys. Condens. Matter* **2008**, *20*, 064201.

Chapter 6

(1) Zhang, L.; Qin, L.; Wang, X.; Cao, H.; Liu, M. *Adv. Mater.* **2014**, *26*, 6959.

(2) Romeo, A.; Castriciano, M. A.; Occhiuto, I.; Zagami, R.; Pasternack, R. F.; Scolaro, L. M. *J. Am. Chem. Soc*. **2013,** *136,* 40.

(3) Das, R. K.; Kandanelli, R.; Linnanto, J.; Bose, K.; Maitra, U. *Langmuir* **2010**, *26*, 16141.

(4) Nandi, N.; Vollhardt, D. *Acc. Chem. Res.* **2007**, *40*, 351.

(5) Wang, Z.; Ma, K.; Xu, B.; Li, X.; Tian, W. *Sci. China Chem.* **2013**, *56*, 1234.

(6) Rogers, M. A.; Weiss, R. G. *New J. Chem*. **2014**.

(7) Palmer, L. C.; Leung, C.; Kewalramani, S.; Kumthekar, R.; Newcomb, C. J.; Olvera, M.; Cruz, D.; Bedzyk, M. J.; Stupp, S. I. *J. Am. Chem. Soc.* **2014**, *136*, 14377.

(8) Yang, Y.; Zhang, Y.; Wei, Z. *Adv. Mater.* **2013**, *25*, 6039.

(9) Dong, X.-W.; Liu, T.; Hu, Y.-Z.; Liu, X.-Y.; Che, C.-M. *Chem. Commun.* **2013**, *49*, 7681.

(10) Sohtome, Y.; Tanatani, A.; Hashimoto, Y.; Nagasawa, K. *Chem. Pharm. Bull*. **2004**, *52*, 477.

(11) Estroff, L. A.; Hamilton, A. D. *Chem. Rev.* **2004**, *104*, 1201.

(12) Kao, J.; Thorkelsson, K.; Bai, P.; Rancatore, B. J.; Xu, T. *Chem. Soc. Rev.* **2013**, *42*, 2654.

(13) Janáky, C.; Visy, C. *Anal. Bioanal. Chem.* **2013**, *405*, 3489.

(14) Gupta, B.; Joshi, L.; Prakash, R. *Macromol. Chem. Phys.* **2011**, *212*, 1692.

(15) Zhou, W.; Xu, J.; Du, Y.; Yang, P. *Int. J. Hydrogen Energy* **2011**, *36*, 1903.

(16) Briseno, A. L.; Mannsfeld, S. C. B.; Formo, E.; Xiong, Y.; Lu, X.; Bao, Z.; Jenekhe, S. A..; Xia, Y. *J. Mater. Chem.* **2008**, *18*, 5395.

(17) Leghrib, R.; Dufour, T.; Demoisson, F.; Claessens, N.; Reniers, F.; Llobet, E. *Sensors Actuators B Chem.* **2011**, *160*, 974.
(18) Cui, Z. H.; Guo, X. X. *J. Power Sources* **2014**, *267*, 20.
(19) Kim, F. S.; Ren, G.; Jenekhe, S. A. *Chem. Mater.* **2011**, *23*, 682.
(20) Barakat, N. a. M.; Motlak, M.; Kim, B.-S.; El-Deen, A. G.; Al-Deyab, S. S.; Hamza, a. M. *J. Mol. Catal. A Chem.* **2014**, *394*, 177.
(21) Li, X.-H.; Antonietti, M. *Chem. Soc. Rev.* **2013**, *42*, 6593.

Appendix 1

(1) Williams, A. T. R.; Winfield, S. A.; Miller, J. N. *Analyst* **1983**, *108*, 1067.
(2) Scott, T. A. J. *J. Phys. Chem.* **1946**, 406.
(3) Wankhede, D. S. *Int. J. Chem. Res.* **2011**, *2*, 23.
(4) Melhuish, W. H. *J. Phys. Chem.* **1961**, *97*, 229.

Appendices

Appendix 1. Determination of quantum yields.

Fluorescence quantum yields (Φ_{fl}) were determined using the relative quantum yield method developed by Williams *et al.*[1] The dye used for the analysis was anthracene, which was dissolved in absolute ethanol, and cross checked against quinine sulfate.[53] Information regarding solvents used and their indices of refraction are addressed individually in the experimental sections of Chapters 2 and 3. In this appendix, the determination of Φ_{fl} for compound **3e** is outlined, which performed using equation 1.

$$\Phi_x = \Phi_{st}\left(\frac{m_x}{m_{st}}\right)\left(\frac{\eta_x^2}{\eta_{st}^2}\right) \quad (1)$$

Where the subscripts *x* and *st* refer to the sample and standard, respectively. Other parameters include: quantum yield (Φ), *m* is the slope of the line of best fit found from plotting the integral of the fluorescence spectra versus the absorption at 356 nm (see Figure A1-1), and η is the refractive index of solvent. The quantum yield of anthracene used, Φ_{st}, was the value of 0.27 reported by Melhuish *et al.*, and the refractive indices for ethanol, η_{st} is 1.359 and for THF is 1.405.[2-4]

$$\Phi_x = \Phi_{st}\left(\frac{m_x}{m_{st}}\right)\left(\frac{\eta_x^2}{\eta_{st}^2}\right)$$

$$= 0.27\left(\frac{22803}{54608}\right)\left(\frac{1.405}{1.359}\right)$$

$$= 0.12$$

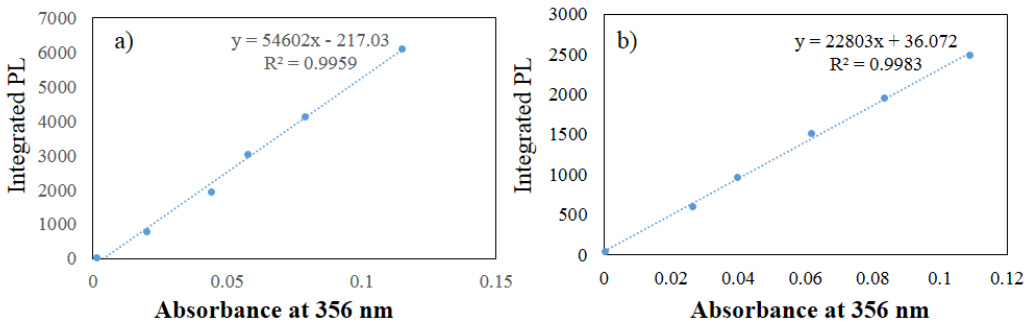

Figure A1-1. The integrated PL intensity as a function of absorbance of a) anthracene in ethanol, and b) **3e** in THF for the determination of the quantum yield.

A1.1 References

(1) Williams, A. T. R.; Winfield, S. A.; Miller, J. N. *Analyst* **1983**, *108*, 1067.

(2) Scott, T. A. J. *J. Phys. Chem.* **1946**, 406.

(3) Wankhede, D. S. *Int. J. Chem. Res.* **2011**, *2*, 23.

(4) Melhuish, W. H. *J. Phys. Chem.* **1961**, *97*, 229.

Appendix 2:

Preparation of carbazole macrocycles: characterization.

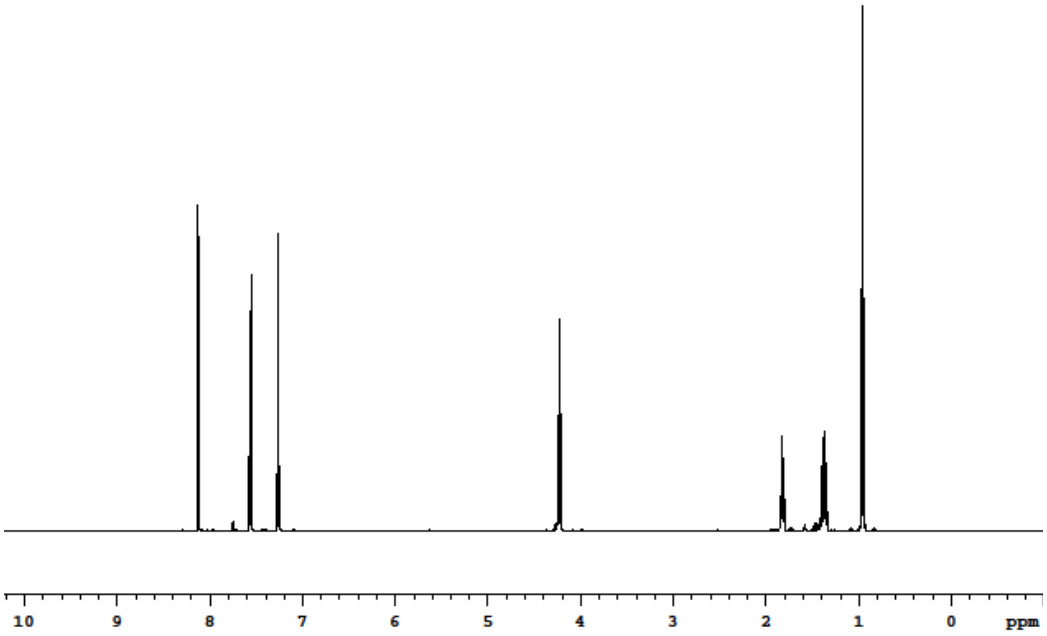

Figure A2-1. ^{1}H NMR spectrum of 3,6-dibromo-N-butyl carbazole (**2a**) in $CDCl_3$.

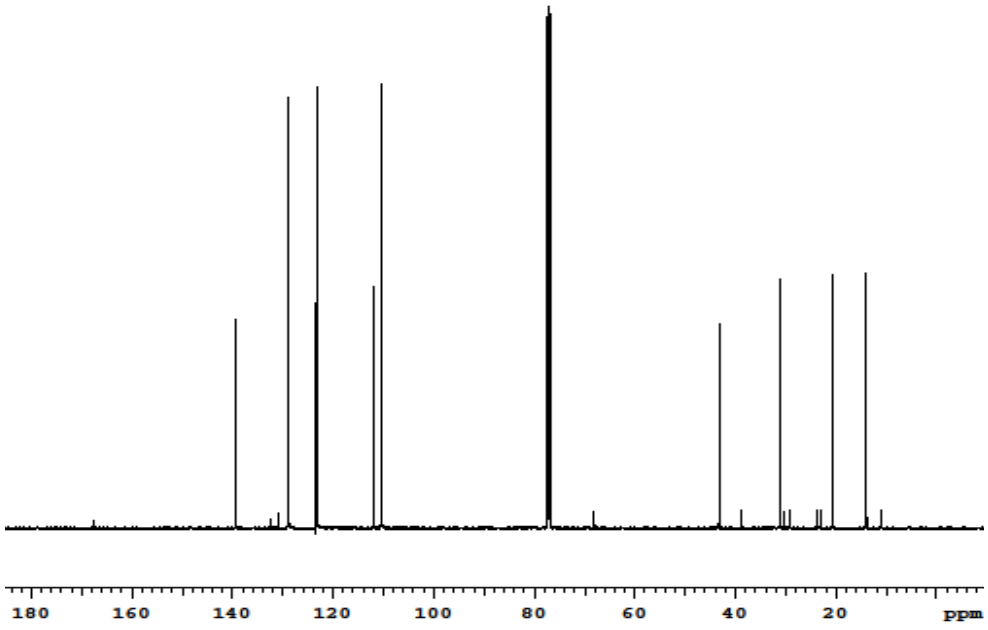

Figure A2-2. ^{13}C NMR spectrum of 3,6-dibromo-N-butyl carbazole (**2a**) in $CDCl_3$.

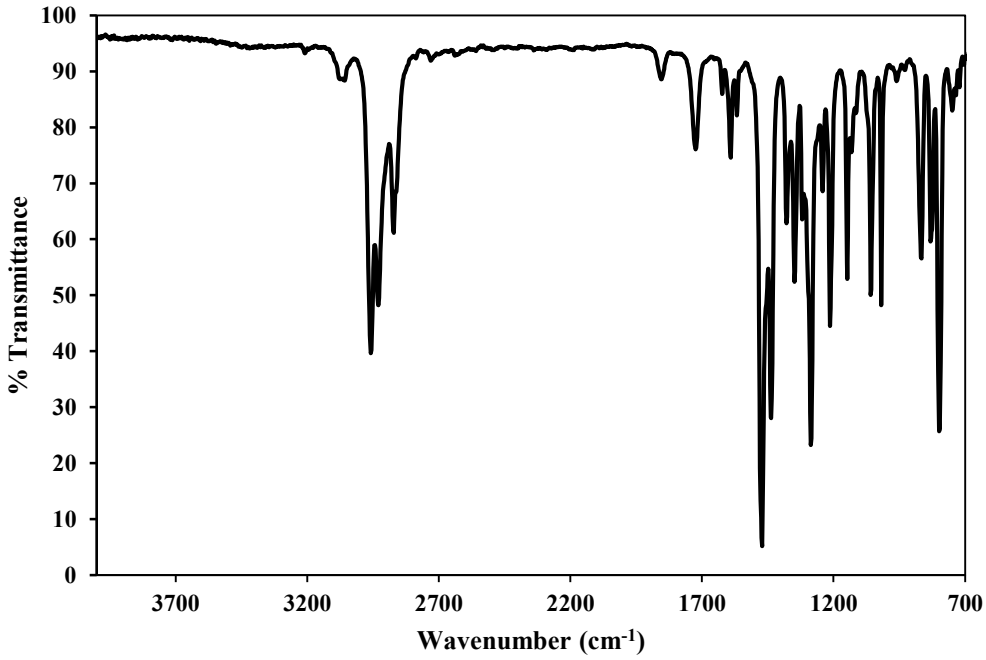

Figure A2-3. IR spectrum of 3,6-dibromo-N-butyl carbazole (**2a**) as thin film on KBr.

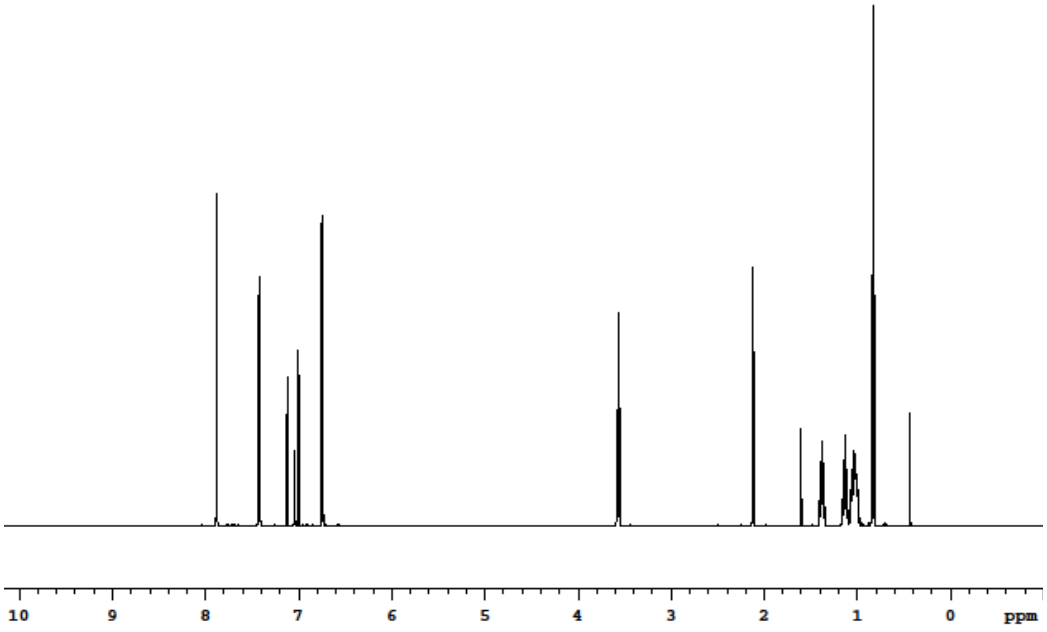

Figure A2-4. ^{1}H NMR spectrum of 3,6-dibromo-N-hexyl carbazole (**2b**) in toluene d8.

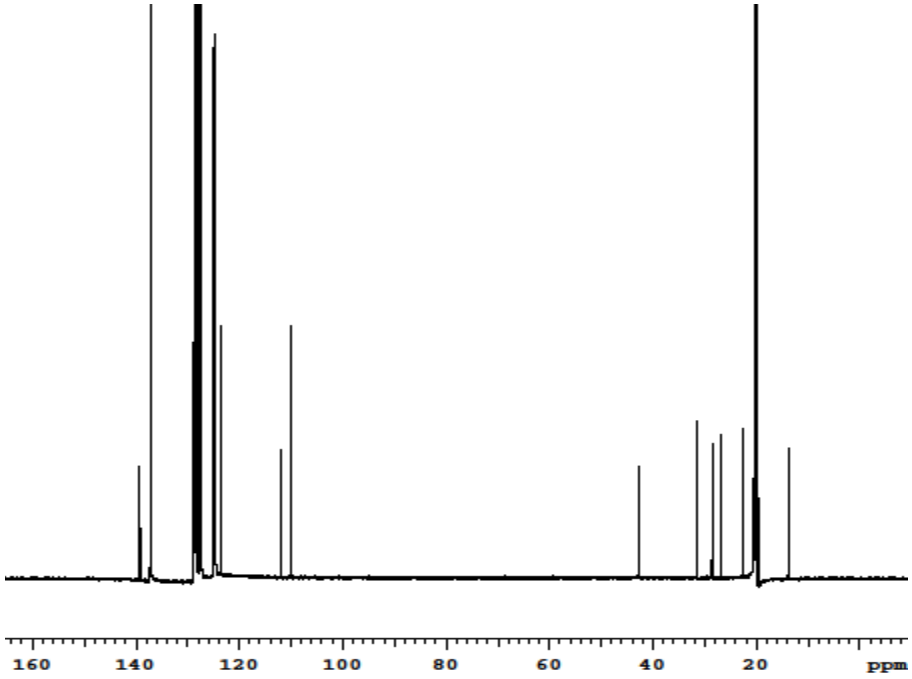

Figure A2-5. ^{13}C NMR spectrum of 3,6-dibromo-N-hexyl carbazole (**2b**) in toluene d8.

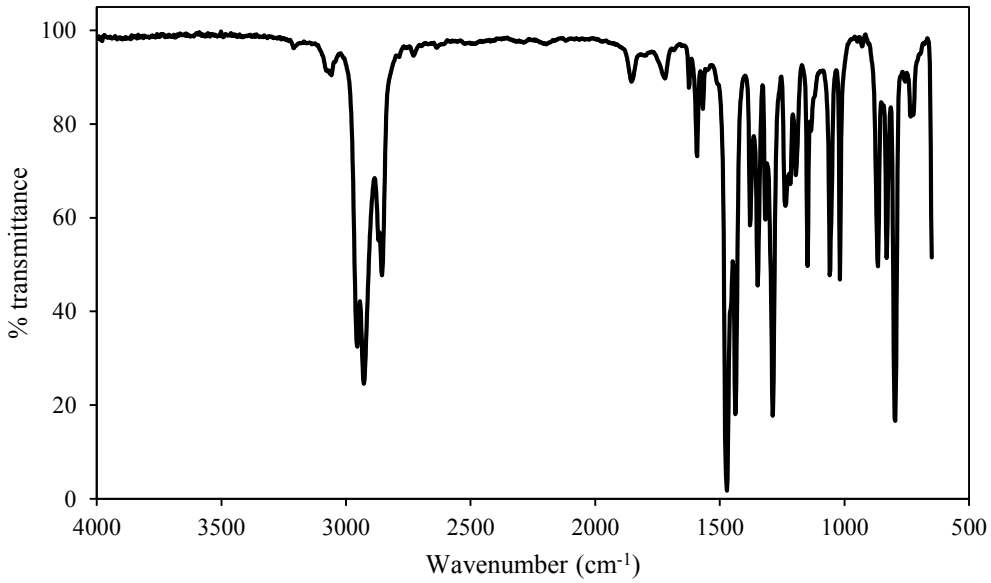

Figure A2-6. IR spectrum of 3,6-dibromo-N-hexyl carbazole (**2b**) as thin film on KBr.

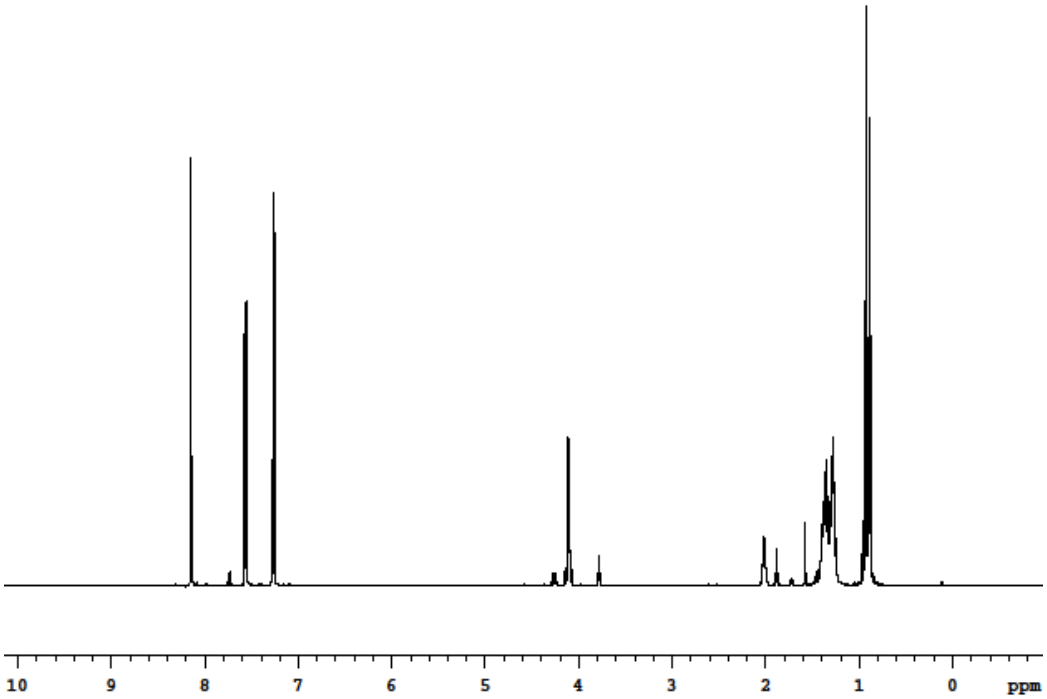

Figure A2-7. ^{1}H NMR spectrum of 3,6-dibromo-N-octyl carbazole (**2c**) in acetone d6.

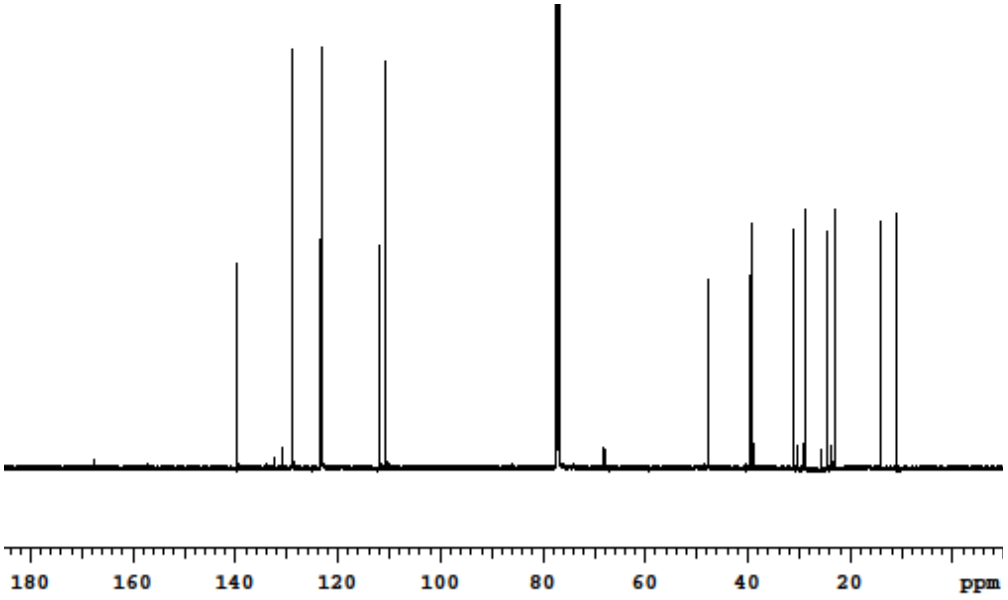

Figure A2-8. ^{13}C NMR spectrum of 3,6-dibromo-N-octyl carbazole (**2c**) in acetone d6.

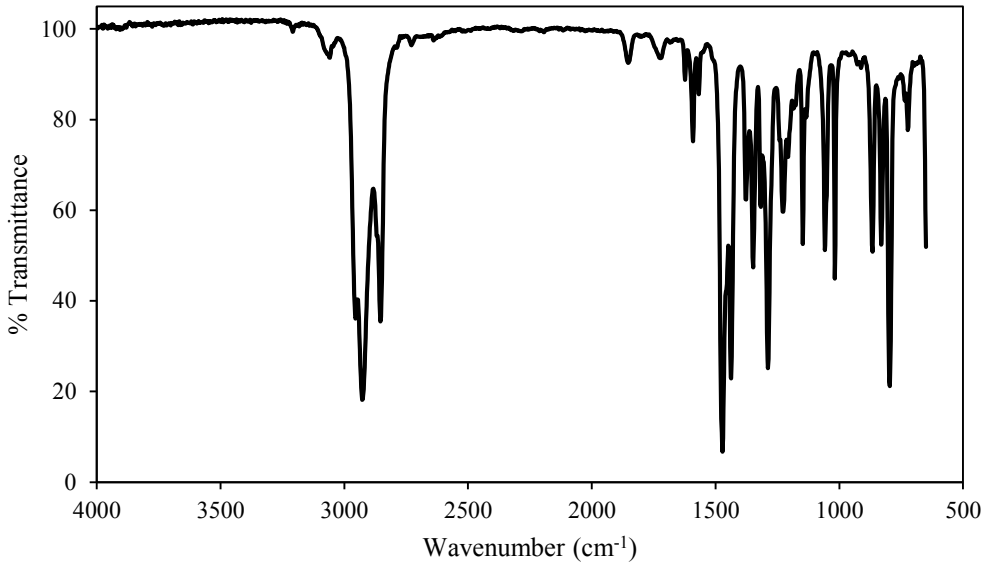

Figure A2-9. IR spectrum of 3,6-dibromo-N-octyl carbazole (**2c**) as thin film on KBr.

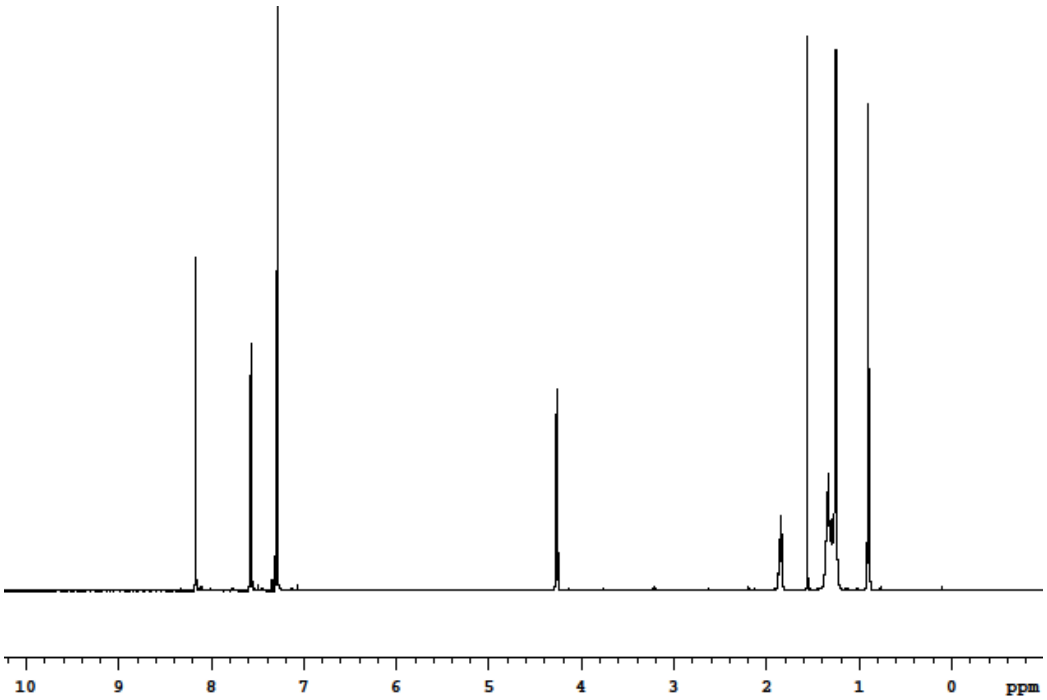

Figure A2-10. ^{1}H NMR spectrum of 3,6-dibromo-N-decyl carbazole (**2d**) in $CDCl_3$.

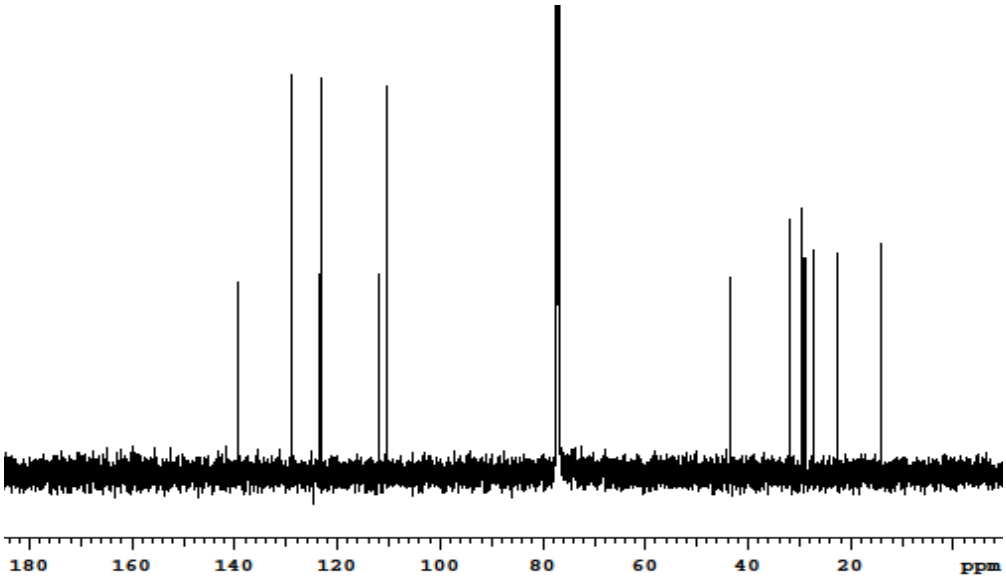

Figure A2-11. ^{13}C NMR spectrum of 3,6-dibromo-N-decyl carbazole (**2d**) in $CDCl_3$.

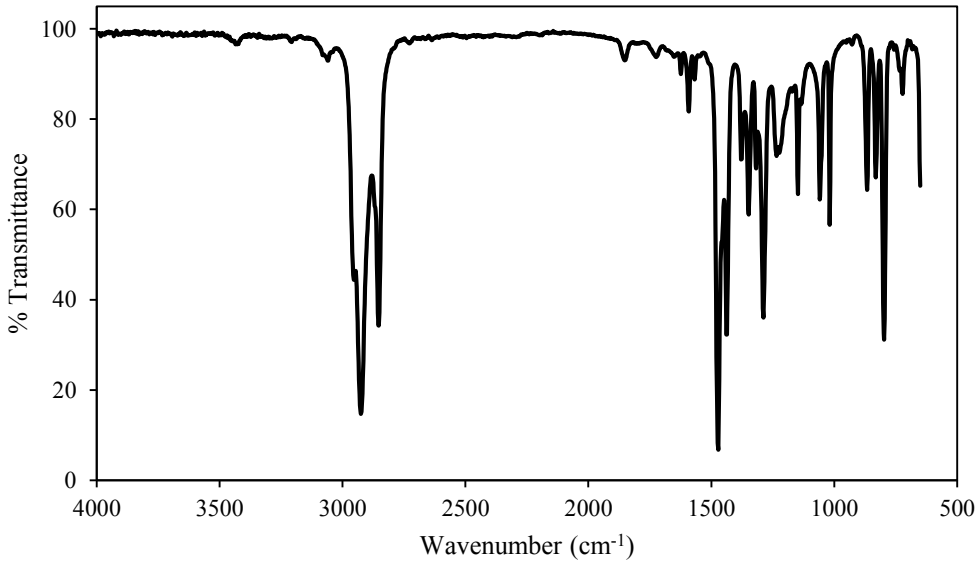

Figure A2-12. IR spectrum of 3,6-dibromo-N-decyl carbazole (**2d**) as thin film on KBr.

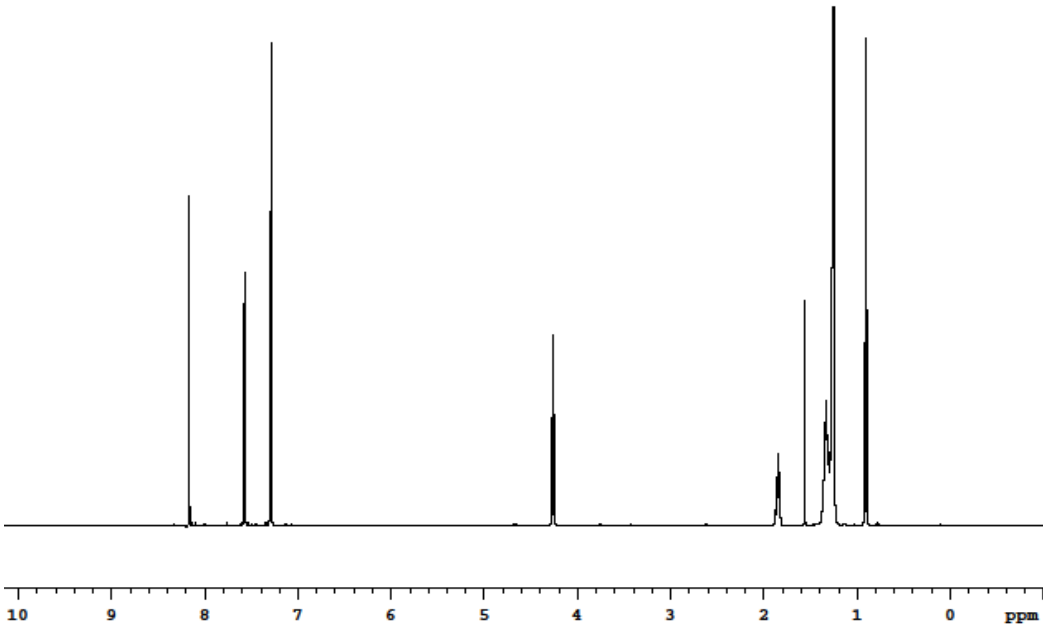

Figure A2-13. ^{1}H NMR spectrum of 3,6-dibromo-N-dodecyl carbazole (**2e**) in $CDCl_3$.

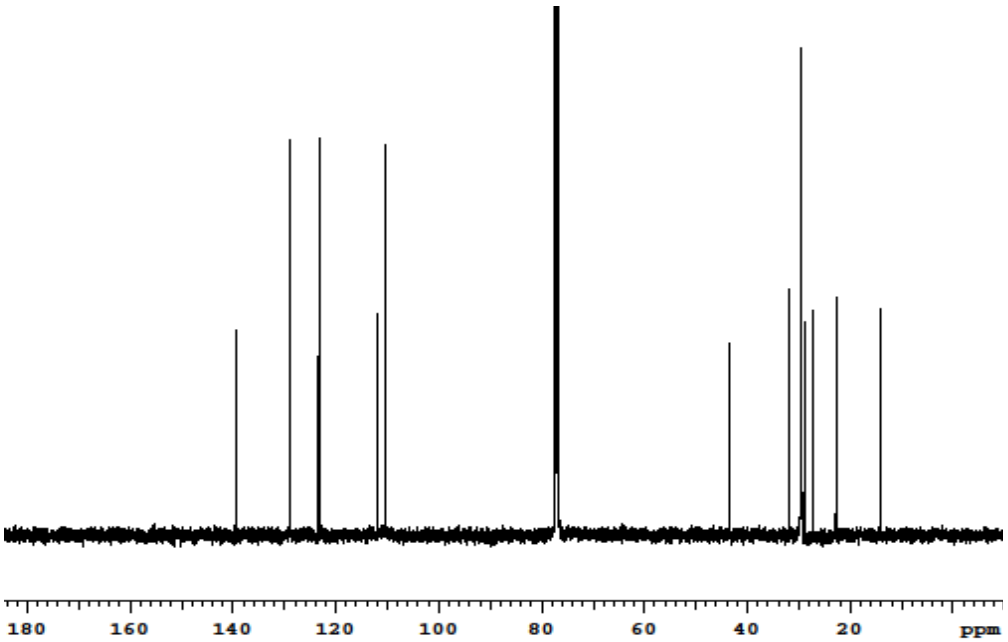

Figure A2-14. ^{13}C NMR spectrum of 3,6-dibromo-N-dodecyl carbazole (**2e**) in $CDCl_3$.

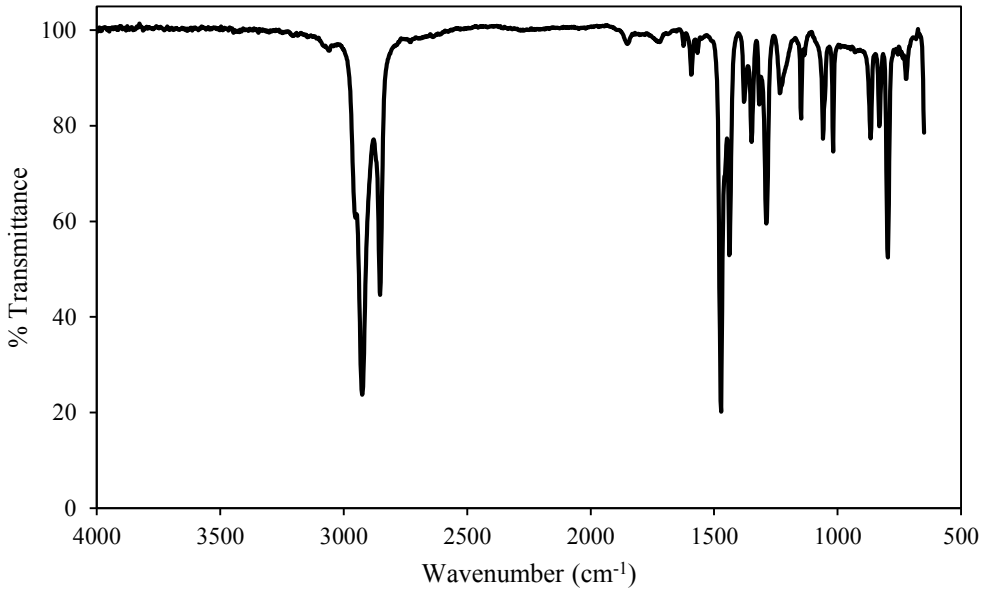

Figure A2-15. IR spectrum of 3,6-dibromo-N-dodecyl carbazole (**2e**) as thin film on KBr.

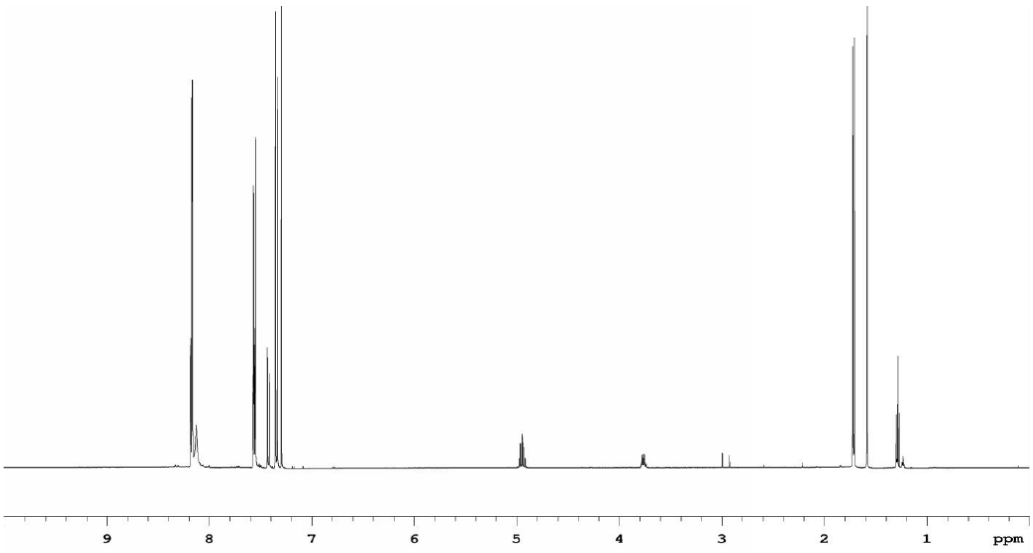

Figure A2-16. ^{1}H NMR spectrum of 3,6-dibromo-N-isopropyl carbazole (**2f**) in toluene-d8.

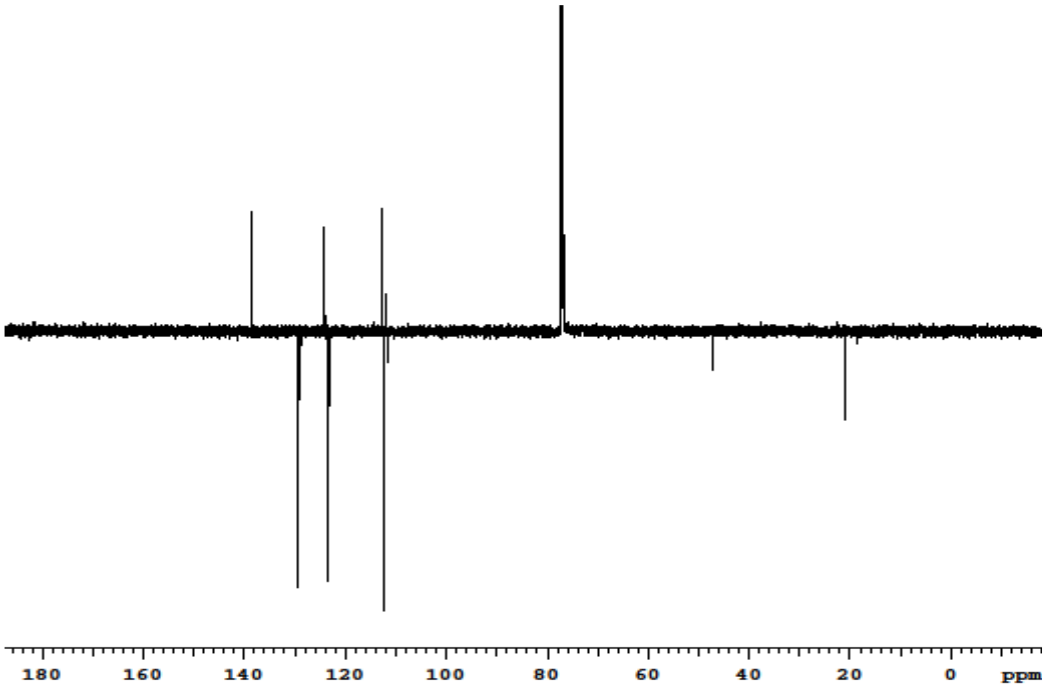

Figure A2-17. ^{13}C NMR spectrum of 3,6-dibromo-N-isopropyl carbazole (**2f**) in toluene-d8.

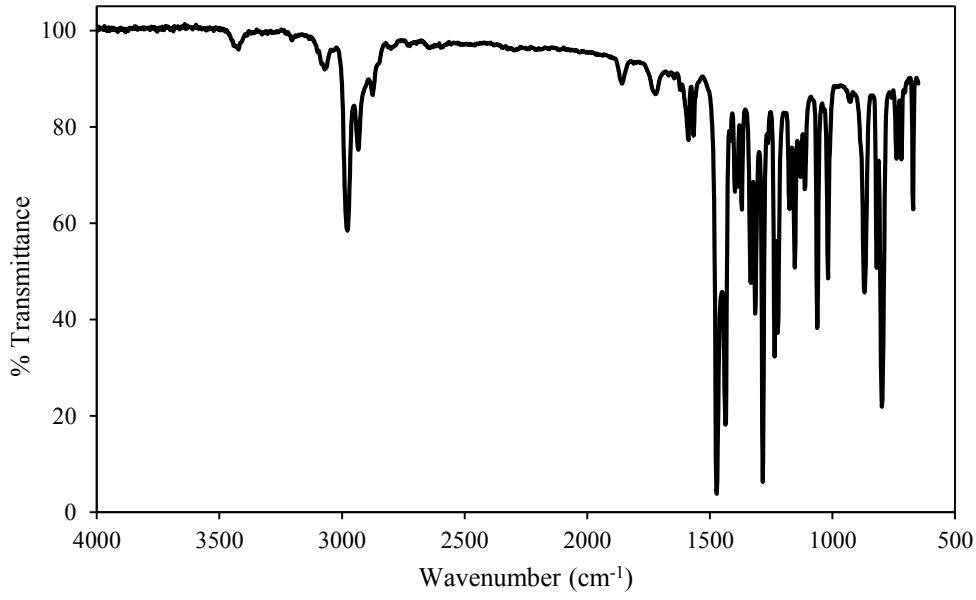

Figure A2-18. IR spectrum of 3,6-dibromo-N-isopropyl carbazole (**2f**) as thin film on KBr.

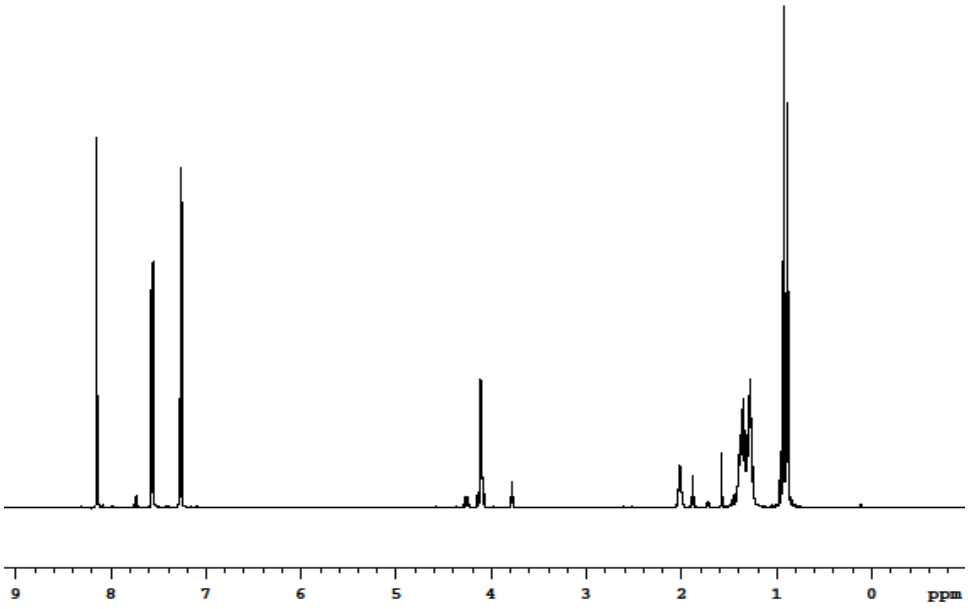

Figure A2-19. ^{1}H NMR spectrum of 3,6-dibromo-N-(2-ethylhexyl) carbazole (**2g**) in $CDCl_3$.

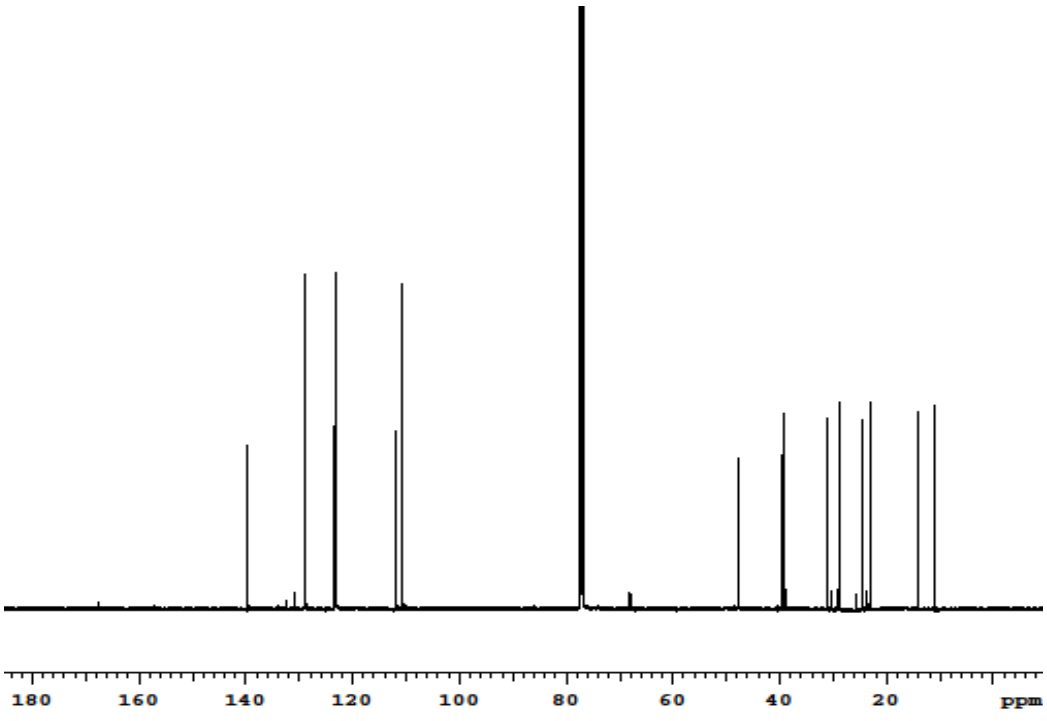

Figure A2-20. ^{13}C NMR spectrum of 3,6-dibromo-N-(2-ethylhexyl) carbazole (**2g**) in $CDCl_3$.

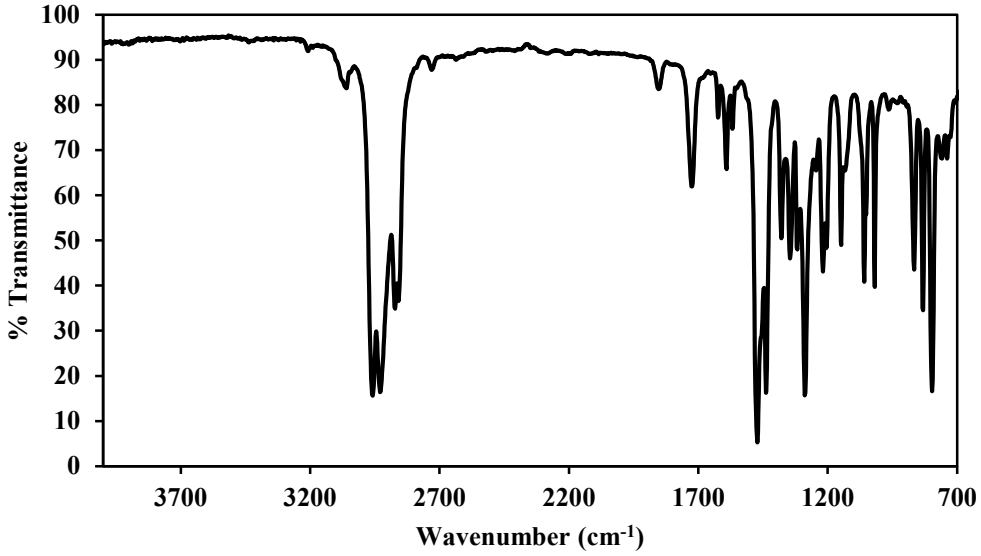

Figure A2-21. IR spectrum of 3,6-dibromo-N-(2-ethylhexyl) carbazole (**2g**) as thin film on KBr.

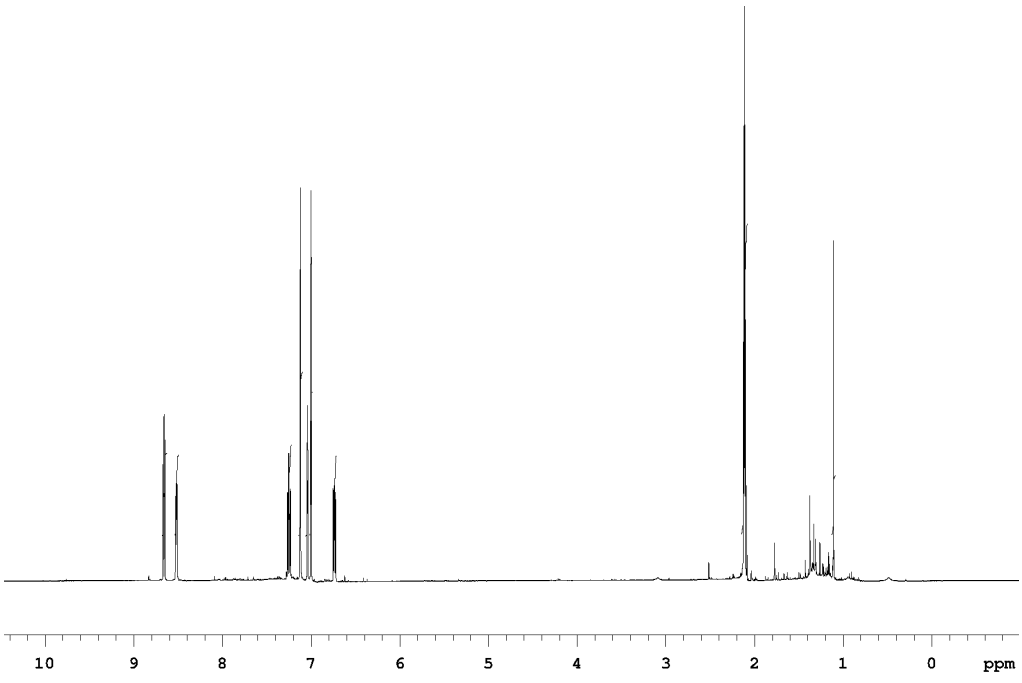

Figure A2-22. ^{1}H NMR spectrum of cyclo-3,6-tetracarbazole (**1**) in toluene d8.

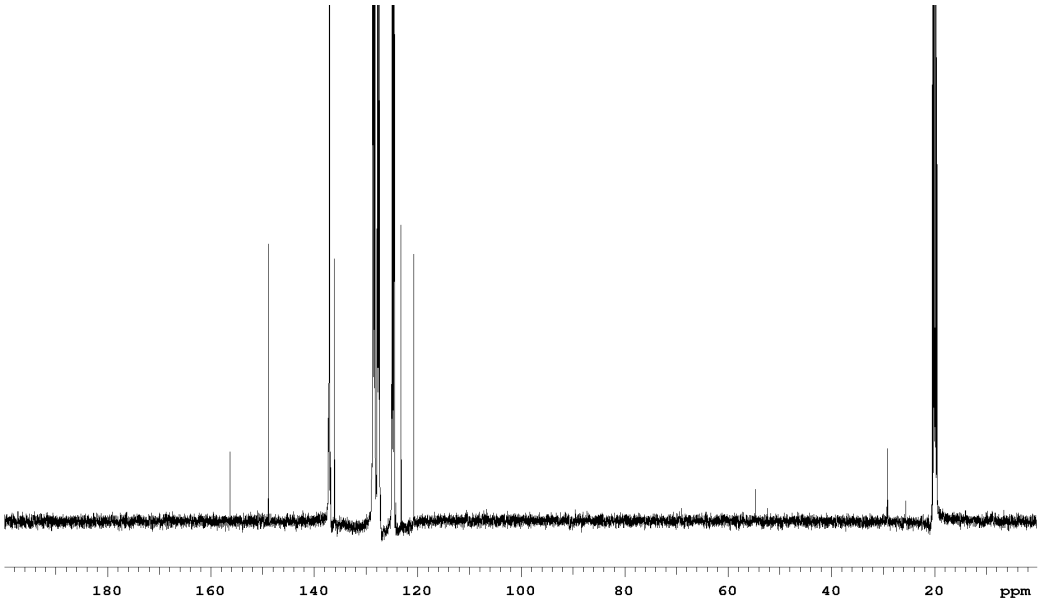

Figure A2-23. ^{13}C NMR spectrum of cyclo-3,6- tetracarbazole (**1**) in toluene d8.

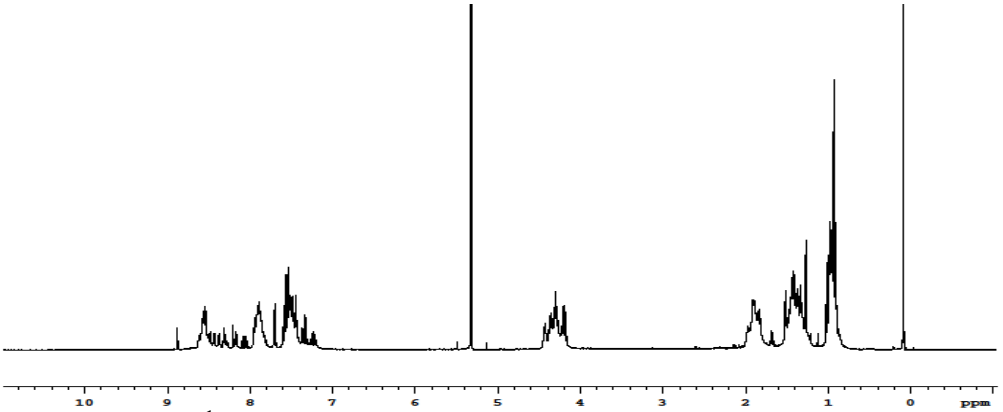

Figure A2-24. ^{1}H NMR spectrum of cyclo-3,6-tetra-N-butyl carbazole (**3a**) in $CDCl_3$.

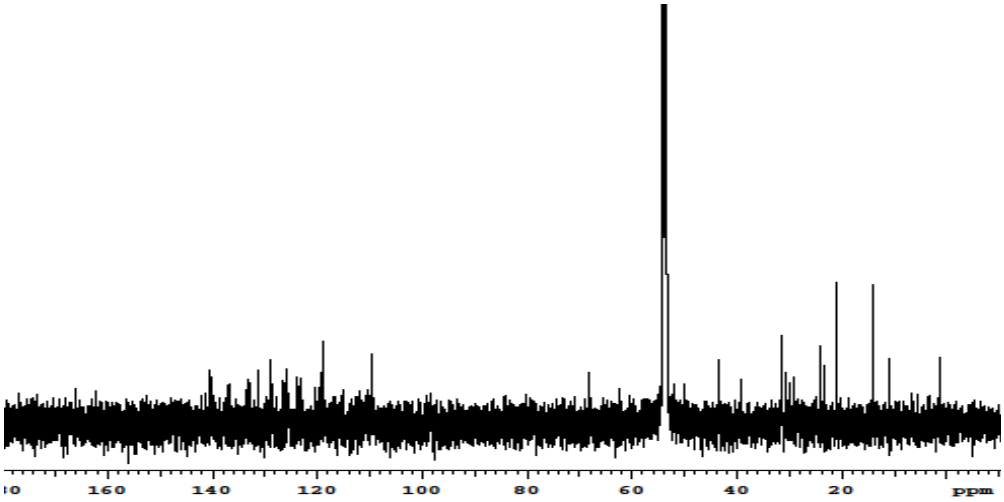

Figure A2-25. ^{13}C NMR spectrum of cyclo-3,6- tetra-N-butyl carbazole (**3a**) in $CDCl_3$.

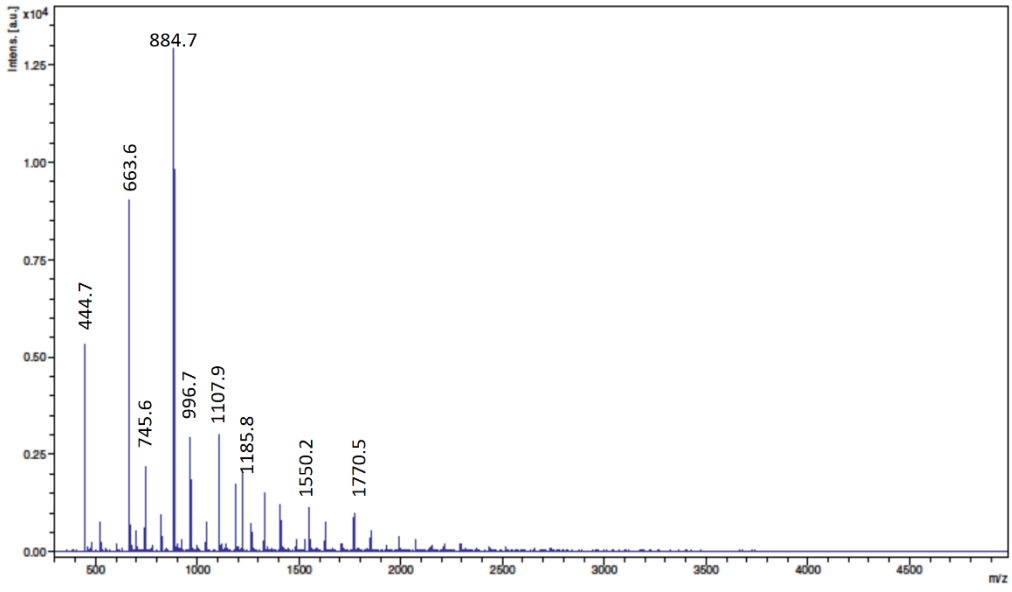

Figure A2-26. MALDI-TOF spectrum of cyclo-3,6- tetra-N-butyl carbazole (**3a**) in DCTB matrix.

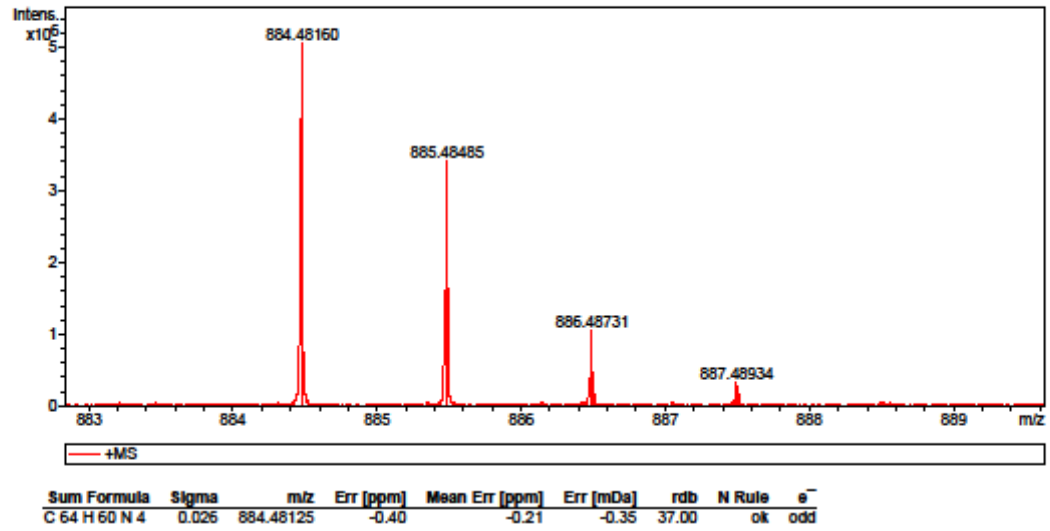

Figure A2-27. MALDI-FTICR spectrum of cyclo-3,6- tetra-N-butyl carbazole (**3a**) in DCTB matrix.

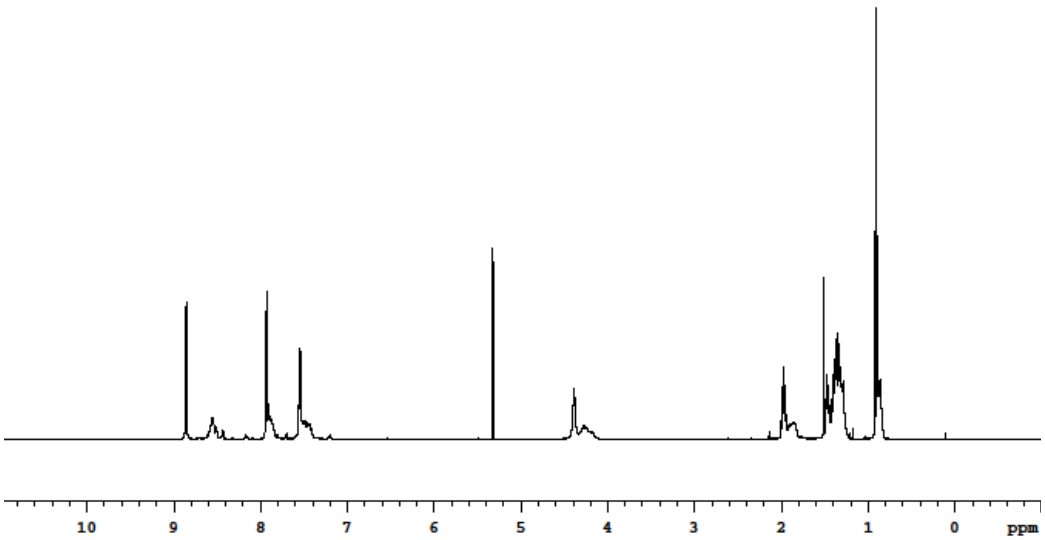

Figure A2-28. ^{1}H NMR spectrum of cyclo-3,6-tetra-N-hexylcarbazole (**3b**) in CD_2Cl_2.

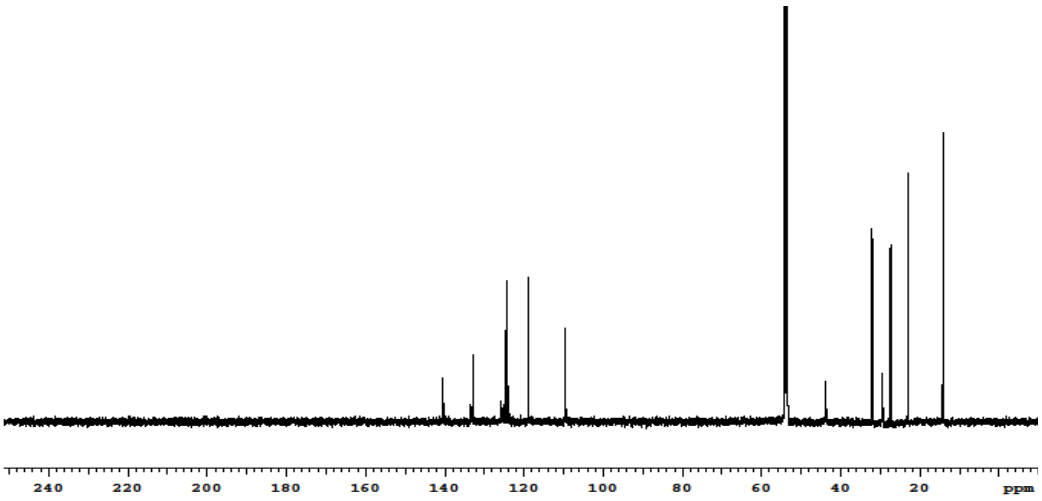

Figure A2-29. ^{13}C NMR spectrum of cyclo-3,6-tetra-N-hexylcarbazole (**3b**) in CD_2Cl_2.

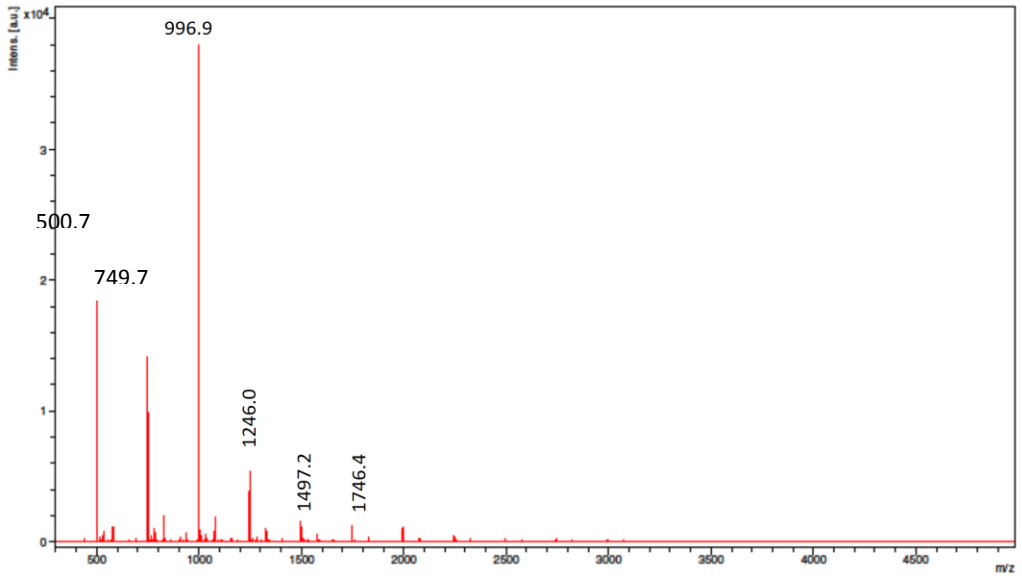

Figure A2-30. MALDI-TOF spectrum of cyclo-3,6-tetra-N-hexylcarbazole (**3b**) in DCTB matrix.

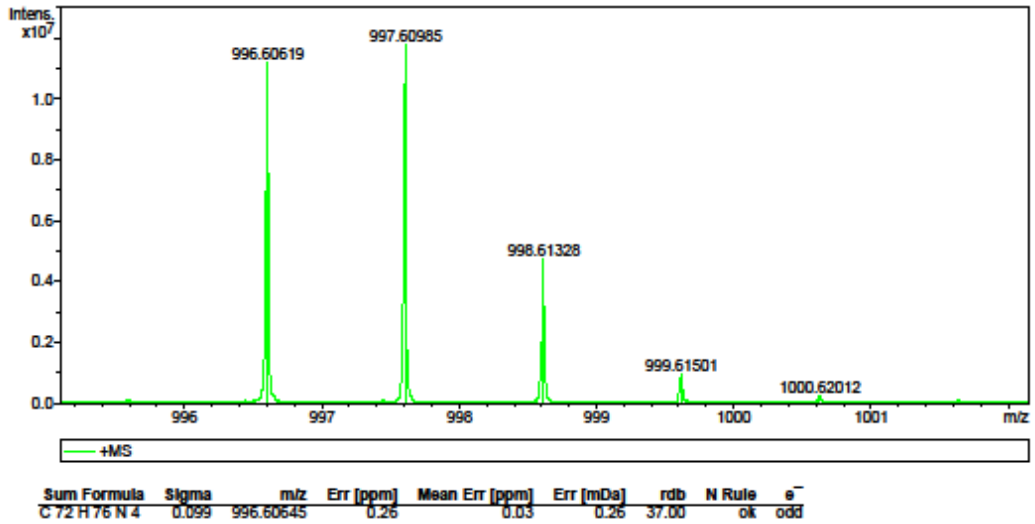

Figure A2-31. MALDI-FTICR spectrum of cyclo-3,6-tetra-N-hexylcarbazole (**3b**) in DCTB matrix.

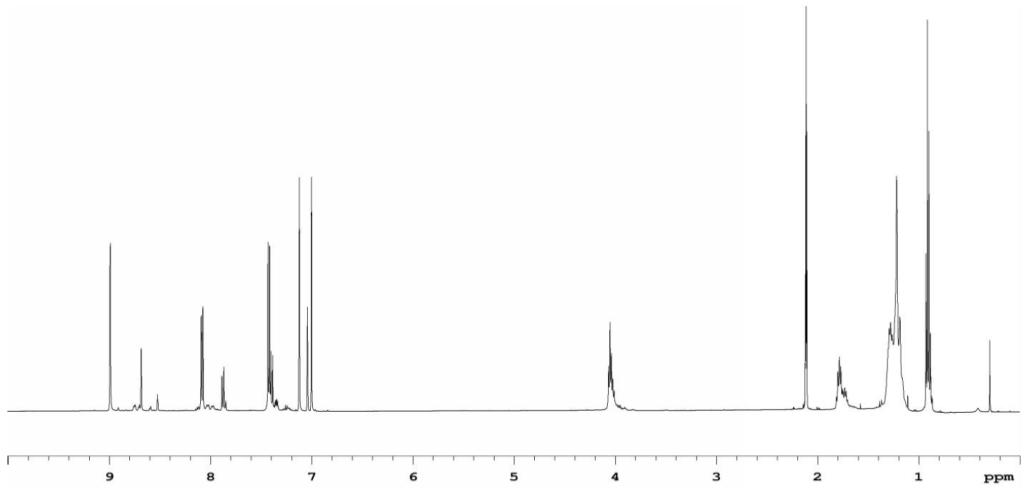

Figure A2-32. ^{1}H NMR spectrum of cyclo-3,6-tetra-N-octylcarbazole (**3c**) in toluene-d8.

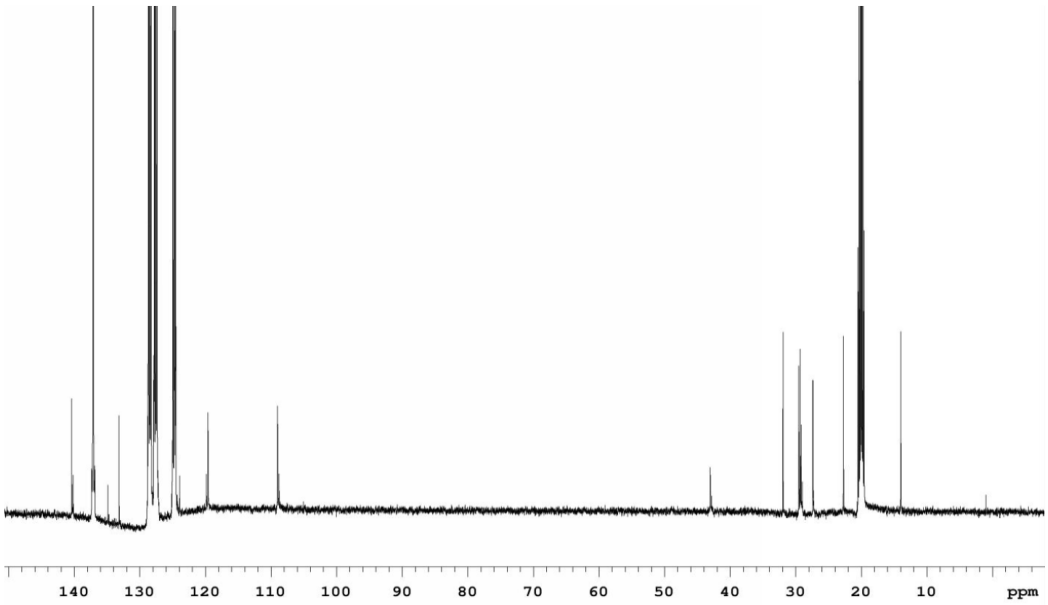

Figure A2-33. ^{13}C NMR spectrum of cyclo-3,6-tetra-N-octylcarbazole (**3c**) in toluene-d8.

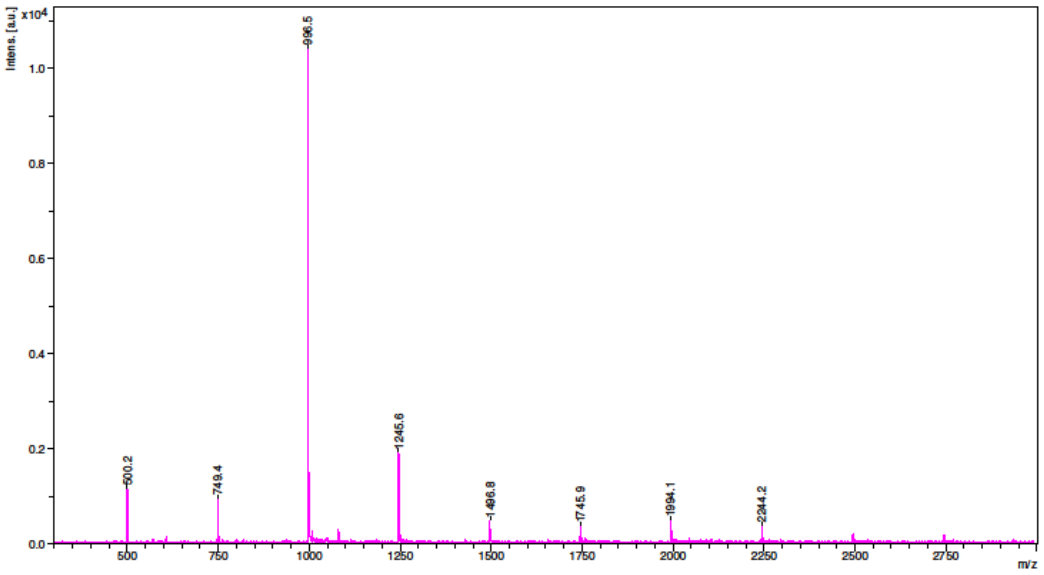

Figure A2-34. MALDI-TOF spectrum of cyclo-3,6-tetra-N-octylcarbazole (**3c**) in DCTB matrix.

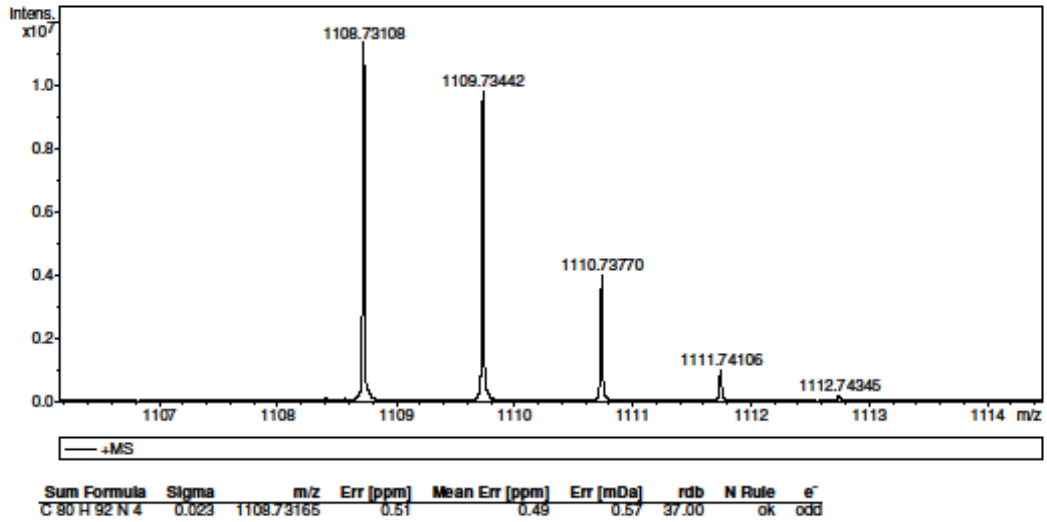

Figure A2-35. MALDI-FTICR spectrum of cyclo-3,6-tetra-N-octylcarbazole (**3c**) in DCTB matrix.

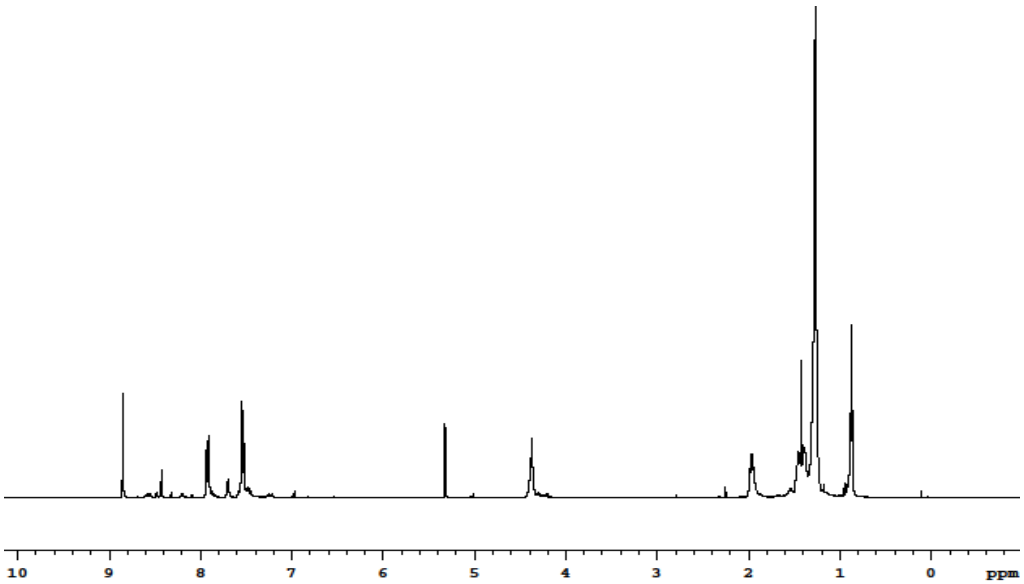

Figure A2-36. ^{1}H NMR spectrum of cyclo-3,6-tetra-N-decylcarbazole (**3d**) in CD_2Cl_2.

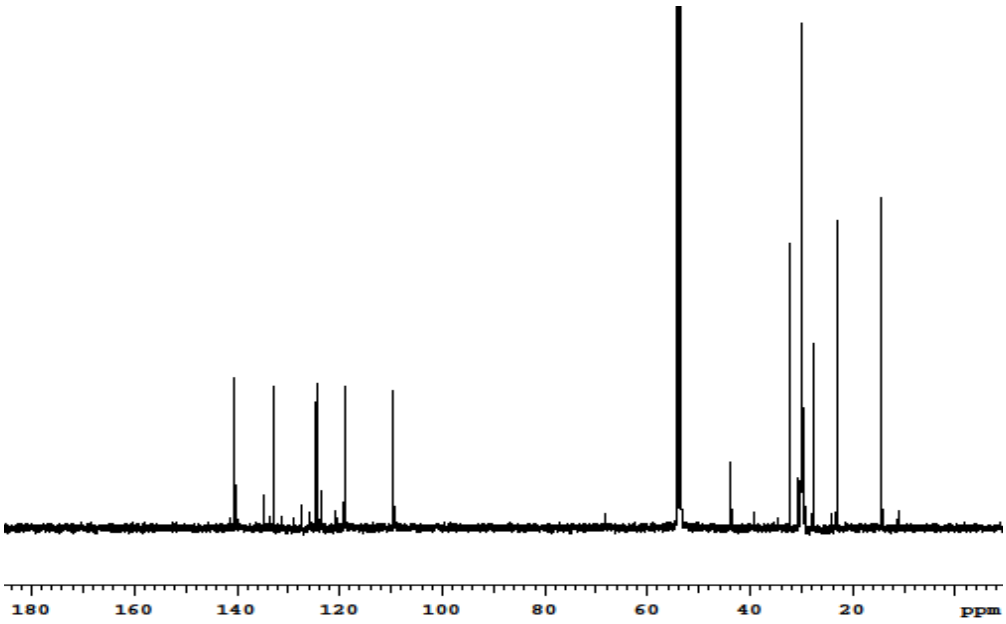

Figure A2-37. ^{13}C NMR spectrum of cyclo-3,6-tetra-N-decylcarbazole (**3d**) in CD_2Cl_2.

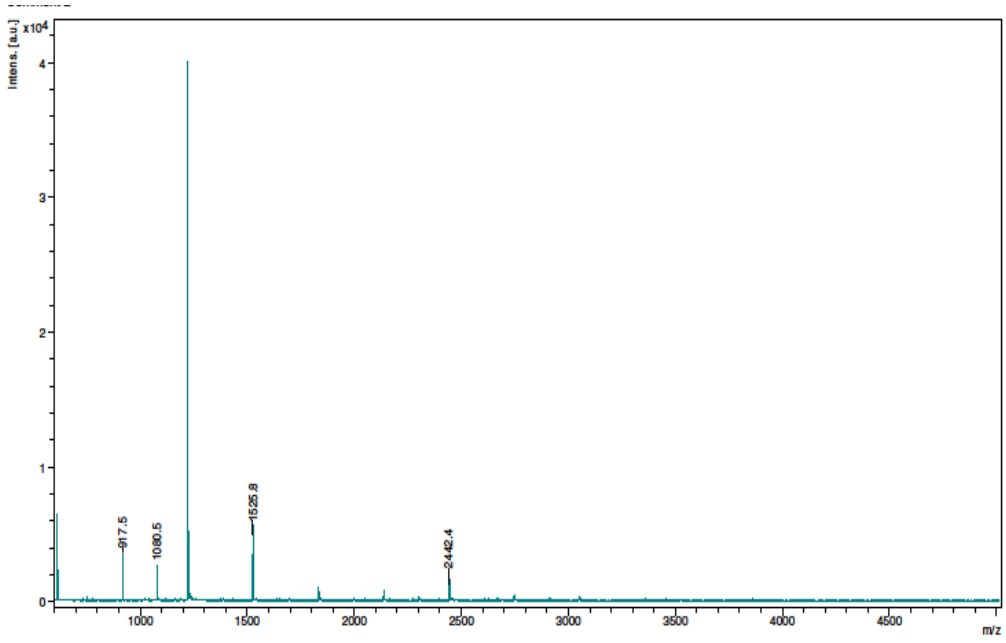

Figure A2-38. MALDI-TOF spectrum of cyclo-3,6-tetra-N-decylcarbazole (**3d**) in DCTB matrix.

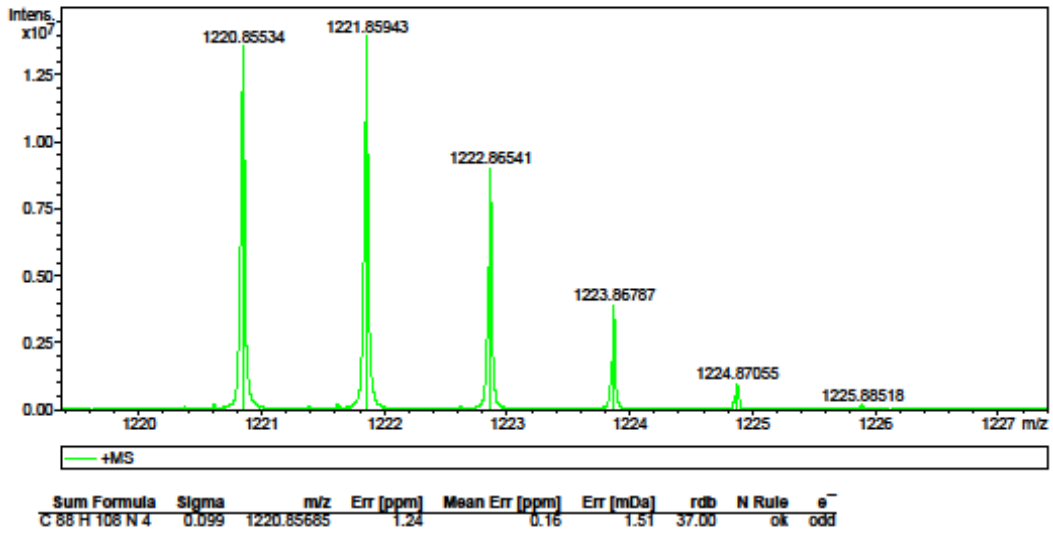

Figure A2-39. MALDI-FTICR spectrum of cyclo-3,6-tetra-N-decylcarbazole (**3d**) in DCTB matrix.

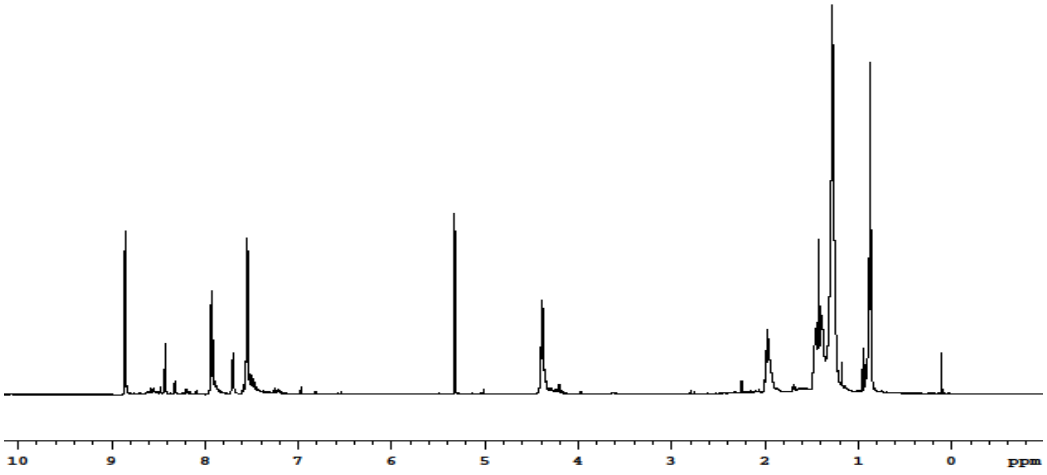

Figure A2-40. ^{1}H NMR spectrum of cyclo-3,6-tetra-N-dodecylcarbazole (**3e**) in CD_2Cl_2.

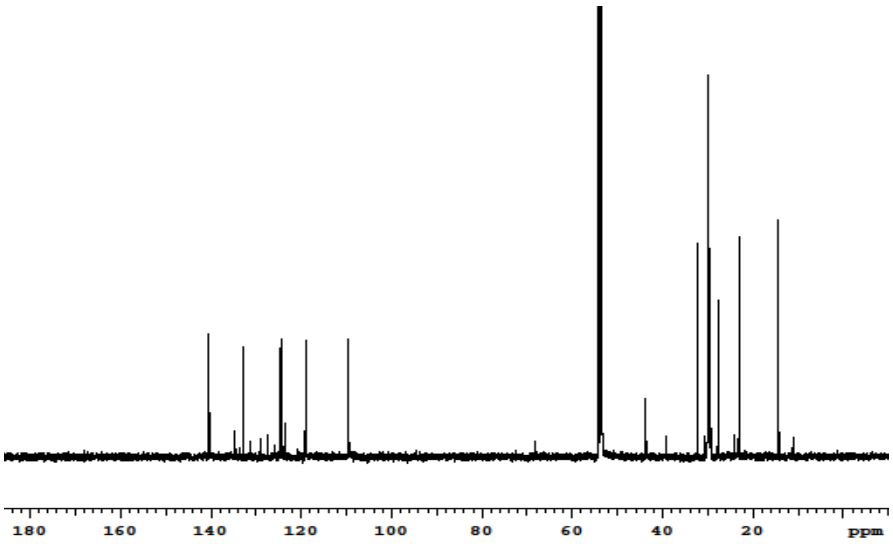

Figure A2-41. ^{13}C NMR spectrum of cyclo-3,6-tetra-N-dodecylcarbazole (**3e**) in CD_2Cl_2.

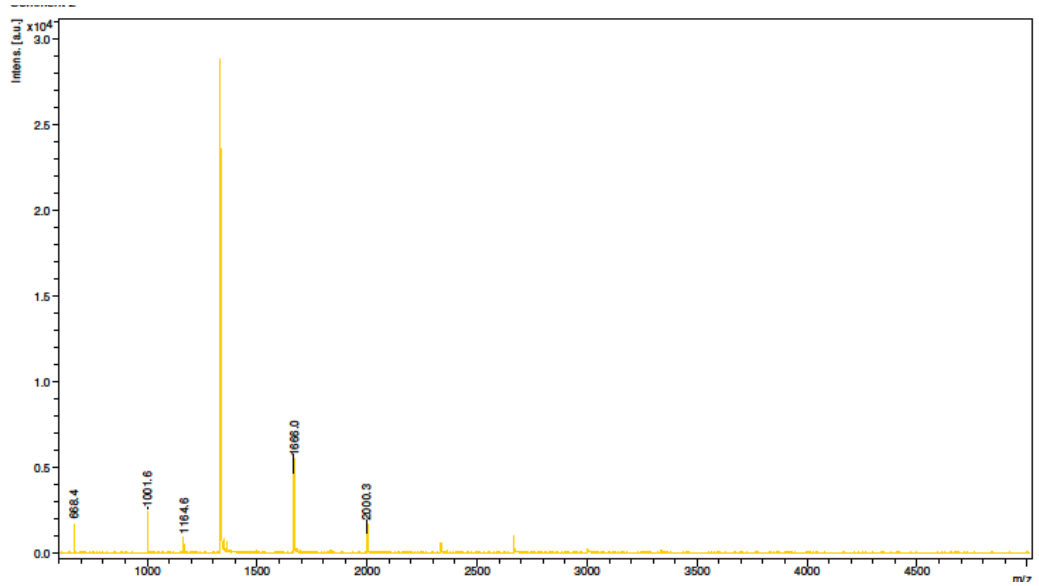

Figure A2-42. MALDI-TOF spectrum of cyclo-3,6-tetra-N-dodecylcarbazole (**3e**) in DCTB matrix.

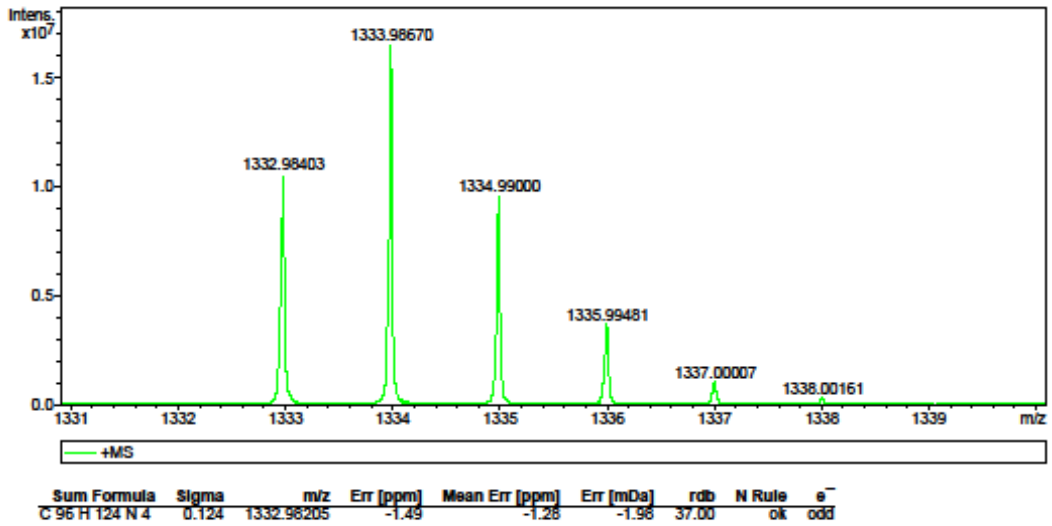

Figure A2-43. MALDI-FTICR spectrum of cyclo-3,6-tetra-N-dodecylcarbazole (**3e**) in DCTB matrix.

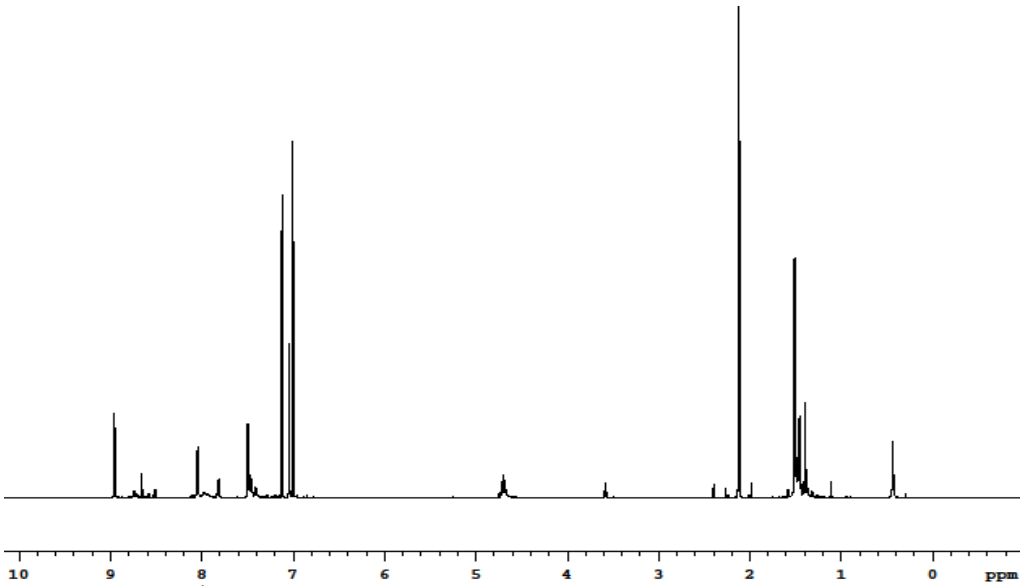

Figure A2-44. ^{1}H NMR spectrum of cyclo-3,6- tetra-N-isopropylcarbazole (**3f**) in toluene-d8.

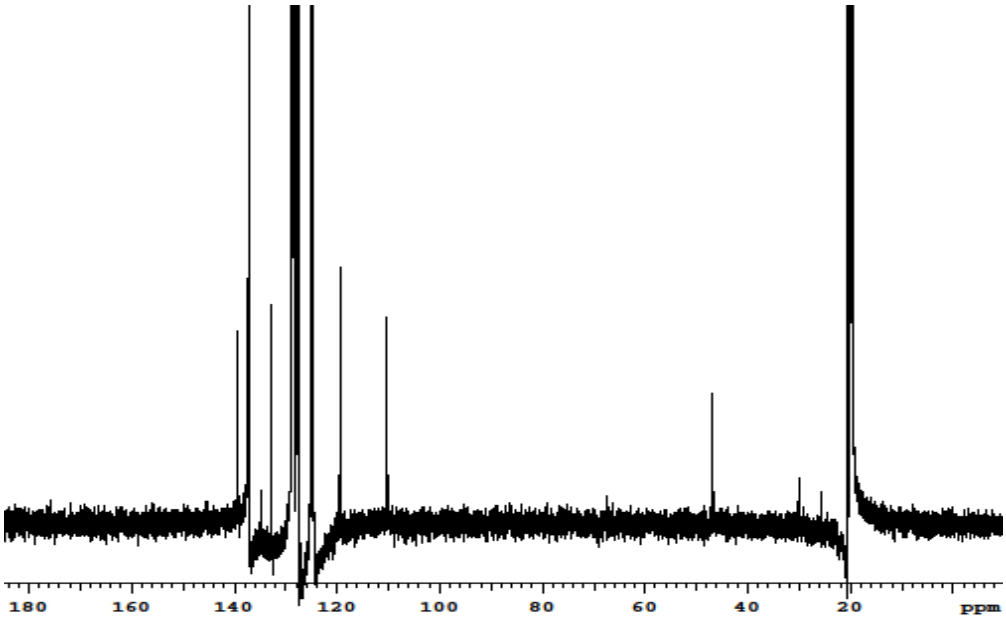

Figure A2-45. ^{13}C NMR spectrum of cyclo-3,6- tetra-N-isopropylcarbazole (**3f**) in toluene-d8.

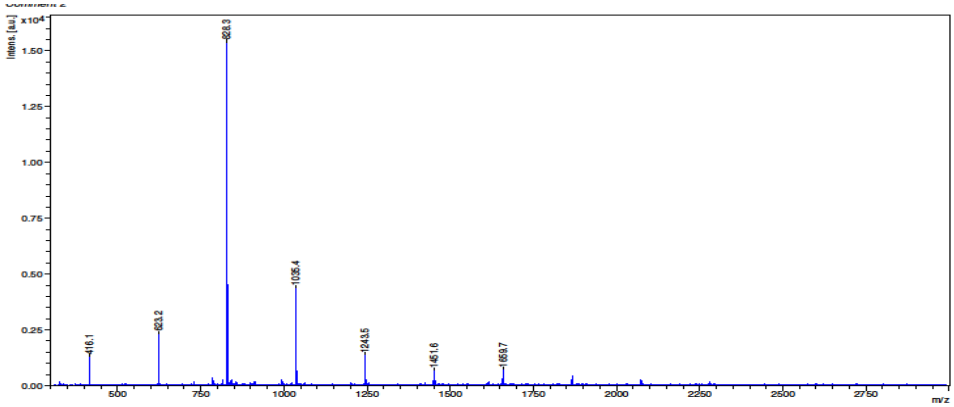

Figure A2-46. MALDI-TOF spectrum of cyclo-3,6- tetra-N-isopropylcarbazole (**3f**) in DCTB matrix.